# Characterization of Reaction Intermediates and Adsorbate Interactions on the Ru(001) Surface

Thesis by

Malina Manon Hills

In Partial Fulfillment of the Requirements

for the Degree of

Doctor of Philosophy

California Institute of Technology

Pasadena, California

1987

(Submitted 12 January 1987)

**To my family**

**for their love and support**

## Acknowledgments

One of the best aspects of Caltech is the eagerness of people to help each other. During my stay here, I have enjoyed the assistance and friendship of many people, only a few of whom may be named in this space. Tony Stark, John Yehle, Floyd Litreal and Chick Nakawatase not only built and repaired numerous pieces of equipment for me, but also taught me how equipment is constructed and how it works. Kathy Lewis applied patience and a sense of humor to all the lengthy typing tasks I brought her.

Many of the current and former members of the Weinberg group have been both good friends and the source of many enlightening discussions. I am particularly indebted to Charles Buddie Mullins for his assistance in collecting the data discussed in Chapter II, and to John Parmeter for all the sweet EEL spectra. I have profited much from my associations with John and Buddie and truly enjoyed working with them. My research advisor, Henry Weinberg, offered numerous suggestions concerning my work and encouraged me to be thorough in my analysis. He allowed me to work independently in the laboratory and to explore beyond the originally drawn boundaries of my research.

Finally, I would like to thank the people who kept me sane during the past few years. Carol Jones, Julia Lester and Jackie Shanks have been true comrades, sharing all the pleasures and pains of graduate school. Through her guidance and caring, Barbara Ellenhorn has helped me to see myself from a more accurate perspective. Last, but not least, Phil Hookham has shared my burdens, calmed me down and made me laugh.

## Abstract

The adsorption and reaction of ethylene and methylamine on the Ru(001) surface have been investigated in order to characterize reaction intermediates and adsorbate interactions. Experiments were conducted under ultrahigh vacuum conditions using electron energy loss spectroscopy and thermal desorption mass spectrometry. Molecularly chemisorbed ethylene is di-σ-bonded and the carbon atoms of the ethylene are rehybridized to $sp^3$. Upon annealing to room temperature, ethylene forms ethylidyne ($CCH_3$) and acetylide (CCH) via unstable $\eta^2$-$CHCH_2$ and $\eta^2$-$CCH_2$ intermediates. These species decompose below 400 K to carbon adatoms and methylidyne (CH) with concurrent evolution of hydrogen.

The interactions of ethylene and its decomposition intermediates with hydrogen and also with carbon monoxide have been explored. Hydrogen and carbon monoxide reduce the adsorption and decomposition of ethylene by blocking adsites. Neither coadsorbed hydrogen nor carbon monoxide alter the identities of the decomposition intermediates, although the selectivity of the reaction is altered. Thus on the clean, hydrogen-precovered and carbon monoxide-precovered Ru(001) surfaces, ethylene tends to decompose via $sp^3$-hybridized, $\eta^2$-bonded intermediates.

Oxygen overlayers perturb the electronic structure of the Ru(001) surface, changing both the bonding of coadsorbates and the decomposition intermediates. For example, ethylene adsorbed molecularly on the Ru(001)-p(2x2)O surface is $sp^2$-hybridized and π-bonded. This ethylene dehydrogenates to ethylidyne which forms vinylidene ($CCH_2$). The vinylidene is coordinated to the surface via one carbon atom with π-electron donation from the carbon-carbon double bond to the surface occurring. Thus the presence of oxygen changes the nature of the molecularly adsorbed ethylene and the decomposition intermediates, favoring $sp^2$-hybridized, $\eta^1$-bonded adspecies. This result holds also for adspecies such as acetylene, acetone and formaldehyde and is discussed using the Dewar-Chatt-Duncanson model.

Methylamine adsorbed on the Ru(001) surface is coordinated through the lone pair of electrons on the nitrogen atom. This species dehydrogenates to a $CH_2NH_2$ intermediate at 300 K, that dehydrogenates to $CHNH_2$ upon annealing to 350 K. The lone pair of electrons, previously located on the nitro-

gen, are delocalized over the ruthenium-carbon and carbon-nitrogen bonds of $CHNH_2$. This species decomposes below 400 K via two competing pathways, forming carbon adatoms and ammonia or dehydrogenating to side-on bonded C=N with concurrent evolution of hydrogen.

## Table of Contents

# CHAPTER I

## Introduction

Progress in ultrahigh vacuum (UHV) investigations of the reactions of gases with well-characterized transition metal surfaces has advanced significantly our understanding of the interactions of simple molecules (especially diatomics such as $H_2$ and CO) with these surfaces. A brief summary of the surface sensitive spectroscopies that have been used to examine the chemistry of adsorbate-substrate interactions may be found in Ref. (1). The information derived from these surface science techniques has established a foundation for more recent studies concerning the interactions of larger molecules, and in particular hydrocarbons, with these surfaces and also the effects of coadsorption of atoms and diatomic molecules with these species. This thesis details the adsorption and reaction, i.e. the chemistry, of various organic molecules with the Ru(001) surface as a function of fractional surface coverage and temperature. We have focused primarily upon the reactions of ethylene and acetylene and their coadsorption with hydrogen and oxygen. Additionally, the adsorption and reaction of methylamine and formic acid have been studied.

The spectroscopic techniques used in these investigations were thermal desorption mass spectrometry, high-resolution electron energy loss spectroscopy (EELS), low-energy electron diffraction (LEED) and Auger electron spectroscopy. Auger spectroscopy, which may be used to identify which chemical elements are present on the surface and in what concentration was used only to verify the cleanliness of the Ru(001) surface because the overlap of the ruthenium MNN Auger transition and the carbon KLL transition made estimates of the carbon coverage quite uncertain (2). The thermal desorption experiments were designed to elucidate the adsorption and desorption kinetics and thermal stabilities of decomposition intermediates of the various adspecies. Specifically, these experiments address the following: (1) What species desorb from the surface as a function of temperature; (2) The existence of different apparent bonding states and possibly different adsorption sites; (3) The nature of lateral interactions among adspecies; and (4) Desorption kinetics. Electron energy loss spectroscopy is a vibrational spectroscopy that discloses what species exist on the surface as a function of temperature and coverage and may also indicate their bonding geometry and adsorption sites. This technique has proven extremely useful in studying the adsorption and decomposition of hydrocarbons. Low-energy electron diffraction experiments allow determination of whether long-range order exists in an overlayer and may

under certain circumstances provide absolute fractional coverages.

The adsorption and reaction of ethylene and acetylene with the Ru(001) surface were examined for several reasons. These studies improve our understanding of the hydrogenation and decomposition of alkenes and alkynes and establish possible intermediates in the hydrogenolysis, hydrogenation, isomerization and dehydrogenation reactions of other hydrocarbons over ruthenium catalysts. In particular, we have examined the dehydrogenation, hydrogenation and desorption of these species, identified the decomposition intermediates and their possible bonding configurations. The observed temperatures of desorption and thermal decomposition have also been used to estimate bond strengths and activation energies of desorption. Recent investigations of the decomposition of ammonia under both UHV conditions and at higher pressures of nearly one atmosphere indicate that these activation energies and the associated preexponential factors may be applicable over broad ranges in pressure (3). Thus, the kinetic, thermodynamic and mechanistic data generated from the ethylene investigations should prove valuable in understanding the hydrogenation of ethylene over supported ruthenium catalysts at higher pressures. These studies also facilitate comparison of the reactions of hydrocarbon species on the surface with those of similar ligands in organometallic clusters (4). Finally, the interaction of ethylene with the Ru(001) surface precovered with oxygen adatoms was examined in order to elucidate the role of poisons in the surface chemistry of hydrocarbons.

Previous investigations of the molecular adsorption of unsaturated hydrocarbons on Group VIII transition metal surfaces display a tendency for the carbon atoms of these species to rehybridize upon adsorption (5-26). On most surfaces, the carbon atoms of ethylene rehybridize to nearly $sp^3$, although on cobalt and palladium surfaces the ethylene is thought to be $\pi$-bonded (5-20). The carbon atoms of chemisorbed acetylene rehybridize to between $sp^2$ and $sp^3$ following adsorption on the Fe(110), Fe(111), Ni(111), Ni(110), Pd(110), Rh(111), Pd(111), Pd(100) and Pt(111) surfaces (5,6,8,19,21-26). This parallels the tendency of alkynes to react with metal clusters such that the carbon atoms bond with three or four metal atoms with extensive rehybridization occurring (27). The decomposition intermediates of unsaturated hydrocarbons on these metal surfaces have also been identified spectroscopically. There appears to be a general tendency towards more complete dehydrogenation on the reactive iron, cobalt

and nickel surfaces upon which ethylene decomposes rapidly to acetylene, acetylide (CCH) or carbon adatoms (**5-10**), and acetylene forms methylidyne (CH) (**5,6,8,12,21-22**). In contrast, on platinum, rhodium and palladium, ethylene forms ethylidyne ($CCH_3$) or vinyl ($HCCH_2$) (**11-20**), while acetylene forms vinylidene ($CCH_2$), acetylide (CCH) or ethylidyne (**19,21,23-26**). In none of these investigations, however, was a full decomposition mechanism for either ethylene or acetylene delineated.

This thesis attempts to describe fully the decomposition reactions of ethylene and acetylene on the Ru(001) surface by examining adsorption on the clean surface, coadsorption experiments with hydrogen and carbon monoxide, and isotopic exchange experiments with deuterium. Additionally, we have investigated the reaction of ethylene with a chemically modified surface, the Ru(001) surface precovered with well-characterized, submonolayers of oxygen. The addition of oxygen to a transition metal surface lowers the Fermi level with respect to the vacuum level. The resultant increased separation between the Fermi level and the unoccupied $\pi^*$ orbital of an unsaturated hydrocarbon, such as ethylene, may inhibit backdonation of electron density to the adsorbate. Consequently, ethylene adsorbed on oxygen precovered surfaces tends to be $\pi$-bonded rather than di-$\sigma$-bonded. The addition of oxygen also lowers the binding energies of coadsorbates and therefore may alter the decomposition intermediates of ethylene.

The reaction of methylamine with the clean Ru(001) surface was investigated as a comparison to the surface chemistry of both methanol (**28**), in which the $NH_2$ group of methylamine is replaced by an OH group, and formamide ($NH_2CHO$), which has also been investigated previously (**29**). This work further elucidates the effects of the lone pairs of electrons on the nitrogen (or oxygen) atom upon the bonding of these species. Finally, the interaction of formic acid with ruthenium was explored further to better understand the details of the decomposition reactions (**30**).

**References**


1. Ertl, G.; Küppers, J., *Low Energy Electrons and Surface Chemistry*, VCH, Weinheim, Federal Republic of Germany, 1985.
2. Madey, T.E.; Engelhardt, H.A.; Menzel, D. *Surface Sci.* **1975**, 48, 304.
3. Tsai, W.; Vajo, J.J.; Weinberg, W.H., *J. Phys. Chem.* **1985**, 89, 4926.
4. Muetterties, E.L.; Rhodin, T.N.; Band, E.; Brucker, C.F.; Pretzer, W.R., *Chem. Rev.* **1979**, 79, 91.
5. Erley, W.; Baro, A.M.; McBreen, P.; Ibach, H., *Surface Sci.* **1982**, 120, 273.
6. Seip, U.; Tsai, M.-C.; Küppers, J.; Ertl, G., *Surface Sci.* **1984**, 147, 65.
7. Stroscio, J.A.; Bare, S.R.; Ho, W., *Surface Sci.* **1984**, 148, 499.
8. Lehwald, S.; Ibach, H., *Surface Sci.* **1979**, 89, 425.
9. Carr, R.G.; Sham, T.K.; Eberhardt, W.E., *Chem. Phys. Lett.* **1985**, 133, 63.
10. Albert, M.R.; Sneddon, L.G.; Plummer, E.W., *Surface Sci.* **1984**, 147, 127.
11. Demuth, J.E., *Surface Sci.* **1979**, 84, 315.
12. Steininger, H.; Ibach, H.; Lehwald, S., *Surface Sci.* **1982**, 117, 685.
13. Gates, J.A.; Kesmodel, L.L., *Surface Sci.* **1982**, 120, L461.
14. Gates, J.A.; Kesmodel, L.L., *Surface Sci.* **1983**, 124, 68.
15. Tysoe, W.T.; Nyberg, G.L.; Lambert, R.M., *J. Phys. Chem.* **1984**, 88, 1960.
16. Kesmodel, L.L.; Gates, J.A., *Surface Sci.* **1981**, 111, L747.
17. Stuve, E.M.; Madix, R.J., *J. Phys. Chem.* **1985**, 89, 105.
18. Stuve, E.M.; Madix, R.J. Brundle, C.R., *Surface Sci.* **1985**, 152/153, 552.
19. Dubois, L.H.; Castner, D.G.; Somorjai, G.A., *J. Chem. Phys.* **1980**, 72, 5234.
20. Gupta, N.M.; Kamble, V.S.; Iyer, R.M., *J. Catal.* **1984**, 88, 457.
21. Bandy, B.J.; Chesters, M.A.; Pemble, M.E.; McDougall, G.S.; Sheppard, N., *Surface Sci.* **1984**, 139, 87.

22. Ibach, H.; Lehwald, S. J., *Vacuum Sci. Technol.* **1981**, 17, 625.

23. Gates, J.A.; Kesmodel, L.L., *J. Chem. Phys.* **1982**, 76, 4281.

24. Kesmodel, L.L.; Waddill, G.D.; Gates, J.A., *Surface Sci.* **1984**, 138, 464.

25. Kesmodel, L.L., *J. Chem. Phys.* **1983**, 79, 4646.

26. Ibach, H.; Lehwald, S., *J. Vacuum Sci. Technol.* **1978**, 15, 407.

27. Ittel, S.D.; Ibers, J.A., *Adv. Organomet. Chem.* **1976**, 14, 33.

28. Hrbek, J.; dePaola, R.A.; Hoffmann, F.M., *J. Chem. Phys.* **1984**, 81, 2818.

29. Parmeter, J.E.; Schwalke, U.; Weinberg, W.H., *J. Am. Chem. Soc.*, to be published.

30. Avery, N.R.; Toby, B.H.; Anton, A.B.; Weinberg, W.H., *Surface Sci.* **1982**, 122, L574.

# CHAPTER II

## The Interaction of Ethylene with the Ru(001) Surface



[This chapter was published as a paper by M. M. Hills, J. E. Parmeter, C. B. Mullins and W. H. Weinberg in *The Journal of the American Chemical Society* **108**, 3554 (1986).]

**Abstract**

The interaction of ethylene with the Ru(001) surface has been investigated via high resolution electron energy loss spectroscopy and thermal desorption mass spectrometry. Following desorption of an ethylene multilayer at 110 K, di-σ-bonded molecular ethylene is present on the surface. Competing desorption of molecular ethylene and dehydrogenation to form adsorbed ethylidyne ($CCH_3$) and acetylide (CCH) as well as hydrogen adatoms occur between approximately 150 and 260 K. The ethylidyne is stable to approximately 330 K, whereupon it begins to decompose to carbon and hydrogen adatoms. The desorption of hydrogen occurs in a sharp peak centered at 355 K, resulting from simultaneous ethylidyne decomposition and desorption of surface hydrogen. Further annealing of the overlayer to 380 K causes cleavage of the carbon-carbon bond of the acetylide, creating carbon adatoms and adsorbed methylidyne (CH). The methylidyne decomposes above 500 K with accompanying hydrogen desorption, leaving only carbon adatoms on the surface at 700 K.

## I. Introduction

The adsorption and reaction of ethylene on single crystalline surfaces of the Group VIII transition metals (**1-17**) has been the subject of intense study both as a prototype for olefin hydrogenation and dehydrogenation reactions (**18-21**) and to provide a basis for comparing the bonding of olefins to surfaces with the bonding that has been observed to occur in multinuclear homogeneous organometallic cluster compounds. Spectroscopic studies of ethylene adsorbed on these surfaces have shown that both the nature of the bonding of molecular ethylene to the substrate as well as the thermal decomposition pathway of the adsorbed ethylene vary widely. For example, ethylene rehybridizes to a di-$\sigma$-bonded molecular species when adsorbed on Fe(110), Fe(111), Ni(110), Ni(111), Ni[5(111)x(110)], Pt(111) and Pt(100) (**1-7**), whereas molecularly adsorbed ethylene on Co(001) at 115 K is $\pi$-bonded (**8**), as is ethylene adsorbed on Pd(111) at 150 K and on Pd(110) at 110 K (**6,9-13,17**). A mixed overlayer of $\pi$- and di-$\sigma$-bonded ethylene forms on Pd(100) at 150 K (**14,15**). Ethylene adsorption on the Ru(001) surface has been studied recently by Barteau, and co-workers (**22**). A detailed comparison between our more complete study and the preliminary results of Barteau, et al. (**22**) is presented in Sect. IV.

The thermal decomposition of ethylene (ultimately to hydrogen and surface carbon) on the surfaces mentioned above has been investigated by vibrational electron energy loss spectroscopy (EELS), thermal desorption mass spectrometry (TDMS), and UV photoelectron spectroscopy. The thermal decomposition intermediates in ethylene dehydrogenation on Fe(110), Ni(111), Ni[5(111)x(110)] and Ni(110) are acetylene and acetylide (CCH) (**1,3,4**). Stuve and Madix have postulated the formation of a vinyl group from ethylene adsorbed on Pd(100) (**14,15**). On Co(001) and Fe(111) no stable surface intermediates were observed; chemisorbed ethylene evidently dehydrogenates completely just below room temperature to carbon and hydrogen (**2,8**). On Pt(111), Rh(111), Pd(111) and Pt(100), chemisorbed ethylene dehydrogenates to form ethylidyne below 300 K (**7,9-13,16,23**). Thus ethylene adsorbed on the close-packed surfaces of each of the 4d and 5d Group VIII metals studied previously forms ethylidyne (**24**). On the other hand, ethylene adsorbed on all of the surfaces of the 3d Group VIII metals studied to date, including the close-packed surfaces, dehydrogenates more completely to acetylene, acetylide or directly to carbon. Hence it is of fundamental interest to determine whether

ethylene adsorbed on the Ru(001) surface behaves as it does on the other hexagonal 4d and 5d transition metal surfaces studied previously [Rh(111), Pd(111), Pt(100) and Pt(111)], or whether it dehydrogenates more completely, as it does on the hexagonal Ni(111) and Co(001) surfaces.

## II. Experimental Procedures

The experimental measurements were conducted in two different ultrahigh vacuum (UHV) chambers, each with base pressures below 1 x $10^{-10}$ Torr. The first UHV chamber is equipped with a quadrupole mass spectrometer, a single pass cylindrical mirror electron energy analyzer with an integral electron gun for Auger electron spectroscopy, and LEED optics. All thermal desorption measurements were carried out in this chamber; data were collected using an LSI-11 DEC laboratory computer, and linear heating rates of 5-15 K/s were employed. A glass enclosure was placed around the ionizer of the mass spectrometer, and a small aperture in the front of the glass envelope permited sampling of gas that was desorbed only from the well-oriented front of the single crystal. Thus the effects of desorption from the edge of the crystal, the support leads, and the manipulator are excluded from the thermal desorption spectra (**26**).

The second UHV chamber contains both a quadrupole mass spectrometer and a home-built EELS spectrometer of the Kuyatt-Simpson type (**27,28**). The energy-dispersing elements in the EELS monochromator and rotatable analyzer are 180° hemispherical deflectors. The "off-specular" EEL spectra were measured with the analyzer rotated 7-10° from the specular direction, toward the surface normal. All EEL spectra were measured using a beam energy of 4 eV and with the incident beam approximately 60° from the surface normal. The instrumental resolution (full-width at half-maximum of the elastically scattered peak) varied between 60 and 80 $cm^{-1}$, while maintaining a count rate of approximately 3 x $10^5$ cps in the elastic peak. A more extensive description of these UHV chambers as well as the procedures followed for cutting, polishing, mounting and cleaning the Ru(001) crystals have been discussed in detail previously (**27-30**). The cleanliness of the surfaces was monitored with Auger spectroscopy in the first chamber and with EELS in the second.

Research purity hydrogen (99.9995%), and C.P. grade deuterium and ethylene (99.5%) were purchased from Matheson. Research purity tetradeuterated ethylene (99.99%) was obtained from Merck

and Co. The $H_2$, $D_2$ and $C_2D_4$ were used without further purification, whereas the $C_2H_4$ was subjected to freeze-thaw-pumping cycles prior to use. The purity of all gases was verified *in situ* with mass spectrometry.

## III. Results

Typical thermal desorption spectra following exposure of the Ru(001) surface to 1L (1L ≡ 1 Langmuir = 1 x $10^{-6}$ Torr-s) or more of $C_2H_4$ at 90 K are shown in Fig. 1(a) and (b) (31). Only hydrogen and ethylene are observed to desorb from the surface. In particular, no ethane, methane or acetylene are detected as judged by the absence of 30 and 16 AMU peaks and by comparison of the 28, 27 and 26 AMU peaks to the cracking pattern of ethylene.

Figure 1(b) establishes that most of the hydrogen, after an ethylene exposure exceeding 0.6 L, desorbs in a sharp peak centered at 355 K (independent of coverage), with a small high temperature shoulder above 400 K and a broad tail extending from 500 to 700 K, of which the latter represents 10-15% of the desorbing hydrogen. It will be shown below that the major peak corresponds to the desorption of hydrogen enhanced by the decomposition of ethylidyne (one of the decomposition products of ethylene), the shoulder corresponds to desorption-limited hydrogen from the surface, and the high temperature tail corresponds to the dehydrogenation of surface methylidyne (another decomposition product). The thermal desorption spectrum of molecular ethylene [cf. Fig. 1(a)] shows that ethylene desorbs in a sharp peak centered near 110 K, followed by a broad peak, of which the tail extends to approximately 250 K. As discussed below, EEL spectra of the surface on which ethylene is adsorbed and which is annealed to various temperatures show that the higher temperature peak corresponds to the desorption of di-σ-bonded ethylene, while multilayer ethylene desorbs in the lower temperature peak. The "multilayer" peak shown in Fig. 1(a) actually corresponds to only desorption from a second layer. This multilayer peak does not saturate with increasing ethylene exposure, however, and is sufficiently intense following a 15 L exposure of ethylene that it obscures the desorption peak due to chemisorbed ethylene.

For lower exposures of ethylene, below 0.6 L, the hydrogen thermal desorption spectra are quite different. The thermal desorption spectrum of $H_2$ after an ethylene exposure of 0.2 L, shown in Fig.

1(c), contains a high temperature tail terminating below 600 K, which is due to methylidyne decomposition, and a rather broad peak centered at 420 K that shifts to lower temperature as the initial surface coverage of chemisorbed ethylene increases. The latter is essentially identical to that which is observed after adsorption of hydrogen on the clean Ru(001) surface (32). The maximum rate of $H_2$ desorption shifts from 420 K for an ethylene exposure of 0.2 L to 395 K for a 0.4 L exposure, and then drops to 355 K for all ethylene exposures exceeding 0.6 L. The decrease in peak temperature for exposures of ethylene below 0.6 L is indicative of second-order desorption kinetics of surface hydrogen. For these lower exposures of ethylene, below 0.6 L, no desorption of molecular ethylene is observed.

Figures 2(a) and (b) show the EEL spectra of 4 L of $C_2H_4$ and 3 L of $C_2D_4$, respectively, adsorbed at 80 K on the Ru(001) surface. Consistent with the thermal desorption spectra, a comparison of the observed energy loss features to IR and Raman spectra of gaseous, liquid and solid ethylene [cf. Table 1 (33,34)] demonstrates that the overlayers of Fig. 2 correspond to molecular multilayers. Note the intense $CH_2$ wagging mode at 970 $cm^{-1}$, which is the best fingerprint of molecular ethylene multilayers, and also of the carbon-hydrogen stretching mode at 3000 $cm^{-1}$. The frequencies of both these modes are characteristic of an $sp^2$ hybridized carbon atom. Table 1 also shows that the isotopic shifts for multilayer $C_2D_4$ on Ru(001) are in good agreement with those of $C_2D_4$(g).

Annealing these overlayers to 110 K desorbs the multilayer, as shown in the thermal desorption spectra [cf. Fig. 1(a)], leaving di-σ-bonded ethylene, which is stable to 150 K. The EEL spectra of this chemisorbed species are exhibited in Fig. 3(a) for $C_2H_4$ and Fig. 3(b) for $C_2D_4$. The rehybridization of the carbon atoms to nearly $sp^3$ is reflected in the shifts of the $CH_2$ wagging mode and the carbon-hydrogen stretching mode to 1145 and 2985 $cm^{-1}$, respectively. The shoulder at 1040 $cm^{-1}$ is probably due to the carbon-carbon stretching mode, but it is poorly resolved from the $CH_2$ twisting mode in $C_2H_4$ and the $CD_2$ wagging mode in $C_2D_4$ both of which are at 900 $cm^{-1}$. A carbon-carbon stretching frequency of 1040 $cm^{-1}$ is consistent with the rehybridization of the carbon atoms of ethylene to $sp^3$. Other modes of di-σ-bonded ethylene are the symmetric ruthenium-carbon stretching mode at 460 $cm^{-1}$ (420 $cm^{-1}$ for $C_2D_4$), the $CH_2$ rocking mode at 775 $cm^{-1}$, the $CH_2$ twisting mode at 900 $cm^{-1}$ (700 $cm^{-1}$ for $C_2D_4$) and the $CH_2$ scissoring mode at 1450 $cm^{-1}$ (1210 $cm^{-1}$ for $C_2D_4$). The $CD_2$ rocking mde of

di-σ-bonded $C_2D_4$ was not resolved in Fig. 3(b) due to the poorer cutoff in the elastic peak. The symmetric ruthenium-carbon stretching mode of di-σ-bonded $C_2D_4$ also contains a small contribution from ν(Ru-CO). The symmetric and asymmetric carbon-hydrogen stretching modes of $C_2H_4$ at 2940 and 3050 $cm^{-1}$ were resolved in spectra similar to Fig. 3(a).

Peak assignments for di-σ-bonded ethylene (both $C_2H_4$ and $C_2D_4$) on Ru(001) are compared in Table 2 with these data as well as with IR data for $C_2H_4Br_2$(g), $C_2H_4$(g), Zeise's salt, and low-valent nickel complexes [$Ni(C_2H_4)_n$ and $Ni_2(C_2H_4)_n$, n = 1,2,3] (**1-4,7,33,35,36**). A comparison of the frequencies of the modes of di-σ–bonded $C_2H_4$ on Ru(001) to these data shows that ethylene undergoes rehybridization on the Ru(001) surface as on Ni(110), Ni(111) and Fe(110) (**1,3-5**). The existence of a π-bonded ethylene admolecule can be excluded by a comparison to the IR data for Zeise's salt and Ozin's nickel complexes, which have, among other differences, higher frequency $CH_2$ rocking modes and carbon-carbon stretching modes.

A comparison of EEL spectra of di-σ-bonded ethylene with spectra of diazomethane led to an original assignment of the spectrum of Fig. 3(a) as a bridging methylene species (**37**). However, a subsequent review of these and other spectra has shown that the reaction of $CH_2N_2$ to form $C_2H_4$ and $N_2$ may occur in the gas-dosing lines prior to introduction into the UHV chamber. An assignment of EEL spectra of uncontaminated diazomethane, which produces $\mu_2$–$CH_2$ groups on Ru(001), is listed in the last column in Table 2. Additional vibrational data concerning bridging methylene may be found elsewhere (**39-43**). The adsorption of $C_2H_4$ on Ru(001) with annealing to 110 K produces di-σ-bonded molecular ethylene, which can be distinguished from $\mu_2$–$CH_2$ by the intense $CH_2$ twisting mode at 900 $cm^{-1}$. In agreement with this conclusion, the thermal desorption spectra of ethylene on Ru(001) show desorption of molecular ethylene up to 250 K.

In an effort to describe further the character of the di-σ-bonded ethylene on Ru(001), isotopic exchange, thermal desorption experiments of coadsorbed $C_2H_4$ and $C_2D_4$ were carried out. In all cases, only $C_2H_4$ and $C_2D_4$ desorbed from the multilayer. However, all five isotopically labeled species ($C_2H_4$, $C_2H_3D$, $C_2H_2D_2$, $C_2HD_3$ and $C_2D_4$) appeared in the di-σ-bonded ethylene that desorbs molecularly. Figure 4 shows the relative ratios of these five species that desorb molecularly above 150 K.

These ratios were obtained by correcting the areas under the thermal desorption peaks of the 26-32 AMU spectra, both for the cracking patterns of the five species and for the relative sensitivity of the mass spectrometer to each species. (These ratios *exclude* multilayer $C_2H_4$ and $C_2D_4$.) Figure 4 shows that isotopic exchange is limited, and no one mixed species ($C_2H_3D$, $C_2H_2D_2$ or $C_2HD_3$) is favored over the other two. On the other hand, the corresponding $H_2/HD/D_2$ thermal desorption spectra exhibited complete isotopic exchange. The above results suggest that the isotopic mixing observed for chemisorbed ethylene that desorbs molecularly results from exchange between an ethylene admolecule and a hydrogen (or deuterium) adatom, since the onset of desorption of the mixed molecular ethylene species ($C_2H_xD_{4-x}$, $1 \leq x \leq 3$) coincides with the initial decomposition of ethylene to ethylidyne, acetylide and surface hydrogen via carbon-hydrogen bond cleavage.

Annealing di-σ-bonded ethylene to 250 K produces two new carbon-containing surface species as well as hydrogen adatoms. The modes due to surface hydrogen were not resolved in the corresponding EEL spectrum shown in Fig. 5(a). The weak losses of hydrogen adatoms, which occur at 845 and 1115 $cm^{-1}$ (**44**), were obscured by various carbon-hydrogen and carbon-carbon modes. However, the presence of hydrogen adatoms was confirmed by stoichiometric considerations and hydrogen postadsorption experiments, which will be discussed later. The two hydrocarbon fragments present on the surface have been identified as ethylidyne and acetylide from the EEL spectrum of Fig. 5(a), the corresponding EEL spectrum of the deuterated species, off-specular EELS measurements, and EEL spectra measured following annealing to various temperatures.

Peak assignments for $CCH_3$ and $CCD_3$ are compared in Table 3 to IR data for a tricobalt ethylidyne complex as well as EELS results for ethylidyne adsorbed on various close-packed Group VIII metal surfaces (**4,7,16,45**). A triruthenium ethylidyne complex has also been synthesized, but no relevant IR data have been published (**46**). For all of the ethylidyne adspecies listed in Table 3, the carbon-carbon stretching mode produces a strong, dipolar enhanced peak. By analogy to the structure of the triruthenium and tricobalt organometallic compounds, and considering the relative intensities of the (dipolar enhanced) carbon-carbon stretching modes, the carbon-carbon bond axis of each of the ethylidyne adspecies is nearly perpendicular to the surface plane. A comparison of the EELS losses for

$CCH_3$ and $CCD_3$ on Ru(001) with IR data for $(CO)_9Co_3(\mu_3\text{-}CCH_3)$ and $(CO)_9Co_3(\mu_3\text{-}CCD_3)$ (cf. Table 3) shows that the structure and bonding of the ethylidynes in the two cases are quite similar.

The acetylide species is characterized by a carbon-hydrogen bending mode at 750 $cm^{-1}$, a carbon-hydrogen stretching mode at 2960 $cm^{-1}$, and a carbon-carbon stretching mode at 1290 $cm^{-1}$. The vibrational modes of acetylide are partially obscured by the ethylidyne modes because the ratio of ethylidyne to acetylide present in Fig. 4(a) is approximately 3:2, on the basis of hydrogen thermal desorption measurements. Annealing this overlayer to 360 K decomposes the ethylidyne, leaving acetylide, carbon and a small concentration of hydrogen adatoms on the surface. Thus the modes of the acetylide are completely resolved in spectra measured after annealing the overlayer to 360 K [cf. Fig. 5(b)]. This acetylide also forms from the thermal decomposition of acetylene and is discussed in greater detail in a separate paper (**47**). We merely note here that these assignments agree quite well with those of Kesmodel et al. for acetylide on Pd(100) for which $\delta$(CH) is 750 $cm^{-1}$, $\nu$(CC) is 1340 $cm^{-1}$ and $\nu$(CH) is 3000 $cm^{-1}$ (**48,49**).

The EEL spectra of the deuterated acetylide show that the carbon-deuterium bending mode of CCD downshifts to 550 $cm^{-1}$ from 750 $cm^{-1}$ for CCH (cf. Table 4), which compares well with the value of $\delta$(CD) of 540 $cm^{-1}$ for CCD on Pd(100) (**48,49**). We also observe a slight shift in $\nu$(CC) from 1290 $cm^{-1}$ in CCH to 1260 $cm^{-1}$ in CCD, and the expected shift in $\nu$(CD) from 2960 $cm^{-1}$ in CCH to approximately 2210 $cm^{-1}$ in CCD. These losses persist up to 380 K, where cleavage of the carbon-carbon bond of the acetylide occurs, forming surface carbon and methylidyne.

The adsorbed methylidyne is identified from the EEL spectrum of Fig. 5(c) with $\nu$(RuC) at 465 $cm^{-1}$, $\delta$(RuCH) at 810 $cm^{-1}$ and $\nu$(CH) at 3010 $cm^{-1}$, of which the latter two are significantly higher than the corresponding modes of the acetylide. The disappearance of the 1290 $cm^{-1}$ carbon-carbon stretching mode of acetylide upon annealing to 500 K also assists us in distinguishing acetylide and methylidyne. The mode at 570 $cm^{-1}$ in Fig. 5(c) is the carbon-metal stretching mode of carbon adatoms and/or carbon dimers. The broad feature at 1100-1600 $cm^{-1}$ may be attributed to the carbon-carbon stretching mode of these dimers. The vibrational modes of the methylidyne are compared in Table 5 to those of high temperature (T>400 K) methylidynes on various transition metal surfaces, as

well as tricobalt and triruthenium $\mu_3$-CH complexes (**1,2,4,9,10,50-53**). Our assignments agree quite well with those of methylidyne adsorbed on the Fe(111), Ni(111) and Pd(111) surfaces and are consistent with those of the organometallic complexes. The isotopic shifts of the vibrational modes of methylidyne adsorbed on Ru(001) are also in agreement with those of $(CO)_4Co_3(\mu_3\text{-CD})$.

All of the methylidyne modes are eliminated by annealing the Ru(001) surface above 700 K. After this annealing, weak modes near 600 $cm^{-1}$ and 1100-1600 $cm^{-1}$ are observed, which are attributed to $\nu$(RuC) of carbon adatoms and dimers, and $\nu$(CC) of carbon dimers. These modes are present in the EEL spectra of both $C_2H_4$ and $C_2D_4$. No other features are present in the high temperature EEL spectra, supporting the thermal desorption results, which show complete desorption of hydrogen (and ethylene) below 700 K.

Bearing in mind what we have learned from EELS concerning the decomposition of ethylene on Ru(001), we now return to a more detailed analysis of the thermal desorption spectra. In the case of ethylene adsorbed on the Ru(001) surface, three reactions generate surface hydrogen below 400 K, namely: (1) $C_2H_4$ dehydrogenation to CCH(a) and 3H(a), beginning at 150 K; (2) $C_2H_4$ dehydrogenation to $CCH_3$(a) and H(a), also beginning at 150 K; and (3) $CCH_3$ decomposition to 2C(a) or $C_2$(a) and 3H(a), beginning at 330 K. As shown in Fig. 1(b), a large ethylene exposure produces a sharp peak at 355 K with a shoulder near 400 K in the hydrogen thermal desorption spectrum, followed by a long, high temperature tail. Since the high temperature tail corresponds exclusively to methylidyne decomposition and represents a small fraction of the total hydrogen that is desorbed (approximately 10%), a hydrogen mass balance requires that the desorption that occurs below 500 K corresponds to surface hydrogen from acetylide and ethylidyne formation as well as from ethylidyne decomposition.

For rather low exposures of ethylene, below 0.6 L, the hydrogen thermal desorption spectra are quite different, although the EEL spectra of all coverages of ethylene adsorbed on Ru(001) are qualitatively the same. The thermal desorption spectrum of hydrogen following a low ethylene exposure contains a prominent peak (which shifts as a function of coverage) and also a high temperature tail [cf. Fig. 1(c)]. As shown by the EELS results, the tail corresponds to hydrogen desorption that is limited by methylidyne decomposition. The hydrogen desorbing in the major peak is due to surface hydrogen

from ethylene decomposition to ethylidyne and acetylide, and ethylidyne decomposition to surface carbon, as is the hydrogen desorbing in the 355 K peak following higher ethylene exposures. The shift in this peak as a function of ethylene coverage indicates that the desorption of this hydrogen is desorption-limited. This is confirmed by experiments conducted on the carbonaceous residue that remains after annealing to 700 K the ruthenium surface that had been exposed to 0.4 L $C_2H_4$ at 100 K. Hydrogen was adsorbed on this carbonaceous residue at 90 K, and then a thermal desorption measurement was carried out. The thermal desorption spectra showed that the major hydrogen thermal desorption peak was repopulated, confirming that this peak is due to desorption of surface hydrogen.

The sharp peak at 355 K in the thermal desorption spectra of hydrogen following an exposure of ethylene *exceeding* 0.6 L consists of surface hydrogen formed from ethylene decomposition at lower temperatures (150-280 K) and driven by the presence of that hydrogen from ethylidyne decomposition. The maximum rate of the latter occurs at 355 K. The high temperature shoulder on this peak (near 400 K) corresponds to desorption of residual surface hydrogen. That the sharp peak at 355 K and its high temperature shoulder are derived from surface hydrogen has been confirmed by hydrogen postadsorption experiments. First, the Ru(001) surface was exposed to 5 L of $C_2H_4$ at 90 K, annealed to 800 K, cooled to 90 K, and exposed to 30 L of hydrogen. A subsequent thermal desorption spectrum [Fig. 6(b)] shows a peak at 355 K with a high temperature shoulder (**54**). A comparison with the hydrogen thermal desorption spectrum after an exposure of 5 L of $C_2H_4$ [Fig. 6(a)] shows that less hydrogen is present in the 355 K peak of Fig. 6(b) and that the leading edge of the peak in this spectrum is not so sharp. These differences are due solely to the presence of ethylidyne decomposition in Fig. 6(a) and its absence in Fig. 6(b).

In a second experiment, the ruthenium surface was exposed to 0.4 L of $C_2H_4$, followed by 1 L of $H_2$ at 90 K. A subsequently measured hydrogen thermal desorption spectrum [Fig. 7(a)] was unlike that following an exposure of 0.4 L of $C_2H_4$ [Fig. 7(b)]. Rather, it appears qualitatively similar to that observed after an exposure of 1 L of $C_2H_4$ [cf. Fig. 1(b)], in that both spectra contain sharp peaks at 355 K. The major difference between the two spectra of Fig. 7 is that more hydrogen adatoms are present in spectrum (a), and this is reflected in the much more prominent high temperature shoulder.

Furthermore, more ethylidyne is formed relative to acetylide following the postadsorption of hydrogen, suggesting that this branching ratio is a function of hydrogen coverage. This will be discussed in greater detail in Sect. IV.

To summarize, at all coverages ethylene adsorbs in a di-σ-bonded configuration that decomposes to ethylidyne, acetylide and surface hydrogen above 150 K. The ethylidyne dehydrogenates above 330 K generating additional surface hydrogen. The surface hydrogen desorbs at a temperature that, decreases with increasing coverage following ethylene exposures below 0.6 L, and at 355 K following higher exposures of ethylene. The acetylide decomposes to carbon adatoms and methylidyne near 380 K. Finally, methylidyne decomposes, evolving hydrogen, after annealing above 500 K. For exposures of ethylene below 0.6 L, complete decomposition of methylidyne occurs below 600 K. For higher ethylene exposures, the carbon adatoms (which are present in a higher concentration on the surface) stabilize the methylidyne, such that methylidyne decomposition extends up to 700 K. A plot of ethylene coverage as a function of ethylene exposure as well as a plot of the fractional coverage of ethylene which desorbs molecularly as a function of ethylene exposure are presented in Fig. 8.

## IV. Discussion

As described in Sect. III, ethylene chemisorbs on the Ru(001) surface in a di-σ-bonded configuration (at a surface tempeature below 150 K), and at 80 K condenses into a molecular multilayer that resembles the free ethylene molecule (cf. Table 1). As may be seen in Fig. 2, all five IR active modes of ethylene appear in the EEL spectra of the molecular multilayer. In addition, the carbon-carbon stretching mode, the $CH_2$ rocking mode, and the asymmetric $CH_2$ scissoring mode were resolved in some spectra. These modes are excited via an impact scattering mechanism.

Chemisorbed ethylene, which is stable below 150 K, is di-σ-bonded to the Ru(001) surface, and assignments of the observed vibrational modes are listed in Table 2. This molecularly chemisorbed ethylene on the Ru(001) surface appears to undergo a somewhat greater degree of rehybridization than it does on the Ni(110), Ni(111) and Fe(110) surfaces (**1,3-5**). The differences in frequency between the $CH_2$ twisting and scissoring modes of $C_2H_4$ on Ru(001) and on Fe(111) are not unexpected, since ethylene on Fe(111) is severely tilted with respect to the surface plane such that two hydrogens are

subject to multicenter interactions, which are manifest by a softened ν(CH) mode at 2725 $cm^{-1}$ (2). This distorted geometry downshifts both the $CH_2$ wagging and scissoring modes.

Rather little can be said conclusively concerning the symmetry of the di-σ-bonded ethylene on Ru(001). Application of the dipolar selection rule would imply that the symmetry of the adsorbate-substrate complex is $C_1$, since both the $CH_2$ rocking and twisting modes appear in Fig. 3(a). However, EEL spectra measured off-specular show that these modes are largely impact excited, and therefore, the dipolar selection rule does not apply. Hence, the symmetry of di-σ-bonded ethylene on Ru(001) remains indeterminant. A near-edge X-ray absorption fine structure (NEXAFS) study of ethylene adsorbed on Pt(111) at 90 K by Horsley and co-workers (**55**) has shown that ethylene is symmetrically di-σ-bonded to two platinum atoms with the carbon-carbon bond axis parallel to the surface and a carbon-carbon bond length of 1.49 ± 0.03 angstrom. We expect that di-σ-bonded ethylene would be absorbed similarly on the Ru(001) surface.

Barteau et al. (**22**) have reported a di-σ-bonded ethylene species on Ru(001) with a carbon-carbon stretching mode at 1330 $cm^{-1}$. Our results indicate that their assignments are incorrect, however, for the following reasons. First, they adsorbed ethylene at 170 K, a temperature at which we have shown that di-σ-$C_2H_4$ has begun to decompose, forming a mixed overlayer of $C_2H_4$(a), $CCH_3$(a), CCH(a) and H(a). Thus the modes they identify as resulting from di-σ-$C_2H_4$ are, in fact, a combination of di-σ-$C_2H_4$, $CCH_3$ and CCH modes. The 1330 $cm^{-1}$ loss, which they assign to ν(CC), is actually the $\delta_s(CH_3)$ mode of ethylidyne. This feature becomes more intense with further annealing, which decomposes the $C_2H_4$(a) and produces more ethylidyne. Furthermore, our EEL spectra of $C_2D_4$ on Ru(001) annealed to 170 K show clearly that the previous assignment (**22**) is incorrect, because the 1330 $cm^{-1}$ loss downshifts to 1000 $cm^{-1}$ in the deuterated spectra, and there are no modes of comparable intensity to the 1330 $cm^{-1}$ mode between 1150 and 2190 $cm^{-1}$ in the deuterated spectra. Barteau and coworkers (**22**) did not measure any EEL spectra of deuterated ethylene and thus could not distinguish carbon-carbon vibrational modes from hydrogenic modes. A comparison of the EEL spectra of $C_2H_4$ and $C_2D_4$ is essential to the correct identification of these vibrational modes. As shown in Tables 2, 3 and 4, EEL spectra of $C_2D_4$ on Ru(001) annealed between 110 and 400 K confirm our mode assignments for the

three adspecies, di-σ-bonded ethylene, ethylidyne and acetylide. Finally, we note that a carbon-carbon stretching frequency of 1040 $cm^{-1}$ is more reasonable than one of 1330 $cm^{-1}$ for an $sp^3$ hybridized hydrocarbon species, and it is consistent with the carbon-carbon stretching mode observed at 1135 $cm^{-1}$ for acetylene chemisorbed on Ru(001) (47). It would be expected that ν(CC) of chemisorbed ethylene on Ru(001) would be lower than this value, ruling out the assignment of the 1145 $cm^{-1}$ mode to ν(CC) of $C_2H_4$. Furthermore, the 1145 $cm^{-1}$ mode shifts considerably (to 900 $cm^{-1}$) in the spectra of $C_2D_4$ and certainly cannot be due to ν(CC).

No LEED patterns other than the (1x1) of the substrate were observed for the ethylene overlayer between 90 and 300 K. Hence LEED measurements cannot aid in a determination of the ethylene surface structure or absolute coverages. However, thermal desorption results for $C_2H_4$ and $H_2$ have been used to estimate the ethylene coverage using the known saturation fractional coverage of hydrogen (0.86) (32). The ethylene coverage (excluding the multilayer) is presented as a function of ethylene exposure in Fig. 8(a). From this figure, we see that the saturation (fractional) coverage of chemisorbed ethylene is approximately 0.30. Figure 8(a) was used also to obtain the initial probability of adsorption of ethylene at 100 K, which was found to be unity within the limits of experimental uncertainty. The activation energy of desorption (equal to the heat of adsorption) of di-σ-bonded $C_2H_4$ was estimated from the thermal desorption measurements. Using the method of Redhead (56) and assuming a preexponential factor of $10^{13}$–$10^{14}$ $s^{-1}$, we obtain a value of approximately 11.6 ± 1 kcal/mole. Considering the changes in bond strengths due to rehybridization of the carbon atoms, we have also estimated that the binding energy of di-σ-bonded ethylene is between 105 and 135 kcal/mole. *Thus, the observation of a low heat of adsorption for chemisorbed ethylene on Ru(001) does not imply that the ruthenium-carbon bond is weak.*

When the saturated overlayer of chemisorbed ethylene is annealed to 250 K, approximately 20% of the ethylene desorbs, while the remainder dehydrogenates to ethylidyne, acetylide and surface hydrogen. The stoichiometry of the ethylidyne formed by ethylene decomposition on Pt(111) was confirmed by hydrogen thermal desorption spectra in which approximately 25% of the total hydrogen desorbed from the surface at 300 K, the same temperature at which ethylidyne was shown to form via EELS

(57). Unfortunately, the hydrogen from ethylidyne formation remains adsorbed on the Ru(001) surface, ultimately desorbing with hydrogen from ethylidyne decomposition. Hence, we are unable to confirm *directly* the stoichiometry of the ethylene decomposition products from hydrogen thermal desorption spectra. The ethylidyne on Ru(001) begins to decompose at approximately 330 K, whereas the ethylidyne formed on Pt(111) is stable to 400 K (7). The reduced stability of ethylidyne on Ru(001) is undoubtedly due to the stronger metal-hydrogen and metal-carbon bonds formed on the ruthenium surface, which makes the decomposition of ethylidyne via metal-hydrogen and metal-carbon bond formation more favorable both thermodynamically and kinetically.

The identification of ethylidyne and acetylide as the decomposition products of di-σ-bonded ethylene on Ru(001) can be contrasted to the results of Barteau et al. (22), who only identified ethylidyne. We also note that Barteau assigned the $\rho(CH_3)$ mode of ethylidyne to a loss at 870 $cm^{-1}$. We observed no such mode in our EEL spectra and cannot account for this discrepancy, but merely mention that our assignment of the 1000 $cm^{-1}$ loss to $\rho(CH_3)$ and the observed isotopic shift to 800 $cm^{-1}$ for $\rho(CD_3)$ are in agreement with the frequencies observed for other ethylidyne species.

Our EEL spectra of the thermal evolution of ethylidyne and acetylide on Ru(001) and complementary thermal desorption spectra show that virtually all of the ethylidyne dehydrogenates to surface carbon below 360 K leaving only CCH(a) and H(a) on the surface. Thus, an EEL spectrum measured after annealing to 360 K [Fig. 5(b)] contains only the loss features of acetylide, permitting unambiguous identification of this intermediate. The observation of the carbon-hydrogen bending mode of acetylide at 280 K, prior to the onset of ethylidyne dehydrogenation implies that acetylide is not a decomposition product of ethylidyne. Further proof of this assertion comes from CO and $C_2H_4$ coadsorption experiments (58).

By analogy to all relevant organometallic ethylidyne complexes synthesized to date, it is almost certain that the carbon-carbon bond axis of ethylidyne on Ru(001) is very nearly perpendicular to the surface. This configuration is also supported by the strong intensity of the ν(CC) mode of ethylidyne at 1140 $cm^{-1}$ in the EEL spectrum of Fig. 5(a) and its predominantly dipolar character. Furthermore it is very probable that ethylidyne is bonded to the Ru(001) surface in a threefold hollow site both by anal-

ogy to the trimetal $\mu_3$-$CCH_3$ complexes (**45-46**) and by the observation of ethylidyne only on hexagonal surfaces (**4,7,16**). A further indication of this bonding of ethylidyne on Ru(001) is provided by NEXAFS results of ethylidyne on Pt(111) (**55**), which showed that the ethylidyne is symmetrically bonded to three platinum atoms with the carbon-carbon bond axis essentially perpendicular to the surface.

Next, we consider the effects of simultaneous ethylidyne decomposition and hydrogen desorption on the observed shape of the hydrogen thermal desorption peak. When the Ru(001) surface on which ethylene is adsorbed (exposures above 0.6 L) is annealed to 300 K, hydrogen desorption is observed. In these measurements, hydrogen desorbs at this low temperature due to its higher surface coverage. As the overlayer is annealed to 330 K, additional hydrogen desorbs, and ethylidyne begins to dehydrogenate, replenishing the supply of surface hydrogen. Thus, adjacent to the decomposing ethylidyne, an area of high local density of hydrogen adatoms is formed, which accelerates the rate of desorption of hydrogen and gives the hydrogen thermal desorption peak a sharp leading edge. Comparing Figs. 6(a) and (b), we see that the high temperature shoulder on the 355 K hydrogen thermal desorption peak results from residual surface hydrogen.

For these higher exposures of ethylene, the temperature of the hydrogen thermal desorption peak remains at 355 K independent of coverage. Ethylidyne decomposition dictates this hydrogen desorption since the desorption of hydrogen occurs at a lower temperature in a broader peak at higher hydrogen adatom coverages (from the adsorption of hydrogen). The adsorption and decomposition of ethylene at high coverages is otherwise identical to that for lower coverages with three exceptions. First, a multilayer of ethylene forms which desorbs at 110 K. Second, some of the di-$\sigma$-bonded ethylene desorbs [cf. Fig. 8(b)]. Finally, the ratio of ethylidyne to acetylide that is formed is increased. Recall that annealing to 400 K the Ru(001) surface on which ethylene is adsorbed not only decomposes the ethylidyne, but also causes cleavage of the carbon-carbon bond of the acetylide, leaving methylidyne and carbon adatoms. The high temperature tail of the hydrogen thermal desorption peak after ethylene adsorption corresponds to dehydrogenation of methylidyne. Consequently, the ratio of ethylidyne to acetylide that is formed from ethylene can be obtained from the relative areas of the 355 K peak and the tail. The acetylide coverage is equal to the coverage of the hydrogen desorbing in the high temperature tail.

The ethylidyne coverage is obtained by subtracting three times the acetylide coverage from the coverage of hydrogen desorbing in the 355 K hydrogen thermal desorption peak and its high temperature shoulder, and dividing this number by four. We find that a saturation exposure of ethylene decomposes to ethylidyne and acetylide in the approximate ratio of 60:40, whereas a lower exposure, 0.4 L of $C_2H_4$, yields a ratio of 50:50. Consequently, ethylidyne formation is favored at higher surface coverages. This result may be interpreted in terms of the number of hydrogen adatoms generated by ethylene decomposition to ethylidyne (one per $C_2H_4$) versus acetylide (three per $C_2H_4$). At higher surface coverages more threefold sites, required for hydrogen adatoms, will be either occupied or blocked. Also, the coverage of hydrogen will be greater as ethylene dehydrogenation proceeds. Thus, the decomposition product that requires fewer vacant surface sites for formation and is composed of more hydrogen atoms, ethylidyne, is favored. The dependence of the ratio of ethylidyne to acetylide formed upon the hydrogen coverage has also been confirmed by hydrogen thermal desorption experiments measured following a saturation ethylene exposure at 350 K. At this temperature, the hydrogen adatom concentration on the surface is reduced. This lower hydrogen coverage caused the acetylide coverage to increase by approximately 50% compared to the coverage of acetylide formed following a saturation ethylene exposure at 80 K, and annealing to 350 K, as judged by the relative intensities of the high temperature tails in the hydrogen thermal desorption spectra.

Finally, we discuss briefly the mechanism of dehydrogenation of ethylidyne. The EEL spectra measured immediately following the decomposition of ethylidyne show no enhancement of the carbon-hydrogen bending mode of acetylide and provide no evidence for methylidyne formation. Thus, we can rule out both acetylide and methylidyne formation from ethylidyne decomposition and conclude that ethylidyne must dehydrogenate completely to either carbon-carbon dimers [with $\nu$(CC) at 1100-1600 $cm^{-1}$ in the EEL spectra of Figs. 5(b) and (c)], and hydrogen or carbon adatoms and hydrogen. The observed complete dehydrogenation of ethylidyne at a temperature at which acetylide is stable on the surface is quite important. It implies that the reaction coordinate that results in the loss of the first hydrogen atom from ethylidyne is not the one that would lead to the stable surface acetylide. A plausible but most certainly speculative scenario for the dehydrogenation of ethylidyne would involve interac-

tion with an adjacent threefold hollow site, whereas the stable acetylide (almost certainly not oriented parallel to the surface plane) has a structure that is rotated 60° with respect to this reaction coordinate.

## V. Conclusions

Ethylene chemisorbs on Ru(001) in a di-σ-bonded configuration at temperatures below approximately 150 K. Upon heating, competing molecular desorption, dehydrogenation to acetylide and dehydrogenation to ethylidyne occur.The resulting thermal decomposition scheme for a saturation coverage of chemisorbed ethylene ($\theta$ = 0.30) may be depicted as follows:

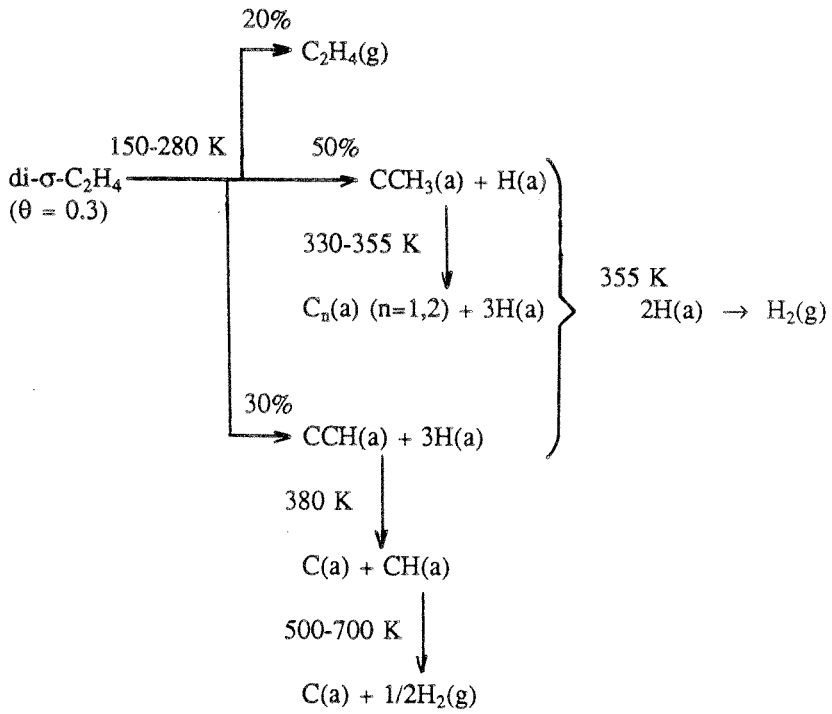


The ethylidyne formed on Ru(001) is less stable than on other Group VIII metal surfaces; e.g., it begins to decompose to carbon and hydrogen adatoms near 330 K compared to the decomposition temperature of approximately 400 K observed on Pt(111) and Rh(111). Carbon-carbon bond cleavage of the acetylide occurs at 380 K, producing surface carbon and methylidyne of which the latter dehydrogenates between 500 and 700 K. Following ethylene exposures exceeding 0.6 L, desorption of hydrogen occurs in a sharp peak with a maximum rate of desorption at 355 K, which is limited by ethylidyne decomposition, in a shoulder at approximately 400 K on this peak due to desorption-limited hydrogen, and also in a high temperature tail due to methylidyne decomposition. Hydrogen desorption following

lower ethylene exposures becomes desorption-limited, except for the hydrogen that is evolved from the decomposition of methylidyne.

To summarize, ethylene adsorbed on Ru(001) produces both ethylidyne and the more extensively dehydrogenated acetylide. Thus, the behavior of ethylene adsorbed on Ru(001) appears to be intermediate between the more complete dehydrogenation observed on Ni(111) and Co(001) and the exclusive formation of the less dehydrogenated stable ethylidyne species found on the hexagonal surfaces of rhodium, palladium, and platinum.

**Acknowledgments**

This work was supported by the National Science Foundation under Grant No. CHE-8516615. Acknowledgment is also made to the donors of the Petroleum Research Fund, administered by the American Chemical Society, for the partial support of this research under Grant No. 15454-AC5.

**References**


1. Erley, W.; Baro, A.M.; McBreen, P.; Ibach, H., *Surface Sci.* **1982**, 120, 273.
2. Seip, U.; Tsai, M.-C.; Küppers, J.; Ertl, G., *Surface Sci.* **1984**, 147, 65.
3. Stroscio, J.A.; Bare, S.R.; Ho, W., *Surface Sci.* **1984**, 148, 499.
4. Lehwald, S.; Ibach, H., *Surface Sci.* **1979**, 89, 425.
5. Carr, R.G.; Sham, T.K.; Eberhardt, W.E., *Chem. Phys. Letters* **1985**, 113, 63.
6. Demuth, J.E., *Surface Sci.* **1979**, 84 315.
7. Steininger, H.; Ibach, H.; Lehwald, S., *Surface Sci.* **1982**, 117, 685.
8. Albert, M.R.; Sneddon, L.G.; Plummer, E.W., *Surface Sci.* **1984**, 147, 127.
9. Gates, J.A.; Kesmodel, L.L., *Surface Sci.* **1982**, 120, L461.
10. Gates, J.A.; Kesmodel, L.L., *Surface Sci.* **1983**, 124, 68.
11. Tysoe, W.T.; Nyberg, G.L.; Lambert, R.M., *J. Phys. Chem.* **1984**, 88, 1960.
12. Ratajczykowa, I.; Szymerska, I., *Chem. Phys. Letters* **1983**, 96, 243.
13. Kesmodel, L.L.; Gates, J.A., *Surface Sci.* **1981**, 111, L747.
14. Stuve, E.M.; Madix, R.J., *J. Phys. Chem.* **1985**, 89, 105.
15. Stuve, E.M.; Madix, R.J.; Brundle, C.R., *Surface Sci.* **1985**, 152/153, 532.
16. Dubois, L.H.; Castner, D.G.; Somorjai, G.A., *J. Chem. Phys.* **1980**, 72, 5234.
17. Gupta, N.M.; Kamble, V.S.; Iyer, R.M., *J. Catal.* **1984**, 88, 457.
18. Chesters, M.A.; McDougall, G.S.; Pemble, M.E.; Sheppard, N., *Appl. Surface Sci.* **1985**, 22/23, 369.
19. Boudart, M.; McDonald, M.A., *J. Phys. Chem.* **1984**, 88, 2185.
20. Henrici-Olive´, G.; Olive´, S., *Angew. Chem. Int. Ed. Engl.* **1976**, 15, 136.
21. Dixit, R.S., Tavlarides, L.L., *Ind. Eng. Chem. Process Des. Dev.* **1983**, 22, 1.
22. Barteau, M.A.; Broughton, J. Q.; Menzel, D., *Appl. Surface Sci.* **1984**, 19, 92.

23. Ibach, H. *Proceedings of the International Conference on Vibrations in Adsorbed Layers*, Julich, **1978**, 64.

24. The Pt(100) surface reconstructs to a slightly buckled, close-packed (5x20) superstructure (25).

25. Heilmann, P.; Heinz, K.; Müller, K., *Surface Sci.* **1979**, 83, 487.

26. Feulner, P.; Menzel, D., *J. Vac. Sci. Technol.* **1980**, 17, 662.

27. Thomas, G.E.; Weinberg, W.H., *Phys. Rev. Letters* **1978**, 41, 1181.

28. Thomas, G.E.; Weinberg, W.H., *Rev. Sci. Instrum.* **1979**, 50, 497.

29. Williams, E.D.; Weinberg, W.H., *Surface Sci.* **1979**, 82, 93.

30. Williams, E.D.; Weinberg, W.H., *J. Vac. Sci. Technol.* **1982**, 20, 534.

31. All exposures reported are uncorrected for the sensitivity of the ion gauge to the various gases.

32. Shimizu, H.; Christmann, K.; Ertl, G., *J. Catal.* **1980**, 61, 412.

33. Shimanouchi, T., *NSRDS-NBS Publication 39*, **1972**, 74.

34. Brecher, C.; Halford, R.S., *J. Chem. Phys.* **1961**, 35, 1109.

35. Hiraishi, J., *Spectrochim. Acta*, Part A **1969**, 25, 749.

36. Ozin, G.A., *J. Am. Chem. Soc.* **1978**, 100, 4750.

37. George, P.M.; Avery, N.R.; Weinberg, W.H.; Tebbe, F.N., *J. Am. Chem. Soc.* **1983**, 105, 1393.

38. EEL spectra of 2.5 L of $H_2CN_2$ dosed at 80 K, annealed to 192-316 K and cooled to 80 K prior to measurement.

39. Fox, D.J.; Schaefer, H.F., *J. Chem. Phys.* **1983**, 78, 328.

40. Theopold, K.H.; Bergman, R.G., *J. Am. Chem. Soc.* **1981**, 103, 2489.

41. Oxton, I.A.; Powell, D.B.; Sheppard, N.; Burgess, K.; Johnson, B.F.G.; Lewis, J., *J. Chem. Soc., Chem. Commun.* **1982**, 719.

42. McBreen, P.H.; Erley, W.; Ibach, H., *Surface Sci.* **1984**, 148, 292.

43. Chang, S.-C., Kafafi, Z.H.; Hauge, R.H.; Billups, W.E.; Margave, J.L., *J. Am. Chem. Soc.* **1985**, 107, 1447.

44. Barteau, M.A.; Broughton, J.Q.; Menzel, D., *Surface Sci.* **1983**, 133, 443.

45. Skinner, P.; Howard, M.W.; Oxton, I.A.; Kettle, S.F.A.; Powell, D.B.; Sheppard, N., *J. Chem. Soc., Faraday Trans. 2* **1981**, 77, 1203.

46. Sheldrick, G.M.; Yesinowski, J.P., *J. Chem. Soc. Dalton Trans.* **1975**, 873.

47. Parmeter, J.E.; Hills, M.M.; Weinberg, W.H., *J. Am. Chem. Soc. (submitted).*

48. Kesmodel, L.L., *J. Vac. Sci. Technol. A* **1984**, 2, 1083.

49. Kesmodel, L.L., Wadill, G.D.; Gates, J.A., *Surface Sci.* **1984**, 138, 464.

50. Demuth, J.E.; Ibach, H., *Surface Sci.* **1978**, 78, L238.

51. Erley, W.; McBreen, P.H.; Ibach, H., *J. Catal.* **1983**, 84, 229.

52. Oxton, I.A., *Spectochim. Acta* **1982**, 38A, 181.

53. Howard, M.W.; Kettle, S.F.; Oxton, I.A.; Powell, D.B.; Sheppard, N.; Skinner, P., *J. Chem. Soc., Faraday Trans. 2* **1981**, 77, 397.

54. EEL spectra of this adlayer support the presence of only carbon and hydrogen adatoms; in particular, no modes of methylidyne are observed.

55. Horsley, J.A.; Stöhr, J.; Koestner, R.J., *J. Chem. Phys.* **1985**, 83, 3146.

56. Redhead, P.A., *Vacuum* **1962**, 203.

57. Ibach, H.; Mills, D.L. *Electron Energy Loss Spectroscopy and Surface Vibrations*, Academic Press, N.Y., 1982.

58. Hills, M. M.; Parmeter, J. E.; Weinberg, W. H. (in preparation).

**Table 1.** Comparison of vibrational frequencies of multilayer $C_2H_4$ adsorbed on Ru(001) at 80 K with $C_2H_4$ (g), $C_2H_4$ ($l$) and $C_2H_4$ (s).

| No./Repr. | Mode | $C_2H_4$(g) (33) Raman | $C_2H_4$(g) (33) IR | $C_2H_4$($l$) (34) Raman | $C_2H_4$($l$) (34) IR | $C_2H_4$(s) (34) IR | Multilayer $C_2H_4$ on Ru(001) |
|---|---|---|---|---|---|---|---|
| $\nu_1$ $A_g$ | $\nu_s(CH_2)$ | 3026 | f | 3019 | 3016 | | 3000 |
| $\nu_{11}$ $B_{2u}$ | | f | 2989 | | 2983 | 2973 | |
| $\nu_5$ $B_{1g}$ | $\nu_a(CH_2)$ | 3103 | f | 3075 | | | 3095 |
| $\nu_9$ $B_{2u}$ | | f | 3105 | | 3085 | 3075 | |
| $\nu_2$ $A_g$ | $\nu$(CC) | 1623 | f | 1621 | 1620 | 1616 | 1630 |
| $\nu_3$ $A_g$ | $CH_2$ scis. | 1342 | f | 1340 | 1339 | 1336 | 1350 |
| $\nu_{12}$ $B_{3u}$ | | f | 1444 | | 1437 | 1438 | 1460 |
| $\nu_4$ $A_u$ | $CH_2$ twist | f | f | | ~1010 | | n.r. |
| $\nu_6$ $B_{1g}$ | $CH_2$ rock | | f | 1236 | 1239 | | |
| $\nu_{10}$ $B_{2u}$ | | f | 810 | | 828 | 827 | 860 |
| $\nu_7$ $B_{1u}$ | $CH_2$ wag | f | 949 | | 960 | 970 | 970 |
| $\nu_8$ $B_{2g}$ | | 950 | f | 943 | | | |
| | $\nu_s$(RuC) | | | | | | 440 |

| No./Repr. | Mode | $C_2D_4$(g) (33) | Multilayer $C_2D_4$ on Ru(001) |
|---|---|---|---|
| $\nu_1$ $A_g$ | $\nu_s(CD_2)$ | 2251 | 2310 |
| $\nu_{11}$ $B_{2u}$ | | 2200 | |
| $\nu_5$ $B_{1g}$ | $\nu_a(CD_2)$ | 2304 | n.r. |
| $\nu_8$ $B_{2u}$ | | 2345 | |
| $\nu_2$ $A_g$ | $\nu$(CC) | 1515 | 1550 |
| $\nu_3$ $A_g$ | $CD_2$ scis. | 981 | 1015 |
| $\nu_{12}$ $B_{3u}$ | | 1078 | 1175 |
| $\nu_4$ $A_u$ | $CD_2$ twist | 728 | n.r. |
| $\nu_6$ $B_{1g}$ | $CD_2$ rock | 1009 | n.r. |
| $\nu_{10}$ $B_{2u}$ | | 586 | |
| $\nu_7$ $B_{1u}$ | $CD_2$ wag | 720 | 735 |
| $\nu_8$ $B_{2g}$ | | 780 | |
| | $\nu_s$(RuC) | | 425 |

n.r. = not resolved
f = forbidden

**Table 2.** Comparison of vibrational frequencies of di-σ-bonded $C_2H_4$ on Ru(001) at 130 K with other chemisorbed ethylene species, gaseous ethylene compounds, organometallic ethylene compounds, and a surface methylene species.

| Mode $C_2H_4$ (or $CH_2$) | di-σ-$C_2H_4$ on | | | | | | $C_2H_4$(g) | gauche $C_2H_4Br_2$(g) | $K[PtCl_3(C_2H_4)]H_2O$ | $Ni_2(C_2H_4)$ | $CH_2$ on Ru(001) |
|---|---|---|---|---|---|---|---|---|---|---|---|
| | Ru(001) | Ni(110) (3) | Ni(111) (4) | Fe(110) (1) | Fe(111) (2) | Pt(111) (7) | (33) | (33) | (35) | (36) | (38) |
| $\nu_s$(CM) | 460 | 420 | 450 | 480 | 580 | 470 | | | | 376 | n.r. |
| $\nu_a$(CM) | n.r. | n.r. | 610 | 410 | 450 | 560 | | | | | n.r. |
| $CH_2$ rock | 775 | 715 | 720 | 720 | n.r. | 660 | 826 | 848 | 841 | 910 | 785 |
| $CH_2$ twist | 900 | 850 | 880 | 915 | 870 | 790 | f | 1104 | | | |
| $CH_2$ wag | 1145 | 1145 | 1110 | 1105 | n.r. | 980 | 949 | 1278 | 975 | 1180 | 1155 |
| $CH_2$ scissors | 1450 | 1435 | 1430 | 1410 | 1385 | 1430 | 1444 | 1420 | 1515 | 1208 | |
| $\nu_s(CH_2)$ | 2940 | 2970 | 2930 | 2960 | 2980 | 2980 | 2989 | 2953 | 3013 | 2880 | 2965 |
| $\nu_a(CH_2)$ | 3050 | n.r. | n.r. | n.r. | n.r. | 3000 | 3096 | 3005 | 3075 | 2908 | n.r. |
| ν(CC) | 1040 | n.r. | 1200 | 1250 | 1115 | 1060 | 1623 | 1019 | 1243 | 1488 | |
| Mode $C_2D_4$ | | | | | | | | | | | |
| $\nu_s$(CM) | 420 | 390 | 420 | 440 | | 450 | | | | | |
| $\nu_a$(CM) | n.r. | n.r. | 590 | n.r. | | n.r. | | | | | |
| $CD_2$ rock | n.r. | 615 | 650 | 635/540 | | n.r. | 586 | 712 | | | |
| $CD_2$ twist | 700 | 725 | 740 | 700 | | 600 | f | 791 | | | |
| $CD_2$ wag | 900 | 925 | 870 | 850 | | 740 | 720 | 947 | | | |
| $CD_2$ scissors | 1210 | 1235 | 1200 | 1040 | | 1150 | 1078 | 1141 | | | |
| $\nu_s(CD_2)$ | 2210 | 2170 | 2170 | 2175 | | 2150 | 2251 | 2174 | | | |
| $\nu_a(CD_2)$ | 2295 | 2290 | 2270 | n.r. | | 2250 | 2304 | 2271 | | | |
| ν(CC) | n.r. | n.r. | n.r. | 1160 | | 900 | 1515 | 1014 | | | |

f = forbidden
n.r. = not resolved

**Table 3.** Comparison of vibrational frequencies of ethylidyne.

| Mode | $CCH_3$ on Ru(001) at 280K | $CCH_3$ on Pd(111) at 300K (**4**) | $CCH_3$ on Pt(111) at 300K (**7**) | $CCH_3$ on Rh(111) at 300K (**16**) | $(CO)_9Co_3(\mu_3\text{-}CCH_3)$ (**45**) |
|---|---|---|---|---|---|
| $\nu_s(CM)$ $A_1$ | 480* | 409 | 435vs | 450 | 401 |
| $\nu_a(CM)$ E | n.r. | n.r. | 600w | n.r. | 555 |
| $\rho(CH_3)$ E | 1000 | n.r. | 980sh | n.r. | 1004 |
| $\nu(CC)$ $A_1$ | 1140 | 1080s | 1130vs | 1130 | 1163 |
| $\delta_s(CH_3)$ $A_1$ | 1370 | 1334vs | 1355vs | 1350 | 1356 |
| $\delta_a(CH_3)$ E | 1450 | 1400 | 1420sh | n.r. | 1420 |
| $\nu_s(CH_3)$ $A_1$ | 2945 | 2900m | 2920 | 2900 | 2888 |
| $\nu_a(CH_3)$ E | 3045 | n.r. | 3050 | 3000 | 2930 |
| Deuterated Species | | | | | |
| $\nu_s(CM)$ $A_1$ | 480 | n.r. | 410 | | 393 |
| $\nu_a(CM)$ E | n.r. | n.r. | ~600 | | 536 |
| $\rho(CD_3)$ E | 800 | n.r. | 790 | | 828 |
| $\nu(CC)$ $A_1$ | 1150 | 1120 | 1160 | | 1182 |
| $\delta_s(CD_3)$ $A_1$ | 1000 | n.r. | 990 | | 1002 |
| $\delta_a(CD_3)$ E | n.r. | n.r. | 1030 | | 1031 |
| $\nu_s(CD_3)$ $A_1$ | 2190 | 2181 | 2080 | | n.r. |
| $\nu_a(CD_3)$ E | 2280 | n.r. | 2220 | | 2192 |

n.r. = not resolved. *Identified from spectra similar to that of Fig. 5(a), but without CO contamination.

**Table 4.** Comparison of vibrational frequencies of acetylide.

| Mode | CCH on Ru(001) at 360 K | CCH on Pd(100) at 400 K (**48,49**) |
|---|---|---|
| $\nu_s$(CM) | 435 | n.r. |
| $\nu_a$(CM) | n.r. | n.r. |
| $\delta$(CH) | 750 | 750 |
| $\nu$(CH) | 2960 | 3000 |
| $\nu$(CC) | 1290 | 1340 |
| Mode | CCD | CCD |
| $\nu_s$(CM) | n.r. | n.r. |
| $\nu_a$(CM) | n.r. | n.r. |
| $\delta$(CD) | 550 | 540 |
| $\nu$(CD) | 2210 | 2220 |
| $\nu$(CC) | 1260 | 1340 |

n.r. = not resolved

**Table 5.** Comparison of vibrational frequencies of surface methylidyne species to those of $(CO)_4Co_3(\mu_3\text{-}CH)$ and $(CO)_9H_3Ru_3(\mu_3\text{-}CH)$.

| Mode | CH on Ru(001) | CH on Fe(111) (2) | CH on Fe(110) (1,50) | CH on Ni(111) (4,51) | CH on Pd(111) (9,10) | $(CO)_9H_3Ru_3(\mu_3\text{-}CH)$ (52) | $(CO)_4Co_3(\mu_3\text{-}CH)$ (53) |
|---|---|---|---|---|---|---|---|
| $\nu$(CH) | 3010 | 3015 | 3050 | 2980 | 3002 | 2988 | 3041 |
| $\delta$(MCH) (e) | 810 | 795 | 880 | 790 | 762 | 894 | 850 |
| $\nu_s$(MC) ($a_1$) | 465 | | | | | 670 | 715 |
| $\nu_a$(MC) (e) | n.r. | | | | | 424 | 417 |
| $\nu$(CD) | 2250 | | | | | | 2268 |
| $\delta$(MCD) (e) | 615 | | | | | | 680 |
| $\nu_s$(MC) ($a_1$) | 415 | | | | | | 696 |
| $\nu_a$(MC) (e) | n.r. | | | | | | 410 |

**Figure Captions**

Figure 1. Thermal desorption spectra after $C_2H_4$ adsorption on Ru(001) at 90 K. (a) $C_2H_4$ and (b) $H_2$ desorption following a 1 L exposure; and (c) $H_2$ desorption following a 0.2 L exposure.

Figure 2. EEL spectra of molecular multilayers of ethylene on Ru(001). (a) 4 L of $C_2H_4$ at 80 K, and (b) 3 L of $C_2D_4$ at 80 K.

Figure 3. EEL spectra of di-σ-bonded ethylene on Ru(001). (a) 4 L of $C_2H_4$ annealed to 139 K, and (b) 3 L of $C_2D_4$ annealed to 123 K.

Figure 4. Coadsorption of $C_2H_4$ and $C_2D_4$. Relative coverages of $C_2H_4$, $C_2H_3D$, $C_2H_2D_2$, $C_2HD_3$ and $C_2D_4$ from thermal desorption spectra. (a) 0.6 L exposure of $C_2H_4$ followed by 3 L of $C_2D_4$ at 110 K; and (b) 1 L exposure of $C_2H_4$ followed by 3 L of $C_2D_4$ at 110 K.

Figure 5. EEL spectra of 4 L of $C_2H_4$ adsorbed on Ru(001) at 80 K and annealed to (a) 280 K, (b) 360 K, and (c) 500 K. Spectrum (a) exhibits the modes of both ethylidyne and acetylide. Spectrum (b) is characteristic of acetylide. Spectrum (c) corresponds to methylidyne.

Figure 6. Hydrogen thermal desorption following: (a) exposure of 5 L of $C_2H_4$, and (b) exposure of 5 L of $C_2H_4$ followed by annealing to 800 K, cooling to 90 K and exposure to 30 L of $H_2$.

Figure 7. Hydrogen thermal desorption following exposures of: (a) 0.4 L of $C_2H_4$ followed by 2 L of $H_2$, and (b) 0.4 L of $C_2H_4$ at 100 K.

Figure 8. (a) Fractional coverage of chemisorbed $C_2H_4$ as a function of exposure, and (b) fractional coverage of chemisorbed $C_2H_4$ that desorbs molecularly as a function of exposure. The temperature of adsorption is 80 K.

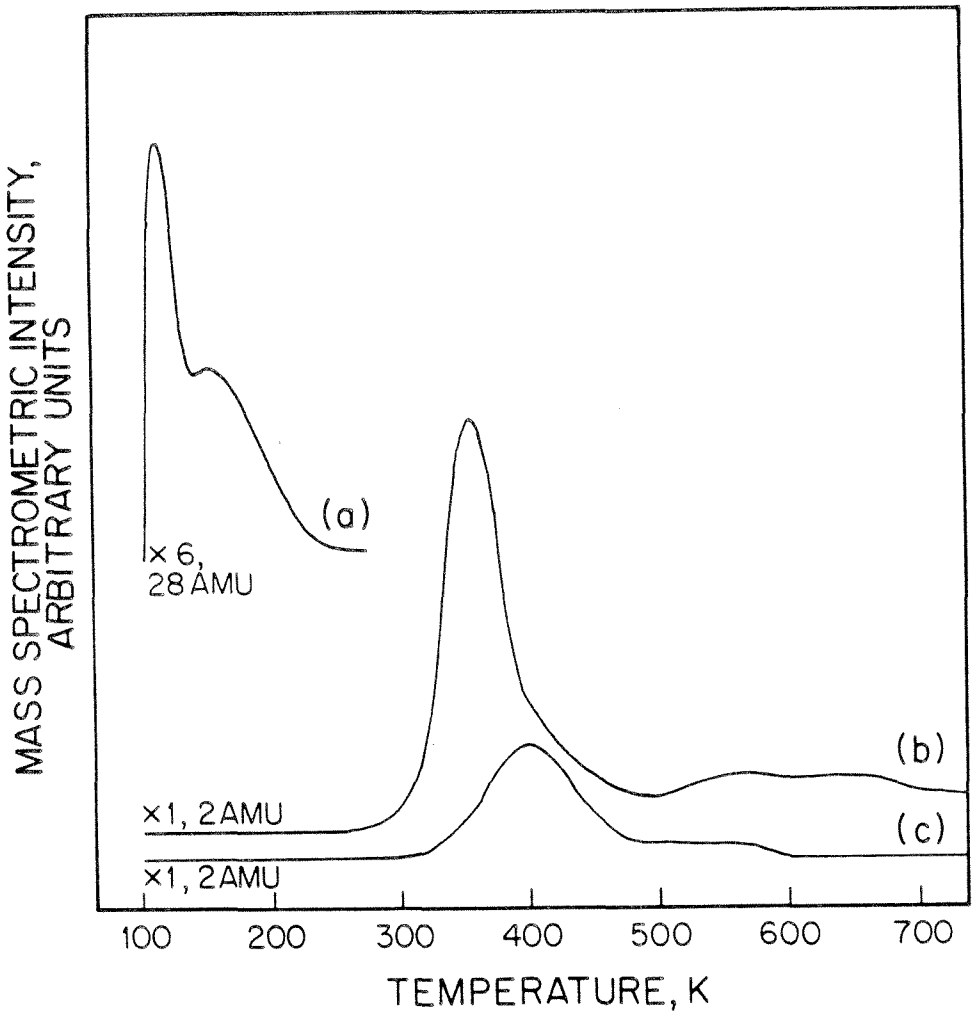
MASS SPECTROMETRIC INTENSITY, ARBITRARY UNITS
(a)
×6, 28 AMU
(b)
×1, 2 AMU
(c)
×1, 2 AMU
100
200
300
400
500
600
700
TEMPERATURE, K

Figure 1

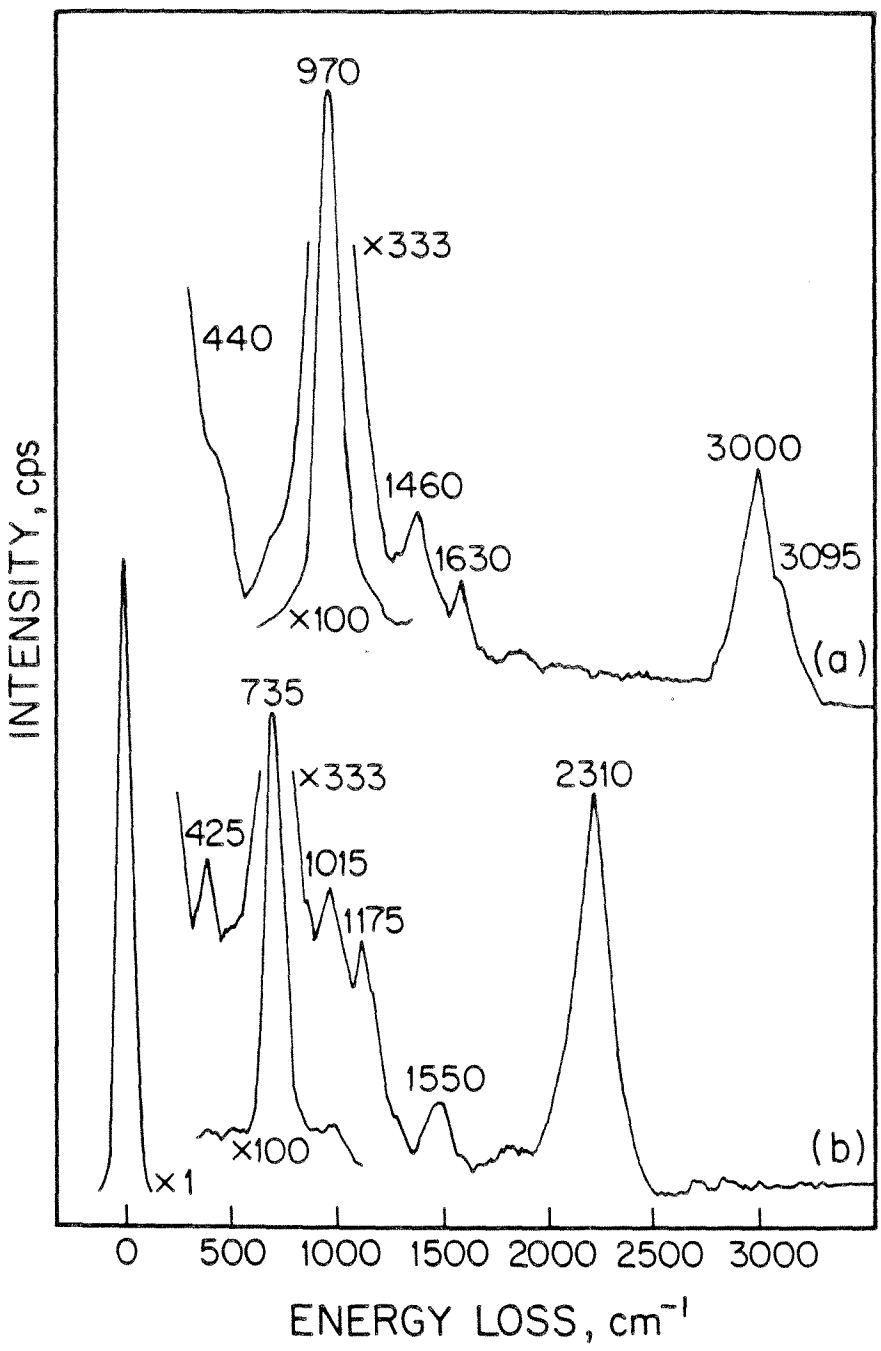
970
×333
440
3000
1460
1630
3095
×100
(a)
735
×333
2310
425
1015
1175
1550
×100
(b)
×1
INTENSITY, cps
0
500
1000
1500
2000
2500
3000
ENERGY LOSS, cm⁻¹

Figure 2

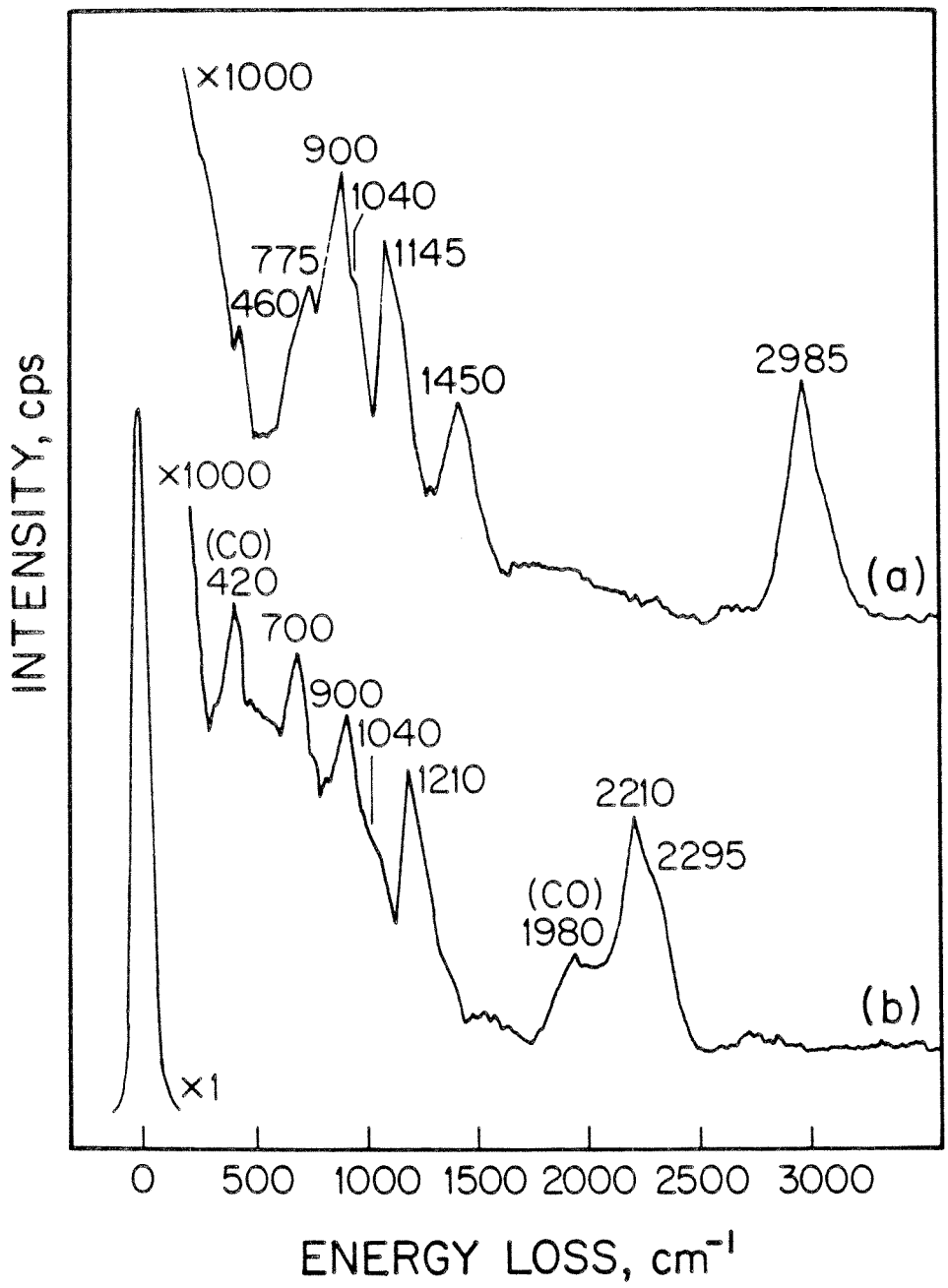
×1000
900
1040
775
1145
460
1450
2985
×1000
(CO)
420
700
900
1040
1210
2210
2295
(CO)
1980
(a)
(b)
×1
INTENSITY, cps
0
500
1000
1500
2000
2500
3000
ENERGY LOSS, cm⁻¹

Figure 3

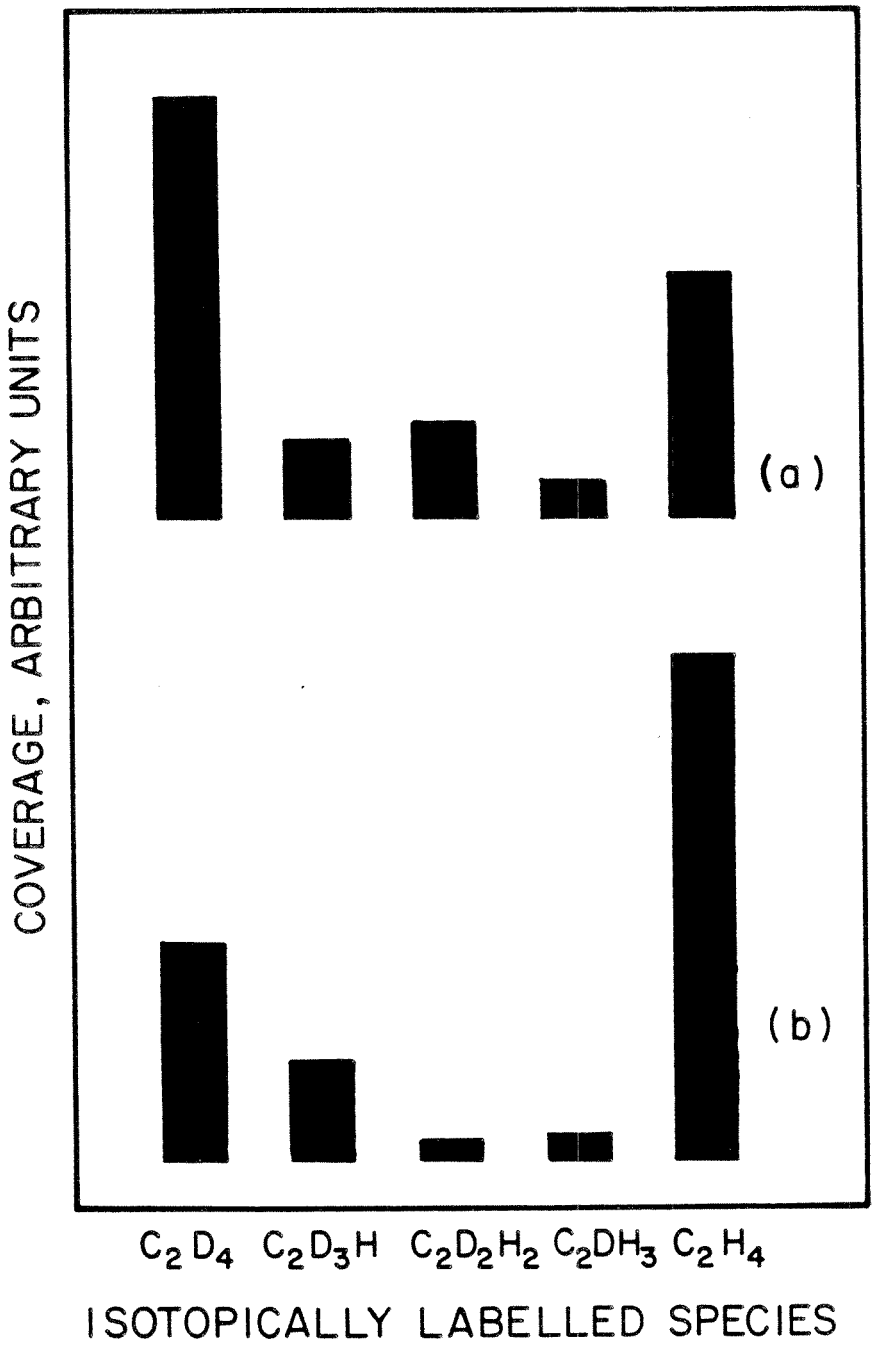
COVERAGE, ARBITRARY UNITS
(a)
(b)
$C_2D_4$ $C_2D_3H$ $C_2D_2H_2$ $C_2DH_3$ $C_2H_4$
ISOTOPICALLY LABELLED SPECIES

Figure 4

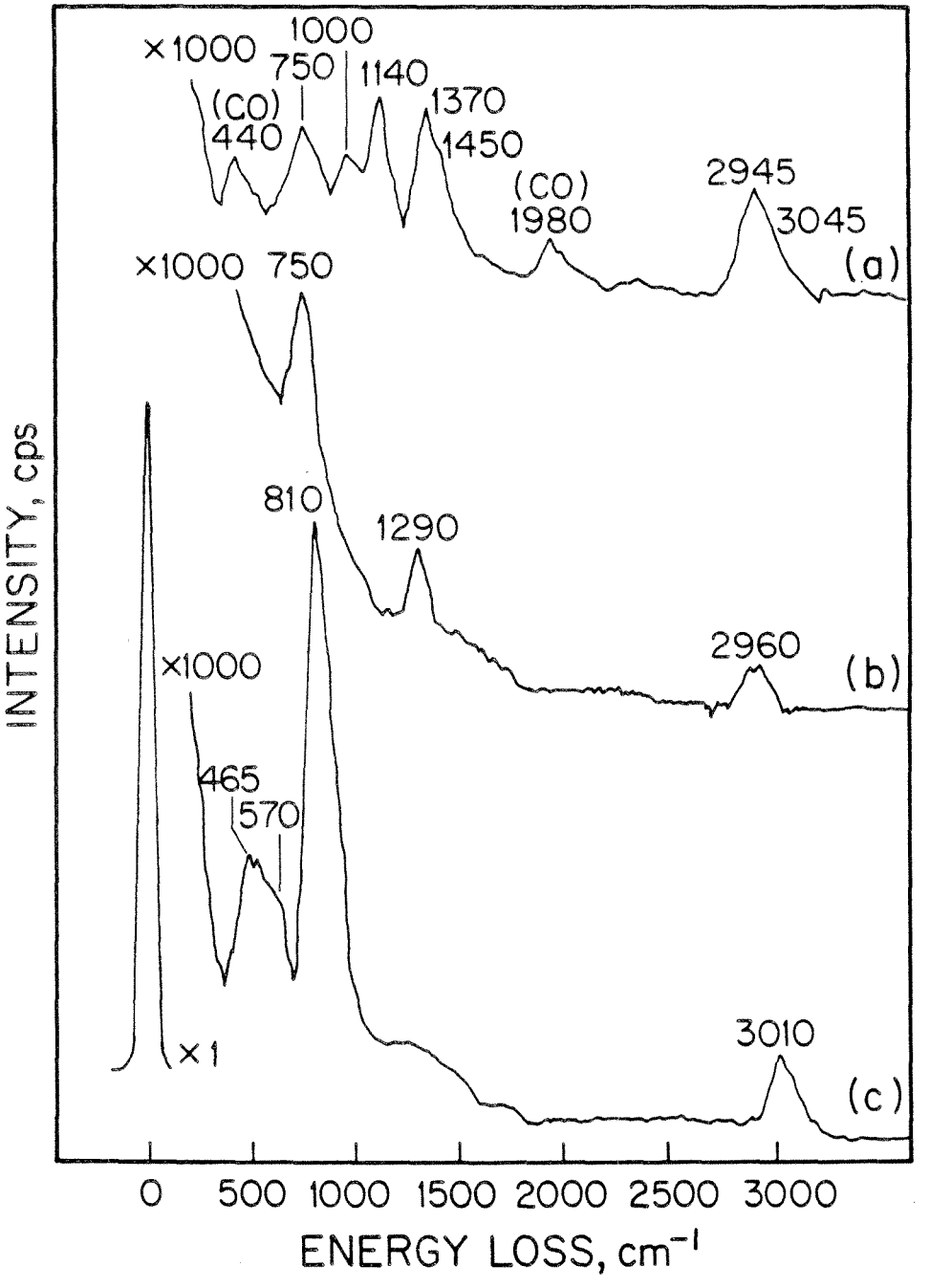
×1000
1000
750
1140
(CO)
440
1370
1450
(CO)
1980
2945
3045
(a)
×1000
750
810
1290
2960
(b)
×1000
465
570
×1
3010
(c)
INTENSITY, cps
0
500
1000
1500
2000
2500
3000
ENERGY LOSS, cm⁻¹

Figure 5

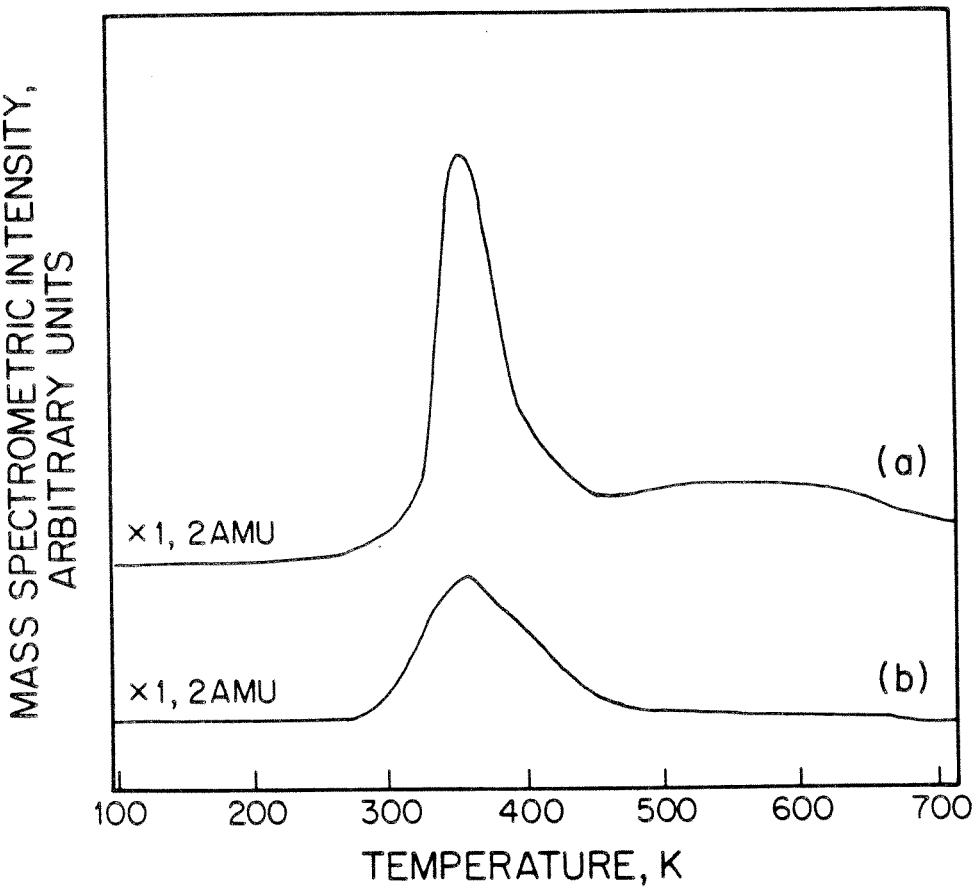
MASS SPECTROMETRIC INTENSITY, ARBITRARY UNITS
×1, 2AMU
(a)
×1, 2AMU
(b)
100
200
300
400
500
600
700
TEMPERATURE, K

Figure 6

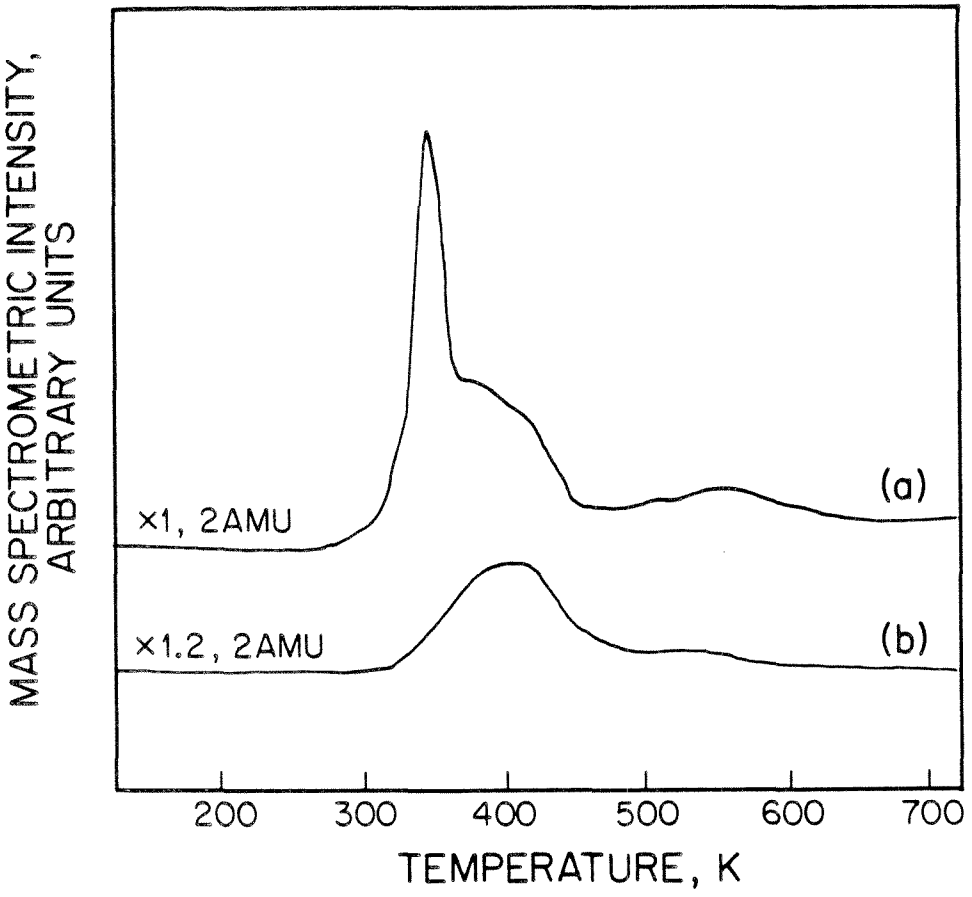
MASS SPECTROMETRIC INTENSITY, ARBITRARY UNITS
×1, 2AMU
(a)
×1.2, 2AMU
(b)
200
300
400
500
600
700
TEMPERATURE, K

Figure 7

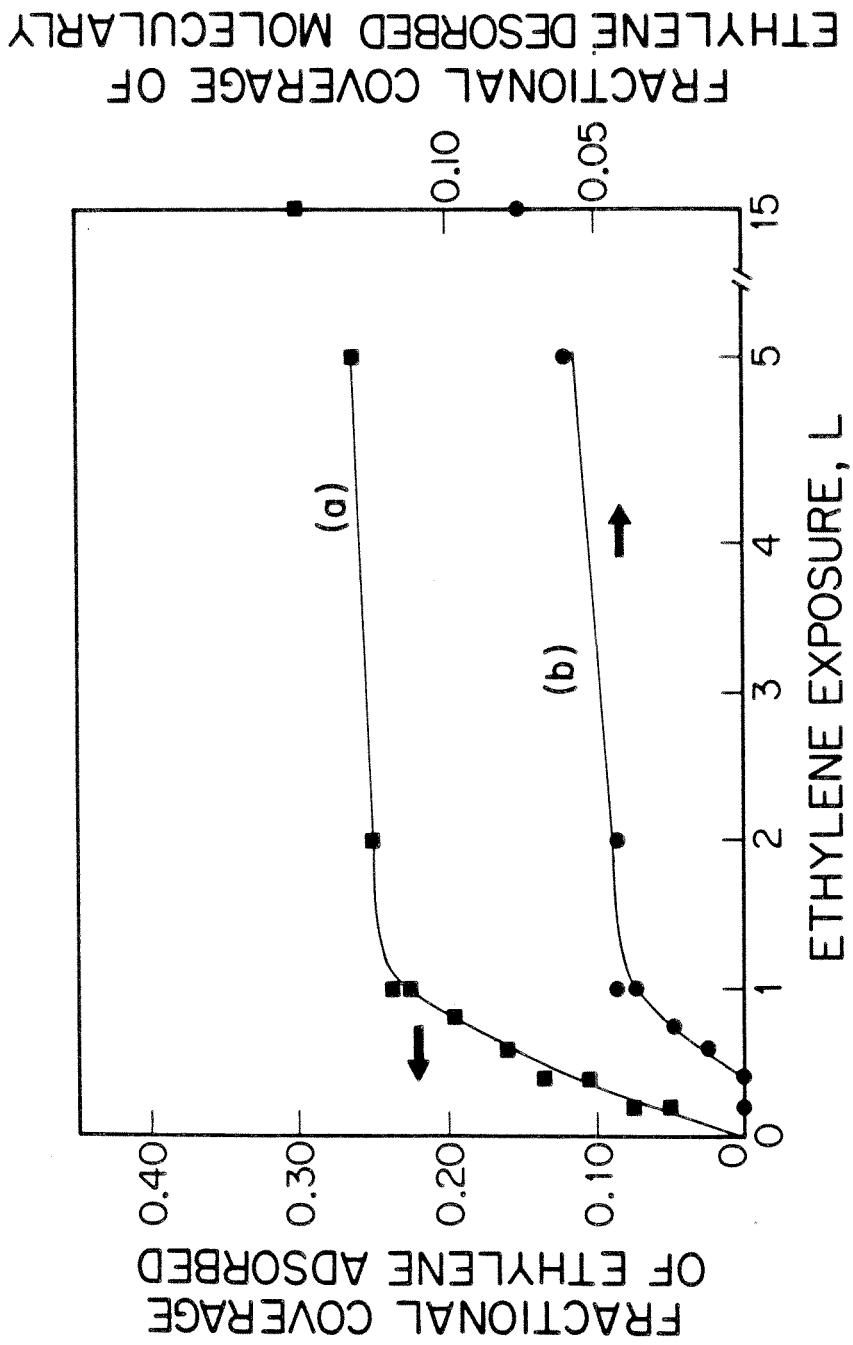
FRACTIONAL COVERAGE OF ETHYLENE ADSORBED
0.40
0.30
0.20
0.10
0
0
1
2
3
4
5
15
ETHYLENE EXPOSURE, L
(a)
(b)
0.10
0.05
FRACTIONAL COVERAGE OF ETHYLENE DESORBED MOLECULARLY

Figure 8

# CHAPTER III

## The Coadsorption of Hydrogen and Ethylene, and Carbon Monoxide and Ethylene on the Ru(001) Surface



[This chapter has been accepted for publication as an article by M. M. Hills, J. E. Parmeter and W. H. Weinberg in *The Journal of the American Chemical Society.*]

## Abstract

A detailed investigation of the coadsorption of ethylene with both preadsorbed hydrogen and preadsorbed carbon monoxide on the Ru(001) surface is reported here. Both preadsorbed hydrogen and carbon monoxide reduce the saturation coverage of subsequently chemisorbed ethylene. The coadsorption of hydrogen with ethylene results in detectable hydrogenation of ethylene to ethane below 280 K, whereas no self-hydrogenation of ethylene to ethane is observed. High resolution electron energy loss spectra show that ethylene coadsorbed with either hydrogen or carbon monoxide decomposes to ethylidyne ($CCH_3$) and acetylide (CCH), as it does on the clean surface. Carbon monoxide preadsorption enhances the stability of the ethylidyne such that it decomposes at approximately 420 K, rather than at 355 K as on the initially clean Ru(001) surface. Preadsorbed carbon monoxide also reduces the ratio of ethylidyne to acetylide that is formed from ethylene, compared to the ratio observed from an equivalent coverage of ethylene on the clean surface; hydrogen preadsorption, on the other hand, increases this ratio.

## I. Introduction

Surprisingly little spectroscopic information is available concerning the interaction of either hydrogen or carbon monoxide with ethylene on well-characterized, single crystalline transition metal surfaces, although much insight regarding the hydrogenation and dehydrogenation of ethylene can be obtained from these measurements. Ratajczykowa and Szymerska (1) have employed mass spectrometry under ultrahigh vacuum (UHV) conditions to investigate the coadsorption of ethylene, hydrogen and carbon monoxide on Pd(111) between 300 and 330 K, temperatures at which molecularly adsorbed ethylene and ethylidyne ($CCH_3$) coexist on the clean surface (2). The relative rates of ethylene hydrogenation and dehydrogenation were compared as functions of hydrogen and carbon monoxide coverage. It was found that the coverage of carbon monoxide controlled the hydrogen coverage, which governed the rate of ethylene hydrogenation relative to ethylene dehydrogenation.

Self-hydrogenation of ethylene to ethane on the Pt(111) surface been reported by Godbey et al. (3). The maximum rate of ethane formation occurs at 300 K, and this is reduced to 250 K in the presence of preadsorbed hydrogen. Coadsorption of deuterium with ethylene led to the evolution of all isotopically labeled ethane molecules ($C_2H_xD_{6-x}$; x = 0, 1, ..., 6).

Isotopic exchange between deuterium adatoms and the ethylidyne that is formed from the thermal decomposition of ethylene has been studied on the Pt(111) and Rh(111) surfaces (**4,5**). Using static secondary ion mass spectrometry and thermal desorption mass spectrometry, Ogle and White (4) have estimated that this exchange reaction on Pt(111) has an activation barrier of approximately 7 kcal/mole. Using electron energy loss spectroscopy (EELS), Koel et al. (**5**) found that deuterium incorporation into ethylidyne on Rh(111) at 350 K was slow in the sense that significant isotopic exchange was observed after only a few minutes following exposure of ethylidyne to 1 atm of deuterium, and they postulated the existence of an ethylidene ($CDCH_3$) intermediate in the exchange reaction. In neither investigation was ethylidyne directly observed to be hydrogenated to ethylidene, ethylene or ethane.

The coadsorption of hydrogen and ethylene on ruthenium is of particular interest due to the high reactivity of this metal for ethylene hydrogenation and its selectivity in the hydrogenation of monosubstituted olefins (**6**). Only rhodium is a more active catalyst than ruthenium for ethylene hydrogenation.

Knowledge of the interactions of ethylene and hydrogen on the Ru(001) surface will not only clarify the nature of the hydrogenation reaction of ethylene, but it will also allow important comparisons to the interactions of ethylene and hydrogen on Pt(111) and Rh(111) surfaces, each of which has hexagonal symmetry. The interaction between carbon monoxide and ethylene on ruthenium provides information concerning the effects of a nonreactive coadsorbate on the adsorption, desorption and dehydrogenation of ethylene. This investigation will also complement previous results for ethylene, acetylene and acetylene plus hydrogen on the Ru(001) surface (**7-10**).

To understand the interactions of hydrogen and carbon monoxide with ethylene on the Ru(001) surface, it is necessary first to understand the interaction of hydrogen, carbon monoxide and ethylene separately with the clean surface. Both the binding site and the adsorption and desorption kinetics of hydrogen on the Ru(001) surface are well characterized. Hydrogen adsorbs dissociatively in threefold hollow sites, producing weak electron energy loss peaks at 845 and 1115 $cm^{-1}$ at saturation coverage (**11**). Thermal desorption spectra of hydrogen exhibit two peaks at high surface coverages, which result from interactions among the adatoms rather than the occupation of geometrically inequivalent surface sites (**12**). The high temperature peak appears first at low coverages with a maximum rate of desorption, which downshifts from 450 to 380 K with increasing coverage. The low temperature peak appears at fractional surface coverages exceeding 0.35, with a maximum rate of desorption occurring near 325 K. The saturation fractional coverage is estimated to be 0.85 ± 0.15 (**11**). The activation energy of desorption and the corresponding preexponential factor of the desorption rate coefficient are 16.5 kcal/mole and $10^{-3}$ $cm^2/s$ for fractional coverages of hydrogen below 0.2. The activation energy of desorption decreases to 10 kcal/mole as the lower binding energy chemisorption state is populated. The initial probability of adsorption is 0.25 ± 0.1 at 200 K, decreasing to 0.12 as the higher binding energy chemisorption state is filled, and then dropping precipitously to 0.05 as the lower binding energy state is populated.

Carbon monoxide adsorbs molecularly on Ru(001) with a single carbon-oxygen stretching frequency, which shifts from 1980 to 2060 $cm^{-1}$ as the coverage increases (**13,14**). Under no circumstances has CO been observed to dissociate on the clean Ru(001) surface under UHV conditions. A

$(\sqrt{3} \times \sqrt{3})R30°$-CO low energy electron diffraction (LEED) pattern is formed with an optimal fractional surface coverage of 1/3. For this and lower coverages, the magnitude of the carbon-oxygen stretching frequency suggests that the CO is adsorbed in on-top sites. The observation of bridging CO on this surface has not been reported previously. Michalk and co-workers (**15**) have confirmed the on-top site symmetry of the $(\sqrt{3} \times \sqrt{3})R30°$ overlayer with dynamical LEED calculations. They found also that the CO is adsorbed essentially perpendicularly to the Ru(001) surface with a ruthenium-carbon bond length of 2.0 ± 0.1 Å and a carbon-oxygen bond length of 1.10 ± 0.1 Å. The fractional CO coverage at saturation is 0.65, where a $(5\sqrt{3} \times 5\sqrt{3})R30°$ coincidence LEED pattern, presumably due to a compressed CO overlayer, is observed (**13**). Two peaks are observed in the thermal desorption spectra of CO (**16**). The high temperature peak has a maximum desorption rate at approximately 480 K, while the low temperature peak, which is present at fractional coverages exceeding 1/3, has a maximum rate of desorption near 410 K. The activation energy of desorption is 38 kcal/mole at low fractional coverages ($\theta_{CO} < 0.23$) and increases to 42 kcal/mole at $\theta_{CO} = 0.33$, at which coverage the higher binding energy peak has filled. It then decreases rapidly to 29 kcal/mole, reaching 26 kcal/mole at saturation coverage. The preexponential factor of the desorption rate coefficient behaves similarly: its initial value is $2 \times 10^{16}$ $s^{-1}$, increasing to $10^{19}$ $s^{-1}$ at $\theta_{CO} = 0.33$, and then decreasing to $10^{14}$ $s^{-1}$ as saturation coverage is approached (**16**).

The interaction of ethylene with the clean Ru(001) surface has been discussed in detail recently (7). To summarize, below 150 K ethylene is chemisorbed molecularly in a di-σ-bonded configuration. Competing molecular desorption and dehydrogenation of the di-σ-bonded ethylene to ethylidyne, acetylide (CCH) and hydrogen adatoms occurs between 150 and 250 K. As shown by near-edge X-ray absorption, fine structure and LEED calculations, the ethylidyne on Pt(111) is adsorbed in threefold hollow sites (**17,18**), and it dehydrogenates completely to hydrogen adatoms and either carbon-carbon dimers or carbon adatoms with no spectroscopically observable, partially dehydrogenated intermediates (**17**). The hydrogen desorbs in a sharp peak at 355 K with a shoulder near 420 K for a saturation coverage of chemisorbed ethylene. Cleavage of the carbon-carbon bond of the acetylide, which yields methylidyne (CH) and surface carbon, is observed at 380 K. Reaction-limited hydrogen desorption

occurs between 500 and 700 K as the methylidyne dehydrogenates.

Peebles et al. (**19**) have shown that preadsorption of carbon monoxide suppresses the high temperature thermal desorption peak of postadsorbed hydrogen on the Ru(001) surface. The lower temperature thermal desorption peak of hydrogen both decreases in intensity and shifts to lower temperature (from approximately 325 to 305 K) with increasing carbon monoxide coverage (**20**). Although it is not known whether these observations are the result of lateral H-CO repulsive interactions giving rise to the formation of high density islands of hydrogen adatoms in the presence of carbon monoxide or a weakening of the Ru-H bond due to the presence of the coadsorbed carbon monoxide, the former explanation was shown to be correct by a LEED investigation of the coadsorption of hydrogen and CO on Rh(111), where nearly complete segregation of the two species was observed on the surface (**21**).

These observations raise several questions. First, how do preadsorbed hydrogen and carbon monoxide affect the subsequent adsorption of ethylene? Second, is the thermal decomposition of ethylene altered by the presence of hydrogen or carbon monoxide, and, if so, how? For example, are ethylidyne and acetylide formed, and, if so, in the same relative concentrations? Finally, can ethylene hydrogenation to ethane be observed under UHV conditions when hydrogen and ethylene are coadsorbed?

## II. Experimental Procedures

Thermal desorption mass spectrometry experiments were conducted in a UHV apparatus, which has been described in detail previously (**22,23**). Briefly, the chamber is pumped by both a 220 *l*/s noble ion pump and a titanium sublimation pump, which reduce the base pressure below $10^{-10}$ Torr. The crystal is cooled to below 100 K using liquid nitrogen. Linear heating rates of 5-20 K/s are achieved via resistive heating, controlled by a power supply interfaced to an LSI-11 DEC laboratory computer. This UHV chamber contains a UTI-100C quadrupole mass spectrometer enclosed in a glass envelope for selective sampling of gases that desorb from only the well-oriented front surface of the single crystal (**24**). Low-energy electron diffraction optics and a rotatable Faraday cup are available for the display of LEED patterns and the measurement of LEED beam profiles. A single pass cylindrical mirror electron energy analyzer with an integral electron gun is available for Auger electron spectroscopy.

A second UHV chamber was used to conduct high resolution electron energy loss spectroscopic experiments. This chamber also has a base pressure below $10^{-10}$ Torr using similar pumping techniques; and liquid nitrogen cooling and resistive heating of the crystal were similarly employed. The home-built Kuyatt-Simpson type EEL spectrometer is described in detail elsewhere (**25,26**). It was operated such that the kinetic energy of the electron beam incident upon the crystal was approximately 4 eV at an angle of incidence of 60° with respect to the surface normal. The spectra were measured with a resolution of 60-80 $cm^{-1}$ (full-width at half-maximum of the elastically scattered peak), while a count rate of 1.5-3 x $10^5$ cps was maintained in the elastic channel. This UHV chamber also contains a quadrupole mass spectrometer, but it was not, in general, employed in the thermal desorption measurements reported here.

The techniques used for orienting, cutting, polishing and mounting the Ru(001) crystals have been described previously (**25,26**). The crystals were cleaned using periodic argon ion sputtering and routine annealing to 1000 K in 7 x $10^{-8}$ Torr of $O_2$, followed by annealing to 1700 K *in vacuo*. Surface cleanliness was monitored in the two UHV chambers by Auger electron spectroscopy, EELS and hydrogen thermal desorption.

Research purity (99.9995% min.) hydrogen, C.P. grade (99.5%) deuterium and ethylene, and research purity (99.99% min.) carbon monoxide were obtained from Matheson. The ethylene was purified further by three freeze-thaw-pump cycles. Research purity (99.99%) ethylene-$d_4$ was purchased from Merck and Co. The purity of all gases was verified *in situ* by mass spectrometry in both UHV chambers.

## III. Results

### A. Coadsorption of Carbon Monoxide and Ethylene

Preadsorbed CO alters significantly the thermal desorption spectra of hydrogen from adsorbed ethylene on Ru(001). Figure 1(a) shows the hydrogen thermal desorption spectrum following a saturation exposure of 1 L of $C_2H_4$ (1 L ≡ 1 Langmuir ≡ $10^{-6}$ Torr-s) at 130 K, while Figs. 1(b)-(e) show a series of hydrogen thermal desorption spectra for various preexposures of carbon monoxide, followed by

a constant ethylene exposure of 1 L at 130 K (at which temperature no multilayer of ethylene forms). Figure 1(f) shows the hydrogen thermal desorption spectrum following the adsorption of 0.4 L of ethylene on the clean surface. As the precoverage of CO increases, new desorption peaks of hydrogen appear at 290 and 420 K, while the 355 K peak decreases in intensity, disappearing completely at CO exposures of 0.8 L or more. In addition, the high temperature tail (above 480 K) shifts to lower temperature, and the total amount of hydrogen that desorbs decreases with increasing carbon monoxide coverage.

The inhibition in the chemisorption of ethylene by preadsorbed CO ($\theta_{C_2H_4}$ vs. $\theta_{CO}$) is illustrated in Fig. 2(a), where $\theta_{C_2H_4}$ includes both the reversibly and irreversibly chemisorbed ethylene. This relationship was derived from the data of Fig. 1, together with the corresponding thermal desorption spectra of molecular ethylene. In the presence of CO, approximately 20% of the chemisorbed ethylene desorbs molecularly, as is observed also on the clean surface. Displacement of CO by ethylene was not observed. However, for all CO precoverages the thermal desorption peaks of CO coadsorbed with ethylene are downshifted by approximately 20 K with respect to the desorption of equivalent coverages of CO from the otherwise clean Ru(001) surface.

The preadsorption of 0.4 L ($\theta_{C_2H_4} \simeq 0.13$) of ethylene, followed by 2 L of carbon monoxide ($\theta_{CO} \simeq 0.20$), produced hydrogen thermal desorption spectra similar to Fig. 1(c). Greater initial ethylene coverages blocked carbon monoxide adsorption to a larger extent, and the preadsorption of 1 L of ethylene followed by any exposure of CO resulted in $H_2$ and $C_2H_4$ thermal desorption spectra that were nearly identical to those of ethylene adsorbed on the clean Ru(001) surface.

Electron energy loss spectra for various precoverages of carbon monoxide followed by an exposure of ethylene at 80 K are similar to those of ethylene adsorbed on the clean surface. As on the clean Ru(001) surface, multilayers of ethylene condense at 80 K. Annealing the crystal to 110 K desorbs this multilayer, leaving an overlayer composed of carbon monoxide and di-σ-bonded ethylene. Figure 3(a) shows an EEL spectrum measured after annealing a saturation coverage of ethylene adsorbed on the clean Ru(001) surface to 110 K and is indicative of di-σ-bonded ethylene. The mode assignments for this di-σ-bonded ethylene are discussed in detail elsewhere (7). Briefly, di-σ-bonded ethylene on

Ru(001) produces strong $CH_2$ twisting and wagging modes at 900 and 1145 $cm^{-1}$ and a symmetric carbon-hydrogen stretching mode at 2940 $cm^{-1}$, which reflect the rehybridization of the carbon atoms in ethylene to nearly $sp^3$. Additional energy loss features at 460, 650, 775, 1040, 1450 and 3050 $cm^{-1}$ are due, respectively, to the symmetric and asymmetric carbon-ruthenium stretching modes, the $CH_2$ rocking mode, the carbon-carbon stretching mode, the $CH_2$ scissoring mode, and the asymmetric carbon-hydrogen stretching mode of the molecularly chemisorbed ethylene. Although not all of these modes are resolved in Fig. 3(a), they have been assigned from other EEL spectra.

Figure 3(c) is an EEL spectrum measured following an exposure of 0.6 L of CO ($\theta_{CO}$ = 0.33) and then 1 L of $C_2H_4$ ($\theta_{C_2H_4}$ = 0.08-0.09) at 80 K with subsequent annealing to 110 K. [Figure 3(b) is an EEL spectrum measured following an exposure of 1 L of $H_2$ and then 1 L of $C_2H_4$, and will be discussed in Sect. IIIB.] The mixed overlayer of Fig. 3(c) consists of di-$\sigma$-bonded $C_2H_4$ and linearly bonded CO. The modes of both ethylene and carbon monoxide are unchanged compared to those observed when ethylene and carbon monoxide are adsorbed separately on the Ru(001) surface. The symmetric Ru-CO stretching mode and the C≡O stretching mode are observed at 465 and 2020 $cm^{-1}$ in Fig. 3(c). All mode assignments of ethylene coadsorbed with carbon monoxide were confirmed by EEL spectra of CO coadsorbed with deuterated ethylene.

Annealing the mixed overlayer to between 230 and 280 K causes competing desorption and dehydrogenation of the di-$\sigma$-bonded ethylene. A subsequently measured EEL spectrum [Fig. 3(d)] indicates the presence of ethylidyne and acetylide, the same decomposition products formed from ethylene that is adsorbed on the clean surface.The ethylidyne is characterized by the $\nu$(CC) mode at 1140 $cm^{-1}$, the $\delta_s(CH_3)$ mode at 1370 $cm^{-1}$, the $\rho(CH_3)$ mode at 1000 $cm^{-1}$, and the $\nu(CH_3)$ mode at 2945 $cm^{-1}$ (7). Note that ethylidyne produces no losses below 1000 $cm^{-1}$ except for $\nu_s$(Ru-C) at 480 $cm^{-1}$ [which is unresolved from $\nu$(Ru-C) of CO]; the loss at 750 $cm^{-1}$ is due to the carbon-hydrogen bending mode of acetylide. In Fig. 3(d), the carbon-carbon stretching mode of acetylide at 1290 $cm^{-1}$ and the carbon-hydrogen stretching mode of acetylide at 2960 $cm^{-1}$ are unresolved from the $\delta_s(CH_3)$ and $\nu(CH_3)$ modes of ethylidyne. This overlayer contains a small concentration of bridging CO in addition to linearly bonded CO, as indicated by the shoulder at 1840 $cm^{-1}$ in Fig. 3(d) (27). This $\mu$-CO forms near 220 K

when acetylide and ethylidyne are formed and disappears near 450 K as the CO begins to desorb. The CO thermal desorption spectrum of the overlayer corresponding to Fig. 3(d) was virtually identical to that of a CO coverage of 0.33 adsorbed on the clean surface, except for being downshifted by approximately 20 K. No unusual features were observed which might be attributed to the presence of the bridging CO.

Annealing the surface above 350 K initiates decomposition of the ethylidyne, forming hydrogen adatoms, carbon adatoms and (possibly) carbon dimers. The hydrogen from ethylidyne decomposition desorbs in either the 355 K or the 420 K thermal desorption peaks (cf. Fig. 1), depending upon the CO coverage. Hydrogen thermal desorption spectra have been used to obtain the ratio (R) of ethylidyne to acetylide that is formed from ethylene coadsorbed with CO. This ratio is plotted in Fig. 4(a) as a function of the coverage of the irreversibly chemisorbed ethylene. These data were obtained by exposing the Ru(001) surface to a variable precoverage of CO, followed by a saturation exposure of ethylene. As shown in Figs. 4(a) and (b), preadsorbed CO decreases the ratio of ethylidyne to acetylide that is formed from postadsorbed ethylene, relative to the ratio observed for an equivalent coverage of ethylene on the clean surface. However, this ratio does increase with increasing ethylene coverages (lower CO precoverages), as it does for ethylene adsorbed on the clean surface. This issue will be discussed in detail in Sect. IV.A.2.

The carbon-carbon bond of the acetylide is cleaved, forming carbon adatoms and methylidyne, when the overlayer is annealed to 400 K. An EEL spectrum of coadsorbed methylidyne and CO is shown in Fig. 3(e). The characteristic modes of methylidyne are a carbon-hydrogen bending mode at 810 $cm^{-1}$ and a carbon-hydrogen stretching mode at 3010 $cm^{-1}$. The Ru-CH stretching mode (at 440 $cm^{-1}$) is obscured by the $\nu$(Ru-CO) mode at 460 $cm^{-1}$. Annealing to 600 K decomposes all of the methylidyne, desorbing hydrogen and CO, leaving only surface carbon with $\nu$(Ru-C) at approximately 600 $cm^{-1}$.

### B. Coadsorption of Hydrogen and Ethylene

Electron energy loss spectra of hydrogen and ethylene coadsorbed on Ru(001) are similar to those of ethylene adsorbed on the clean surface with the exception that the modes due to ethylidyne,

following annealing to 280 K, are more intense relative to the modes of acetylide. This indicates that the thermal decomposition products of ethylene adsorbed on the clean and the hydrogen precovered Ru(001) surfaces are the same under our experimental conditions. Figures 3(a) and (b) compare, respectively, the EEL spectrum of a saturation coverage of ethylene adsorbed on the clean surface at 80 K and annealed to 110 K ($\theta_{C_2H_4}$ = 0.30) with that of the Ru(001) surface exposed to 1 L of $H_2$ ($\theta_H$ = 0.65) followed by a saturation coverage of ethylene ($\theta_{C_2H_4}$ = 0.13) at 80 K and subsequently annealed to 110 K. The spectrum of Fig. 3(b) is less intense because less ethylene is adsorbed. It is apparent, however, that these spectra correspond to the same surface species, namely, di-σ-bonded ethylene. Hydrogen adatoms are also present in the overlayer corresponding to the spectrum of Fig. 3(b). The weak ruthenium-hydrogen modes, which occur at 780 and 1115 $cm^{-1}$ (at this hydrogen coverage) with an intensity less than 0.04% of the elastic peak (11), are obscured, however, by losses due to the adsorbed ethylene. A small amount of carbon monoxide is also present in the overlayer corresponding to the spectrum of Fig. 3(b), as indicated by the presence of the ν(C≡O) mode of CO at 2200 $cm^{-1}$. The weak intensity of this mode in Fig. 3(b) [cf. Fig. 3(c)-(e)] implies that the fractional coverage of CO in this overlayer is less than 0.01, and it has no influence on the chemisorption and reaction of hydrogen and ethylene.

Annealing the coadsorbed hydrogen and ethylene overlayer to higher temperatures results in EEL spectra similar to those of ethylene adsorbed on the clean Ru(001) surface. The di-σ-bonded ethylene ($\theta_{C_2H_4} \simeq 0.13$) dehydrogenates to ethylidyne and acetylide between 150 and 280 K. The ratio of ethylidyne to acetylide is approximately 2.5, as judged by the areas of the hydrogen thermal desorption peaks of Fig. 5(b), compared to a branching ratio of 1.3 for a coverage of ethylene of 0.13 on the clean Ru(001) surface. The dependence of the ratio of ethylidyne to acetylide upon the coverage of irreversibly adsorbed ethylene for preadsorbed deuterium (hydrogen) followed by a saturation postexposure of $C_2H_4$ ($C_2D_4$) is compared to that observed for ethylene adsorbed on the clean surface in Figs. 4(b) and (c). Although there are large uncertainties in the data of Fig. 4(c) due to the small acetylide coverages, the preadsorption of hydrogen clearly results in an increased ratio of ethylidyne to acetylide relative to the ratio observed following the dehydrogenation of an equivalent coverage of ethylene on the clean

surface. Indeed, a saturation hydrogen precoverage ($\theta_H \approx 0.85$ and $\theta_{C_2H_4} \approx 0.05$) completely inhibits acetylide formation. The ethylidyne decomposes to carbon (possibly dimers) and hydrogen adatoms below 355 K. Near 400 K the carbon-carbon bond of the acetylide cleaves, forming methylidyne and surface carbon. Finally, the methylidyne decomposes, evolving hydrogen, above 480 K.

The thermal desorption spectra of hydrogen and ethylene coadsorbed on Ru(001) and ethylene adsorbed on the clean surface are somewhat different. Figure 5(a) illustrates the hydrogen thermal desorption spectrum after 1 L of $C_2H_4$ is adsorbed on this surface. There is a sharp peak at 345 K, a shoulder near 420 K, and a high temperature tail extending from 480 to 700 K. Figure 5(b) shows the hydrogen thermal desorption spectrum after an exposure of 1 L of $H_2$ followed by 1 L of $C_2H_4$ at 100 K. This spectrum exhibits a much more prominent shoulder on the high temperature side of the (sharper) 345 K peak, and the high temperature tail terminates between 600 and 650 K. As discussed previously (7), and confirmed by the carbon monoxide and ethylene coadsorption experiments, the 345 K peak of Fig. 5(a) corresponds to desorption of hydrogen limited by ethylidyne decomposition. Due to the similarity of the EEL spectra of ethylene adsorbed on the clean surface and ethylene coadsorbed with hydrogen, the high temperature tails (above approximately 480 K) of Figs. 5(a) and (b) correspond to decomposition-limited desorption of hydrogen from the same species, methylidyne.

The shoulder near 420 K in the hydrogen thermal desorption spectrum of coadsorbed hydrogen and ethylene [Fig. 5(b)] is due to desorption-limited hydrogen from the Ru(001) surface. This shoulder occurs at approximately the same temperature at which a similar coverage of hydrogen desorbs from the clean surface, as may be seen in Fig. 5(c), and the area under the shoulder increases with increasing hydrogen precoverage. Proof that this shoulder corresponds to desorption-limited hydrogen was provided by additional thermal desorption measurements in which the hydrogen and ethylene overlayer was annealed to 800 K, and then the (uncleaned) surface was exposed to hydrogen. The subsequent hydrogen thermal desorption spectrum indicated that the shoulder (now a peak since the 345 K peak was absent) was repopulated, demonstrating that the shoulder of Fig. 5(b) represents desorption-limited hydrogen from the surface. No other hydrogen thermal desorption peaks were observed, implying that no carbon-hydrogen bonds were formed. Complementary EEL spectra measured after annealing the

carbon- and hydrogen-covered surface to various temperatures supported the presence of only C(a) and H(a); i.e., no hydrogen-containing species such as CH, $CH_2$ or $CH_3$ were observed under any conditions. This disagrees with the results of Barteau et al. (**28**), who reported the hydrogenation of surface carbon to methylidyne on Ru(001).

In addition to the desorption of hydrogen, annealing the mixed hydrogen and ethylene overlayer resulted in the desorption of ethylene and the formation and desorption of ethane, as shown in Figs. 5(d) and (e). Condensed ethylene desorbed in a multilayer peak at 110 K [cf. Fig. 5(d)]. Ethane and chemisorbed ethylene desorbed in broad peaks, the tails of which extend to approximately 250 K. The intermediate to ethane formation, presumably ethyl, was not sufficiently stable to be observed spectroscopically by EELS. Ethane was formed following fractional precoverages of hydrogen exceeding 0.4 and subsequent saturation exposures of ethylene. The amount of ethane that desorbed corresponds to an effective fractional surface coverage of only approximately 0.01, which is less than one-third of the amount of ethylene, which desorbs molecularly. The fraction of chemisorbed ethylene that desorbs molecularly increases from 0.2 to 0.6 as the initial fractional coverage of hydrogen increases from zero to 0.85.

Thermal desorption measurements of preadsorbed deuterium and postadsorbed ethylene were carried out to examine both the extent of isotopic mixing among the adspecies and the inhibition of ethylene adsorption by deuterium. Considerable isotopic mixing occurred in the desorbed hydrogen [cf. Fig. 6]. These experiments also showed that within our experimental uncertainty, postexposures of 1 L or more of ethylene did not displace any preadsorbed deuterium. Coadsorption of deuterium (hydrogen) with molecularly chemisorbed $C_2H_4$ ($C_2D_4$) indicated that isotopic exchange between these two species was slight in that only minor amounts of any ethylene and ethane desorption products except $C_2H_4$ ($C_2D_4$) and $C_2H_4D_2$ ($C_2D_4H_2$) were observed.

The results of isotopic exchange experiments between both $CCH_3$ and CCH and deuterium adatoms are discussed in a separate paper (**29**). Briefly, electron energy loss spectra of acetylide and ethylidyne formed from $C_2H_2$ and coadsorbed with deuterium provide evidence for isotopic exchange between deuterium and CCH but no exchange between deuterium and ethylidyne.

Isotopic exchange experiments between deuterated methylidyne and postadsorbed hydrogen [and equivalently between CH(a) and D(a)] were also carried out. Deuterated methylidyne (coadsorbed with carbon adatoms) was formed by exposing the Ru(001) surface to 4 L of $C_2D_4$ at 100 K and annealing to 440 K such that $\theta_C \approx 0.38$ and $\theta_{CD} \approx 0.10$. The surface was then cooled to 100 K, exposed to a saturation coverage of hydrogen ($0.3 < \theta_H < 0.4$), and a thermal desorption experiment conducted. Hydrogen, HD and $D_2$ were detected in desorption-limited peaks at 400 K, and in tails above 500 K due to dehydrogenation of CH and CD. No other species such as methane were observed to desorb. A comparison of the areas under the high temperature tails of the $H_2$, HD and $D_2$ thermal desorption spectra shows that 20% to 30% of the deuterated methylidyne underwent isotopic exchange. The observation of deuterium desorption below 400 K indicates that isotopic exchange occurs also below this temperature. The occurrence of isotopic exchange between CH coadsorbed with deuterium has also been confirmed with EELS, and is reported elsewhere (9). These EELS measurements showed no hydrogenation of methylidyne to stable methylene or methyl species.

The extent of inhibition of ethylene adsorption by preadsorbed deuterium was estimated from the $H_2$, HD, $D_2$, ethylene and ethane thermal desorption spectra for various initial surface coverages of deuterium followed by a saturation exposure of ethylene. These data were used to construct Fig. 2(b), a plot of $\theta_{C_2H_4}$ versus $\theta_D$, where $\theta_D$ was determined from the HD, $D_2$ and $C_2H_4D_2$ thermal desorption spectra. Clearly, a saturation precoverage of deuterium does not completely inhibit ethylene adsorption. The inhibition of ethylene adsorption by deuterium adatoms is weaker than that by preadsorbed carbon monoxide.

## IV. Discussion

### A. Coadsorption of Carbon Monoxide and Ethylene

#### *1. Adsorption*

From Fig. 1 and the corresponding thermal desorption spectra of molecular ethylene, it was determined that the fraction of the di-σ-bonded ethylene which desorbed molecularly from the CO preexposed and subsequently ethylene *saturated* surface was 20% of the total fractional coverage of chem-

isorbed ethylene, independent of the CO coverage. This fraction is approximately the same as that observed when a saturated overlayer of ethylene is chemisorbed on the clean Ru(001) surface. This result shows that preadsorbed CO does not inhibit ethylene thermal decomposition on the surface *relative* to molecular desorption. However, preadsorbed CO does inhibit ethylene adsorption as illustrated in Fig. 2.

The approximately linear decrease in the ethylene coverage with carbon monoxide coverage suggests that CO is simply (geometrically) blocking the surface for ethylene adsorption. The reciprocal of the magnitude of the slope of the line in Fig. 2(a) indicates that 1.7 CO admolecules poison the adsorption of one ethylene molecule. Assuming that the areas occupied by a carbon monoxide admolecule and an ethylene admolecule are inversely proportional to the saturation fractional coverages of CO (0.65) and ethylene (0.30), respectively, then 2.2 (i.e. 0.65/0.30) CO admolecules would block adsorption of one ethylene molecule. We observe that fewer CO admolecules are required to block adsorption of one ethylene molecule because ethylene has a significantly lower heat of adsorption than carbon monoxide, and, unlike CO, does not form a compressible overlayer.

2. *Thermal Decomposition*

The results of Peebles et al. (**19**) and unpublished data from our laboratory indicate that the peak at 290 K in the hydrogen thermal desorption spectra for coadsorbed CO and $C_2H_4$ [cf. Figs. 1(b)-(e)] is due to surface hydrogen that desorbs at a slightly lower temperature than does hydrogen coadsorbed with CO for the same coverages of CO and surface hydrogen. This is presumably the result of a higher effective hydrogen density due to the presence of ethylidyne and acetylide. That the peak at 290 K results from desorption-limited hydrogen was confirmed by hydrogen thermal desorption spectra of coadsorbed hydrogen and carbon monoxide on a carbon precovered surface ($\theta_C \approx 0.15$), which showed hydrogen desorption in a single peak at 290 K for fractional coverages of CO exceeding 0.35. From the observed EEL spectra both of ethylene adsorbed on the clean surface (**7**) and of ethylene coadsorbed with carbon monoxide, it is clear that this surface hydrogen is derived from ethylene dehydrogenation to acetylide and ethylidyne below 250 K.

The peak at 420 K in the hydrogen thermal desorption spectra of Figs. 1(b)-(e) results from the decomposition of ethylidyne. Without coadsorbed CO, the ethylidyne begins to decompose near 330 K, reaching a maximum rate at 355 K. This is manifest as a rather sharp peak in the hydrogen thermal desorption spectrum at this temperature, as may be seen in Fig. 1(a). Preadsorbed CO not only decreases the amount of ethylidyne that is formed relative to acetylide (cf. Fig. 4), but also shifts the ethylidyne decomposition to a higher temperature. The *onset* of ethylidyne decomposition in the presence of a fractional coverage of CO of 0.4 occurs at the same temperature (approximately 380 K) at which CO begins to desorb, as shown both by thermal desorption and EELS results. This suggests that CO inhibits ethylidyne decomposition (effectively stabilizing the ethylidyne), e.g. by geometrically blocking the surface adjacent to the ethylidyne that is necessary for its decomposition. Thus, as the precoverage of CO is increased, more ethylidyne is prevented from dehydrogenating prior to CO desorption. A fractional surface precoverage of CO exceeding 0.4 prevents any dehydrogenation of the ethylidyne at 355 K.

The final changes in the hydrogen thermal desorption spectra of carbon monoxide coadsorbed with ethylene on Ru(001) are a shift to lower temperature and an increased intensity (*relative* to the 355 and 420 K peaks) of the high temperature tail above approximately 480 K, which is due to methylidyne decomposition. The former is due to the lower coverage of ethylene on the surface when CO is preadsorbed and is associated with the greater availability of vacant adsites at the temperature of methylidyne decomposition, i.e. a lower concentration of adsorbed carbon (**30**). The increasing intensity of the high temperature tail in the hydrogen thermal desorption spectra due to methylidyne decomposition relative to the 355 and 420 K peaks is a consequence of a reduction in ethylidyne formation relative to acetylide formation, as shown in Fig. 4. Recall that methylidyne is derived only from acetylide. The enhancement of acetylide formation with increasing CO precoverage also causes the increasing relative intensity of the 290 K peak in the hydrogen thermal desorption spectra, since acetylide formation produces two more hydrogen adatoms than does ethylidyne formation, and these two adatoms desorb in the 290 K peak in the presence of CO. The enhanced acetylide formation relative to ethylidyne formation in the presence of CO is obviously greater than that which would be expected due to the lower ethylene

surface coverage in the presence of CO (cf. Fig. 4). A reasonable explanation for this effect is that the net balance of interaction energies among hydrogen, carbon monoxide and the intermediate(s) to ethylidyne and acetylide formation is repulsive with respect to the interaction energy which results in the absence of hydrogen. This inhibits the reaction of hydrogen with the precursor to ethylidyne formation and, therefore, favors dehydrogenation to acetylide with respect to ethylidyne formation (31). This point of view is consistent with the repulsive interactions that occur between coadsorbed hydrogen and CO, which result in phase separation of these two species.

Thus, the assignment of peaks in the hydrogen thermal desorption spectra is as follows: the $\beta_1$ peak at 290 K is composed of surface hydrogen from ethylene dehydrogenation to acetylide and ethylidyne, downshifted by the presence of CO; the $\gamma_1$ peak at 355 K is composed of hydrogen from the decomposition of ethylidyne; the $\gamma_2$ peak at 420 K is composed of hydrogen from the decomposition of ethylidyne that is stabilized by coadsorbed CO; and the $\gamma_3$ peak near 530 K is composed of hydrogen from methylidyne decomposition. These assignments are consistent with the observed ratios of the peak areas. For example, for the case of Fig. 1(e), where no peak at 355 K is observed, the stoichiometry required by the above peak assignments is $\beta_1 = \frac{\gamma_2}{3} + 3\gamma_3$. This stoichiometry has been confirmed by the thermal desorption spectrum of Fig. 1(e), which exhibits relative peak areas for $\beta_1 : \gamma_2 : \gamma_3$ of 0.55 : 0.3 : 0.15. Thus, the carbon monoxide-hydrogen repulsive interactions, which cause phase separation and the lower binding energy of surface hydrogen that results in desorption at a lower temperature, allow us to confirm the stoichiometry of the decomposition products of ethylene adsorbed on the Ru(001) surface, which were identified by EELS. The ratios of these peaks also confirm that only a small fraction, *if any*, of the ethylidyne decomposes to methylidyne. If we assume that ethylidyne can decompose to methylidyne, then the ratios of the peaks in these hydrogen thermal desorption spectra indicate that, *at most*, 10% of the ethylidyne decomposes to methylidyne.

Finally, we have observed that the adsorption of ethylene also affects the bonding of preadsorbed carbon monoxide. Postadsorption of ethylene induced the formation of a small fraction of bridging carbon monoxide, which is not observed at any coverage of CO on the otherwise clean Ru(001) surface. Furthermore, the presence of carbon and methylidyne following ethylene dehydrogenation reduced the

binding energy of preadsorbed carbon monoxide such that the CO desorbed at approximately 20 K below the temperature at which an equivalent fractional coverage of CO desorbs from the clean surface.

**B. Coadsorption of Hydrogen and Ethylene**

*1. Adsorption*

Figure 2(b) shows that preadsorbed deuterium does not inhibit ethylene adsorption so effectively as does preadsorbed carbon monoxide. The ethylene coverage that is plotted is the fractional coverage of *chemisorbed* ethylene following multilayer desorption. Preadsorbed deuterium decreases the ethylene coverage approximately linearly, and a saturation coverage of deuterium ($\theta_D \approx 0.85$) does not completely block ethylene adsorption. The linear dependence of ethylene coverage upon deuterium pre-coverage suggests that the deuterium, like preadsorbed carbon monoxide, is geometrically blocking the surface with respect to the subsequent adsorption of ethylene. The results shown in Fig. 2(b) suggest that 3.3 hydrogen adatoms poison the adsorption of one ethylene molecule. As expected, the number of hydrogen atoms required to block the adsorption of one ethylene molecule is greater than the number of carbon monoxide molecules (1.7). The extrapolated intercept of the abscissa of Fig. 2(b) indicates a hydrogen coverage of one adatom per ruthenium unit cell is necessary to poison the surface essentially completely with respect to the subsequent adsorption of ethylene.

*2. Thermal Decomposition*

The preadsorption of deuterium atoms into the threefold sites on Ru(001) decreases the availability of vacant threefold sites for the products of ethylene decomposition. The ethylene decomposition products, ethylidyne and acetylide, require one and three vacant threefold sites, respectively, for hydrogen adatoms. Thus, as the deuterium precoverage is increased and fewer threefold sites are available, a larger fraction of the chemisorbed ethylene is desorbed molecularly as $C_2H_4$ or is hydrogenated to ethane, compared to chemisorbed ethylene on the otherwise clean Ru(001) surface. The fraction of chemisorbed ethylene, which desorbs molecularly as $C_2H_4$ increases from 0.2 to 0.6 as the fractional hydrogen precoverage, increases from zero to 0.85. The higher concentration of hydrogen (deuterium) adatoms on the surface below 280 K facilitates ethane formation, which was not observed when ethylene was adsorbed on the clean Ru(001) surface. Ethane evolution was observed only in the

coverage range $0.4 \leq \theta_H$ (preceding a saturation exposure of ethylene), and the ethane that desorbed corresponds to an effective fractional surface coverage of approximately 0.01. We note further that ethane forms via the hydrogenation of di-σ-bonded ethylene, not ethylidyne or acetylide, which are not present on the surface at the temperature at which ethane evolution is initiated.

Thermal desorption experiments of coadsorbed deuterium and $C_2H_4$ or hydrogen and $C_2D_4$ showed that the majority ethane species were $C_2D_2H_4$ in the first case and $C_2H_2D_4$ in the latter. The predominant ethylene species that desorbed molecularly from these overlayers were $C_2H_4$ and $C_2D_4$, respectively; i.e., very little isotopic mixing with the molecularly adsorbed ethylene occurred. These results suggest that ethane formation occurs via the irreversible addition of two surface hydrogen or deuterium adatoms to ethylene.

Thermal desorption and EEL spectra of deuterium coadsorbed with CH or hydrogen coadsorbed with CD indicated that approximately 20% of the methylidyne underwent isotopic exchange. On the other hand, isotopic exchange between surface hydrogen and $CCD_3$ did not occur. Similarly, acetylide underwent limited isotopic exchange with surface hydrogen. The mechanisms by which these exchange reactions proceed will be discussed elsewhere (**29**). This is in agreement with the results of Koel et al. (**5**) who identified via EELS an ethylidyne on Rh(111) at 300 K following $C_2H_4$ adsorption, and $H_2$ and $C_2H_4$ coadsorption. This ethylidyne underwent H-D exchange when exposed to deuterium only at high deuterium pressures (1 atm).

As discussed earlier, the 345 K peak in the hydrogen thermal desorption spectra of hydrogen and ethylene coadsorbed on Ru(001) [cf. Fig. 5(b)] corresponds to the desorption of hydrogen that is limited by ethylidyne decomposition. The high temperature tail, above approximately 480 K, in the spectra corresponds to the reaction-limited desorption of hydrogen from the decomposition of methylidyne that is formed by the cleavage of the carbon-carbon bond of acetylide at 400 K. The observed change in the areas of these two peaks indicates that the ratio of ethylidyne to acetylide increases with hydrogen precoverage, as shown in Fig. 4. Indeed, one might expect that an increase in hydrogen or deuterium precoverage would favor ethylidyne over acetylide, since the former is composed of two more hydrogen atoms.

As may be seen in Fig. 5(b), the shoulder at 420 K in the hydrogen thermal desorption spectra of hydrogen and ethylene adsorbed on Ru(001) is enhanced relative to that of hydrogen thermal desorption from ethylene adsorbed on the clean surface. The temperature corresponding to the maximum rate of hydrogen desorption from this shoulder is approximately 20 K lower than that at which an equivalent amount of hydrogen desorbs from the clean Ru(001) surface. However, this shoulder could be repopulated by adsorbing hydrogen on the (uncleaned) surface that results from annealing coadsorbed hydrogen and ethylene to 700 K, which desorbs the hydrogen completely. This indicates that this shoulder corresponds to desorption-limited surface hydrogen.

## V. Conclusions

Both preadsorbed carbon monoxide and hydrogen (deuterium) inhibit ethylene postadsorption on the Ru(001) surface. Of the two, carbon monoxide more effectively inhibits ethylene adsorption. The EEL spectra were virtually identical for ethylene adsorbed on Ru(001), ethylene adsorbed with preadsorbed hydrogen, and ethylene adsorbed with preadsorbed carbon monoxide. In all three cases, the ethylene decomposed upon heating to ethylidyne and acetylide. The ethylidyne dehydrogenated completely to carbon and hydrogen adatoms with further heating, while the acetylide underwent carbon-carbon bond cleavage to form carbon adatoms and methylidyne. The preadsorption of CO causes surface hydrogen to desorb at a lower temperature (290 K) and ethylidyne to decompose at a higher temperature (420 K). The observed ratios of peak areas in the hydrogen thermal desorption spectra confirm the identity of the stable ethylene decomposition products, ethylidyne and acetylide, as observed via EELS.

The preadsorption of hydrogen initiated ethane formation and desorption (with a maximum rate at approximately 200 K). The desorption of ethylene and the formation of ethane were enhanced with increasing hydrogen precoverage, compared to the dehydrogenation products, ethylidyne and acetylide.

The presence of preadsorbed CO and hydrogen alters the ratio of the ethylene decomposition products, ethylidyne and acetylide. Carbon monoxide preadsorption enhances acetylide formation relative to ethylidyne formation from postadsorbed ethylene, compared to an equivalent coverage of ethylene adsorbed on the clean surface, while hydrogen preadsorption enhances ethylidyne formation,

such that a saturation preexposure of hydrogen completely suppresses acetylide formation.

The presence of hydrogen initiated ethane formation and desorption (with a maximum rate at approximately 200 K). The desorption of ethylene and the formation of ethane were enhanced with increasing hydrogen precoverage, compared with the dehydrogenation products, ethylidyne and acetylide.

**Acknowledgment** This work was supported by the National Science Foundation under Grant No. CHE-8516615.

**References and Notes**


1. Ratajczykowa, I.; Szymerska, I., *Chem. Phys. Letters* **1983**, 96, 243.

2. Gates, J.A.; Kesmodel, L.L., *Surface Sci.* **1982**, 120, L461.

3. Godbey, D.; Zaera, F.; Yeates, R.; Somorjai, G.A. Somorjai, *Surface Sci.* **1986**, 167, 150.

4. Ogle, K.M.; White, J.M., *Surface Sci.* **1986**, 165, 234.

5. Koel, B.E.; Bent, B.E.; Somorjai, G.A., *Surface Sci.* **1984**, 146, 211.

6. Boudart, M.; McDonald, M.A., *J. Phys. Chem.* **1984**, 88, 2185; Henrici-Olive, G.; Olive, S., *Angew. Chem. Int. Ed. Engl.* **1976**, 15, 136; Dixit, R.S.; Tavlarides, L.L., *Ind. Eng. Chem. Process Des. Dev.* **1983**, 22, 1.

7. Hills, M.M.; Parmeter, J.E.; Mullins, C.B.; Weinberg, W.H., *J. Am. Chem. Soc.* **1986**, 108, 3554.

8. Parmeter, J.E.; Hills, M.M.; Weinberg, W.H., *J. Am. Chem. Soc.* **1986**, 108, 3563.

9. Parmeter, J.E.; Hills, M.M.; Weinberg, W.H., *J. Am. Chem. Soc.*, in press.

10. Barteau, M.A.; Broughton, J.Q.; Menzel, D., *Appl. Surface Sci.* **1984**, 19, 92 (1984).

11. Barteau, M.A.; Broughton, J.Q.; Menzel, D., *Surface Sci.* **1983**, 133, 443.

12. Shimizu, H.; Christmann, K.; Ertl, G., *J. Catal.* **1980**, 61, 412.

13. Thomas, G.E.; Weinberg, W.H., *J. Chem. Phys.* **1979**, 70, 1437.

14. Pfnür, H.; Menzel, D.; Hoffmann, F. M.; Ortega, A.; Bradshaw, A. M., *Surface Sci.* **1980**, 93, 431.

15. Michalk, G.; Moritz, W.; Pfnür, H.; Menzel, D., *Surface Sci.* **1983**, 129, 92.

16. Pfnür, H.; Feulner, P.; Menzel, D.; *J. Chem. Phys.* **1983**, 79, 2400/4613.

17. Horsley, J.A.; Stöhr, J.; Koestner, R.J., *J. Chem. Phys.* **1985**, 83, 3146.

18. Koestner, R.J.; Van Hove, M.A.; Somorjai, G.A., *J. Chem. Phys.* **1983**, 87, 203.

19. Peebles, D.E.; Schreifels, J.A.; White, J.M., *Surface Sci.* **1982**, 116, 117.

20. These results were confirmed independently in our laboratory.

21. Williams, E.D.; Thiel, P.A.; Weinberg, W.H.; Yates, Jr., J.T., *J. Chem. Phys.* **1980**, 72, 3496.

22. Williams, E.D.; Weinberg, W.H., *Surface Sci.* **1979**, 82, 93.

23. Williams, E.D.; Weinberg, W.H., *J. Vacuum Sci. Tech.* **1982**, 20, 534.

24. Feulner, P.; Menzel, D., *J. Vacuum Sci. Tech.* **1980**, 17, 662.

25. Thomas, G.E.; Weinberg, W.H., *Phys. Rev. Letters* **1978**, 41, 1181.

26. Thomas, G.E.; Weinberg, W.H., *Rev. Sci. Instrum.* **1979**, 50, 497.

27. The bridging CO accounts for approximately 8% of the total concentration of CO, based on the intensities of the CO stretching modes of linear and bridge-bonded CO, and assuming that the dipole derivatives of the CO that is bridge bonded and linearly bonded are equal.

28. Barteau, M.A.; Feulner, P.; Stengl, R.; Broughton, J.Q.; Menzel, D., *J. Catal.* **1985**, 94, 51.

29. Parmeter, J.E.; Hills, M.M.; Weinberg, W.H., in preparation.

30. Note that the high temperature tail in Fig. 1(d) is similar to the tail in the hydrogen thermal desorption spectrum following the adsorption of 0.4 L of $C_2H_4$ on the clean Ru(001) surface, shown in Fig. 1(f).

31. This explanation implies that the precursor to ethylidyne formation is $CCH_2$. Evidence for the existence of this precursor is provided by the combined results of experiments of coadsorbed ethylene and hydrogen and coadsorbed acetylene and hydrogen. This will be discussed in detail elsewhere (**29**).

**Figure Captions**

Figure 1. Thermal desorption spectra of hydrogen after $C_2H_4$ adsorption on the clean and CO precovered Ru(001) surface at 130 K. (a) 1 L of $C_2H_4$; (b) 0.2 L of CO followed by 1 L of of $C_2H_4$; (c) 0.4 L of CO followed by 1 L of of $C_2H_4$; (d) 0.6 L of CO followed by 1 L of of $C_2H_4$; (e) 0.8 L of CO followed by 1 L of of $C_2H_4$; (f) 0.4 L of $C_2H_4$.

Figure 2. Inhibition of ethylene adsorption by deuterium (hydrogen) or CO precoverages. (a) Fractional coverage of chemisorbed $C_2H_4$ as a function of CO precoverage. (b) Fractional coverage of chemisorbed $C_2H_4$ ($C_2D_4$) as a function of deuterium (hydrogen) precoverage.

Figure 3. EEL spectra of ethylene on Ru(001). (a) 4 L of $C_2H_4$ annealed to 120 K; (b) 1 L of $H_2$ followed by 1 L of of $C_2H_4$ annealed to 120 K; (d) 0.6 L of CO followed by 1 L of of $C_2H_4$ annealed to 120 K; (d) 0.6 L of CO followed by 1 L of of $C_2H_4$ annealed to 280 K; (e) 0.6 L of CO followed by 1 L of $C_2H_4$ annealed to 400 K.

Figure 4. The ratio of ethylidyne to acetylide formed from ethylene ($R$) as a function of the saturation coverage of irreversibly chemisorbed ethylene for: (a) $\Delta$ a mixed CO and ethylene overlayer; (b) • ethylene on the clean surface; (c) □ a hydrogen (deuterium) and $C_2D_4$ ($C_2H_4$) overlayer.

Figure 5. Thermal desorption spectra after $C_2H_4$ or $H_2$ adsorption on the clean and hydrogen precovered surfaces at 100 K. (a) $H_2$ thermal desorption following a 1 L expsure of $C_2H_4$; (b) $H_2$ thermal desorption after a 1 L exposure of $H_2$ followed by 1 L of $C_2H_4$; (c) $H_2$ thermal desorption following a 0.4 L exposure of $H_2$; (d) $C_2H_4$ thermal desorption after a 1L exposure of $H_2$ followed by 1 L of $C_2H_4$; (e) $C_2H_6$ thermal desorption after a 1 L exposure of $H_2$ followed by 1 L of $C_2H_4$.

Figure 6. Thermal desorption spectra after a 1 L exposure of $D_2$ followed by 1 L of $C_2H_4$ at 130 K: (a) $H_2$ thermal desorption (c) HD thermal desorption; (c) $D_2$ thermal desorption.

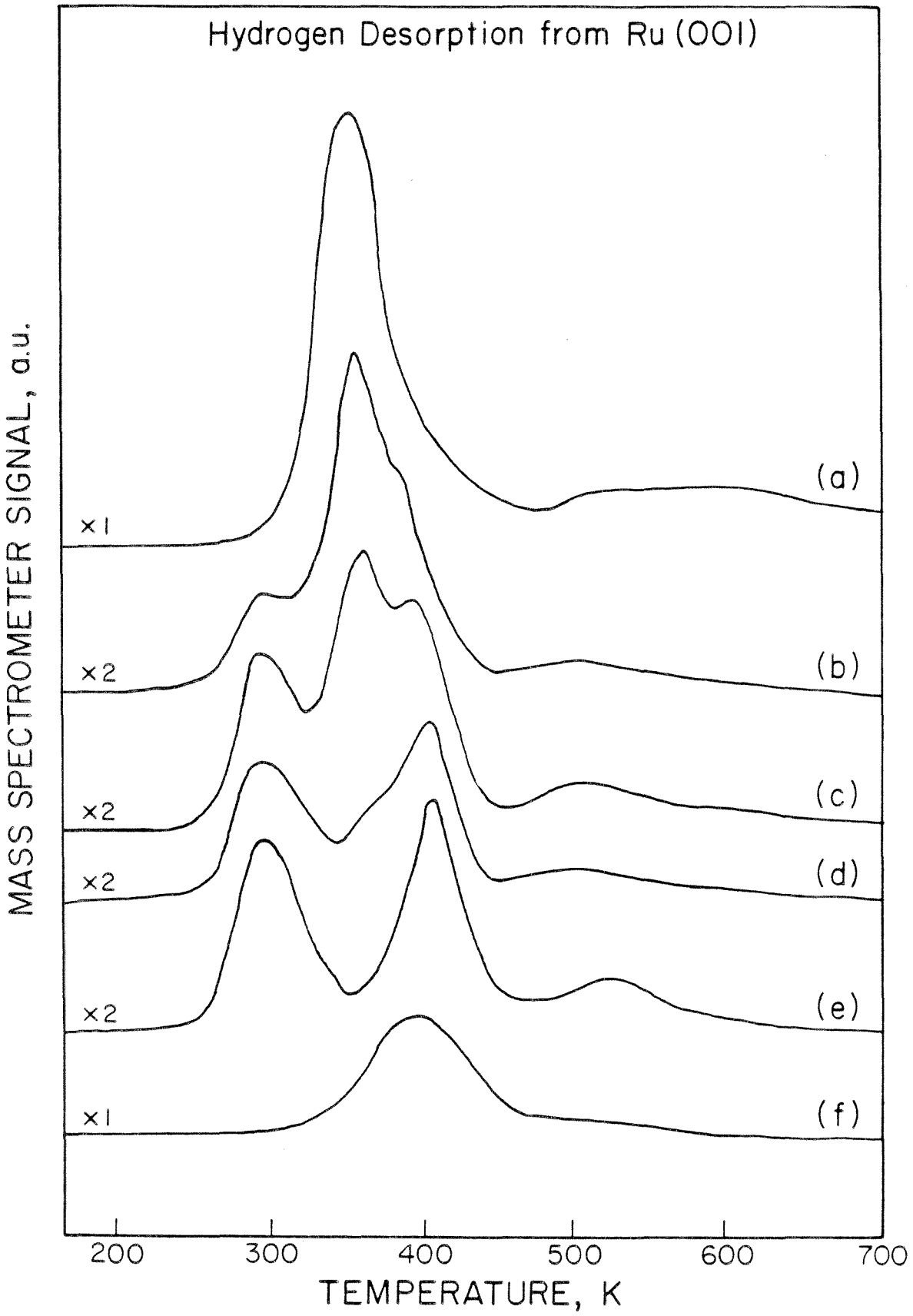
Hydrogen Desorption from Ru (001)
MASS SPECTROMETER SIGNAL, a.u.
×1
×2
×2
×2
×2
×1
(a)
(b)
(c)
(d)
(e)
(f)
200
300
400
500
600
700
TEMPERATURE, K

Figure 1

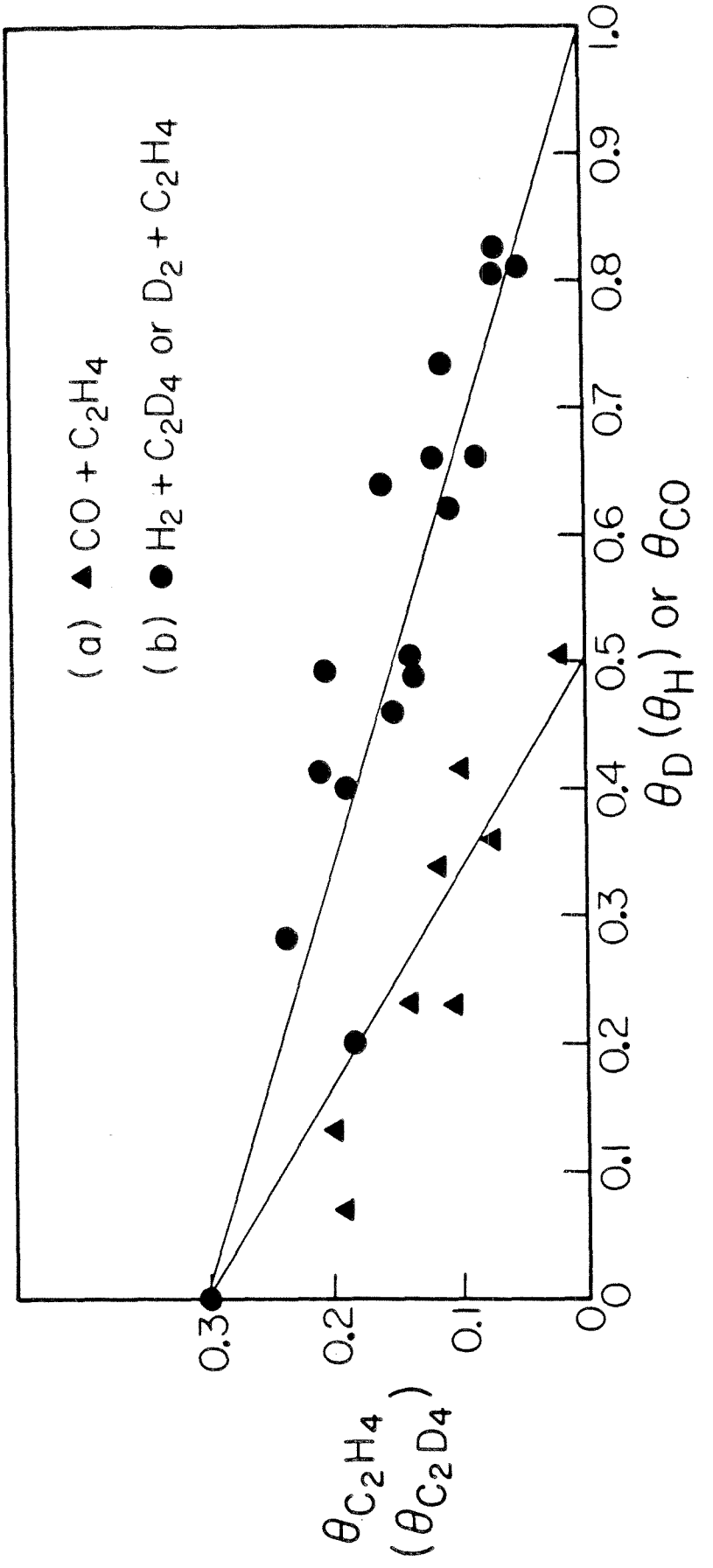
(a) ▲ CO + C2H4
(b) ● H2 + C2D4 or D2 + C2H4
θC2H4 (θC2D4)
θD (θH) or θCO
0.3
0.2
0.1
0
0.1
0.2
0.3
0.4
0.5
0.6
0.7
0.8
0.9
1.0

Figure 2

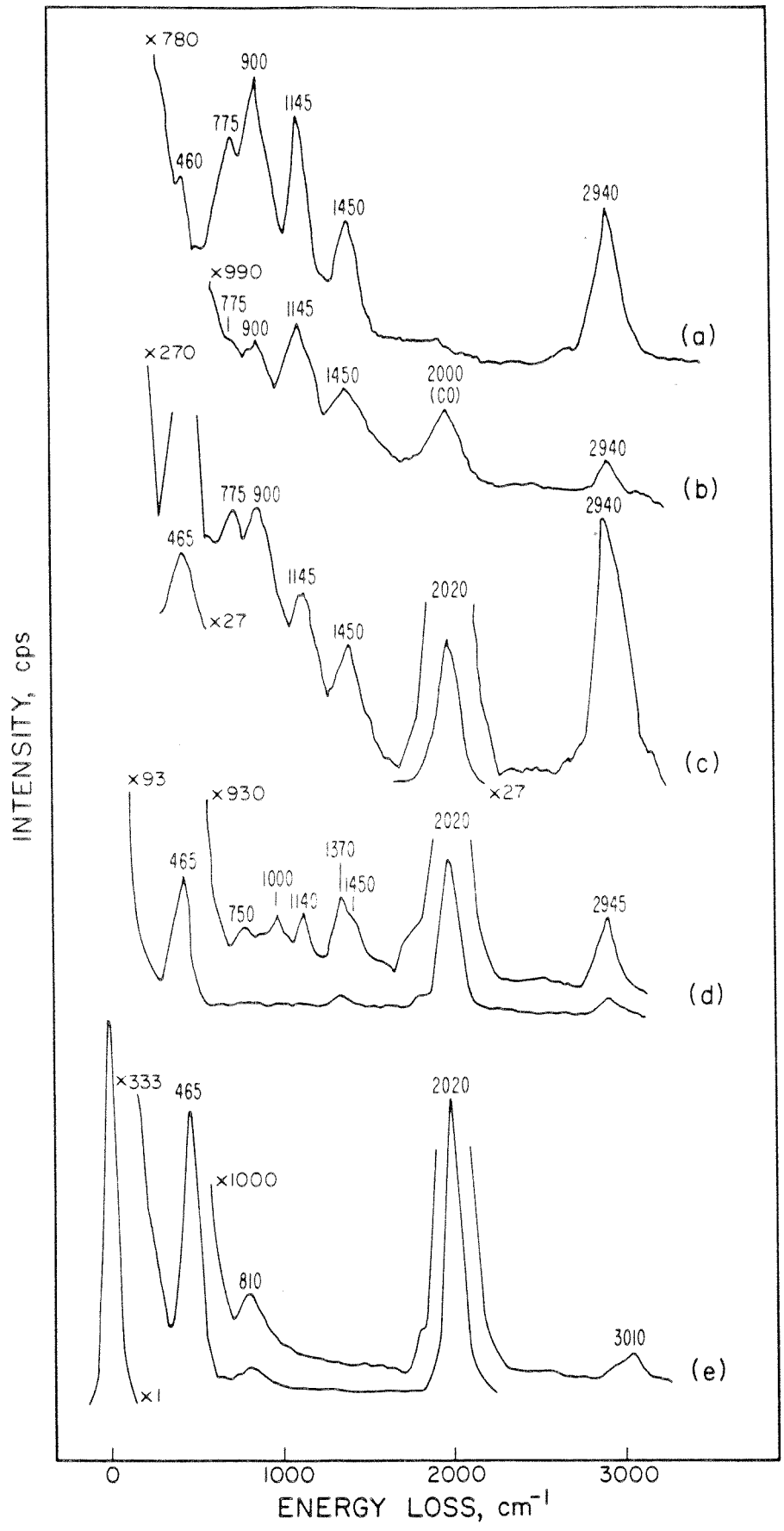
×780
900
1145
775
460
1450
2940
(a)
×990
775
900
1145
1450
2000
(CO)
2940
(b)
×270
775 900
465
1145
2020
2940
×27
1450
(c)
×27
×93
×930
2020
465
1370
1000
1140
1450
750
2945
(d)
×333
465
2020
×1000
810
3010
(e)
×1
INTENSITY, cps
0
1000
2000
3000
ENERGY LOSS, cm⁻¹

Figure 3

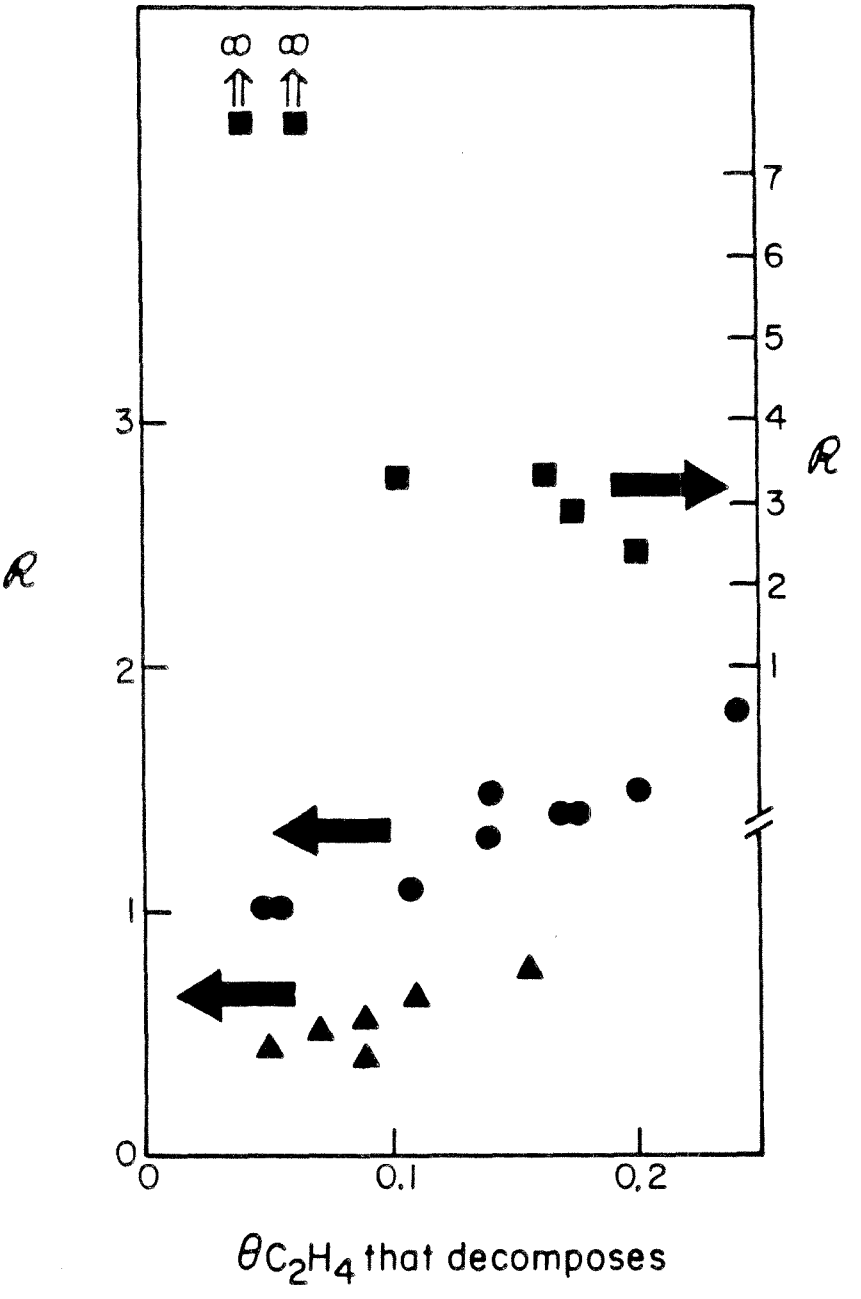


Figure 4

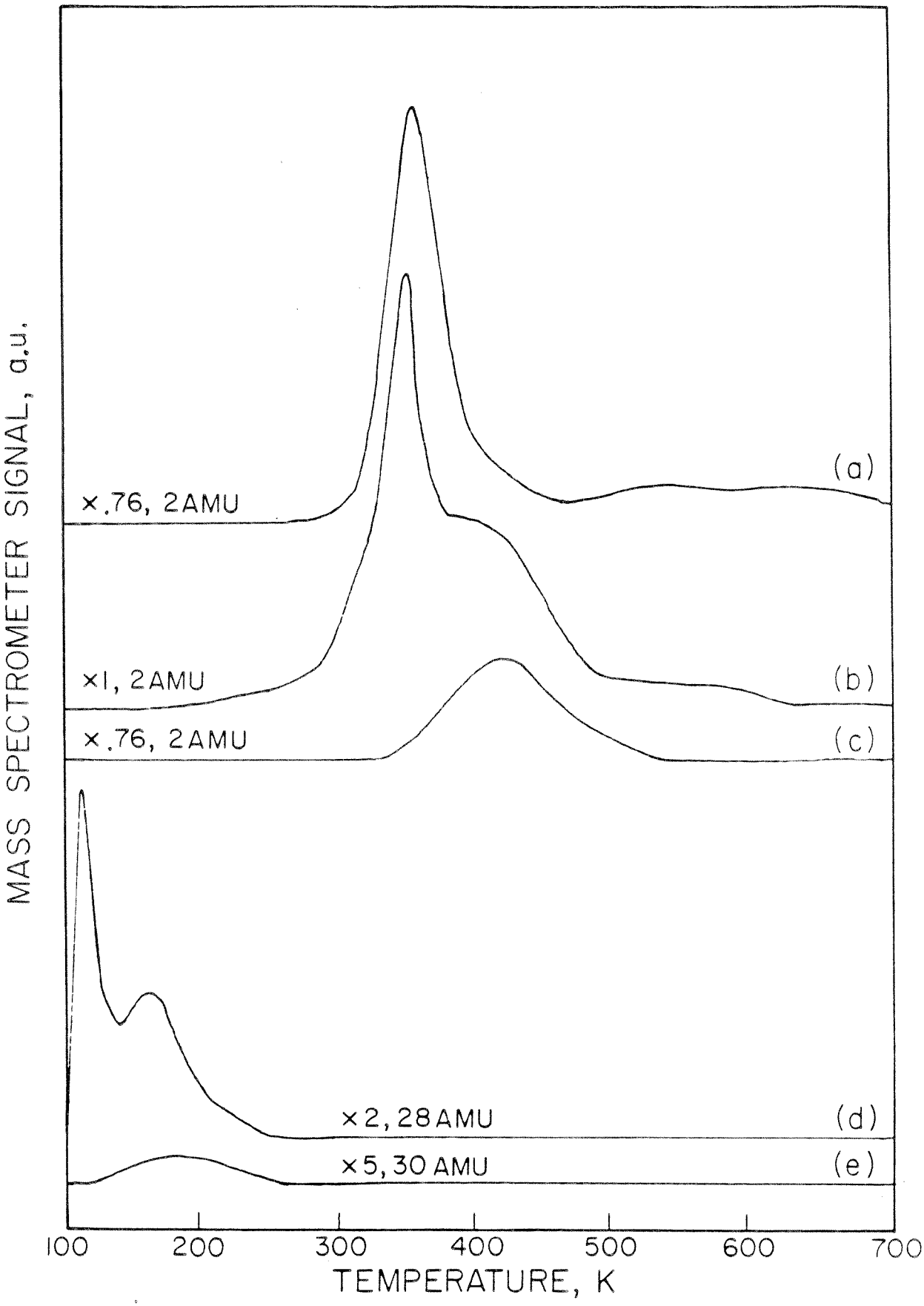
MASS SPECTROMETER SIGNAL, a.u.
×.76, 2AMU
(a)
×1, 2AMU
(b)
×.76, 2AMU
(c)
×2, 28AMU
(d)
×5, 30 AMU
(e)
100
200
300
400
500
600
700
TEMPERATURE, K

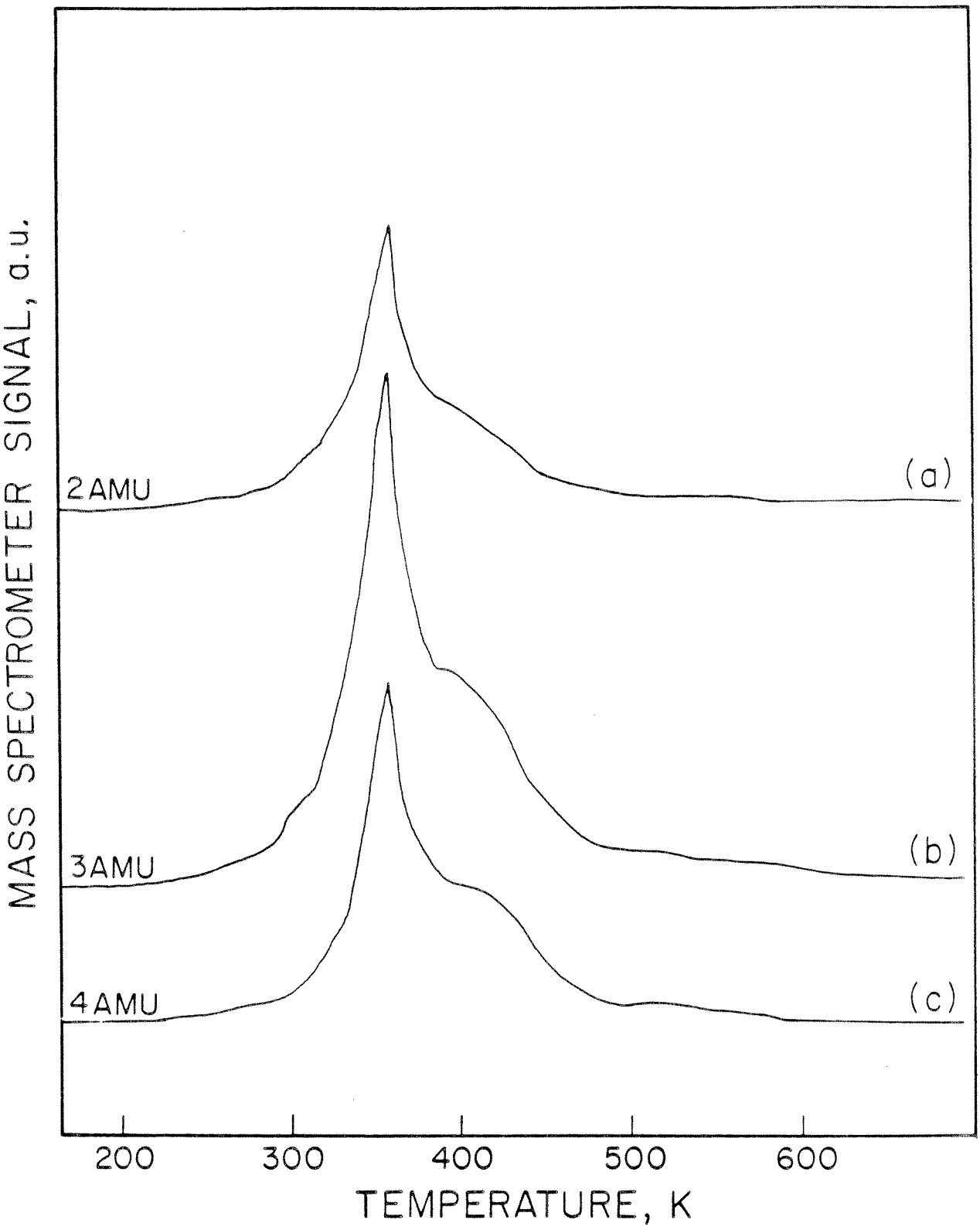
MASS SPECTROMETER SIGNAL, a.u.
2AMU
(a)
3AMU
(b)
4AMU
(c)
200
300
400
500
600
TEMPERATURE, K

Figure 6

# CHAPTER IV

## The Isolation and Characterization of Vinylidene from the Dehydrogenation of Ethylidyne on the Ru(001)-p(2x2)O Surface

[This chapter has been accepted for publication as a Communication by M. M. Hills, J. E. Parmeter and W. H. Weinberg in *The Journal of the American Chemical Society*.]

**Abstract**

The first unambiguous identification of a surface vinylidene species has been observed using high resolution electron energy loss spectroscopy following the thermal decomposition at 250 K of ethylidyne that was formed from π-bonded ethylene on the Ru(001)-p(2x2)O surface. This is also the first observation of the partial dehydrogenation of adsorbed ethylidyne that does not involve carbon-carbon bond cleavage as well. The carbon atoms of the vinylidene are very nearly $sp^2$–hybridized, and the vinylidene is tilted with respect to the surface normal since π-electron donation from the carbon-carbon double bond to the surface is observed. Decomposition of the vinylidene to methylidyne and surface carbon occurs above 350 K with simultaneous evolution of hydrogen.

Although the structure and bonding of a variety of adsorbed species on transition metal surfaces have been compared to those of similar ligands in homogeneous metal compounds, the chemical reactions which these two entities undergo have not been related. This connection represents the logical and necessary next step in relating the organometallic chemistry of homogeneous compounds with that of extended surfaces, i.e. the relationship between homogeneous catalysis by organometallic compounds and heterogeneous catalysis by metallic surfaces. It has been found that ethylene reacts with $Os_3(CO)_{12}$ to form a μ-vinylidene complex, $H_2Os_3(CO)_9(CCH_2)$, which can be hydrogenated to a μ-ethylidyne complex, $H_3Os_3(CO)_9(CCH_3)$ (**1-3**). Similarly, ethylene adsorbed on the hexagonal Ru(001) (**4**), Pt(111) (**5**), Pt(100) (**6,7**), Pd(111) (**9**) and Rh(111) (**10**) surfaces at room temperature forms ethylidyne, which dehydrogenates at higher surface temperatures. However, vinylidene has been neither isolated nor unambiguously identified as an intermediate in either the formation or the decomposition of adsorbed ethylidyne (**11**). This communication reports the first conclusive spectroscopic identification of adsorbed vinylidene, which was observed following the annealing of adsorbed ethylidyne on the Ru(001)-p(2x2)O surface (**12**).

The high resolution electron energy loss spectroscopic (EELS) measurements were carried out in an ultrahigh vacuum system that has been described in detail previously (**14**). The p(2x2) oxygen overlayer on the Ru(001) surface, which is depicted in Fig. 1(a), corresponds to a fractional surface coverage of atomic oxygen of 0.25. The existence of this ordered overlayer was confirmed by EEL spectra, which exhibit a $\nu_{\perp}$(Ru-O) mode at 535 $cm^{-1}$ and a phonon mode characteristic of the ordered overlayer at 250 $cm^{-1}$ (**15**).

Exposure of the Ru(001)-p(2x2)O surface to ethylene at temperatures below 240 K results in the adsorption of π-bonded molecular ethylene (**13,16**). Upon annealing to 250 K, the π-bonded ethylene reacts to form chemisorbed ethylidyne with the desorption of hydrogen. The ethylidyne is identified by intense ν(CC) and $\delta_s(CH_3)$ modes at 1140 and 1370 $cm^{-1}$ (1150 and 1000 $cm^{-1}$ for $CCD_3$), which are evident in the EEL spectra of Fig. 1(b) and (c) (**17**).

Upon heating to approximately 350 K, the ethylidyne reacts quantitatively to form vinylidene with simultaneous evolution of hydrogen. The EEL spectra of adsorbed vinylidene are shown in Fig.

1(d) and (e). The intense feature at 1435 $cm^{-1}$ in Fig. 1(d) is due to the overlapping ν(CC) and $\delta(CH_2)$ modes of $CCH_2$. The $\delta(CD_2)$ mode shifts to 1010 $cm^{-1}$ in the deuterated spectrum [Fig. 1(e)], permitting the observation of the ν(CC) mode of $CCD_2$ at 1350 $cm^{-1}$. The modes of the adsorbed vinylidene are assigned and compared to those of vinylidene in $H_2Os_3(CO)_9(CCH_2)$ in Table 1. The excellent agreement between the vibrational frequencies of the vinylidene ligand and the adsorbed vinylidene suggests that the bonding of the two is quite similar. An X-ray crystallographic structural determination of the triosmium cluster has shown that the $CCH_2$ ligand is bridge-bonded to two osmium atoms, that the carbon-carbon bond length of 1.38 Å is only slightly elongated from that of gaseous ethylene (1.34 Å), and that there is π-electron donation from the carbon-carbon double bond to the third osmium atom (**1-3**). The carbon-carbon bond length of the vinylidene ligand suggests that the carbon atoms are nearly $sp^2$–hybridized, and due to the good agreement between the ν(CC) modes of the vinylidene ligand and the adsorbed vinylidene, the carbon atoms of the latter are also expected to be nearly $sp^2$–hybridized. The frequency of the ν(CC) mode of the adsorbed $CCH_2$ is lowered from that of $CH_2CBr_2$ [1593 $cm^{-1}$ (**18**) and that of the μ–vinylidene ligand in $Cp_2Mn_2(CO)_4(CCH_2)$ [1542 $cm^{-1}$ (19)] due to π-electron donation from the carbon-carbon bond of the vinylidene to the ruthenium surface upon which the p(2x2) oxygen overlayer is present. This π-electron donation implies that the adsorbed vinylidene is tilted with respect to the surface normal, as is observed in $H_2Os_3(CO)_9(CCH_2)$.

Annealing the adsorbed vinylidene to 400 K initiates decomposition to methylidyne (identified by EELS) and surface carbon with simultaneous evolution of hydrogen, and the methylidyne decomposes above 500 K, creating additional surface carbon and evolving hydrogen (**13**). Hydrogen thermal desorption spectra are also consistent with this decomposition mechanism. These spectra show that half of the total amount of hydrogen desorbs below 350 K, indicating that the species present on the surface at this temperature has a stoichiometry of $C_2H_2$. Another quarter of the hydrogen desorbs in a peak centered at 400 K in accordance with the decomposition of vinylidene to methylidyne. The final quarter of the hydrogen desorbs between 500 and 700 K as the methylidyne decomposes.

In contrast to the formation of vinylidene from ethylidyne (**20**) and the subsequent decomposition of vinylidene to methylidyne on the Ru(001)-p(2x2)O surface, ethylidyne decomposes completely near

355 K to carbon and hydrogen on the Ru(001) surface (**4,21**). The fact that methylidyne is a stable intermediate in the decomposition of ethyidyne on the Ru(001)-p(2x2)O surface, while it is not on the Ru(001) surface, implicates the existence of different mechanisms of the decomposition reactions on the two surfaces. On Ru(001), $sp^3$ hybridization and σ-bonding to the surface are favored, whereas on Ru(001)-p(2x2)O $sp^2$ hybridization and π-donation to the surface are favored, as judged, for example, by the di-σ-bonded and π-bonded molecularly adsorbed ethylene that is observed on the respective surfaces. Hence, the π-bonded vinylidene that was isolated on the Ru(001)-p(2x2)O surface is unlikely to be an (unstable) intermediate in ethylidyne decomposition on Ru(001), although a different, more nearly $sp^3$-hybridized, vinylidene may well be involved (**22**).

To summarize, adsorbed vinylidene has been isolated following the decomposition of ethylidyne on the Ru(001)-p(2x2)O surface at 350 K. The bonding of the adsorbed vinylidene is analogous to that of the vinylidene ligand in $H_2Os_3(CO)_9(CCH_2)$, with very nearly $sp^2$–hybridized carbon atoms and tilting of the vinylidene with respect to the surface normal due to π-electron donation from the carbon-carbon double bond to the surface. Indeed, the formation of vinylidene from adsorbed ethylidyne is analogous to the reverse of the hydrogenation reaction of $H_2Os_3(CO)_9(CCH_2)$ to $H_3Os_3(CO)_9(CCH_3)$. The decomposition of ethylidyne to vinylidene on the Ru(001)-p(2x2)O surface differs from the decomposition mechanism of ethylidyne on the Ru(001) surface due to electronic perturbations of the ruthenium surface by the ordered oxygen overlayer. These perturbations are also manifest in the observed π-bonding of molecular ethylene at 200 K, as opposed to the di-σ-bonded molecular ethylene that is observed on the Ru(001) surface.

**Acknowledgment:** This work was supported by the National Science Foundation under Grant no. CHE-8516615.

**References**


[1] Deeming, A.J.; Underhill, M., *J.C.S. Chem. Comm.* **1983**, 277.

[2] Deeming, A.J.; Underhill, M., *J.C.S. Dalton Trans.* **1974**, 1415.

[3] Andrews, J.R.; Kettle, S.F.A.; Powell, D.B.; Sheppard, N., *Inorg. Chem.* **1982**, 21, 2874.

[4] Hills, M.M.; Parmeter, J.E.; Mullins, C.B.; Weinberg, W.H., *J. Am. Chem. Soc.* **1986**, 108, 3554.

[5] Steininger, H.; Ibach, H.; Lehwald, S., *Surface Sci.* **1982**, 117, 685.

[6] Ibach, H. in: *Proc. Conf. on Vibrations in Adsorbed Layers*, Jülich, 1978.

[7] The Pt(100) surface reconstructs to a slightly buckled, close-packed (5x20) superstructure (8).

[8] Heilman, P.; Heinz, K.; Müller K., *Surface Sci.* **1979**, 83, 487.

[9] Gates, J.A.; Kesmodel, L.L., *Surface Sci.* **1983**, 124, 68.

[10] Koel, B.E.; Bent, B.E.; Somorjai, G.A., *Surface Sci.* **1984**, 146, 211.

[11] Indeed, *no intermediate* has been observed in the reaction of molecularly adsorbed ethylene to ethylidyne. Likewise, no intermediate in the decomposition of adsorbed ethylidyne has been observed heretofore in which carbon-carbon bonding is preserved.

[12] The ethylidyne is a stable intermediate in the dehydrogenation of $\pi$-bonded, molecular ethylene on the Ru(001) surface on which an ordered p(2x2) overlayer of oxygen adatoms is present (13).

[13] Hills, M.M.; Parmeter, J.E.; Weinberg, W.H., in preparation.

[14] Thomas, G.E.; Weinberg, W.H., *Rev. Sci. Instrum.* **1979**, 50, 497.

[15] Rahman, T.S.; Anton, A.B.; Avery, N.R.; Weinberg, W.H., *Phys. Rev. Lett.* **1983**, 51, 1979.

[16] The nature of this chemisorption bond is very different from that of the di-$\sigma$-adsorbed ethylene on the clean Ru(001) surface (**4**).

[17] A detailed discussion of the assignment of all the observed vibrational modes of adsorbed ethylidyne has been presented elsewhere (**4**).

[18] De Hemptinne, M., *Trans. Faraday Soc.* **1946**, 42, 5.

[19] Folting, K.; Huffman, J.C.; Lewis, L.N.; Coulton, K.G., *Inorg. Chem.* **1979**, 18, 3483.

[20] The observation of ethylidyne decomposition to vinylidene, but not the reverse reaction, is a consequence of the negligible coverage of hydrogen on the surface at the temperatures at which vinylidene is stable. The recombinative desorption of hydrogen occurs below 220 K on the Ru(001)-p(2x2)O surface.

[21] On the Ru(001) surface, ethylene also reacts to form acetylide (CCH), which decomposes to methylidyne at 360 K. The methylidyne dehydrogenates between 500 and 700 K (4).

[22] Weinberg, W.H.; Parmeter, J.E.; Hills, M.M., in preparation.

**Table 1.** Comparison of vibrational frequencies (in $cm^{-1}$) of vinylidene on the Ru(001)-p(2x2)O surface with $Os_3H_2(CO)_9(CCH_2)$.

| Mode | $CCH_2$ on Ru(001)-p(2x2)O | $CCD_2$ on Ru(001)-p(2x2)O | $Os_3H_2(CO)_9(CCH_2)$ (3) |
|---|---|---|---|
| $\nu$(RuC) | 455 | 435 | 255-311 |
| $\tau(CH_2)$ or $\tau(CD_2)$ | n.r. | n.r. | 808 |
| $\omega(CH_2)$ or $\omega(CD_2)$ | 895 | 700 | 959 |
| $\rho(CH_2)$ or $\rho(CD_2)$ | 965 | n.r. | 1048 |
| $\delta(CH_2)$ or $\delta(CD_2)$ | 1435 | 1010 | 1328 |
| $\nu$(CC) | 1435 | 1350 | 1467 |
| $\nu_s(CH_2)$ or $\nu_s(CD_2)$ | 2985 | 2180 | 2990 |
| $\nu_a(CH_2)$ or $\nu_a(CD_2)$ | 3050 | 2290 | 3052 |

n.r. = not resolved.

**Figure Caption**

Fig. (a) The unit cell and basis of the p(2x2) ordered oxygen overlayer on the Ru(001) surface. The EEL spectra that result from 2 L exposures of (b), (d) $C_2H_4$ and (c), (e) $C_2D_4$ on the Ru(001)-p(2x2)O surface at 80 K and heated to:(b), (c) 250 K and (d), (e) 350 K. The intense peak at 535 $cm^{-1}$ in all spectra is due to the $\nu_{\perp}$(Ru-O) mode of the p(2x2) oxygen overlayer. The peak at 2025 $cm^{-1}$ in spectrum (e) is due to the $\nu$(C≡O) mode of a small amount ($\theta_{CO} < 0.01$) of coadsorbed carbon monoxide.

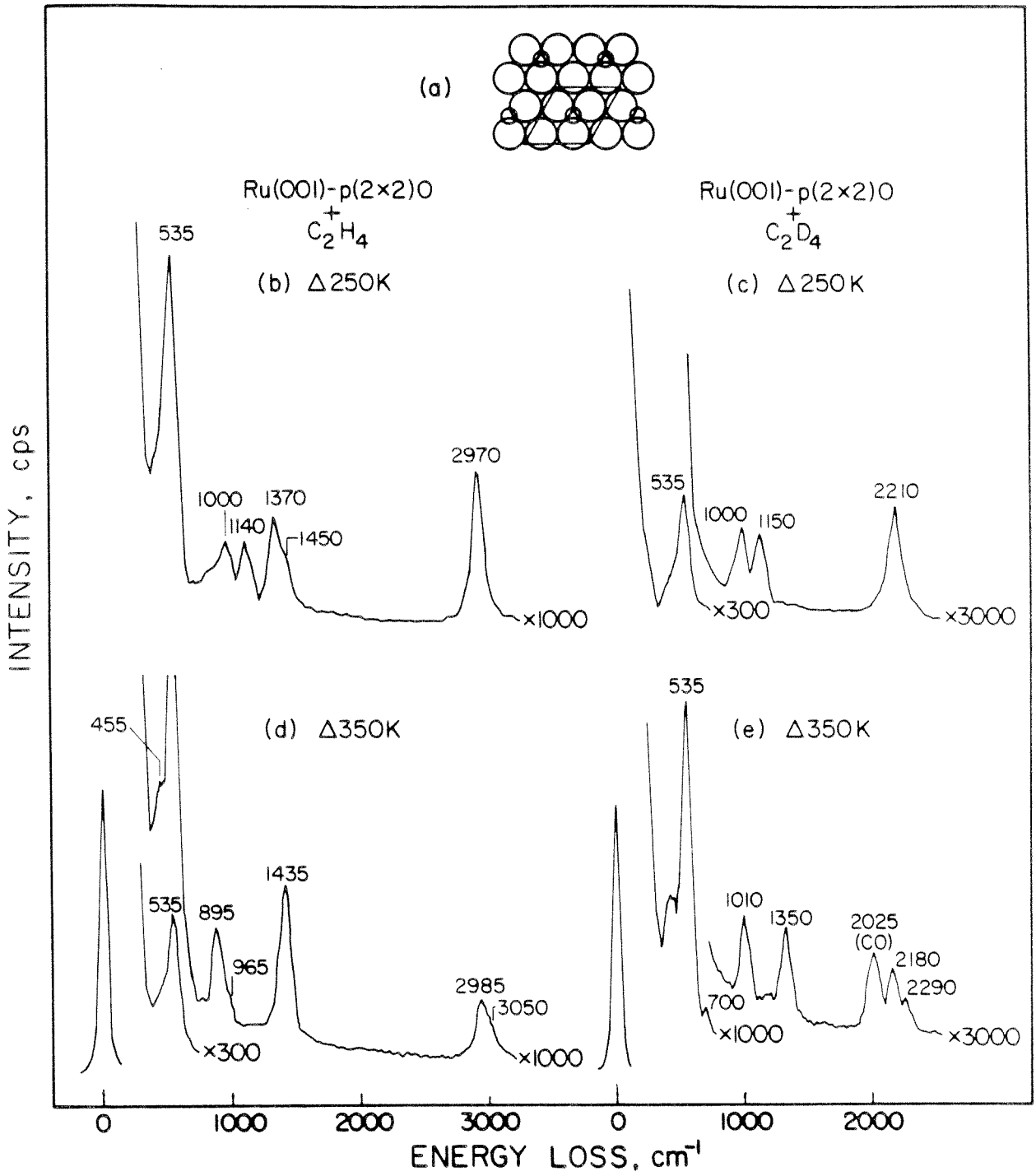
(a)
Ru(001)-p(2×2)O
+
$C_2H_4$
(b) Δ250K
535
1000
1140
1370
1450
2970
×1000
Ru(001)-p(2×2)O
+
$C_2D_4$
(c) Δ250K
535
1000
1150
2210
×300
×3000
(d) Δ350K
455
535
895
965
1435
2985
3050
×300
×1000
(e) Δ350K
535
700
1010
1350
2025
(CO)
2180
2290
×1000
×3000
INTENSITY, cps
0
1000
2000
3000
0
1000
2000
ENERGY LOSS, $cm^{-1}$

# CHAPTER V

## The Coadsorption and Reaction of Ethylene on Chemically Modified Ru(001) Surfaces

**Abstract**

The adsorption and reaction of ethylene on a Ru(001) surface on which ordered p(2x2) and p(1x2) overlayers of oxygen adatoms are present have been investigated using high-resolution electron energy loss spectroscopy, thermal desorption mass spectrometry and low-energy electron diffraction. In contrast to the di-σ-bonded ethylene that is observed on clean Ru(001), ethylene chemisorbs molecularly in a π-bonded configuration at temperatures below 200 K on both the Ru(001)-p(2x2)O and Ru(001)-p(1x2)O surfaces. All of the ethylene that is chemisorbed on Ru(001)-p(1x2)O desorbs reversibly at 160 and 240 K, whereas approximately one-third of the ethylene on the Ru(001)-p(2x2)O surface desorbs molecularly at these temperatures. Upon annealing to 250 K, the irreversibly adsorbed ethylene on the Ru(001)-p(2x2)O surface dehydrogenates to ethylidyne ($CCH_3$), which dehydrogenates further to vinylidene ($CCH_2$) below 350 K. This represents the first unambiguous identification of a surface vinylidene species, as well as the first isolation of an intermediate in the decomposition of surface ethylidyne that preserves carbon-carbon bonding. The vinylidene decomposes to adsorbed carbon and methylidyne (CH) below 400 K, and the methylidyne decomposes with the evolution of hydrogen between 500 and 700 K.

## I. Introduction

Recent spectroscopic investigations of the interaction of ethylene and acetylene with the Ru(001) surface have revealed both the nature of the molecularly chemisorbed species and the decomposition products of these unsaturated hydrocarbons (**1,2**). Coadsorption experiments of hydrogen with ethylene, carbon monoxide with ethylene, and hydrogen with acetylene have clarified further the decomposition mechanisms (**3,4**). The combined results of these studies (**5**) have led to the following mechanistic picture (**1-5**): (1) Both ethylene and acetylene chemisorb molecularly below 150 K on the Ru(001) surface, with rehybridization of the carbon atoms to nearly $sp^3$ occurring; (2) Upon heating to between 150 and 280 K, both ethylene and acetylene form a $HCCH_2$ species, while acetylene also forms acetylide (CCH) at these temperatures; (3) The $HCCH_2$ species reacts rapidly to form acetylide and ethylidyne ($CCH_3$); (4) The ethylidyne decomposes to carbon adatoms and hydrogen near 350 K, while the acetylide decomposes via carbon-carbon bond cleavage near 380 K, forming methylidyne (CH) and carbon adatoms; and (5) The methylidyne dehydrogenates, evolving hydrogen above approximately 500 K.

We report here the results of a study of the interaction of ethylene with Ru(001) surfaces on which preadsorbed overlayers of dissociatively adsorbed oxygen are present. We have concentrated on the reproducible and well-characterized Ru(001)-p(2x2)O and Ru(001)-p(1x2)O surfaces, although we have also examined the effects of disordered oxygen overlayers, the fractional coverages of which varied from approximately 0.05 to 0.5. The p(2x2)O overlayer corresponds to a fractional surface coverage of oxygen adatoms of 0.25, while the p(1x2)O overlayer consists of three independent domains that are rotated by 120° with respect to one another and corresponds to a fractional surface coverage of oxygen adatoms of 0.5 (**6,7**). These two structures are shown schematically in Figs. 1(a) and (b). As may be seen in Figs. 1(c) and (d), electron energy loss (EEL) spectra of the p(2x2)O overlayer exhibit a $\nu_s$(RuO) mode at 535 $cm^{-1}$ and a surface phonon at 250 $cm^{-1}$ (**7**). Similarly, EEL spectra of the p(1x2)O overlayer exhibit a $\nu_s$(RuO) mode at 585 $cm^{-1}$, a surface phonon at 240 $cm^{-1}$, and a $\nu_a$(RuO) mode at 430 $cm^{-1}$ (**7**). It is these spectroscopic signatures that render reproducible the synthesis of these two well-characterized surfaces.

There are several important reasons for our interest in this system. Oxygen overlayers increase

the effective "Lewis acidity" of transition metal surfaces, i.e. the propensity of the surface metal atoms to accept electrons is increased. The extent of charge transfer from the ruthenium to the oxygen adatoms of the p(2x2)O overlayer can be estimated using the observed change in the work function of +0.20 eV following the adsorption of oxygen into the p(2x2) overlayer (**6**) [making use of the previously determined ruthenium-oxygen bond length (**7**), and assuming that depolarization effects are negligible]. It is found that approximately 0.03 electron is transferred from the ruthenium to each oxygen adatom of the overlayer. Similarly, it is estimated that approximately 0.04 electron is transferred from the ruthenium to each oxygen adatom of the p(1x2) overlayer, using the measured change in the work function of +0.80 eV and correcting for depolarization effects. This charge transfer increases the separation between the Fermi level of the ruthenium surface and the $\pi^*$-orbital of ethylene, and this transfer could result in the adsorption of $\pi$-bonded ethylene on the oxygen precovered ruthenium surface by inhibiting backdonation into the $\pi^*$-orbital. For example, the preadsorption of oxygen on Pd(100), Fe(111) and Pt(111) induces the formation of $\pi$-bonded molecular ethylene, as opposed to the di-$\sigma$-bonded ethylene observed on the clean surfaces (**8-10**). Furthermore, the charge transfer from the ruthenium to the oxygen weakens both the metal-carbon and metal-hydrogen bonding and therefore could result in the formation of different intermediates in the ethylene decomposition reaction, possibly, although not necessarily, via the formation of oxygen-containing intermediates. Finally, the coadsorption of oxygen and ethylene permits a quantification of the extent of poisoning of molecular chemisorption of ethylene by both ordered and disordered oxygen overlayers, as well as the reduction in the extent of ethylene decomposition compared to the reduced (clean) surface.

## II. Experimental Procedures

Thermal desorption mass spectrometry and low-energy electron diffraction (LEED) measurements were carried out in an ultrahigh vacuum (UHV) apparatus that has been described in detail previously (**11**). Briefly, the chamber is pumped by both a 220 l/s noble ion pump and a titanium sublimation pump, which reduce the base pressure to below $10^{-10}$ Torr. The crystal is cooled to below 100 K with liquid nitrogen, and linear heating rates of the crystal of 5-20 K/s are achieved via resistive heating controlled by a power supply that is interfaced with an LSI-11 DEC laboratory computer. This UHV

chamber contains a UTI-100C quadrupole mass spectrometer enclosed in a glass envelope for selective sampling of gases that desorb from only the well-oriented front surface of the single crystal (12). Low-energy electron diffraction optics and a rotatable Faraday cup are available for the display of LEED patterns and the measurement of LEED beam profiles. A single-pass cylindrical mirror electron energy analyzer with an integral electron gun is available for Auger electron spectroscopy.

A second UHV chamber was used to conduct high-resolution electron energy loss spectroscopic (EELS) measurements. This chamber also has a base pressure below $10^{-10}$ Torr using similar pumping techniques, and liquid nitrogen cooling and resistive heating of the crystal were similarly employed. The home-built Kuyatt-Simpson type EEL spectrometer has been described in detail elsewhere (13,14). It was operated such that the kinetic energy of the electron beam incident upon the crystal was approximately 4 eV, at an angle of incidence of 60° with respect to the surface normal. The spectra were measured with a resolution of 60-80 $cm^{-1}$ (full-width at half-maximum of the elastically scattered peak), while maintaining a count rate of 1-3 $\times$ $10^5$ cps in the elastic channel. This UHV chamber also contains a quadrupole mass spectrometer, but it was not, in general, employed in the thermal desorption measurements reported here.

The techniques used for orienting, cutting, polishing and mounting the Ru(001) crystals have been described previously (13,14). The crystals were cleaned using periodic argon ion sputtering and routine annealing to 1000 K in 7 $\times$ $10^{-8}$ Torr of $O_2$, followed by annealing to 1700 K *in vacuo*. Surface cleanliness was monitored in the two UHV chambers by Auger electron spectroscopy, EELS and hydrogen thermal desorption.

Research purity (99.98% min.) oxygen ($^{16}O_2$) and C.P. grade (99.5%) ethylene were obtained from Matheson. The ethylene was purified further by three freeze-thaw-pump cycles. Research purity (99.98% min. oxygen, 99% $^{18}O_2$) isotopically labeled oxygen was obtained from Merck and Co. The purity of all gases was verified *in situ* by mass spectrometry in both chambers. Gas exposures are reported in units of Langmuirs, where 1 Langmuir = 1L $\equiv$ $10^{-6}$ Torr-s. The quoted exposures have not been corrected for the relative ionization probabilities of the different gases.

## III. Results

### A. Molecularly Chemisorbed Ethylene on the Ru(001)-p(2x2)O and Ru(001)-p(1x2)O Surfaces

The ordered p(2x2) and p(1x2) oxygen overlayers were synthesized on the Ru(001) surface by exposing the crystal at 90 K to 0.8 and 3 L of $O_2$, respectively, followed by annealing to 400 K. The existence of these ordered overlayers was verified both by LEED (**6**) and by EELS (**7**), and their structures are shown in Fig. 1, together with the corresponding EEL spectra.

Exposure of the Ru(001)-p(2x2)O and Ru(001)-p(1x2)O surfaces at 80 K to 2 L or more of ethylene gives rise to a molecular multilayer that is identical to that observed on the clean surface (**1**). This multilayer desorbs at 115 K, leaving a chemisorbed overlayer composed of the oxygen adatoms and $\pi$-bonded molecular ethylene. Submonolayer coverages of ethylene adsorbed at 80 K are also $\pi$-bonded. Low-energy electron diffraction patterns of these overlayers of molecularly chemisorbed ethylene continue to exhibit the indistinguishable p(2x2) and p(1x2) superstructures due to the oxygen adatoms. Figures 2(a) and (b) are EEL spectra of $C_2H_4$ and $C_2D_4$ coadsorbed with the p(1x2)O overlayer at 80 K and annealed to 200 K, while Figs. 2(c) and (d) are EEL spectra of $C_2H_4$ and $C_2D_4$ coadsorbed with the p(2x2)O overlayer at 80 K and annealed to 200 K. These spectra indicate that $\pi$-bonded molecular ethylene is formed on both surfaces. The intense $\nu_s$(RuO) mode appears at 585 $cm^{-1}$ in Figs. 2(a) and (b) and at 535 $cm^{-1}$ in Figs. 2(c) and (d). The $\nu_a$(RuO) mode is not resolved from the $\nu_s$(RuO) mode in Figs. 2(a) and (b), nor are the surface phonons resolved from the elastic peak in Figs. 2(a), (c) and (d). The peaks in the spectra of Fig. 2 that are due to $\pi$-bonded ethylene are assigned as follows. The intense feature at 950 $cm^{-1}$ (695 $cm^{-1}$ for $C_2D_4$) is the $CH_2$ ($CD_2$) wagging mode. The peak at 3040 $cm^{-1}$ in Figs. 2(a) and (c) is the symmetric carbon-hydrogen stretching mode from which the asymmetric stretching mode was not resolved. These modes were resolved in the EEL spectra of deuterated ethylene [cf. Figs. 2(b) and (d)], with $\nu_s(CD_2)$ observed at 2220 $cm^{-1}$ and $\nu_a(CD_2)$ at 2300 $cm^{-1}$. The frequencies of the carbon-hydrogen (carbon-deuterium) stretching modes as well as the $CH_2$ ($CD_2$) wagging modes are indicative of nearly $sp^2$-hybridized carbon atoms in the adsorbed ethylene. The modes at 1245 and 1520 $cm^{-1}$ in the EEL spectra of chemisorbed $C_2H_4$ are the strongly coupled

$CH_2$ scissoring and carbon-carbon stretching modes. The $CD_2$ scissoring and carbon-carbon stretching modes are essentially uncoupled in the spectra of deuterated ethylene and occur at 975 and 1350 $cm^{-1}$, respectively. The frequency of the $\nu$(CC) mode in the spectra of deuterated ethylene indicates that this species is $\pi$-bonded to the surface. The strong coupling of the $CH_2$ scissoring and carbon-carbon stretching modes in the $\pi$-bonded $C_2H_4$ is in agreement with the observed coupling of these modes of $C_2H_4$ in Zeise's salt **(15,17,18)**. Although not resolved from the ruthenium-oxygen stretching mode in Figs. 2(a)-(d), the $\nu$(Ru-$C_2H_4$) mode was observed at 440 $cm^{-1}$ in EEL spectra measured 10° off-specular, in which the $\nu_s$(RuO) mode exhibits a much lower intensity due to its largely dipolar character and strong dynamic dipole and in which the elastic peak has also decreased in intensity.

These mode assignments are compared in Table 1 to those of multilayer and di-$\sigma$-bonded ethylene on Ru(001), $C_2H_4$(g), Zeise's salt, and $\pi$-bonded, molecularly chemisorbed ethylene on other Group VIII transition metal surfaces **(1,8-10,15,16,18)**. These comparisons confirm that molecularly chemisorbed ethylene on both Ru(001)-p(2x2)O and Ru(001)-p(1x2)O is $\pi$-bonded to the surfaces and that the carbon atoms of the ethylene are very nearly $sp^2$-hybridized, as judged by the frequencies of the $\nu_s(CH_2)$, $\nu_s(CD_2)$, $\nu_a(CD_2)$ and $\nu$(CC) (of $C_2D_4$) modes, as well as the good agreement of all mode assignments with those of Zeise's salt, a paradigm of $\pi$-bonded ethylene. On the other hand, the carbon atoms of di-$\sigma$-bonded ethylene on the Ru(001) surface are almost completely rehybridized to $sp^3$, as judged by the significantly lower frequencies of the carbon-carbon and carbon-hydrogen stretching modes, and the upshifts in the $CH_2$ and $CD_2$ wagging modes.

Annealing the $\pi$-bonded ethylene on the Ru(001)-p(1x2)O surface above 240 K results in the reversible molecular desorption of all of the ethylene. This was demonstrated both by EEL spectra that were measured following the annealing of adsorbed ethylene overlayers to 240 K, which exhibited only the $\nu_s$(RuO), $\nu_a$(RuO) and phonon modes as in Fig. 1(d), and by thermal desorption spectra of these overlayers that showed only the desorption of molecularly chemisorbed ethylene in a shoulder and a peak centered at 160 and 240 K, respectively, and the desorption of the molecular ethylene multilayer at 115 K [cf. Fig. 3(a)]. The fractional saturation coverage of ethylene chemisorbed on Ru(001)-p(1x2)O was estimated to be 0.10 from the ethylene thermal desorption spectra. The activation energy

of desorption (equal to the heat of adsorption since the adsorption is unactivated) of ethylene desorbing in the 160 K peak is approximately 9.8 ± 1 kcal/mole, and that of ethylene desorbing in the 240 K peak is approximately 14.0 ± 1 kcal/mole, assuming preexponential factors of the desorption rate coefficients of $10^{13}$–$10^{14}$ $s^{-1}$ **(19)**.

In contrast to the completely reversible adsorption of ethylene on the Ru(001)-p(1x2)O surface, only one-third of the chemisorbed ethylene on the Ru(001)-p(2x2)O surface desorbs reversibly from a saturated overlayer, the total fractional coverage of which is 0.12. As shown in Fig. 3(b), this reversibly adsorbed ethylene also desorbs in a peak at 240 K and a shoulder at 160 K on the multilayer peak. This thermal desorption measurement was conducted using a p(2x2)$^{18}$O overlayer in order to distinguish molecularly desorbed ethylene from C$^{18}$O that is produced by the surface reaction between carbon (from the decomposition of ethylene) and oxygen [cf. Fig. 3(c)]. However, a small concentration of C$^{16}$O due to background adsorption (fractional surface coverage between 0.01 and 0.02) is also observed to desorb, as indicated by the desorption-limited peak at approximately 450 K in Fig. 3(b).

Although molecularly chemisorbed ethylene on both the Ru(001)-p(2x2)O and Ru(001)-p(1x2)O surfaces desorbs in two peaks at 160 and 240 K, EEL spectra that were measured after annealing to temperatures between 115 and 240 K were identical and indicative of π-bonded ethylene. The identification of the ethylene that desorbs in the 160 K peak as a π-bonded species implies that this peak does not correspond to desorption of a second layer of ethylene.

**B. Thermal Decomposition of Ethylene on the Ru(001)-p(2x2)O Surface and on Disordered Oxygen Overlayers on the Ru(001) Surface**

Electron energy loss spectra which demonstrate the effect of annealing the molecularly chemisorbed ethylene overlayer on the Ru(001)-p(2x2)O surface to higher temperatures are shown in Fig. 4. Comparing the spectra of π-bonded ethylene annealed to 200 K [Figs. 2(c) and (d)] to those of the same overlayers annealed to 250 K [Figs. 4(a) and (b)] indicates that by 250 K the ethylene has converted completely to a new species which can be identified easily as ethylidyne. In fact, π-bonded ethylene reacts to yield ethylidyne at temperatures as low as 230 K. Ethylidyne is formed also from the decomposition of di-σ-bonded ethylene on the Ru(001) surface (1), and is characterized by carbon-carbon

stretching and symmetric methyl deformation modes at 1140 and 1370 $cm^{-1}$ for $CCH_3$, and at 1150 and 1000 $cm^{-1}$ for $CCD_3$. The symmetric and asymmetric carbon-hydrogen stretching modes, expected at 2945 and 3045 $cm^{-1}$ (2190 and 2280 $cm^{-1}$ for $CCD_3$), were not resolved in these spectra, but appear as a single feature at 2970 $cm^{-1}$ (2210 $cm^{-1}$ for $CCD_3$). The asymmetric methyl deformation mode and the methyl rocking mode appear at 1450 and 1000 $cm^{-1}$, respectively, in Fig. 4(a), but are not resolved from the $\delta_s(CD_3)$ and $\nu_s(RuO)$ modes at 1000 and 535 $cm^{-1}$ in Fig. 4(b). The $\nu(Ru{\equiv}CCH_3)$ mode of adsorbed ethylidyne, expected at 480 $cm^{-1}$, is not resolved from the $\nu_s(RuO)$ mode in either of the spectra of Figs. 4(a) and (b). These mode assignments of adsorbed ethylidyne have been discussed in detail elsewhere (**1**).

Electron energy loss spectra that were measured following annealing this overlayer to 350 K [Figs. 4(c) and (d)] demonstrate the total conversion of the ethylidyne to a new species, as judged both by the disappearance of the carbon-carbon stretching modes of $CCH_3$ and $CCD_3$ at 1140 and 1150 $cm^{-1}$ and the $CH_3$ rocking mode at 1000 $cm^{-1}$, as well as by the appearance of new modes which are attributed to a nearly $sp^2$-hybridized vinylidene ($CCH_2$). The EEL spectrum of the deuterated vinylidene [Fig. 4(d)] exhibits three intense peaks at 700, 1010 and 1350 $cm^{-1}$. The peak at 1350 $cm^{-1}$ may be assigned unambiguously to the stretching mode of a carbon-carbon double bond since it is far too high in frequency to correspond either to any carbon-deuterium deformation mode or to $\nu(CC)$ of a single bond. The loss features at 700 and 1010 $cm^{-1}$ are assigned to the $CD_2$ wagging and scissoring modes. The other loss peaks at 435, 2180 and 2290 $cm^{-1}$ are then assigned easily as the $\nu(Ru{=}CCD_2)$, $\nu_s(CD_2)$ and $\nu_a(CD_2)$ modes of the $CCD_2$. The $\nu(CO)$ mode of a small concentration of carbon monoxide that is due to adsorption from the background of the UHV chamber appears at 2035 $cm^{-1}$ in Fig. 4(d). This CO corresponds to a fractional surface coverage of less than 0.02 (**20**), contributes slightly to the loss peak at 435 $cm^{-1}$, and has no effect upon the other adsorbates.

The EEL spectrum of the corresponding hydrogenic species ($CCH_2$) in Fig. 4(c) exhibits two clearly resolved peaks at 895 and 1435 $cm^{-1}$. The peak at 895 $cm^{-1}$ is due to the $CH_2$ wagging mode that has shifted up from 700 $cm^{-1}$ in the deuterated spectrum. The more intense loss feature at 1435 $cm^{-1}$ results from two overlapping peaks that correspond to the carbon-carbon stretching mode and the

$CH_2$ scissoring mode that have shifted up from 1350 $cm^{-1}$ and 1010 $cm^{-1}$, respectively, in $CCD_2$. The other loss peaks at 455, 2985 and 3050 $cm^{-1}$ are the $\nu(Ru{=}CCH_2)$, $\nu_s(CH_2)$ and $\nu_a(CH_2)$ modes of $CCH_2$. The $CH_2$ rocking mode is also evident at 965 $cm^{-1}$ in Fig. 4(c), although the $CD_2$ rocking mode is not resolved from the $CD_2$ wagging mode in the spectrum of $CCD_2$ in Fig. 4(d).

The vibrational frequencies of this vinylidene are compared in Table 2 to those of vinylidene in an $Os_3H_2(CO)_9(CCH_2)$ cluster compound and to two other surface species that have been identified as $CCH_2$ (**21-23**). There is a good correspondence between the vibrational frequencies of the $CCH_2$ in the cluster and the vinylidene that is present on the Ru(001)-p(2x2)O surface. The $CCH_2$ ligand of the complex is bridge-bonded to two osmium atoms with $\pi$-electron donation from the carbon-carbon double bond to the third osmium atom, as shown schematically in Fig. 5(a) (**21**). The structure of this compound, determined by X-ray crystallography, is shown in Fig. 5(b) (**24**).

The existence of a $CCH_2$ species on the Ru(001)-p(2x2)O surface following ethylene adsorption at 80 K and annealing to 350 K is confirmed further by the hydrogen thermal desorption spectrum, shown in Fig. 3(d), from ethylene adsorbed on the Ru(001)-p(2x2)$^{18}$O surface. Approximately half of the hydrogen desorbs below 350 K, indicating that the surface species present at 350 K has a stoichiometry of $C_2H_2$. The hydrogen that desorbs in the two peaks at 210 and 250 K therefore corresponds to hydrogen that results from the dehydrogenation of $\pi$-bonded ethylene to ethylidyne and the subsequent dehydrogenation of ethylidyne to vinylidene. As may be seen by comparing the hydrogen thermal desorption spectrum of Fig. 3(d) with that of hydrogen adsorbed on the Ru(001)-p(2x2)O surface [Fig. 3(e)], most of the hydrogen that results from the dehydrogenation of ethylene and ethylidyne desorbs above the temperature at which chemisorbed hydrogen desorbs from the Ru(001)-p(2x2)O surface, and is therefore a reaction-limited desorption product.

The vinylidene could be rehydrogenated to ethylidyne, indicating that this reaction is reversible. After a saturation coverage of $CCH_2$ was formed, the Ru(001)-p(2x2)O surface was cooled to 80 K, exposed to 10 L of hydrogen and annealed to 200 K. Subsequently measured EEL spectra showed the presence of ethylidyne and a small amount of unreacted vinylidene, indicating that most of the $CCH_2$ had been rehydrogenated. Annealing this overlayer to 350 K results in the dehydrogenation of the

ethylidyne to vinylidene. In another experiment, the vinylidene was exposed to 15 L of deuterium at a surface temperature of 200-250 K. The EEL spectrum of this overlayer indicates the existence of different isotopes of ethylidyne. As expected, the species with the highest coverage is $CCH_2D$ with a $\delta_s(CH_2D)$ mode at 1260 $cm^{-1}$, whereas $CCH_3$ is present at a lower coverage. Neither $CCD_2H$ nor $CCD_3$ was detected.

As shown in Fig. 3(d), annealing the vinylidene overlayer on the Ru(001)-p(2x2)O surface to higher temperatures causes further hydrogen desorption in a peak at 400 K, indicating that the $CCH_2$ has dehydrogenated. Electron energy loss spectra of the overlayer that is formed by annealing the surface to 400 K [cf. Figs. 4(e) and (f)] are consistent with this interpretation. The stable species on the surface at this temperature are carbon adatoms and methylidyne, which are formed via cleavage of the carbon-carbon bond and one carbon-hydrogen bond of vinylidene. No intermediates in the vinylidene decomposition reaction such as methylene ($CH_2$) or acetylide (CCH) were observed by EELS. The existence of methylidyne is indicated both by the presence of a carbon-hydrogen bending mode at 810 $cm^{-1}$ and a carbon-hydrogen stretching mode at 3010 $cm^{-1}$ in Fig. 4(e). The carbon-deuterium bending mode, expected at 615 $cm^{-1}$ for CD, overlaps and is unresolved from the intense $\nu_s(RuO)$ mode in Fig. 4(f). The carbon-deuterium stretching mode, observed at 2250 $cm^{-1}$, is, however, at the same frequency as that of methylidyne on the clean Ru(001) surface (**1,2**). The $\nu_s(Ru{\equiv}CH)$ and $\nu_s(Ru{\equiv}CD)$ modes expected at 465 and 415 $cm^{-1}$ were not resolved from the $\nu_s(RuO)$ mode in these spectra. Note, however, that the phonon mode of the p(2x2) oxygen overlayer was resolved in the spectrum of Fig. 4(f).

Both the hydrogen thermal desorption spectra and the EEL spectra measured following annealing this overlayer to higher temperatures show that the methylidyne dehydrogenates between 500 and 700 K. The surface carbon reacts with the oxygen adatoms ($^{18}O$) to form $C^{18}O$, which desorbs above 500 K, as shown in Fig. 3(c). This carbon monoxide desorption peak is reaction-limited, because this coverage of desorption-limited CO would appear at a much lower temperature (approximately 430 K) on this surface. Neither $CO_2$ nor $H_2O$ was observed to desorb from this overlayer, indicating that the adsorbed oxygen either reacted with carbon above 500 K evolving CO or remained on the surface and desorbed only after annealing to 1700 K. Due to the absence of both spectroscopically observed intermediates

and mass spectrometrically detected reaction products, neither the ethylene, ethylidyne, vinylidene nor methylidyne reacts with the oxygen adatoms on the Ru(001)-p(2x2)O surface.

Finally, the adsorption and reaction of saturation coverages of ethylene on disordered oxygen overlayers on Ru(001) have also been investigated. The disordered oxygen overlayers were prepared by exposing the Ru(001) surface to oxygen at 80-100 K. The fractional surface coverages of oxygen were estimated by using the linear relationship between coverage and exposure, and the known coverage of 0.25 corresponding to a 0.8 L exposure of oxygen (**25**). Hydrogen and ethylene thermal desorption spectra were used to evaluate the inhibition of reversible and irreversible ethylene adsorption by the preadsorbed oxygen. It was found that the fraction of ethylene that chemisorbs reversibly increases with increasing oxygen precoverage, while the amount of irreversibly adsorbed ethylene decreases approximately linearly with the oxygen precoverage. As shown in Fig. 6, a fractional coverage of oxygen of approximately 0.35 inhibits ethylene decomposition completely.

## IV. Discussion

### A. Molecularly Chemisorbed Ethylene

It has been shown that ethylene chemisorbed on the Ru(001)-p(2x2)O and Ru(001)-p(1x2)O surfaces below 230 K is a $\pi$-bonded molecular species, for example, by comparison of the vibrational spectra to that of Zeise's salt. Calculations of the electronic structure of Zeise's anion have suggested that donation of electron density from the $\pi$-orbital of ethylene to the platinum accounts for at least 75% of the total bonding of the ethylene ligand to the platinum, while backdonation from the platinum d-orbitals to the ethylene $\pi^*$-orbital accounts for the rest (**26**). The occurrence of a small amount of backbonding in Zeise's salt is consistent with neutron diffraction results, which show that the hydrogen atoms are bent away from the metal atom such that the carbon atoms are positioned 0.16 Å away from the plane of the four hydrogen atoms and towards the platinum atom (**27**). If no backbonding were to occur, the hydrogen and carbon atoms would remain coplanar. By analogy to Zeise's salt, the bonding of ethylene to these modified ruthenium surfaces may be described in terms of the donation of electron density from the $\pi$-orbital of ethylene to the d-band of the ruthenium of which the local density of *unoccupied* states has been increased by the presence of the electronegative oxygen adatoms, and the

simultaneous backdonation of a small amount of electron density from the ruthenium surface to the $\pi^*$-orbital of chemisorbed ethylene.

The ability of ethylene to act both as a $\pi$-donor and a $\pi^*$-acceptor lowers the vibrational frequency of the carbon-carbon stretching mode of chemisorbed, $\pi$-bonded $C_2D_4$ to 1350 $cm^{-1}$ and of $C_2D_4$ in Zeise's salt to 1353 $cm^{-1}$ from the gas phase value of 1515 $cm^{-1}$. The frequency of the carbon-carbon stretching mode of $\pi$-bonded $C_2H_4$ cannot be compared to that of $C_2H_4(g)$ due to the previously discussed coupling of the $\delta(CH_2)$ and $\nu(CC)$ modes of the chemisorbed ethylene. However, the frequencies of these two modes agree with those of the ethylene ligand in Zeise's salt, suggesting that the degree of mode coupling and the bonding are similar in the two species. The bonding of ethylene to platinum in Zeise's salt increases the carbon-carbon bond length to 1.375 Å from 1.337 Å in gaseous ethylene (**27**), and a similar lengthening of this bond is expected to occur in the ethylene that is $\pi$-bonded to the Ru(001)-p(1x2)O and Ru(001)-p(2x2)O surfaces.

Previous investigations (**1,3**) of ethylene adsorbed on clean, hydrogen precovered, and CO-precovered Ru(001) surfaces have shown that the molecularly chemisorbed ethylene is di-$\sigma$-bonded with a carbon-carbon stretching frequency of 1040 $cm^{-1}$. Hence, the carbon atoms of di-$\sigma$-bonded ethylene on the Ru(001) surface are essentially $sp^3$-hybridized, whereas those of $\pi$-bonded ethylene on the Ru(001)-p(2x2)O and Ru(001)-p(1x2)O surfaces are more nearly $sp^2$-hybridized. The change in the hybridization of the carbon atoms of adsorbed ethylene from $sp^3$ as observed on the clean surface to nearly $sp^2$ as observed on the oxygen precovered surfaces has also been observed for coadsorbed ethylene and oxygen on the Pd(100), Fe(111) and Pt(111) surfaces (**8-10,28**). Moreover, the observed vibrational frequencies of these $\pi$-bonded ethylene species agree quite well with those of $\pi$-bonded ethylene on the Ru(001)-p(2x2)O and Ru(001)-p(1x2)O surfaces, as shown in Table 1. Our results are also in agreement with those of Barteau et al. (**29**) for ethylene chemisorbed on the Ru(001)-p(1x2)O surface at 170 K.

Since there is no indication of any direct chemical interaction between the $C_2H_4$ and the oxygen adatoms, the interaction between ethylene and the Ru(001), the Ru(001)-p(2x2)O and the Ru(001)-p(1x2)O surfaces may be discussed in terms of the "Lewis acidity" of the surface. When oxygen is

adsorbed, the Lewis acidity of the surface; i.e., the ability of the ruthenium atoms to accept electrons, increases. As discussed in Sect. I, approximately 0.03 electron is transferred from the ruthenium to each oxygen adatom of the p(2x2) overlayer, and 0.04 electron is transferred to each oxygen atom of the p(1x2) overlayer. This charge transfer increases the Lewis acidity of the surface ruthenium atoms, making $\pi$-donation from ethylene to the ruthenium more favorable and $\pi^*$-backdonation from the surface less favorable, and this alters the bonding of ethylene from di-$\sigma$- to $\pi$-bonding. A similar effect has been observed when acetone is adsorbed below 200 K on the Ru(001) and the Ru(001)-p(2x2)O surfaces (**30**). On Ru(001), acetone forms largely a side-on bonded $\eta^2$(C,O)-$(CH_3)_2CO$ species, as well as a small amount of $\eta^1$-acetone, which is bonded through a lone pair of electrons on the oxygen atom. Addition of the p(2x2)O overlayer to the surface stabilizes the $\eta^1$-acetone with respect to the $\eta^2$-acetone, since the $\eta^1$-bonding configuration maximizes the net electron transfer from the acetone to the ruthenium. In both cases the increased Lewis acidity of the ruthenium surface increases the selectivity towards the adspecies which donate the most electron density and withdraw the least, $\eta^1$-acetone and $\pi$-bonded ethylene. Similar effects have been observed also for the coadsorption of oxygen with formaldehyde (**31**) and with formamide (**32**) on Ru(001).

On the other hand, the preadsorption of oxygen on Ru(001) does not alter the bonding of acetylene: the carbon atoms of acetylene are rehybridized to nearly $sp^3$ on the Ru(001), Ru(001)-p(2x2)O and Ru(001)-p(1x2)O surfaces (**2,33**). This is a consequence of the different energy levels of the unoccupied $\pi$-orbitals of gaseous ethylene ($1b_{2g}$) and acetylene ($\pi_g$), which lie at -2.85 and -6.1 eV with respect to the vacuum level, respectively (**34,35**). Upon adsorption, these orbital energies will downshift and broaden. Analogously, ultraviolet photoelectron spectroscopic data of Demuth and Eastman (**36**) show that the bonding $\pi$-orbitals, $\pi_u$ of acetylene and $b_{3u}$ of ethylene, shift from -11.4 to -13.1 eV and from -10.5 eV to -11.6 eV upon adsorption of $C_2H_2$ and $C_2H_4$ on Ni(111). The Fermi level of Ru(001) lies at -5.5 eV (**37**), and the Fermi levels of Ru(001)-p(2x2)O and Ru(001)-p(1x2)O lie at -5.7 and -6.3 eV with respect to the vacuum (zero) level (**6**). The energy of the $\pi_g$-orbital of acetylene shifts below the Fermi level of all three surfaces upon adsorption such that backdonation to the empty $\pi_g$ orbital of acetylene occurs, resulting in rehybridization of the carbon atoms to $sp^3$. Similarly, the

energy of the $\pi^*$ ($1b_{2g}$) orbital of ethylene shifts sufficiently near the Fermi level of Ru(001) and broadens upon adsorption to facilitate backdonation, resulting in the formation of di-$\sigma$-bonded ethylene on the clean surface. However, the Fermi levels of the two oxygen precovered surfaces are apparently too low in energy with respect to that of the $\pi^*$-orbital to allow significant backdonation. Hence, ethylene adsorbed on these two surfaces is $\pi$-bonded.

The effect of oxygen adatoms upon the postadsorption of ethylene may be compared with that of carbon, which, like oxygen, is adsorbed in threefold hollow sites on Ru(001) (**7,38,39**). A fractional coverage of 0.25 carbon adatoms (which is equal to the coverage of oxygen adatoms in the p(2x2)O overlayer) produced by the thermal decomposition of ethylene on Ru(001) results in less charge transfer compared to the p(2x2) oxygen overlayer due to the similar electronegativities of ruthenium (2.2) and carbon (2.55), and the greater electronegativity of oxygen (3.44). Electron energy loss spectra of ethylene adsorbed on the Ru(001) surface precovered with a fractional coverage of 0.25 carbon adatoms show that this ethylene is di-$\sigma$-bonded (**40**), confirming that the $\pi$-bonding of molecular ethylene induced by the p(2x2) oxygen overlayer results from an electronic perturbation of the surface.

In addition to the change in the nature of the bonding of chemisorbed ethylene on the Ru(001) surfaces modified chemically by oxygen adatoms, the total coverage of molecularly chemisorbed ethylene is also reduced. As shown by the ethylene and hydrogen thermal desorption spectra, a fractional coverage of oxygen adatoms of 0.5 reduces the saturation fractional coverage of chemisorbed ethylene to 0.10, all of which adsorbs reversibly (cf. a saturation fractional coverage of 0.30 on Ru(001) of which 0.06 desorbs reversibly). The observation that a larger fraction of $\pi$-bonded ethylene desorbs molecularly compared with di-$\sigma$-bonded ethylene is in agreement with results for ethylene adsorbed on the clean and oxygen precovered Pd(100), Fe(111) and Pt(111) surfaces (**8-10**). Indeed, all of the $\pi$-bonded ethylene adsorbed on Pd(100) is thought to desorb reversibly, independent of the oxygen precoverage (**8**).

The appearance of two molecular ethylene desorption peaks above the temperature of multilayer desorption [cf. Fig. 3(a) and (b)] may be related to the local structures of the p(2x2) and p(1x2) oxygen overlayers. The 240 K peak appears with greater intensity in the ethylene thermal desorption spectra of

the p(2x2)O overlayer than in those of the p(1x2)O overlayer, whereas the shoulder at 160 K appears with slightly greater intensity in the spectra of the p(1x2)O overlayer. These observations suggest that the 240 K peak may correspond to ethylene chemisorbed in areas with local p(2x2)O structure, whereas the 160 K peak may correspond to ethylene chemisorbed in areas with local p(1x2)O structure. If this interpretation is correct, the coverages of ethylene corresponding to these two thermal desorption peaks are indicative of the short-range perfection in these two ordered overlayers.

The desorption of π-bonded ethylene at 240 K occurs at a slightly higher temperature than that at which di-σ-bonded ethylene desorbs molecularly (1). The 240 K desorption temperature indicates that the strength of the ruthenium-ethylene π-bond is approximately 14 kcal/mole (perhaps slightly higher due to a small degree of rehybridization). The di-σ-bonded ethylene has a slightly lower heat of adsorption (11 kcal/mole), but a higher binding energy of 80 kcal/mole taking into account the rehybridization that occurs upon adsorption.

**B. Thermal Decomposition of Chemisorbed Ethylene**

As mentioned above, the π-bonded, molecularly chemisorbed ethylene that is observed on the Ru(001)-p(2x2)O surface decomposes to a lesser extent than the di-σ-bonded ethylene on the clean, the hydrogen precovered ($\theta_H$ = 0.25), or the CO precovered ($\theta_{CO}$ = 0.25) ruthenium surfaces. This difference results from the much stronger modification in the electronic structures of the surface by oxygen compared with hydrogen or CO. The primary effects of preadsorbed CO and hydrogen upon ethylene adsorption and reaction are to block the adsorption of ethylene and enhance molecular desorption relative to decomposition by blocking adsorption sites of the decomposition products (3). On the other hand, oxygen adatoms modify the chemical nature of the surface qualitatively, thereby altering the nature of the molecular bonding of ethylene (from di-σ- to π-bonding) and changing its decomposition products. For example, $sp^2$-hybridized vinylidene is observed as a product of the dehydrogenation of ethylene on Ru(001)-p(2x2)O, whereas it is not observed on the reduced Ru(001) surface. It appears that $sp^3$ hybridization and $\eta^2$-bonding are favored on Ru(001), upon which di-σ-bonded ethylene and $sp^3$-hybridized acetylide are formed, and that $sp^2$ hybridization and $\eta^1$-bonding are favored on the Ru(001)-p(2x2)O surface, upon which π-bonded ethylene and $sp^2$-hybridized vinylidene are formed.

Ethylidyne is observed on both Ru(001) ($sp^3$ hybridization) and Ru(001)-p(2x2)O ($\eta^1$-bonding). The presence of coadsorbed oxygen makes $sp^3$ hybridization and $\eta^2$-bonding less favorable due, in part, to a weakening of the ruthenium-carbon bonds. This reduced bond strength is also manifest in less irreversible adsorption on the oxygen precovered surface: preadsorbed oxygen decreases the amount of ethylene that is adsorbed irreversibly in an approximately linear fashion (**41**). Similar linear reductions in the extent of ethylene dehydrogenation by oxygen preadsorption have been observed on the Pd(100), Fe(111) and Pt(111) surfaces (**8-10**).

Electron energy loss spectra of ethylene adsorbed on the Ru(001)-p(2x2)O surface show that $\pi$-bonded ethylene reacts near 230 K to form ethylidyne, all of which dehydrogenates to an $sp^2$-hybridized vinylidene between 250 and 350 K with simultaneous desorption of hydrogen. It is rather likely that the $\pi$-bonded ethylene first dehydrogenates to vinylidene and that this vinylidene rehydrogenates to ethylidyne due to the presence of surface hydrogen at temperatures below 250 K. This postulate is supported by EEL experiments, which showed that vinylidene coadsorbed with hydrogen could be rehydrogenated to ethylidyne.

In contrast to the partially irreversible adsorption of ethylene on the Ru(001)-p(2x2)O surfaces, $\pi$-bonded ethylene on Pd(100), precovered with 0.18 monolayer of oxygen forming a disordered overlayer, adsorbs reversibly (**42**), and a variation in oxygen precoverage merely changes the ratio of di-$\sigma$-bonded to $\pi$-bonded ethylene that is formed (**8**). The di-$\sigma$-bonded ethylene on Pd(100) dehydrogenates at 250 K to $sp^3$-hybridized $CHCH_2$ which decomposes at higher temperatures to methylidyne. As shown by EELS, the $\pi$-bonded ethylene that is chemisorbed on Pt(111) with a fractional precoverage of 0.23 oxygen adatoms forms a new, previously unidentified species upon annealing to 325 K (**10**). Although spectra of the corresponding deuterated species are not available to confirm our assignment, we suggest that the $\pi$-bonded ethylene coadsorbed with a fractional coverage of 0.23 oxygen adatoms on Pt(111) converts to an $sp^2$-hybridized vinylidene. Indeed, the EEL spectrum of this vinylidene is very similar to that of vinylidene on Ru(001)-p(2x2)O. It exhibits an intense and broad loss feature at 1420 $cm^{-1}$ probably due to the (uncoupled) $\delta(CH_2)$ and $\nu(CC)$ modes. The $\nu_s(CH_2)$ and $\nu_a(CH_2)$ modes appear at 2980 and 3080 $cm^{-1}$, respectively. Other modes that appear at 940, 820 and

730 $cm^{-1}$ may be assigned to the $CH_2$ rocking, wagging and twisting modes of vinylidene. On the Pt(111) surface, ethylene is di-σ-bonded and converts to ethylidyne near 300 K, and it is possible that vinylidene on the oxygen precovered surface may also be hydrogenated to ethylidyne. Hence, the interaction of ethylene with ruthenium precovered with a p(2x2)O overlayer is similar to that observed with platinum upon which a comparable fractional coverage of oxygen is present: on both surfaces, π-bonded ethylene converts to vinylidene. Both of these surfaces are more reactive than oxygen precovered Pd(100).

As discussed in Sect. III.B, the identification of adsorbed vinylidene on Ru(001)-p(2x2)O is confirmed by both EEL spectra and by hydrogen thermal desorption spectra, which show that the stoichiometry of the intermediate is $C_2H_2$. Note that the EEL spectra of Figs. 4(c) and (d) cannot be attributed to chemisorbed acetylene due to the absence in Fig. 4(c) of the intense carbon-hydrogen bending mode at 765 $cm^{-1}$, which is characteristic of acetylene chemisorbed on the Ru(001) and Ru(001)-p(2x2)O surfaces, and the observation of $CH_2$ and $CD_2$ scissoring modes at 1435 and 1010 $cm^{-1}$ in Figs. 4(c) and (d). The presence of methylidyne at this temperature can be ruled out due to the absence of an intense CH bending mode in the EEL spectrum of Fig. 4(c), which would be expected at 810 $cm^{-1}$. The existence of $CH_3$ and $CD_3$ groups may also be excluded by examination of the EEL spectra. The vibrational frequencies of the adsorbed vinylidene agree with those of the vinylidene in the $Os_3(CO)_9(CCH_2)H_2$ complex (**21**), the bonding configuration and structure of which are shown in Figs. 5(a) and (b) (**24**). We would expect that the vinylidene is adsorbed similarly on the ruthenium surface with the $CCH_2$ bridge-bonded, the carbon-carbon bond axis tilted with respect to the surface normal, elongation of the carbon-carbon bond compared to that of gaseous ethylene, and with some donation of electron density from the π-orbital of the $CCH_2$ to the d-band of the ruthenium surface [cf. Fig. 5(c)]. The observed ν(CC) mode of adsorbed $CCH_2$ at 1435 $cm^{-1}$ is lowered from those of $C_2H_4$(g) at 1623 $cm^{-1}$ and the $CCH_2$ ligand in $Cp_2Ru_2(CO)_2(\mu\text{–}CO)(\mu\text{–}CCH_2)$ at 1586 $cm^{-1}$ (**43**), due to the π-electron donation from the carbon-carbon bond to the metal surface that occurs in the chemisorbed vinylidene. The overlap of the ν(CC) and $\delta(CH_2)$ modes of adsorbed vinylidene at 1435 $cm^{-1}$ indicates that these modes are not coupled in this species, unlike those of π-bonded ethylene. It cannot

be entirely ruled out that the ν(CC) mode appears at a slightly lower frequency than 1435 $cm^{-1}$, and that the $\delta(CH_2)$ mode "steals" intensity from the ν(CC) mode via mode coupling. However, the absence of any evidence for a shoulder on the low-frequency side of the peak at 1435 $cm^{-1}$ in Fig. 4(c) makes this unlikely.

Gates and Kesmodel (22) have suggested the presence on the Pd(111) surface of a $CCH_2$ adspecies as an intermediate to the formation of ethylidyne from hydrogen and acetylene. This postulated $CCH_2$ adspecies was coadsorbed with acetylene, hydrogen and ethylidyne. Thus, only two of the vibrational modes were identified, ν(CC) and/or $\delta(CH_2)$ at 1437 $cm^{-1}$ and $\nu(CH_2)$ at 2986 $cm^{-1}$ [ν(CC) at 1372 $cm^{-1}$ and $\nu(CD_2)$ at 2206 $cm^{-1}$ for $CCD_2$]. A $CCH_2$ adspecies, an intermediate in the hydrogenation of acetylene to ethylidyne on Pt(111), was tentatively identified by Ibach and Lehwald (23) with mode assignments listed in Table 2. The assignment of the carbon-carbon stretching mode to a loss feature at 1100 $cm^{-1}$ suggests $sp^3$ hybridization of the carbon atoms of the $CCH_2$ on Pt(111), indicating that this species is quite different from the $sp^2$-hybridized $CCH_2$ species observed on Ru(001)-p(2x2)O and the oxygen precovered Pt(111) surfaces. The change in hybridization of the $CCH_2$ species on platinum due to the presence of oxygen supports our earlier assertion that $sp^3$ hybridization is preferred on clean metal surfaces, whereas $sp^2$ hybridization is preferred in the presence of oxygen. Moreover, the observed conversion of $CCH_2$ to ethylidyne on palladium and platinum agrees with our observation that the conversion of ethylidyne to vinylidene is reversible on Ru(001), provided sufficient hydrogen is present.

The thermal evolution of π-bonded ethylene on Ru(001)-p(2x2)O can be summarized as follows. The ethylene reacts to form ethylidyne, possibly via a vinylidene intermediate, below 250 K. In contrast to the total dehydrogenation of ethylidyne to carbon with the simultaneous evolution of hydrogen with no stable intermediate on the Ru(001) surface, the ethylidyne on the Ru(001)-p(2x2)O surface dehydrogenates to vinylidene upon annealing to 350 K. The vinylidene decomposes to methylidyne and carbon adatoms evolving hydrogen between 350 and 450 K, possibly though an unstable acetylide intermediate. Acetylide, which was observed following the adsorption of ethylene on the Ru(001) surface, also decomposes via carbon-carbon bond cleavage to methylidyne at approximately the same tempera-

ture at which vinylidene decomposes on the Ru(001)-p(2x2)O surface. The methylidyne that is formed on Ru(001)-p(2x2)O decomposes between 500 and 700 K. Finally, the carbon reacts with oxygen adatoms to form CO, which desorbs in a reaction-limited step between 500 and 750 K.

The hydrogen thermal desorption spectra from ethylene chemisorbed on the Ru(001)-p(2x2)O surface are completely consistent with this decomposition mechanism. Hydrogen that is evolved from the ethylene and ethylidyne decomposition reactions desorbs in two peaks at 210 and 250 K. These two peaks account for half of the hydrogen desorption from the surface, consistent with the stoichiometry of the vinylidene intermediate observed on the surface at 350 K. The hydrogen thermal desorption peak at 400 K corresponds to one-quarter of the total amount of hydrogen that is desorbed and is therefore consistent with the dehydrogenation of vinylidene to methylidyne and carbon adatoms. The final quarter of the hydrogen desorbs above 500 K as the methylidyne decomposes.

Only $C_2H_4$, $H_2$ and CO were observed to desorb following the chemisorption of ethylene on the Ru(001)-p(2x2)O surface. This result is similar to the coadsorption of ethylene and oxygen on Fe(111), but unlike the coadsorption of ethylene and oxygen on Pd(100) and Pt(111), which exhibited $CO_2$ and $H_2O$ desorption as well (**8-10**). The absence of $CO_2$ and $H_2O$ in the thermal desorption spectra from the ruthenium surface is not surprising since neither the formation of $CO_2$ from coadsorbed CO and oxygen (**44**) nor the formation of water from coadsorbed oxygen and hydrogen has been observed under UHV conditions on the Ru(001) surface in transient thermal desorption experiments (**45**). The lower reactivity of ruthenium and iron for the oxidation of carbon monoxide and hydrogen is a consequence of the stronger metal-oxygen bonds that are formed (**6,46**) compared with those of platinum (**47**) and palladium (**48**).

Finally, the chemistry of ethylene on the Ru(001)-p(2x2)O surface may be compared to the organometallic chemistry of homogeneous compounds. For example, it has been shown that ethylene reacts with $Os_3(CO)_{12}$ to form the vinyl complex, $HOs_3(CH{=}CH_2)(CO)_{10}$, which forms the vinylidene complex, $H_2Os_3(CO)_9(C{=}CH_2)$ (**21**) upon heating. The latter can be hydrogenated to an ethylidyne complex, $H_3Os_3(CO)_9(CCH_3)$ (**21,24,49**), just as chemisorbed vinylidene can be rehydrogenated to ethylidyne on the Ru(001)-p(2x2)O surface. These results also suggest that the conversion of $\pi$-bonded

ethylene to vinylidene on Ru(001)-p(2x2)O occurs via a vinyl intermediate.

## V. Conclusions

The presence of ordered p(2x2) and p(1x2) oxygen overlayers on the Ru(001) surface gives rise to π-bonding of molecularly chemisorbed ethylene, such that the carbon atoms of the ethylene remain nearly $sp^2$-hybridized. This species is qualitatively different from the $sp^3$-hybridized, di-σ-bonded ethylene that is observed on the clean surface. Intuitively, this difference reflects the greater Lewis acidity of the Ru(001)-p(2x2)O and Ru(001)-p(1x2)O surfaces. More precisely, it is a consequence of a significant perturbation in the electronic structure of the ruthenium surface by the ordered oxygen overlayers, which increases the energy separation between the Fermi level and the π*-orbital of ethylene making backdonation unfavorable.

As observed on the oxygen precovered Pt(111), Pd(100) and Fe(111) surfaces, a larger fraction [one-third on Ru(001)-p(2x2)O] of π-bonded ethylene desorbs molecularly than does di-σ-bonded ethylene on the reduced surfaces. The remaining two-thirds of the saturation coverage of ethylene adsorbed on the Ru(001)-p(2x2)O surface dehydrogenates to ethylidyne probably via a vinylidene intermediate upon heating to 250 K. In contrast to the observed total decomposition of ethylidyne to carbon and hydrogen on the Ru(001) surface with no stable intermediates, the presence of oxygen induces the formation of an $sp^2$-hybridized vinylidene species from ethylidyne at 350 K. By analogy to the $H_2Os_3(CO)_9(CCH_2)$ cluster (**21,24,49**), this chemisorbed vinylidene is almost certainly bridge-bonded to two adjacent ruthenium atoms and tilted towards a third ruthenium atom with donation of electron density from the π-orbital to the d-band of the ruthenium surface, as shown in Fig. 5(c). The chemisorbed vinylidene decomposes near 400 K to carbon adatoms and methylidyne, the latter of which dehydrogenates between 500 and 700 K. The vinylidene could be rehydrogenated to ethylidyne in the presence of hydrogen, analogous to the formation of ethylidyne from $CCH_2$ on reduced Pt(111) and Pd(111) (**22,23**). No oxygen-containing intermediates in ethylene decomposition were observed under any conditions of temperature and coverage. Oxygen adatoms reacted only with carbon adatoms, forming CO above 500 K.

Finally, the presence of oxygen favors $\eta^1$-bonding and $sp^2$ hybridization as shown by both the existence of $\pi$-bonded ethylene on the oxygen precovered Pt(111), Pd(100), Fe(111) and Ru(001) surfaces (**8-10**), as well as the formation of $sp^2$-hybridized vinylidene on these chemically modified Ru(001) and Pt(111) surfaces (**10**). On the other hand, $\eta^2$-bonded, $sp^3$-hybridized ethylene was observed in the absence of oxygen on all four surfaces.

**Acknowledgment:** This work was supported by the National Science Foundation under Grant No. CHE-8516615.

**References**


[1.] Hills, M.M.; Parmeter, J.E.; Mullins, C.B.; Weinberg, W.H., *J. Am. Chem. Soc.* **1986**, 108, 3554.

[2.] Parmeter, J.E.; Hills, M.M.; Weinberg, W.H., *J. Am. Chem. Soc.* **1986**, 108, 3563.

[3.] Hills, M.M.; Parmeter, J.E.; Weinberg, W.H., *J. Am. Chem. Soc.* **1986**, 108, 7215.

[4.] Parmeter, J.E.; Hills, M.M.; Weinberg, W.H., *J. Am. Chem. Soc.*, in press.

[5.] Weinberg, W.H., Parmeter, J.E.; Hills, M.M., in preparation.

[6.] Madey, T.E.; Engelhardt, H.A.; Menzel, D., *Surface Sci.* **1975**, 48, 304.

[7.] Rahman, T.S.; Anton, A.B.; Avery, N.R.; Weinberg, W.H., *Phys. Rev. Letters* **1983**, 51, 1979.

[8.] Stuve, E.M.; Madix, R.J.; Brundle, C.R., *Surface Sci.* **1985**, 152/153, 532.

[9.] Seip, U.; Tsai, M.-C.; Küppers, J.; Ertl, G., *Surface Sci.* **1984**, 147, 65.

[10.] Steininger, H.; Ibach, H.; Lehwald, S., *Surface Sci.* **1982**, 117, 685.

[11.] Williams, E.D.; Weinberg, W.H., *Surface Sci.* **1979**, 82, 93.

[12.] Feulner, P.; Menzel, D., *J. Vacuum Sci. Technol.* **1980**, 17, 662.

[13.] Thomas, G.E.; Weinberg, W.H., *J. Chem. Phys.* **1979**, 70, 954.

[14.] Thomas, G.E.; Weinberg, W.H., *Rev. Sci. Instrum.* **1979**, 50, 497.

[15.] Powell, D.B.; Scott, J.G.V.; Sheppard, N., *Spectrochim. Acta Part A* **1972**, 28, 327.

[16.] Shimanouchi, T.; *NSRDS-NBS Publication* **1972**, 39, 74.

[17.] Powell et al. believe that there is considerable $\nu$(CC) and $\delta(CH_2)$ character in both the 1243 and 1515 $cm^{-1}$ bands of Zeise's salt (**15**).

[18.] Hiraishi, J., *Spectrochim. Acta Part A* **1969**, 25, 749.

[19.] Redhead, P.A., *Vacuum* **1962**, 203.

[20.] This estimate is based on the intensity of the $\nu$(CO) mode in this spectrum compared to those of low CO coverages on the Ru(001) surface.

[21.] Andrews, J.R.; Kettle, S.F.A.; Powell, D.B.; Sheppard, N., *Inorg. Chem.* **1982**, 21, 2874.

[22.] Gates, J.A.; Kesmodel, L.L, *Surface Sci.* **1983**, 124, 68.

[23.] Ibach, H.; Lehwald, S., *J. Vacuum Sci. Technol.* **1978**, 15, 407.

[24.] Deeming, A.J.; Underhill, M., *J. Chem. Soc., Dalton Trans.* **1974**, 1415.

[25.] The linear dependence of coverage upon exposure has been shown by Madey et al. (6) to be appropriate for fractional oxygen coverages below 0.35.

[26.] Rosch, N.; Messmer, R.P.; Johnson, K.H., *J. Am. Chem. Soc.* **1974**, 96, 3855.

[27.] Love, R.A.; Koetzle, T.F.; Williams, G.J.B.; Andrews, L.C.; Bau, R., *Inorg. Chem.* 1975, 14, 2653.

[28.] In addition, a small amount of π-bonded ethylene is present on the clean Pd(100) surface.

[29.] Barteau, M.A.; Broughton, J.Q.; Menzel, D., *Appl. Surface Sci.* **1984**, 19, 92.

[30.] Anton, A.B.; Avery, N.R.; Toby, B.H.; Weinberg, W.H., *J. Am. Chem. Soc.* **1986**, 108, 684.

[31.] Anton, A.B.; Parmeter, J.E.; Weinberg, W.H., *J. Am. Chem. Soc.* **1986**, 108, 1823.

[32.] Parmeter, J.E.; Schwalke, U.E.; Weinberg, W.H., *J. Am. Chem. Soc.*, in press.

[33.] Parmeter, J.E.; Weinberg, W.H., to be published.

[34.] Mulliken, R.S., *J. Chem. Phys.* **1979**, 71, 556.

[35.] Dance, D.F.; Walker, I.C., *Chem. Phys. Lett.* **1973**, 18, 601.

[36.] Demuth, J.E.; Eastman, D.E., *Phys. Rev. B* **1976**, 13, 1523.

[37.] Wandelt, K.; Hulse, J.; Küppers, J., *Surface Sci.* **1981**, 104, 212.

[38.] Chan, C.-M.; Weinberg, W.H., *J. Chem. Phys.* **1979**, 71, 2788.

[39.] Feibelman, P.J., *Surface Sci.* **1981**, 103, L149.

[40.] J.E. Parmeter, unpublished results.

[41.] The inhibition of ethylene dissociation by oxygen atoms also results in part from oxygen blocking adsorption sites of the decomposition products.

[42.] As shown by EELS, the irreversibly adsorbed ethylene on the Pd(100) surface preexposed to oxygen is di-σ-bonded (8).

[43.] Evans, J.; McNulty, G. S., *J. Chem. Soc. Dalton Trans.* **1983**, 639.

[44.] Thomas, G.E.; Weinberg, W.H., *J. Chem. Phys.* **1979**, 70, 954.

[45.] M.M. Hills, unpublished results.

[46.] Seip, U.; Tsai, M.-C.; Christmann, K.; Küppers, J.; Ertl, G., *Surface Sci.* **1984**, 139, 29.

[47.] Avery, N. R., *Chem. Physics Lett.* **1983**, 96, 371.

[48.] Nyberg, C.; Tengstal, C. G., *Surface Sci.* **1983**, 126, 163.

[49.] Deeming, A.J.; Underhill, M., *J. Chem. Soc., Chem. Comm.* **1973**, 277.

Table 1. Comparison of vibrational frequencies (in $cm^{-1}$) of π-bonded ethylene on the Ru(001)-p(2x2)O and Ru(001)-p(1x2)O surfaces at 200 K with other ethylene species.

| Mode - $C_2H_4$ | Ru(001)-p(2x2)O and -p(1x2)O | Multilayer $C_2H_4$ on Ru(001) (1) | Di-σ-bonded $C_2H_4$ on Ru(001) (1) | $C_2H_4$(g) (16) | Zeise's Salt $K[PtCl_3(C_2H_4)]$ (15,18) | $C_2H_4$ on Pd(100) + 0.18 ML O (8) | $C_2H_4$ on Fe(111) + 1 L of $O_2$ (9) | $C_2D_4$ on Pt(111) + 0.23 ML O (10) |
|---|---|---|---|---|---|---|---|---|
| $\nu_s$(CH) | 440 | | 460 | | 403 | | | |
| $\nu_a$(CH) | | | | | 490 | | | |
| ρ($CH_2$) | | 860 | 775 | 810 | 841 | | | |
| τ($CH_2$) | | | 900 | | | | | |
| ω($CH_2$) | 950 | 970 | 1145 | 950 | 975 | 940 | 985 | |
| δ($CH_2$) | 1245 + 1520 | 1350/1460 | 1450 | 1347/1444 | 1243 + 1515 | 1510 | 1290 + 1565 | |
| ν(CC) | | 1630 | 1040 | 1623 | | | | |
| $\nu_s$($CH_2$) | 3040 | 3000 | 2940 | 2989/3026 | 3013 | 3020 | 3045 | |
| $\nu_a$($CH_2$) | | 3095 | 3050 | 3104 | 3075 | | | |
| **Mode - $C_2D_4$** | | | | | | | | |
| $\nu_s$(CH) | | | | | | | | |
| $\nu_a$(CH) | | | | | | | | |
| ρ($CD_2$) | | | | 1009/586 | 597/525 | | | |
| τ($CD_2$) | | | 700 | 728 | | | | |
| ω($CD_2$) | 695 | 735 | 900 | 720/780 | 757 | | | 970 |
| δ($CD_2$) | 975 | 1015/1125 | 1210 | 981/1078 | 962 | 985 | | 1370 |
| ν(CC) | 1350 | 1550 | 1040 | 1515 | 1353 | 1340 | | 2230 |
| $\nu_s$($CD_2$) | 2220 | 2310 | 2210 | 2251/2200 | 2224 | 2270 | | 2340 |
| $\nu_a$($CD_2$) | 2300 | | 2295 | 2304/2345 | 2331 | | | |

† = coupled

**Table 2.** Comparison of vibrational frequencies (in $cm^{-1}$) of $CCH_2$ on the Ru(001)-p(2x2)O surface with other $CCH_2$ species.

| Mode | $CCH_2$ on Ru(001)-p(2x2)O | $CCD_2$ on Ru(001)-p(2x2)O | $CCH_2$ on $Os_3H_2(CO)_9(CCH_2)$ (21) | $CCH_2$ on Pd(111) (22) | Pt(111) (23) |
|---|---|---|---|---|---|
| ν(Ru-C) | 455 | 435 | 255-311 | n.r. | n.r. |
| $\tau(CH_2)$ or $(CD_2)$ | n.r. | n.r. | 808 | n.r. | n.r. |
| $\omega(CH_2)$ or $(CD_2)$ | 895 | 700 | 959 | n.r. | 900 |
| $\rho(CH_2)$ or $(CD_2)$ | 965 | n.r. | 1048 | n.r. | n.r. |
| $\delta(CH_2)$ or $(CD_2)$ | 1435 | 1010 | † 1467 | n.r. | 1420 |
| ν(CC) | 1435 | 1350 | † 1328 | 1328 | 1100 |
| $\nu_s(CH_2)$ or $(CD_2)$ | 2985 | 2180 | 2990 | 2986 | 2970 |
| $\nu_a(CH_2)$ or $(CD_2)$ | 3050 | 2290 | 3052 | n.r. | n.r. |

n.r. = not resolved.

† = coupled.

**Figure Captions**

Figure 1. The structures and unit cells of the (a) p(2x2) and (b) p(1x2) ordered oxygen overlayers on the Ru(001) surface. Note that the oxygen occupies threefold hollow sites in both overlayers. Electron energy loss spectra of the (c) p(2x2) and (d) p(1x2) ordered oxygen overlayers.

Figure 2. The EEL spectra that result from 2 L exposures of (a) $C_2H_4$ and (b) $C_2D_4$ on the Ru(001)-p(1x2)O surface, and (c) $C_2H_4$ and (d) $C_2D_4$ on the Ru(001)-p(2x2)O surface at 80 K, followed by heating to 200 K. These spectra are characteristic of π-bonded molecular ethylene on both surfaces.

Figure 3. (a) The ethylene (mass 28) thermal desorption spectrum following a 6 L exposure of $C_2H_4$ on the Ru(001)-p(1x2)O surface at 90 K. (b) The ethylene and $C^{16}O$ (mass 28), (c) the $C^{18}O$ (mass 30) and (d) the hydrogen (mass 2) thermal desorption spectra following a 4 L exposure of $C_2H_4$ on the Ru(001)-p(2x2)$^{18}$O surface at 90 K. (e) The hydrogen (mass 2) thermal desorption spectrum following a 10 L exposure of $H_2$ on the Ru(001)-p(2x2)O surface at 90 K.

Figure 4. The EEL spectra that result from 2 L exposures of $C_2H_4$ [(a), (c), (e)] and $C_2D_4$ [(b), (d), (f)] on the Ru(001)-p(2x2)O surface at 80 K and heated to: (a), (b) 250 K; (c), (d) 350 K; and (e), (f) 400 K.

Figure 5. (a) The bonding configuration and (b) the structure of $CCH_2$ in $Os_3H_2(CO)_9(CCH_2)$ (**24**). (c) The analogous bonding configuration of $CCH_2$ on the Ru(001)-p(2x2)O surface.

Figure 6. The inhibition of irreversible ethylene adsorption by preadsorbed oxygen adatoms.

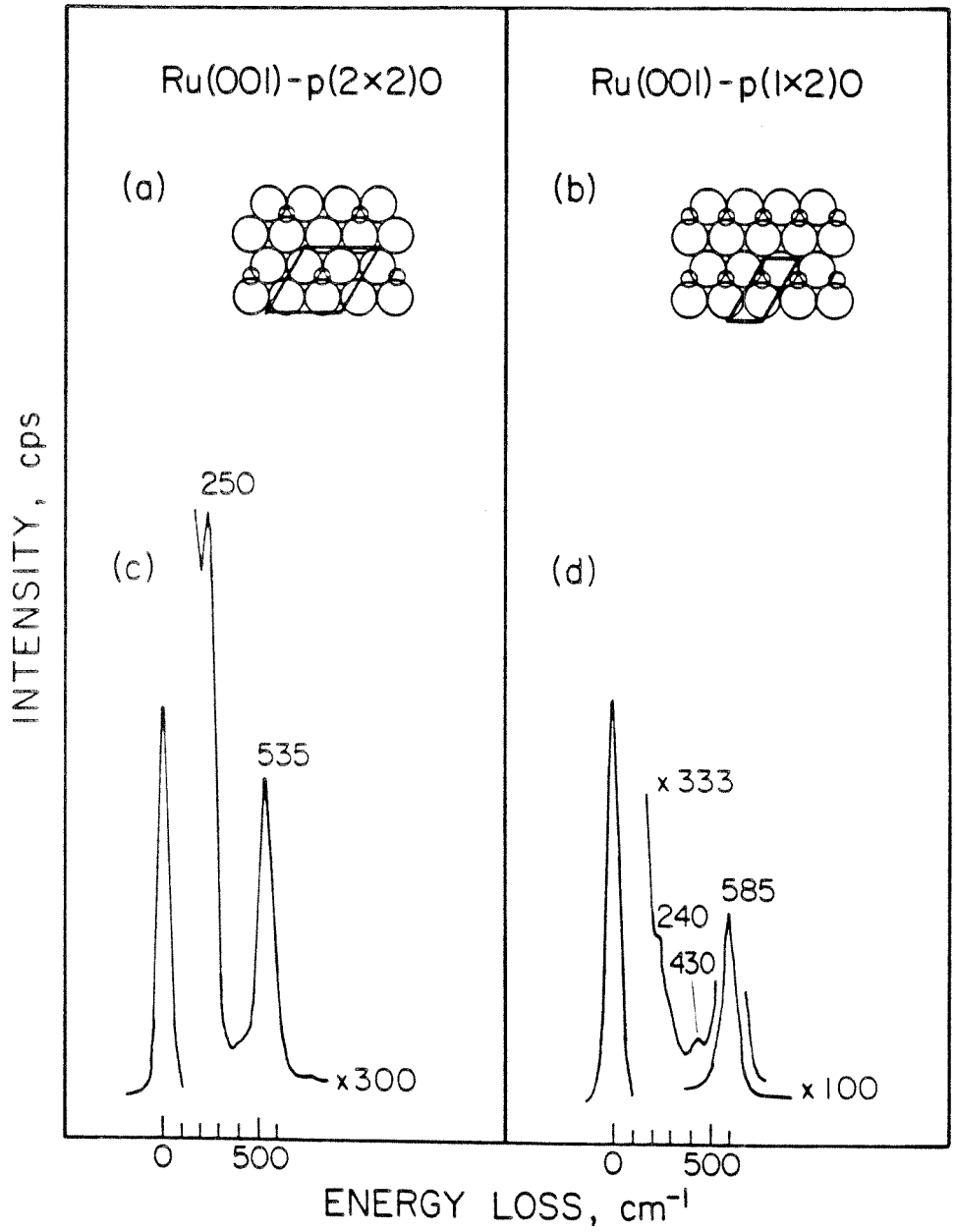
Ru(001)-p(2×2)O
Ru(001)-p(1×2)O
(a)
(b)
(c)
(d)
250
535
x300
x333
585
240
430
x100
INTENSITY, cps
0
500
0
500
ENERGY LOSS, cm⁻¹

Figure 1

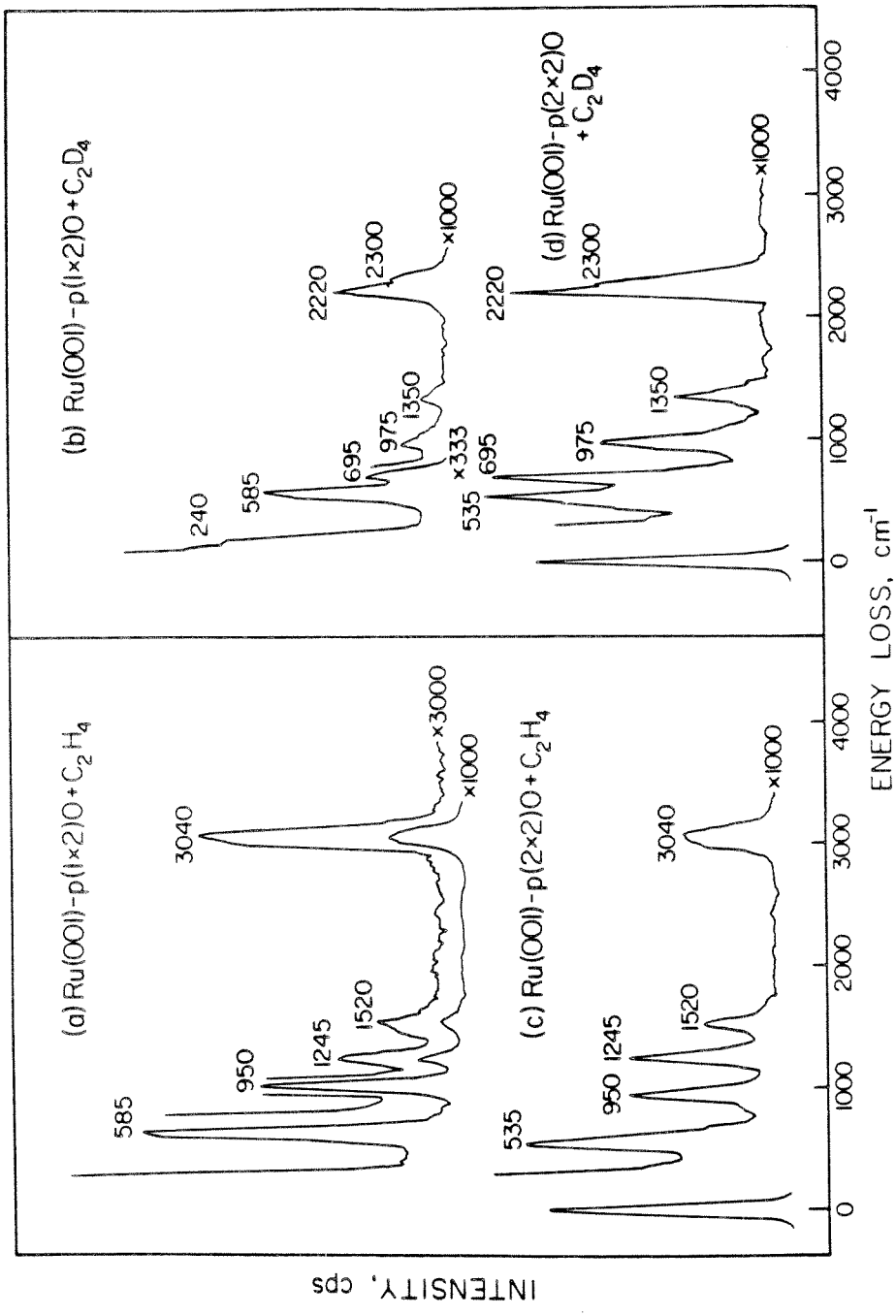
(a) Ru(001)-p(1×2)O + $C_2H_4$
585
950
1245
1520
3040
×3000
×1000
(b) Ru(001)-p(1×2)O + $C_2D_4$
240
585
695
975
1350
2220
2300
×333
×1000
(c) Ru(001)-p(2×2)O + $C_2H_4$
535
950
1245
1520
3040
×1000
(d) Ru(001)-p(2×2)O + $C_2D_4$
535
695
975
1350
2220
2300
×1000
INTENSITY, cps
0
1000
2000
3000
4000
ENERGY LOSS, $cm^{-1}$

Figure 2

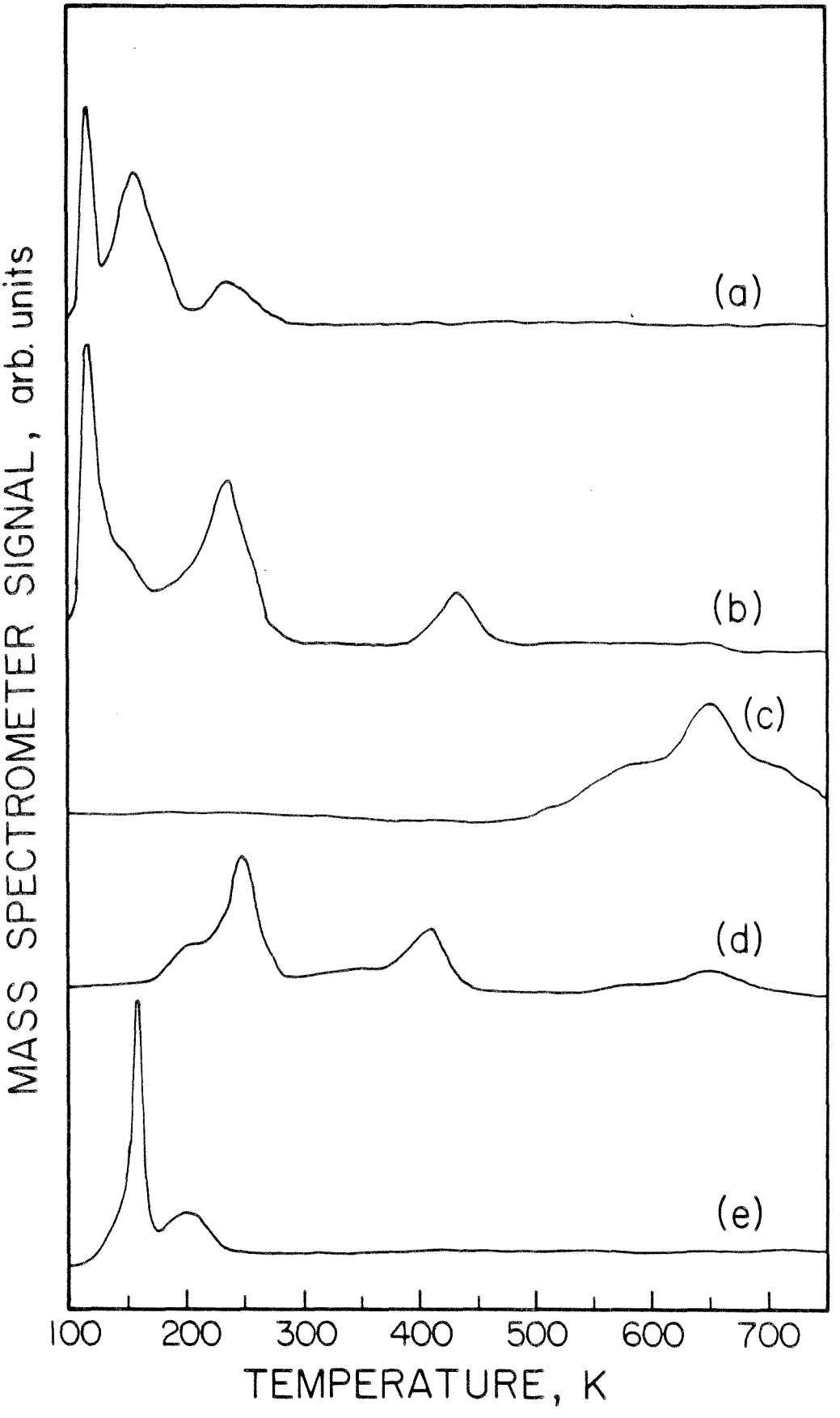
MASS SPECTROMETER SIGNAL, arb. units
(a)
(b)
(c)
(d)
(e)
100
200
300
400
500
600
700
TEMPERATURE, K

Figure 3

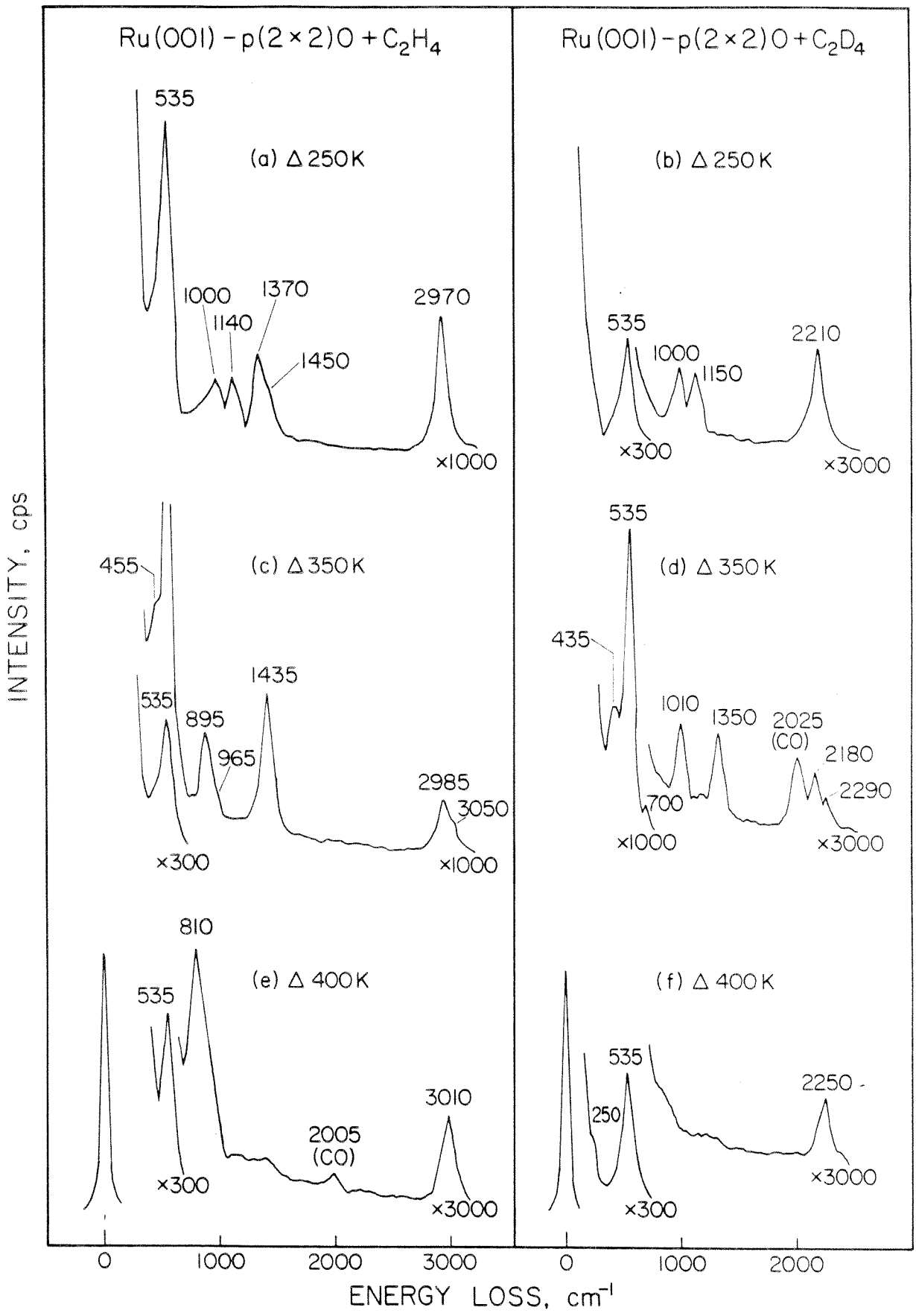
Ru(001) - p(2×2)O + $C_2H_4$
Ru(001) - p(2×2)O + $C_2D_4$
535
(a) Δ 250K
1000
1140
1370
1450
2970
×1000
(b) Δ 250K
535
1000
1150
2210
×300
×3000
455
(c) Δ 350K
535
895
965
1435
2985
3050
×300
×1000
535
(d) Δ 350K
435
1010
1350
2025
(CO)
2180
2290
700
×1000
×3000
810
(e) Δ 400K
535
2005
(CO)
3010
×300
×3000
(f) Δ 400K
535
250
2250
×300
×3000
INTENSITY, cps
0
1000
2000
3000
0
1000
2000
ENERGY LOSS, $cm^{-1}$

Figure 4

(a)

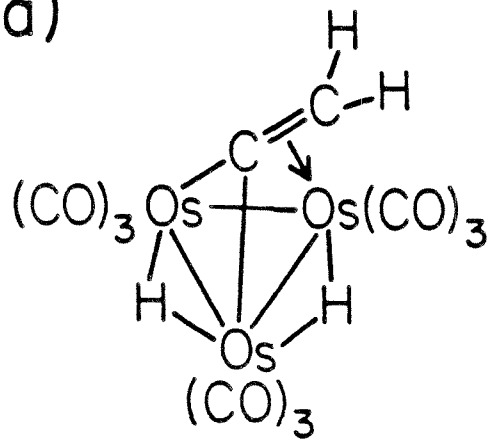
H
C–H
C
(CO)3 Os
Os(CO)3
H
H
Os
(CO)3

(b)

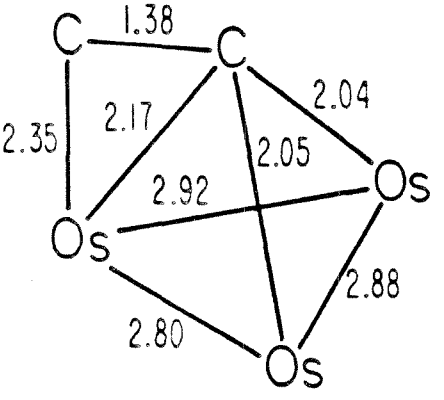
C
1.38
C
2.04
2.35
2.17
2.05
Os
2.92
Os
2.88
2.80
Os

(c)

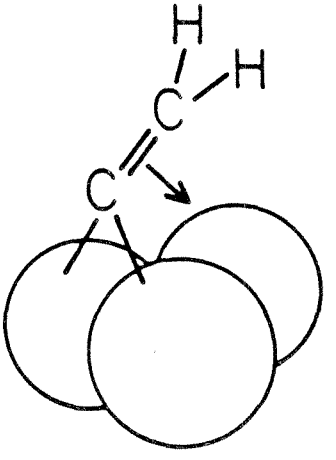
H
H
C
C

Figure 5

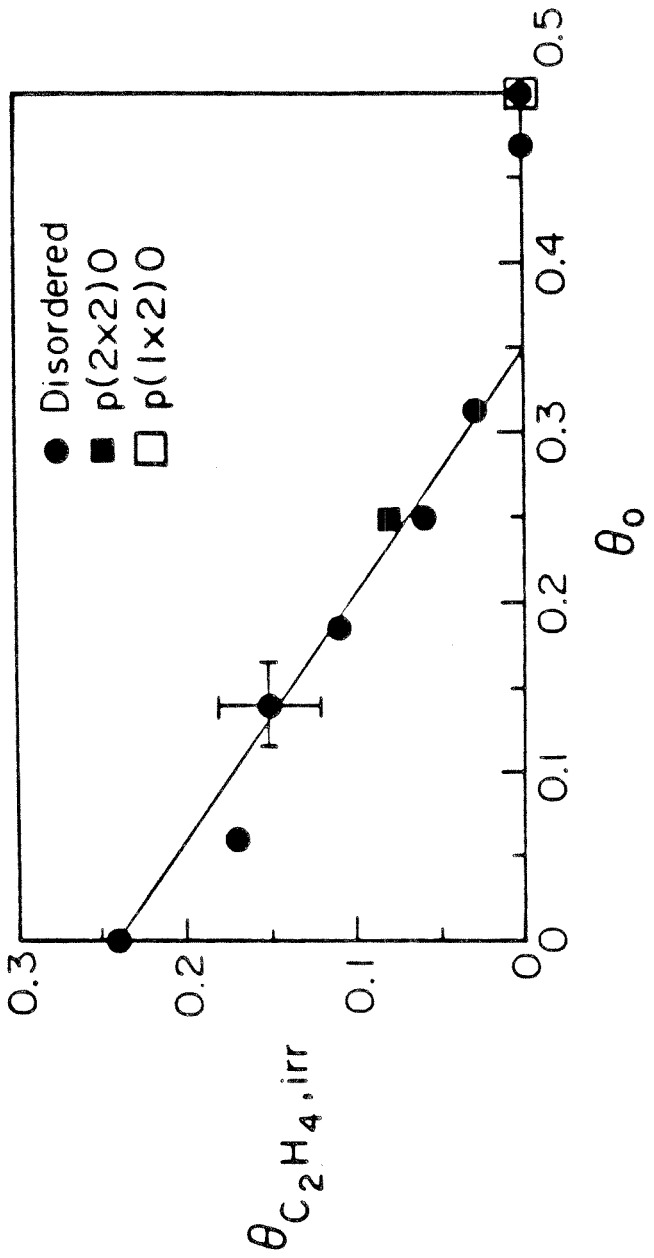
Disordered
p(2x2)O
p(1x2)O
0.3
0.2
0.1
0
0
0.1
0.2
0.3
0.4
0.5
$\theta_{C_2H_4,irr}$
$\theta_O$

Figure 6

# CHAPTER VI

## The Interaction of Methylamine with the Ru(001) Surface

**Abstract**

The chemisorption and decomposition of methylamine on the Ru(001) surface have been investigated using high-resolution electron energy loss spectroscopy and thermal desorption mass spectrometry. Methylamine chemisorbs molecularly below 300 K and is coordinated to the ruthenium via the lone pair of electrons on the nitrogen atom. Annealing to 300 K induces carbon-hydrogen bond cleavage yielding chemisorbed $CH_2NH_2$ and hydrogen adatoms. Further annealing to 350 K results in the formation of $CHNH_2$, which is also bonded to the surface via the carbon atom. The lone pair of electrons originally on the nitrogen atom is delocalized and contributes to the carbon-nitrogen bonding in $CHNH_2$. The frequency of the ν(CN) mode occurs between those expected for unperturbed carbon-nitrogen single and double bonds. The chemisorbed $CHNH_2$ decomposes via two competing pathways. The minority pathway leads to the formation of carbon adatoms and the evolution of ammonia. The majority pathway is the total dehydrogenation to a side-on bonded C=N adspecies with simultaneous evolution of hydrogen occurring. The C=N decomposes to carbon and nitrogen adatoms upon annealing to between 500 and 700 K, and the recombinative desorption of nitrogen is observed above 800 K.

## I. Introduction

Recent spectroscopic investigations of the interaction of ammonia adsorbed on the Ru(001) surface (1-3) and formamide adsorbed on the the Ru(001)-p(1x2)O surface (4) indicate the occurrence of molecular chemisorption at low temperatures, with bonding via a sharing of the lone pair of electrons on the nitrogen (and/or oxygen) atom with the surface. To elucidate further the nature and stability of this type of bonding, we have examined the molecular chemisorption of methylamine on Ru(001). The decomposition of this amine was also studied and serves as a comparison to the decomposition of formamide, ammonia and methanol (5). The decomposition of methylamine should clarify the different propensities for carbon-hydrogen and nitrogen-hydrogen bond cleavage. This also permits a comparison of carbon-nitrogen bond cleavage in the decomposition products of methylamine with carbon-nitrogen bond cleavage in the decomposition products of formamide (4).

Recently, using electron energy loss spectroscopy (EELS), Baca et al. (6) have shown that methylamine is adsorbed molecularly on the Ni(100), Ni(111), Cr(100) and Cr(111) surfaces at 300 K. The spectra of the chemisorbed methylamine indicate that it is bonded on all four surfaces through the lone pair of electrons on the nitrogen atom.

The reactions of methylamine with hydrogen have been examined over thin films of transition metals (7) and silica-supported metal catalysts (8). The two dominant reactions that are observed on supported silver, gold, osmium, palladium, platinum, ruthenium, iridium, rhodium, nickel and cobalt catalysts and thin films, are the formation of ammonia and methane and alkylation to dimethylamine. Additionally, methyl cyanide ($CH_3CN$) is synthesized on supported ruthenium and osmium. The reaction of hydrogen cyanide with hydrogen over metal films produces the same reaction products as methylamine (7). The present work will attempt to identify spectroscopically possible reaction intermediates, which could not be accomplished in these earlier investigations.

## II. Experimental Procedures

The EEL spectrometer used in these studies, as well as the ultrahigh vacuum (UHV) chamber in which it is contained, has been described in detail elsewhere (9). Briefly, the stainless steel UHV

chamber is pumped by both a 220 l/s noble ion pump and a titanium sublimation pump, which reduce the base pressure to below $10^{-10}$ Torr. The home-built EEL spectrometer is of the Kuyatt-Simpson type, with 180° hemispherical deflectors serving as the energy dispersing elements in both the monochromator and the analyzer. The monochromator is spatially fixed, but the analyzer is rotatable to allow off-specular spectra to be measured. All spectra presented and referred to in this paper were collected in the specular direction unless otherwise noted. The impact energy of the incident electron beam was between 4 and 6 eV in all cases, and the beam was incident on the Ru(001) crystal at an angle of 60° with respect to the surface normal. The instrumental energy resolution in these studies, defined as the full-width at half-maximum of the elastically scattered beam, varied from 60 to 80 cm−1 while maintaining count rates in the elastic peak between 1.5 and 3.5 x $10^5$ cps.

The Ru(001) crystal was cooled to 80 K with liquid nitrogen and heated resistively. The crystal was cleaned using periodic argon ion sputtering and routine annealing to 1000 K in 7 x $10^{-8}$ Torr of O2, followed by annealing to 1700 K *in vacuo*. Surface cleanliness was monitored by EELS and hydrogen thermal desorption.

A second UHV apparatus was used to conduct thermal desorption mass spectrometry and low-energy electron diffraction (LEED) measurements (**10**). This chamber also has a base pressure below $10^{-10}$ Torr, using similar pumping techniques, and liquid nitrogen cooling and resistive heating of the crystal were similarly employed. It contains a UTI-100C quadrupole mass spectrometer enclosed in a glass envelope for selective sampling of gases that desorb from only the well-oriented front surface of the single crystal (**11**). This envelope was removed for the ammonia thermal desorption experiments in which very weak signals were observed. Low-energy electron diffraction optics and a rotable Faraday cup are available for the display of LEED patterns and the measurement of LEED beam profiles. No ordered LEED structures other than the (1x1) pattern of the unreconstructed substrate were observed following the adsorption of various coverages of methylamine and annealing to higher temperatures. Hence, no LEED results are discussed here. A single-pass cylindrical mirror electron energy analyzer with an integral electron gun is available for Auger electron spectroscopy. The Ru(001) crystal mounted in this chamber was cleaned as described above, and cleanliness was monitored by both Auger

electron spectroscopy and hydrogen thermal desorption.

Methylamine, $CH3NH_2$ (98.0% min.), was obtained from Matheson, and N-deuterated methylamine (99.1% min., 98% $CH3ND_2$) was obtained from MSD Isotopes. Perdeutero methylamine (98.0% min., 95% $CD_3ND_2$) was obtained from Protech. All three isotopes of methylamine were further purified via three freeze-thaw-pump cycles prior to use. The purity of all gases was verified *in situ* by mass spectrometry in both chambers. Gas exposures are reported in units of Langmuirs, where 1 Langmuir = 1 L ≡ $10^{-6}$ Torr-s. The quoted exposures have not been corrected for the relative ionization probabilities of methylamine and nitrogen.

## III. Results

### A. Thermal Desorption Mass Spectrometry

Thermal desorption spectra that were measured after the adsorption of methylamine on Ru(001) at temperatures below 100 K are displayed in Figs. 1-4. Only molecular methylamine, hydrogen, nitrogen and ammonia desorb from these overlayers. In particular, neither hydrogen cyanide nor methane was observed. Molecular methylamine desorbs in a peak at 330 K for low initial exposures (between 0.2 and 1 L) of methylamine [cf. Fig. 1(a)]. This peak downshifts and broadens with increasing coverage. Assuming a preexponential factor of the desorption rate coefficient of $10^{13}$ to $10^{14}$ $s^{-1}$, the activation energy of desorption of methylamine at low coverage is estimated to be 20 ± 2 kcal/mol (12). At moderate exposures a second peak appears at 240 K as shown in Fig. 1(b). Finally, at high exposures a peak appears at 130 K [cf. Fig. 1(c) and (d)], which does not saturate with increasing exposure and is due to the desorption of a molecular multilayer. The assignment of this peak to a molecular multilayer is confirmed by EELS measurements [cf. Sec. III.B].

In addition to the reversibly adsorbed methylamine, hydrogen desorption is observed which indicates that irreversible (dissociative) adsorption of methylamine occurs. At submonolayer methylamine coverages, the hydrogen thermal desorption peak is purely desorption-limited and shifts to lower temperature with increasing coverage [cf. Fig. 2(a)-(c)]. Hydrogen desorbs in a peak at approximately 380 K and also in a low temperature shoulder for a saturation methylamine coverage [cf. Fig. 2(d)].

Nitrogen thermal desorption occurs between 800 and 1050 K. As shown in the spectra of Fig. 3, the nitrogen desorption peak shifts to lower temperature with increasing coverage. This coverage dependence and the high desorption temperatures are both indicative of the recombinative desorption of nitrogen adatoms. The recombinative desorption of nitrogen atoms following the decomposition of ammonia on Ru(001) (**1-2**) exhibits a similar coverage dependence, although the desorption temperature of the nitrogen is approximately 100 K lower due to the absence of carbon adatoms following ammonia decomposition and the presence of carbon adatoms following methylamine decomposition.

Ammonia desorbs in a reaction-limited peak near 380 K [cf. Fig. 4]. This temperature is above that (approximately 315 K) at which a similar coverage of ammonia desorbs molecularly from the Ru(001) surface (**1-3**). The formation of ammonia represents a minority pathway for the decomposition of irreversibly adsorbed methylamine. At most, a fractional coverage of 0.02 of methylamine decomposes to ammonia and carbon adatoms (**13**). In contrast, the $N_2$ and $H_2$ thermal desorption spectra indicate that a fractional coverage of 0.08 of methylamine decomposes to nitrogen, carbon and hydrogen adatoms following a saturation exposure.

**B. Electron Energy Loss Spectroscopy**

In agreement with the thermal desorption results, the EEL spectra measured after exposing the Ru(001) surface to 4 L or more of methylamine ($CH_3NH_2$) at temperatures below 130 K are indicative of a molecular multilayer. A typical EEL spectrum of the multilayer is shown in Fig. 5(a). Similar EEL spectra have been measured for multilayers of $CH_3ND_2$ and $CD_3ND_2$ adsorbed at 80 K. The frequencies of the modes of multilayer $CH_3NH_2$, $CH_3ND_2$ and $CD_3ND_2$ agree very well with those of methylamine in the solid state and somewhat less well with those of methylamine in the gas phase. These modes are listed and assigned in Table I (**14-16**). The most intense loss feature at 1000 $cm^{-1}$ in the spectrum of $CH_3NH_2$ in Fig. 5(a) is assigned to the carbon-nitrogen stretching mode, and this assignment was confirmed by the EEL spectra of multilayers of $CH_3ND_2$ and $CD_3ND_2$. In the EEL spectrum of multilayer $CH_3NH_2$, this feature also gains some intensity due to an overlap with the $NH_2$ wagging mode that shifts to 780 $cm^{-1}$ in the spectrum of multilayer $CH_3ND_2$ and 730 $cm^{-1}$ for multilayer $CD_3ND_2$. The observed frequency of the $NH_2$ wagging mode (1000 $cm^{-1}$) of multilayer

$CH_3NH_2$ is shifted to a higher frequency than that of $CH_3NH_2$(s) at 955 $cm^{-1}$ (**16**) due to this overlap. The peaks assigned to the $NH_2$ and $ND_2$ wagging modes cannot be assigned to the $NH_2$ and $ND_2$ twisting modes because the infrared inactive twisting mode is expected to be much weaker, if resolved at all. The peak at 1170 $cm^{-1}$ in Fig. 5(a) is the $CH_3$ rocking mode, which occurs at 1185 $cm^{-1}$ for $CH_3ND_2$ and shifts to 835 $cm^{-1}$ for $CD_3ND_2$. The $\rho(CD_3)$ mode of $CD_3ND_2$ is downshifted and it appears as a shoulder on the intense $\omega(ND_2)$ mode at 730 $cm^{-1}$. The symmetric methyl deformation mode occurs at 1440 and 1445 $cm^{-1}$ for multilayers of $CH_3NH_2$ and $CH_3ND_2$ and shifts to 1075 $cm^{-1}$ for $CD_3ND_2$. The asymmetric methyl deformation mode is not resolved in any of these spectra. The $NH_2$ scissoring mode occurs at 1580 cm–1, while the $ND_2$ scissoring mode is observed at 1185 and 1145 $cm^{-1}$ for $CH_3ND_2$ and $CD_3ND_2$, respectively. The symmetric and asymmetric $CH_3$ ($CD_3$) stretching modes are not resolved, and appear at 2930 $cm^{-1}$ (2215 $cm^{-1}$) for $CH_3NH_2$ ($CD_3ND_2$) and 2915 $cm^{-1}$ for $CH_3ND_2$. The symmetric and asymmetric $NH_2$ stretching modes appear at 3260 and 3360 $cm^{-1}$ for multilayer $CH_3NH_2$, while the symmetric and asymmetric $ND_2$ stretching modes appear at 2375 and 2490 $cm^{-1}$ for $CD_3ND_2$ and 2395 and 2485 $cm^{-1}$ for $CH_3ND_2$. The $NH_2$ and $ND_2$ twisting modes are not resolved in any of these spectra.

As discussed in Sect. III.A, the thermal desorption spectra of molecular methylamine indicate that this multilayer desorbs at 130 K and that additional methylamine desorbs molecularly between approximately 200 and 350 K. In agreement with these thermal desorption results, EEL spectra measured after annealing a saturation coverage of $CH_3NH_2$ to 200 K are characteristic of molecularly chemisorbed methylamine. The EEL spectra of chemisorbed $CH_3NH_2$, $CH_3ND_2$ and $CD_3ND_2$ [cf. Fig. 5(b)-(d)] differ only slightly from those of the corresponding isotopes of multilayer methylamine. Features in the EEL spectrum of the chemisorbed $CH_3NH_2$ are sharper compared to those of the multilayer [compare Fig. 5(a) and (b)] due to the orientational order in the former. In addition, a new peak appears at 775 $cm^{-1}$. The overall similarity, however, between the EEL spectra of multilayer and chemisorbed methylamine indicates that the chemisorbed methylamine is perturbed only slightly by bonding to the ruthenium. In particular, no bond cleavage has occurred in the methylamine. This implies that the chemisorbed methylamine is bonded to the ruthenium via donation of the lone pair of electrons on the

nitrogen, analogous to the coordination of chemisorbed ammonia on this surface.

The observed modes of molecularly chemisorbed methylamine are listed and assigned in Table II. The intense feature at 975 to 980 $cm^{-1}$ in the three spectra of Fig. 5 (b)-(d) is the carbon-nitrogen stretching mode. Off-specular EEL measurements of molecularly chemisorbed $CH_3ND_2$ indicate that this mode is strongly dipole-excited, consistent with a carbon-nitrogen bond that is tilted with respect to the plane of the surface. As in the case of the multilayer, in the spectrum of chemisorbed $CH_3NH_2$, the $\nu$(CN) mode gains some intensity due to the overlapping $NH_2$ wagging mode. In the EEL spectra of $CH_3ND_2$ and $CD_3ND_2$, the $ND_2$ wagging mode shifts to 780 and 725 cm–1, respectively. Off-specular EEL measurements indicate that these features are largely dipole-excited, consistent with the assignment of these peaks to the $ND_2$ wagging mode, which is expected to exhibit a larger dynamic dipole perpendicular to the surface than, for example, the $ND_2$ twisting and rocking modes in this bonding configuration. The $NH_2$ scissoring mode of chemisorbed $CH_3NH_2$ occurs at 1575 $cm^{-1}$ in Fig. 5(b), and the $ND_2$ scissoring mode of $CD_3ND_2$ is observed at 1145 $cm^{-1}$ in Fig. 5(d). This mode overlaps the $\rho(CH_3)$ mode at 1165 $cm^{-1}$ in the spectrum of $CH_3ND_2$. The peaks at 1445 and 1470 $cm^{-1}$ in Fig. 5(b) and (c) are assigned to the symmetric methyl deformation modes of $CH_3NH_2$ and $CH_3ND_2$. This mode shifts down to 1095 $cm^{-1}$ for $CD_3ND_2$. In none of the spectra is the asymmetric methyl deformation mode resolved. Off-specular EEL measurements indicate that the $\delta_s(CH_3)$ and $\delta(ND_2)$ modes of $CH_3ND_2$ are primarily due to impact scattering. The symmetric and asymmetric carbon-hydrogen stretching modes are assigned to features at 2875 and 2960 $cm^{-1}$ for $CH_3NH_2$, and 2880 and 2950 $cm^{-1}$ for $CH_3ND_2$. The corresponding carbon-deuterium stretching modes shift to 2085 and 2200 $cm^{-1}$ for perdeuteromethylamine. The $\nu_a(NH_2)$ mode is not resolved from the $\nu_s(NH_2)$ mode at 3250 $cm^{-1}$ for $CH_3NH_2$, nor are the $\nu_a(ND_2)$ and $\nu_s(ND_2)$ modes resolved in the peak at 2430 $cm^{-1}$ for $CH_3ND_2$. However, the symmetric and asymmetric nitrogen-deuterium stretching modes were resolved in Fig. 5(d) at 2360 and 2445 $cm^{-1}$, respectively, for chemisorbed $CD_3ND_2$. The peak that occurs at 775 $cm^{-1}$ in the spectrum of chemisorbed $CH_3NH_2$ is assigned to the $NH_2$ rocking mode, which downshifts to near 600 of $CD_3ND_2$, but which was not resolved in the spectrum of $CH_3ND_2$. The observation of $\rho(NH_2)$ at 775 $cm^{-1}$ is consistent with infrared spectra of cis-$[Pt(CH_3NH_2)_2Cl_2]$ in which the $NH_2$ rock-

ing mode occurs at 740 $cm^{-1}$ (17). This cannot be assigned to the $NH_2$ twisting mode, which should occur at a higher frequency, e.g. 1080 $cm^{-1}$ in the platinum complex. Finally, a weak shoulder at 340 $cm^{-1}$ on the elastic peak of Fig. 5(b)-(d) is due to the ruthenium-nitrogen stretching mode of the chemisorbed methylamine.

Annealing the chemisorbed methylamine to 300 K results in both molecular desorption, as demonstrated by the thermal desorption results, as well as decomposition, as judged by EELS. Figure 6(a) shows an EEL spectrum that was measured after annealing a molecular multilayer of $CH_3NH_2$ to 300 K. In this spectrum, there is no longer a peak at 1175 $cm^{-1}$, and new intense peaks have appeared at 600 and 1205 $cm^{-1}$. In the corresponding EEL spectrum of $CH_3ND_2$, new peaks appear at 555 and 1230 $cm^{-1}$, and the peak at 1165 $cm^{-1}$ has attenuated. The peak at 555 $cm^{-1}$ appears at 535 $cm^{-1}$ in the spectrum of $CD_3ND_2$ annealed to 300 K, the peak at 985 $cm^{-1}$ increases in intensity in this spectrum, and the peak at 835 $cm^{-1}$ has disappeared.

The species stable on the surface after annealing molecularly chemisorbed methylamine to 300 K are surface hydrogen and $CH_2NH_2$, which is formed via the cleavage of a carbon-hydrogen bond. As shown in Fig. 6(a), the EEL spectrum of $CH_2NH_2$ exhibits the unresolved $\nu_s(CH_2)$ and $\nu_a(CH_2)$ modes at 2925 $cm^{-1}$, and the $\nu_s(NH_2)$ and $\nu_a(NH_2)$ modes at 3290 and 3365 $cm^{-1}$, respectively. The data listed in Table III show that the corresponding modes are also observed following $CH_3ND_2$ and $CD_3ND_2$ adsorption and annealing to 300 K. In the spectrum of $CH_2ND_2$, modes at 2930 and 2420 $cm^{-1}$ are assigned to the symmetric carbon-hydrogen and nitrogen-deuterium stretching modes from which the asymmetric stretching modes are not resolved. All four modes are resolved in the spectrum of $CD_2ND_2$ with $\nu_s(CD_2)$ and $\nu_a(CD_2)$ at 2090 and 2190 $cm^{-1}$, and $\nu_s(ND_2)$ and $\nu_a(ND_2)$ at 2400 and 2500 $cm^{-1}$.

The $NH_2$ (or $ND_2$) scissoring mode is observed at 1570 $cm^{-1}$ for $CH_2NH_2$ and 1230 and 1190 $cm^{-1}$ for $CH_2ND_2$ and $CD_2ND_2$. This indicates that the $NH_2$ (or $ND_2$) group is still intact at 300 K, and indeed the $NH_2$ and $ND_2$ wagging modes are still present. The $ND_2$ wag occurs at 735 $cm^{-1}$ in the spectrum of $CD_2ND_2$ and near 810 $cm^{-1}$ for $CH_2ND_2$. The 810 $cm^{-1}$ mode is, in fact, due to the overlapping $ND_2$ wagging and $CH_2$ rocking modes of $CH_2ND_2$, and this probably shifts the wagging mode to a slightly higher frequency than expected (near 735 $cm^{-1}$ as in $CD_3ND_2$). In the EEL spectrum of

$CH_2NH_2$, the $NH_2$ wagging mode overlaps the ν(CN) mode at 1000 $cm^{-1}$. The $ND_2$ rocking modes of $CH_2ND_2$ and $CD_2ND_2$ are not resolved in the corresponding EEL spectra from the intense and broad new peaks at 555 and 535 $cm^{-1}$. However, the $NH_2$ rocking mode persists in the spectrum of $CH_2NH_2$ at 775 $cm^{-1}$, and this mode overlaps the $CH_2$ rocking mode. The $NH_2$ and $ND_2$ twisting modes of all three isotopes were not resolved in any of the EEL spectra.

The persistence of the intense peaks at 1000, 995 and 985 $cm^{-1}$ in the EEL spectra of $CH_3NH_2$, $CH_3ND_2$ and $CD_3ND_2$ annealed to 300 K indicates that the carbon-nitrogen single bond is still intact and has a stretching frequency virtually unchanged from the molecularly chemisorbed methylamine.

The EEL spectra of CH3NH2 and $CH_3ND_2$ annealed to 300 K exhibit new peaks, which appear at 1205 and 1230 $cm^{-1}$, that are due to $CH_2$ wagging modes. The $CD_2$ wagging mode of $CD_2ND_2$ shifts on top of the ν(CN) mode at 985 $cm^{-1}$, increasing the intensity of this feature. The formation of a $CH_2$ group is also supported by the loss of the strong $\delta_s(CH_3)$ mode, which was observed at 1445 and 1470 $cm^{-1}$ for $CH_3NH_2$ and $CH_3ND_2$, respectively, and the loss of the $\delta_s(CD_3)$ mode, which occurred at 1095 $cm^{-1}$ for $CD_3ND_2$. These modes are replaced by weaker $CH_2$ scissoring modes at 1420 $cm^{-1}$ for $CH_2NH_2$ and 1430 $cm^{-1}$ for $CH_2ND_2$, and a $CD_2$ scissoring mode at 1095 $cm^{-1}$ for $CD_2ND_2$. The other modes associated with the $CH_2$ and $CD_2$ groups are also present. The $CH_2$ rocking mode overlaps the $NH_2$ rocking mode at 775 $cm^{-1}$ in Fig. 6(a), and this mode overlaps the $ND_2$ wagging mode at 810 $cm^{-1}$ in the spectrum of $CH_2ND_2$. The $CD_2$ rocking mode overlaps the 535 $cm^{-1}$ peak in the spectrum of $CD_2ND_2$. The assignments of the $CH_2$ ($CD_2$) scissoring, wagging and rocking modes are supported by comparison to those of di-σ-bonded ethylene adsorbed on Ru(001) in which the carbon atoms are also $sp^3$-hybridized (**18**). For example, the $CH_2$ ($CD_2$) scissoring mode occurs at 1450 $cm^{-1}$ (1210 $cm^{-1}$) for di-σ-bonded $C_2H_4$, and at 1420 $cm^{-1}$ (1095 $cm^{-1}$) for $CH_2NH_2$. The low apparent frequency of the $CD_2$ scissoring mode of $CD_2ND_2$ is due to the fact that it appears as a shoulder on the peak at 985 $cm^{-1}$. The $CH_2$ ($CD_2$) wagging mode of ethylene is present at 1145 $cm^{-1}$ (900 $cm^{-1}$) and for $CH_2NH_2$ at 1205 $cm^{-1}$ (985 $cm^{-1}$). The $CH_2$ rocking modes are observed at 775 $cm^{-1}$ for both di-σ-bonded $C_2H_4$ and $CH_2NH_2$. The $CH_2$ ($CD_2$) twisting mode of di-σ-bonded ethylene is at 900 $cm^{-1}$ (700 $cm^{-1}$), but this mode was not resolved in the spectra of $CH_2NH_2$.

Finally, the intense peaks at 600, 535 and 555 $cm^{-1}$ in the spectra of $CH_2NH_2$, $CD_2ND_2$ and $CH_2ND_2$, are attributed to the frustrated translations of these species perpendicular to the surface. As mentioned above, the 535 $cm^{-1}$ peak in the spectra of $CD_2ND_2$ also gains some intensity due to $\rho(CD_2)$ and $\rho(ND_2)$ modes. Off-specular EEL measurements indicate that this mode is strongly dipole-active as would be expected for a frustrated translation.

Annealing the Ru(001) surface upon which the $CH_2NH_2$ species is present to 350 K initiates further decomposition as shown by the corresponding EEL spectrum of Fig. 6(b) in which the intense $T_z$ mode of $CH_2NH_2$ at 600 $cm^{-1}$ does not appear, and a new intense peak is observed at 755 $cm^{-1}$. Furthermore, the relative intensities of the modes have changed such that the peak at 1580 $cm^{-1}$ is now the most intense one in the spectrum other than the new peak at 755 $cm^{-1}$. An EEL spectrum of $CH_3ND_2$ annealed to 350 K shows the loss of the peak at 810 cm–1, the appearance of two intense peaks at 580 and 750 $cm^{-1}$, and an increase in the intensity of the peak at 1255 $cm^{-1}$ relative to peaks at 1005 and 1435 $cm^{-1}$. Finally, the EEL spectrum of $CD_3ND_2$ annealed to 350 K exhibits a new peak at 1440 $cm^{-1}$ and a change in relative intensities such that the peak at 1250 $cm^{-1}$ is more intense than the one at 1010 $cm^{-1}$. As will be discussed below, these changes and other more subtle ones show that annealing molecular methylamine to 350 K results in the formation of a $HCNH_2$ species. The observed frequencies and the mode assignments are listed in Table IV.

The $CHNH_2$ is coordinated to the ruthenium surface via the carbon atom, and this gives rise to a $T_z$ mode at 445 to 450 $cm^{-1}$ in the EEL spectra. The existence of a carbon-nitrogen bond order between one and two in this species is proved by the presence of a peak at 1440 $cm^{-1}$ in the spectrum of $CDND_2$. This peak occurs at too high a frequency to correspond to any carbon-deuterium or nitrogen-deuterium deformational mode. The $\nu$(CN) modes of $CHNH_2$ and $CHND_2$ appear at 1460 and 1435 cm–1. The frequencies of these modes are lower than that of an unperturbed carbon-nitrogen double bond expected near 1638 $cm^{-1}$ as in methyleneimine (19). The increase in the frequency of $\nu$(CN) of $CHNH_2$ compared to that of $CH_2NH_2$ is due to delocalization of the lone pair of electrons from the nitrogen atom.

Modes associated with a $NH_2$ group are also clearly present in the EEL spectrum of $CHNH_2$ in

Fig 6(b). The $NH_2$ scissoring mode of $CHNH_2$ occurs at 1580 $cm^{-1}$, and this mode shifts down to 1250 and 1255 $cm^{-1}$ in the spectra of $CDND_2$ and $CHND_2$. These modes exhibit equivalent intensities in all three spectra. The $NH_2$ ($ND_2$) rocking and wagging modes have shifted in frequency, such that $\omega(NH_2)$ appears at a lower frequency than $\rho(NH_2)$, due to the change in the carbon-nitrogen bond order. This will be discussed in greater detail in Sect. IV.B. The $NH_2$ rocking mode appears at 1220 $cm^{-1}$ for $CHNH_2$, while the $ND_2$ rocking modes appear at 1010 and 1005 $cm^{-1}$ in spectra of $CDND_2$ and $CHND_2$. The intense peak at 755 $cm^{-1}$ in Fig. 6(b) is assigned to the overlapping $NH_2$ wagging and CH bending modes. These two modes shift down to 575 $cm^{-1}$ for $CDND_2$. In the spectrum of $CHND_2$ these modes do not overlap, and the CH bending mode occurs at 750 $cm^{-1}$, whereas the $ND_2$ wagging mode occurs at 580 $cm^{-1}$. The assignments of these modes are supported by the observed intensities in the various spectra. The overlapping CH bending and $NH_2$ wagging modes and the overlapping CD bending and $ND_2$ wagging modes both produce strong loss features, while each of the isolated CH bending and $ND_2$ wagging modes of $CHND_2$ is, as expected, approximately half as intense. Finally, the symmetric and asymmetric nitrogen-hydrogen stretching modes are unresolved and appear at 3230 $cm^{-1}$ for $CHNH_2$. The $\nu_s(ND_2)$ and $\nu_a(ND_2)$ modes shift to 2415 and 2495 $cm^{-1}$ for $CDND_2$, and to 2370 and 2480 $cm^{-1}$ for $CHND_2$.

The loss of a hydrogen atom from $CH_2NH_2$ to form $CHNH_2$ is supported by the absence of the $CH_2$ scissoring and wagging modes, and the observation of a second carbon-hydrogen bending mode at 1000 $cm^{-1}$ for $CHNH_2$ and 1005 $cm^{-1}$ for $CHND_2$. The CD bending mode of $CDND_2$ shifts down to 725 $cm^{-1}$ for $CDND_2$. The corresponding carbon-hydrogen and carbon-deuterium stretching modes occur at 2925, 2920 and 2210 $cm^{-1}$ for $CHNH_2$, $CHND_2$ and $CDND_2$, respectively.

Annealing all three isotopes of methylamine to between 400 and 500 K results in species with identical EEL spectra. The EEL spectrum of $CHNH_2$ annealed to 450 K is shown in Fig. 6(c), and exhibits peaks at 355, 465, 585 and 1670 $cm^{-1}$. The intensity of the 585 $cm^{-1}$ peak increases after annealing to 500 K, as the intensities of the other three peaks decrease, and it is the only peak present in EEL spectra measured after annealing to 700 K. Indeed, this peak decreases in intensity only after annealing to above 800 K. It is therefore attributed to the ruthenium-nitrogen stretching mode of

adsorbed nitrogen atoms and the overlapping ruthenium-carbon stretching mode of carbon adatoms. The decrease in intensity of this peak only after annealing to above 800 K is consistent with thermal desorption spectra, which exhibit recombinative desorption of nitrogen above 800 K [cf. Fig. 3]. This peak still maintains some intensity following nitrogen desorption, due to the presence of carbon adatoms, which give rise to a weaker loss peak near 600 $cm^{-1}$ (18).

The three other loss features in Fig. 6(c) are not due to hydrogenic vibrational modes, because they appear at the same frequencies in the spectra of all three isotopes, and also because the thermal desorption spectra indicate that all the hydrogen has desorbed by 450 K. Thus, these modes are assigned to a side-on bonded C=N species. The loss feature at 1670 $cm^{-1}$ is the carbon-nitrogen stretching mode of a double bond, and the modes at 355 and 465 $cm^{-1}$ are the frustrated translations of the CN species. As discussed above, annealing the C=N to 700 K induces cleavage of the C=N bond to form carbon and nitrogen adatoms. The nitrogen atoms combine and desorb at still higher temperatures. The decomposition mechanism of methylamine is summarized in Fig. 7.

## IV. Discussion

### A. Molecular Methylamine Adsorption

The thermal desorption spectra of methylamine indicate that a portion of the chemisorbed methylamine desorbs molecularly between approximately 200 and 350 K, and that multilayers of methylamine desorb at 130 K. These spectra are similar to those of molecular ammonia adsorbed on Ru(001) (1-3). The ammonia desorbs in a peak at 315 K at low coverages, which broadens and shifts to lower temperatures with increasing coverage until a second desorption peak due also to chemisorbed ammonia appears at 180 K. It has been suggested that the broadening and shifting of the higher temperature ammonia desorption peak are the result of repulsive lateral interactions within the overlayer (3). The chemisorbed ammonia molecules are coordinated to the surface via the nitrogen atom with the threefold axis normal to the surface as shown by electron stimulated desorption ion angular distribution and work function measurements (3). The similarities between the thermal desorption spectra of molecular ammonia and methylamine adsorbed on Ru(001) suggest that the coordination of methylamine to the surface occurs via the lone pair of electrons on the nitrogen atom. However, the broadening and

shifting to lower temperature of the methylamine thermal desorption peak with increasing coverage probably result from an electronic effect. The chemisorbed methylamine donates some electron density from the nitrogen atom to the substrate and this affects the electron donation of subsequently adsorbed methylamine, decreasing the binding energy. The apparent methylamine desorption peak at 240 K probably occurs due to the concommitant dehydrogenation of methylamine to $CH_2NH_2$ and hydrogen adatoms, increasing the effective surface coverage.

The assignments of the vibrational modes of multilayers of methylamine on Ru(001) are very similar to those of solid methylamine obtained from infrared spectra, as shown in Table I. The isotopic shifts of the modes of multilayers of $CH_3ND_2$ and $CD_3ND_2$ also agree with these assignments. The occurrence of the $\nu$(CN) and $\omega(NH_2)$ modes of multilayer $CH_3NH_2$ at 1000 $cm^{-1}$ rather than at 1048 and 955 $cm^{-1}$ as in $CH_3NH_2$(s), is due to the overlap of these features, which causes the peak to appear at an intermediate frequency. Similarly, the symmetric and asymmetric carbon-hydrogen stretching modes of multilayer $CH_3NH_2$ are not resolved, and the peak due to these two modes appears at a frequency between the $\nu_s(CH_3)$ and $\nu_a(CH_3)$ modes of $CH_3NH_2$ in the solid and gas phases. The overall agreement between the vibrational assignments is, however, convincing.

Annealing to 200 K desorbs the methylamine multilayer, leaving molecularly chemisorbed methylamine. The EEL spectra of molecularly adsorbed methylamine are very similar to those of the multilayer with the exception of a slightly lower carbon-nitrogen stretching frequency. The corresponding mode assignments agree well not only with those of the multilayer, but also with those of methylamine adsorbed on Ni(111) at 300 K (**6**), and with those of the methylamine ligand in cis-$[Pt(CH_3NH_2)_2Cl_2]$ (17). A weak mode at 775 cm−1, which is not observed in the EEL spectra of the multilayer, is attributed to the $NH_2$ rocking mode of the molecularly chemisorbed methylamine. The absence of this mode in the EEL spectra of multilayer methylamine is not surprising because the $NH_2$ rocking mode does not occur for methylamine in the gas phase because it is a free rotation. Adsorption of methylamine on the ruthenium surface restricts this rotation, resulting in the $NH_2$ rocking mode at 775 $cm^{-1}$. The $NH_2$ rocking mode occurs at 740 $cm^{-1}$ in the infrared spectrum of cis-$[Pt(CH_3NH_2)_2Cl_2]$ in agreement with this assignment. This mode cannot be attributed to the $NH_2$ twisting mode because $\tau(NH_2)$ would

occur at a higher frequency, e.g. 1080 $cm^{-1}$ in cis-$[Pt(CH_3NH_2)_2Cl_2]$, than the $NH_2$ rocking mode.

The many similarities between the vibrational spectra of chemisorbed, multilayer, gaseous and solid methylamine suggest that the methylamine bonds to the ruthenium surface through the lone pair of electrons on the nitrogen atom. This is the only possible manner in which molecular methylamine can coordinate to the surface. Note that molecularly chemisorbed ammonia on Ru(001) (**1-3**) is also adsorbed through the lone pair of electrons on the nitrogen atom, and that molecular formamide on Ru(001)-p(1x2)O bonds through a lone pair of electrons on the oxygen atoms (**4**). The ruthenium-nitrogen stretching mode of chemisorbed methylamine is observed at 340 $cm^{-1}$. The frequency of this mode is close to the ruthenium-oxygen stretching mode at 310 $cm^{-1}$ of chemisorbed formamide, which is bonded to the Ru(001) surface via a lone pair of electrons of the oxygen atom (**4**).

**B. Decomposition of Methylamine**

The molecularly chemisorbed methylamine after a saturation exposure either desorbs molecularly between 200 and 350 K or dehydrogenates to $CH_2NH_2$ after annealing to 300 K. This indicates that a small coverage of molecularly adsorbed methylamine contributes to the EEL spectra that were measured after annealing to 300 K. In particular, the ν(CN) mode probably gains the most intensity due to the molecular methylamine, since this mode is the most intense in the spectra of chemisorbed methylamine that were measured after annealing to 200 K. The EEL spectrum of Fig. 6(a) cannot be attributed solely to $CH_3NH_2$, however, due to the presence of the 600 $cm^{-1}$ peak and the change in the relative intensities of the 1205, 1420 and 1570 $cm^{-1}$ peaks. The peak at 600 $cm^{-1}$ does not shift significantly upon deuteration (either $CH_3ND_2$ or $CD_3ND_2$), indicating that it is not a hydrogenic vibrational mode. This mode is also too intense to correspond to the ν(Ru-C) or ν(Ru-N) modes of low coverages of carbon or nitrogen adatoms. Hence, it must be attributed to the new species present on the surface at 300 K, namely, $CH_2NH_2$ bound through the carbon atom to the surface. In particular, it is assigned to the frustrated translation of this species perpendicular to the surface. Note that in the infrared spectra of $CH_3MnH$ and $CH_3FeH$, the ν(M–$CH_3$) modes are very intense and occur at 501 and 521 cm–1, respectively (**20**). Thus, the assignment of the intense peaks that occur from 535 to 600 $cm^{-1}$ to ν(Ru-C) of the isotopes of $CH_2NH_2$ appears reasonable. The change of relative intensities of the modes near 1420

and 1570 $cm^{-1}$ occurs because, while the mode at 1570 $cm^{-1}$ is still a $NH_2$ scissoring mode, the mode near 1420 $cm^{-1}$ is no longer $\delta_s(CH_3)$, but rather $\delta(CH_2)$ of CH2$NH_2$, which exhibits a lower intensity. Similarly, the peak at 1205 $cm^{-1}$ in Fig. 6(a) is the $CH_2$ wagging mode of $CH_2NH_2$, which is more intense than the $CH_3$ rocking mode of $CH_3NH_2$ that occurs at 1175 $cm^{-1}$ in Fig. 5(b).

To summarize, the species present at 300 K is assigned to $CH_2NH_2$ with a carbon nitrogen single bond in view of the existence of a carbon-nitrogen stretching mode near 1000 $cm^{-1}$ in the EEL spectra of all three isotopes, the presence of the $NH_2$ and $ND_2$ scissoring and wagging modes, and the appearance of the $CH_2$ and $CD_2$ scissoring and wagging modes.

Annealing the $CH_2NH_2$ to 350 K causes further dehydrogenation to $CHNH_2$. The EEL spectra of this species show the absence of the 600 $cm^{-1}$ peak and greater intensity of the $\delta(NH_2)$ mode at 1580 $cm^{-1}$ relative to the 1000 and 1220 $cm^{-1}$ peaks. The latter occurs because the peak near 1000 $cm^{-1}$ is no longer due to the overlappping $\nu$(CN) mode of a carbon-nitrogen single bond and $\omega(NH_2)$ but is due only to a carbon-hydrogen bending mode. The $\omega(NH_2)$ mode shifts down to 755 cm–1, the frequency expected for a $NH_2$ group bound to a carbon atom with a bond order between one and two (21). Similarly, the peak near 1220 $cm^{-1}$ is no longer $\omega(CH_2)$, but rather $\rho(NH_2)$, which shifts to higher frequency due to the change in the carbon-nitrogen bond order (23).

The existence of $\nu$(CN) at 1460 $cm^{-1}$ is confirmed by EEL spectra of $CDND_2$, which exhibits a mode at 1440 cm–1. This frequency is approximately 200 $cm^{-1}$ lower than that expected for a carbon-nitrogen double bond in, for example, methylamine (19), but more than 400 $cm^{-1}$ higher than that of a single bond in methylamine. This strengthening of the carbon-nitrogen bond is due to a delocalization of the lone pair of electrons from the nitrogen atom.

Electron energy loss spectra of methylamine annealed to 400 K are indicative of only adsorbed C=N and carbon adatoms. The EEL and thermal desorption spectra of methylamine indicate that two decomposition pathways are followed by $CHNH_2$, namely, the formation of C=N, and the formation and desorption of ammonia in a reaction-limited peak at 380 K, the latter of which also produces carbon adatoms. Ammonia exhibits vibrational losses at 480, 600, 1160, 1590, 3240 and 3380 $cm^{-1}$ on the clean surface and desorbs molecularly at 315 K (1-3,24). Ammonia was not observed via EELS under

any conditions of temperature or coverage following methylamine adsorption. There was also no evidence for NH formation. Following the decomposition of formamide on Ru(001), NH exhibits peaks at 690, 1350 and 3315 $cm^{-1}$, which are assigned to the ν(Ru-NH), δ(NH) and ν(NH) modes, respectively. The NH decomposes between 350 and 400 K (**4**). Steady-state ammonia decomposition experiments on Ru(001) indicate that $NH_2$ decomposition to NH and $NH_2$ hydrogenation to $NH_3$ are competing reactions near 400 K (**1**). However, following methylamine decomposition on Ru(001), the fractional coverage of hydrogen on the surface at 350 K must be less than 0.40, which is probably insufficient to hydrogenate NH to ammonia. The low hydrogen coverage and the absence of any NH adsorbed on the surface in the EEL spectra suggest that ammonia formation does not occur via an NH intermediate but can occur via an $NH_2$ intermediate. Any reaction that forms a methylidyne species (CH) can also be eliminated because methylidyne is stable on Ru(001) below 500 K and exhibits an intense δ(CH) mode at 810 $cm^{-1}$, which was not observed in any of the EEL spectra of methylamine. Furthermore, methylidyne dehydrogenation evolves hydrogen between 500 and 750 K, which was not observed in the hydrogen thermal desorption spectra of methylamine. Intramolecular hydrogen transfer on $HNH_2$ to form a carbon adatom and ammonia is considered unlikely due to the observation that adsorption of hydrogen onto the metal surface is usually favored over intramolecular hydrogen transfer reactions. Thus, the following ammonia formation reactions cannot be ruled out following methylamine formation:

$$HCNH_2(a) \rightarrow H(a) + CNH_2(a)$$

$$HCNH_2(a) \rightarrow H(a) + HCNH(a)$$

$$CNH_2(a) \rightarrow C(a) + NH_2(a)$$

$$NH_2(a) + H(a) \rightarrow NH_3(g) \quad .$$

Dehydrogenation of a HCNH or $CNH_2$ intermediate could also lead to the formation of the CN.

The spectroscopically observed conversion of methylamine to $CH_2NH_2$, which dehydrogenates to $CHNH_2$, which leads to ammonia formation, suggests that both $CH_2NH_2$ and $CHNH_2$ are likely intermediates in the formation of ammonia and methane from methylamine on both thin films and supported ruthenium catalysts.

Following the adsorption of a saturation coverage of methylamine and annealing to 400 K, a fractional coverage of less than 0.02 of $CHNH_2$ forms ammonia and carbon atoms. Simultaneously, a coverage of 0.08 of $CHNH_2$ also dehydrogenates to C=N and hydrogen. The desorption of hydrogen near 380 K, following a saturation methylamine exposure, accounts for all of the hydrogen in the chemisorbed methylamine except that which forms ammonia. Thus all that remains on the surface after annealing to 400 K are carbon adatoms and CN. The formation of a small fractional coverage (approximately 0.02) of carbon adatoms from the ammonia formation reaction is consistent with EEL spectra of methylamine measured after annealing to above 380 K. In these spectra, the ν(Ru-C) mode of carbon adatoms occurs near 585 $cm^{-1}$. Decomposition of CN between 500 and 700 K creates both carbon and nitrogen adatoms with overlapping ν(Ru-C) and ν(Ru-N) modes at this frequency. The nitrogen adatoms recombine and desorb below 1000 K, leaving only carbon adatoms on the surface and reducing the intensity of the peak at 585 $cm^{-1}$.

The CN species with frustrated translations at 355 and 465 $cm^{-1}$ and a carbon-nitrogen stretching mode at 1670 $cm^{-1}$ must have a carbon-nitrogen double bond due to the frequency of the latter mode. The double bond indicates that this species is side-on bonded to the surface with the carbon and nitrogen atoms both σ-bonded to the ruthenium and a lone pair of electrons present on the nitrogen atom. Indeed, the frequency of ν(CN) of C=N agrees quite well with that of $\eta^2$(C,N)–$(CH_3)$C=N at 1615 $cm^{-1}$ on the Pt(111) surface (**25**). The intermediates to C=N formation from $HCNH_2$ are unknown. Possible intermediates include HCNH, $CNH_2$, CNH and HCN. In particular, a HCN intermediate to C=N cannot be ruled out because hydrogen thermal desorption experiments indicate that HCN dehydrogenates at temperatures as low as 390 K on Ru(001) and therefore would dehydrogenate immediately if formed from $HCNH_2$ (**26**).

As mentioned above, the carbon-nitrogen bond of C=N cleaves upon annealing to between 500 and 700 K. The nitrogen adatoms due to the decomposition of CN recombine and desorb between 800 and 1000 K, leaving only carbon adatoms on the surface. The decomposition mechanism of methylamine is summarized in Fig. 7.

## V. Conclusions

Molecularly chemisorbed methylamine is coordinated to the Ru(001) surface via the lone pair of electrons on the nitrogen atom. This is analogous to the bonding of ammonia on ruthenium.

The chemisorbed methylamine decomposes via sequential loss of hydrogen. A $CH_2NH_2$ species, bonded through the carbon atom to the surface occurs, after annealing a saturation coverage of methylamine to 300 K. Further annealing to 350 K results in the formation of $CHNH_2$, also bonded to the ruthenium through the carbon atom. The lone pair of electrons on the nitrogen is delocalized and contributes to the carbon-nitrogen bonding. This delocalization causes the frequency of the carbon-nitrogen stretching mode to occur between those expected for carbon-nitrogen single and double bonds.

The $CHNH_2$ decomposes via two competing pathways. Annealing a saturated methylamine monolayer to 400 K produces fractional coverages of approximately 0.02 of carbon adatoms and ammonia, the latter of which desorbs immediately. The mechanism of the formation of ammonia from methylamine on Ru(001) suggests that both $CH_2NH_2$ and $CHNH_2$ are possible intermediates in the formation of ammonia from methylamine over thin films and supported ruthenium catalysts. The remaining $CHNH_2$ (a fractional coverage of 0.08) dehydrogenates completely to CN with simultaneous evolution of hydrogen. The CN species contains a carbon-nitrogen double bond, indicating that it is side-on bonded with the lone pair of electrons localized on the nitrogen atom. Annealing the CN to between 500 and 700 K induces carbon-nitrogen bond cleavage, leaving carbon and nitrogen adatoms on the surface. Finally, the nitrogen adatoms recombine and desorb between 800 and 1000 K.

**References**


1. Tsai, W.; Weinberg, W.H., to be published.
2. Parmeter, J.E., unpublished results.
3. Benndorf, C.; Madey, T.E., *Surface Sci.* **1983**, 135, 164.
4. Parmeter, J.E.; Schwalke, U.; Weinberg, W.H., *J. Am. Chem. Soc.*, submitted.
5. Hrbek, J.; dePaola, R.A.; Hoffmann, F.M., *J. Chem. Phys.* **1984**, 81, 2818.
6. Baca, A.G.; Schulz, M.A.; Shirley, D.A., *J. Chem. Phys.* **1985**, 83, 6001.
7. Anderson, J.R.; Clark, N.J., *J. Catal.* **1966**, 5, 250.
8. Meitzner, G.; Mykytka, W.J.; Sinfelt, J.H., *J. Catal.* **1986**, 98, 513.
9. Thomas, G.E.; Weinberg, W.H., *Rev. Sci. Instrum.* **1979**, 50, 497.
10. Williams, E.D.; Weinberg, W.H., *Surface Sci.* **1979**, 82, 93.
11. Feulner, P.; Menzel, D., *J. Vacuuum Sci. Technol.* **1980**, 17, 662.
12. Redhead, P.A., *Vacuum* **1962**, 203.
13. The generation of carbon adatoms during the formation of ammonia from methylamine is suggested by EELS results.
14. Purnell, C.J.; Barnes, A.J.; Suzuki, S.; Ball, D.F.; Orville-Thomas, W.J., *Chem. Phys.* **1976**, 12, 77.
15. Wolff, H.; Ludwig, H., *J. Chem. Phys.* 1972, 56, 5278.
16. Durig, J.R.; Bush, S.F.; Baglin, I.G., *J. Chem. Phys.* **1968**, 49, 2106.
17. Watt, G.W.; Hutchinson, B.B.; Klett, D.S., *J. Am. Chem. Soc.* **1967**, 89, 2007.
18. Hills, M.M.; Parmeter, J.E.; Mullins, C.B.; Weinberg, W.H., *J. Am. Chem. Soc.* **1986**, 108, 3554.
19. Hamada, Y.; Hashiguchi, K.; Tsuboi, M., *J. Mol. Spectrosc.* **1984**, 105, 70.
20. Billups, W.E.; Konarski, M.M.; Hauge, R.H.; Margrave, J.L., *J. Am. Chem. Soc.* **1980**, 102, 7393.

21. For example, the $NH_2$ wagging mode of $Cl_2{=}N^+H_2$ appears at 784 cm−1 (22).

22. Allenstein, E.; Schmidt, A., *Chem. Ber.* **1964**, 97, 1863.

23. Ibach, H.; Mills, D.L., *Electron Energy Loss Spectroscopy and Surface Vibrations*, Academic Press, New York, 1982, Ch. 4.

24. Even a 0.01 fractional coverage of ammonia can be detected easily via EELS due to the intense 1160 cm−1 mode.

25. Avery, N.R.; Matheson, T.W.; Sexton, B.A., *Appl. Surface Sci.* **1985**, 22/23, 384.

26. Shanahan, K.L. Ph.D. Thesis, Lawrence Berkeley Laboratory, Univ. of Calif., Materials and Molecular Research Division (1984) LBL-17579.

**Table I**

Vibrational Frequencies ($cm^{-1}$) for $CH_3NH_2$, $CH_3ND_2$ and $CD_3ND_2$ Multilayers on Ru(001) at 80 K, for $CH_3NH_2$ and $CD_3ND_2$ in the Gas Phase and for $CH_3NH_2$ in the Solid Phase

| Mode | $CH_3NH_2$ | $CH_3ND_2$ | $CD_3ND_2$ | $CH_3NH_2$(g) | $CH_3ND_2$(g) | $CD_3ND_2$(s) | $CH_3NH_2$(s) |
|---|---|---|---|---|---|---|---|
| | multilayers on Ru(001) | | | (14,15) | (14,15) | (16) | (16) |
| $\tau(NH_2)$ or $\tau(ND_2)$ | n.r. | n.r. | n.r. | 980 | 820 | 1070 | 1353 |
| $\omega(NH_2)$ or $\omega(ND_2)$ | 1000 | 780 | 730 | 780 | 625 | 730 | 955 |
| $\nu(CN)$ | 1000 | 1005 | 1000 | 1044 | 1000 | 942 | 1048 |
| $\rho(CH_3)$ or $\rho(CD_3)$ | 1170 | 1185 | 835 | 1130,1195 | 1117,1187 | 919,929 | 1182,1172 |
| $\delta_s(CH_3)$ or $\delta_s(CD_3)$ | 1440 | 1445 | 1075 | 1430 | 1430 | 1070,1050 | 1467,1441 |
| $\delta_a(CH_3)$ or $\delta_a(CD_3)$ | n.r. | n.r. | n.r. | 1474,1485 | 1465,1485 | 1121 | 1492 |
| $\delta(NH_2)$ or $\delta(ND_2)$ | 1580 | 1185 | 1145 | 1623 | 1229 | 1217,1205 | 1636,1651 |
| $\nu_s(CH_3)$ or $\nu_s(CD_3)$ | 2930 | 2915 | 2215 | 2820 | 2817 | 2190,2061 | 2887,2793 |
| $\nu_a(CH_3)$ or $\nu_a(CD_3)$ | 2930 | 2915 | 2215 | 2985,2962 | 2961,2985 | 2220 | 2942 |
| $\nu_s(NH_2)$ or $\nu_s(ND_2)$ | 3260 | 2395 | 2375 | 3360 | 2479 | 2445 | 3260 |
| $\nu_a(NH_2)$ or $\nu_a(ND_2)$ | 3360 | 2485 | 2490 | 3424 | 2556 | 2485 | 3331 |

n.r.= not resolved

**Table II**

Vibrational Modes of Molecularly Adsorbed Methylamine on Ru(001) at 200 K. All Frequencies are reported in $cm^{-1}$.

| Mode | $CH_3NH_2$ | $CH_3ND_2$ | $CD_3ND_2$ |
|---|---|---|---|
| $\nu$(Ru-N) | 340 | 340 | 340 |
| $\rho(NH_2)$ or $\rho(ND_2)$ | 775 | n.r. | 600 |
| $\nu$(CN) | 980 | 975 | 975 |
| $\omega(NH_2)$ or $\omega(ND_2)$ | 980 | 780 | 725 |
| $\tau(NH_2)$ or $\tau(ND_2)$ | n.r. | n.r. | n.r. |
| $\rho(CH_3)$ or $\rho(CD_3)$ | 1175 | 1165 | 835 |
| $\delta_s(CH_3)$ or $\delta_s(CD_3)$ | 1445 | 1470 | 1095 |
| $\delta_a(CH_3)$ or $\delta_a(CD_3)$ | n.r. | n.r. | n.r. |
| $\delta(NH_2)$ or $\delta(ND_2)$ | 1575 | 1165 | 1145 |
| $\nu_s(CH_3)$ or $\nu_s(CD_3)$ | 2875 | 2880 | 2085 |
| $\nu_a(CH_3)$ or $\nu_a(CD_3)$ | 2960 | 2950 | 2200 |
| $\nu_s(NH_2)$ or $\nu_s(ND_2)$ | 3250 | 2430 | 2360 |
| $\nu_a(NH_2)$ or $\nu_a(ND_2)$ | 3250 | 2430 | 2445 |

n.r.= not resolved

**Table III**

Vibrational Modes Observed for $CH_2NH_2$, $CH_2ND_2$ and $CD_2ND_2$ on the Ru(001) Surface at 300 K due to Methylamine Decomposition. All Frequencies are reported in $cm^{-1}$.

| Mode | $CH_2NH_2$ | $CH_2ND_2$ | $CD_2ND_2$ |
|---|---|---|---|
| $T_s$ | 600 | 555 | 535 |
| $\rho(CH_2)$ or $\rho(CD_2)$ | 775 | 810 | 535 |
| $\rho(NH_2)$ or $\rho(ND_2)$ | 775 | 555 | 535 |
| $\nu(CN)$ | 1000 | 995 | 985 |
| $\tau(CH_2)$ or $\tau(CD_2)$ | n.r. | n.r. | n.r. |
| $\tau(NH_2)$ or $\tau(ND_2)$ | n.r. | n.r. | n.r. |
| $\omega(NH_2)$ or $\omega(ND_2)$ | 1000 | 810 | 735 |
| $\omega(CH_2)$ or $\omega(CD_2)$ | 1205 | 1230 | 985 |
| $\delta(CH_2)$ or $\delta(CD_2)$ | 1420 | 1430 | 1095 |
| $\delta(NH_2)$ or $\delta(ND_2)$ | 1570 | 1230 | 1190 |
| $\nu_s(CH_2)$ or $\nu_s(CD_2)$ | 2925 | 2930 | 2090 |
| $\nu_a(CH_2)$ or $\nu_a(CD_2)$ | 2925 | 2930 | 2190 |
| $\nu_s(NH_2)$ or $\nu_s(ND_2)$ | 3290 | 2420 | 2400 |
| $\nu_a(NH_2)$ or $\nu_a(ND_2)$ | 3365 | 2420 | 2500 |

n.r.= not resolved

**Table IV**

Vibrational Modes Observed for $CHNH_2$, $CHND_2$ and $CDND_2$ Present on the Ru(001) Surface at 350 K due to Methylamine Decomposition. All Frequencies are reported in $cm^{-1}$.

| Mode | $CHNH_2$ | $CHND_2$ | $CDND_2$ |
|---|---|---|---|
| $T_s$ | 450 | 450 | 445 |
| $\delta$(CH) or $\delta$(CD) | 1000 | 1005 | 725 |
| $\delta$(CH) or $\delta$(CD) | 755 | 750 | 575 |
| $\omega(NH_2)$ or $\omega(ND_2)$ | 755 | 580 | 575 |
| $\rho(NH_2)$ or $\rho(ND_2)$ | 1220 | 1005 | 1010 |
| $\nu$(CN) | 1460 | 1435 | 1440 |
| $\tau(NH_2)$ or $\tau(ND_2)$ | n.r. | n.r. | n.r. |
| $\delta(NH_2)$ or $\delta(ND_2)$ | 1580 | 1255 | 1250 |
| $\nu$(CH) or $\nu$(CD) | 2925 | 2920 | 2210 |
| $\nu_s(NH_2)$ or $\nu_s(ND_2)$ | 3230 | 2370 | 2415 |
| $\nu_a(NH_2)$ or $\nu_a(ND_2)$ | 3230 | 2480 | 2495 |

n.r.= not resolved

**Figure Captions**

Figure 1. The methylamine (mass 31) thermal desorption spectra following exposures of (a) 1 L, (b) 3 L, (c) 5L and (d) 10 L of methylamine on the Ru(001) surface at 80 K.

Figure 2. The hydrogen (mass 2) thermal desorption spectra following exposures of (a) 0.2 L, (b) 0.4 L, (c) 1 L and (d) 5 L of methylamine on the Ru(001) surface at 80 K.

Figure 3. The nitrogen (mass 14) thermal desorption spectra following exposures of (a) 0.6 L, (b) 0.8 L, (c) 1 L and (d) 5 L of methylamine on the Ru(001) surface at 80 K.

Figure 4. The ammonia (mass 17) thermal desorption spectra following exposures of (a) 0.4 L, (b) 1 L and (c) 5 L of methylamine on the Ru(001) surface at 80 K.

Figure 5. The EEL spectrum that results following the exposure of the Ru(001) surface to 5 L of $CH_3NH_2$ at 80 K. This spectrum is characteristic of molecular multilayers of $CH_3NH_2$. The EEL spectra that result from 5 L exposures of (b) $CH_3NH_2$, (c) $CH_3ND_2$ and (d) $CD_3ND_2$, and annealing to 200 K. Spectra (b)-(d) are characteristic of molecularly chemisorbed methylamine.

Figure 6. The EEL spectra that result from exposing the Ru(001) surface to 5 L of $CH_3NH_2$ at 80 K and annealing to (a) 300 K, (b) 350 K and (c) 450 K.

Figure 7. The thermal decomposition mechanism of methylamine on Ru(001). Reactions (5) and (6) are not necessarily elementary reaction steps.

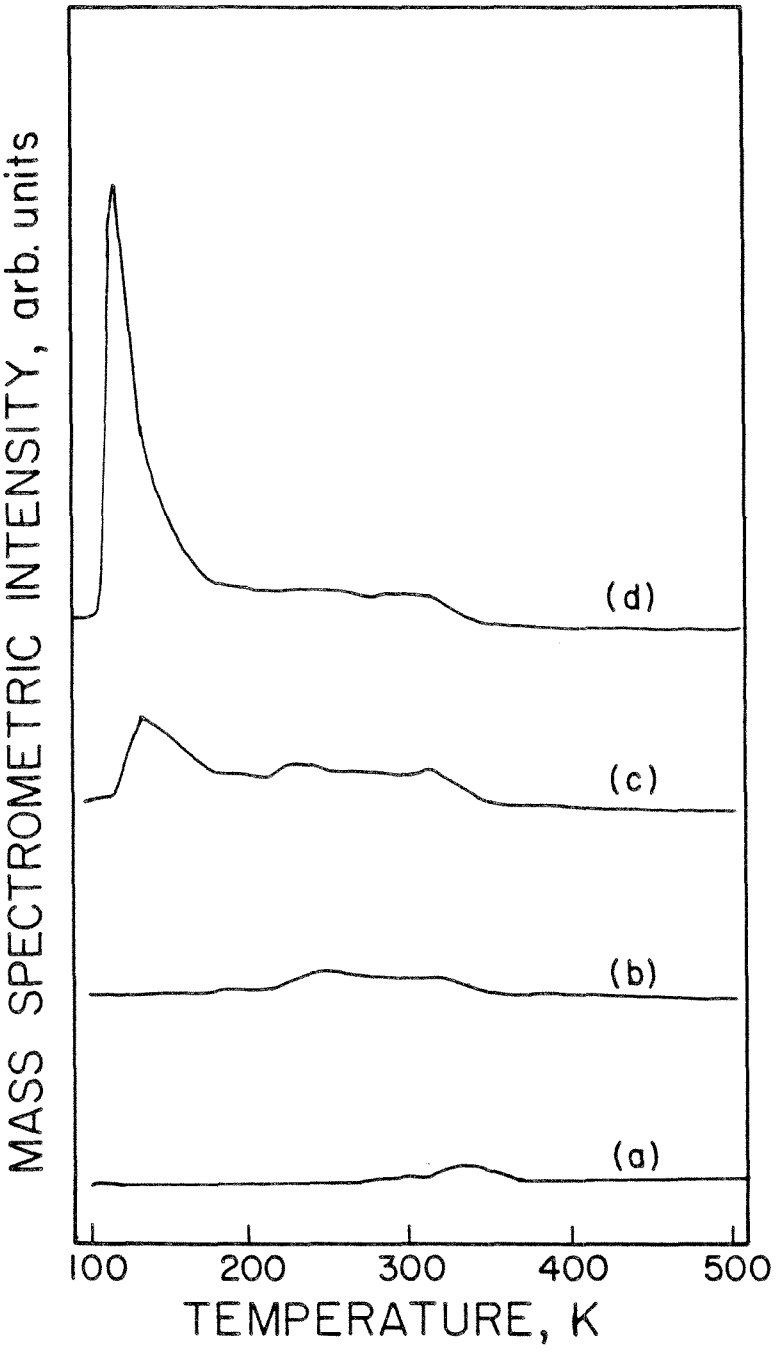
MASS SPECTROMETRIC INTENSITY, arb. units
(d)
(c)
(b)
(a)
100
200
300
400
500
TEMPERATURE, K

Figure 1

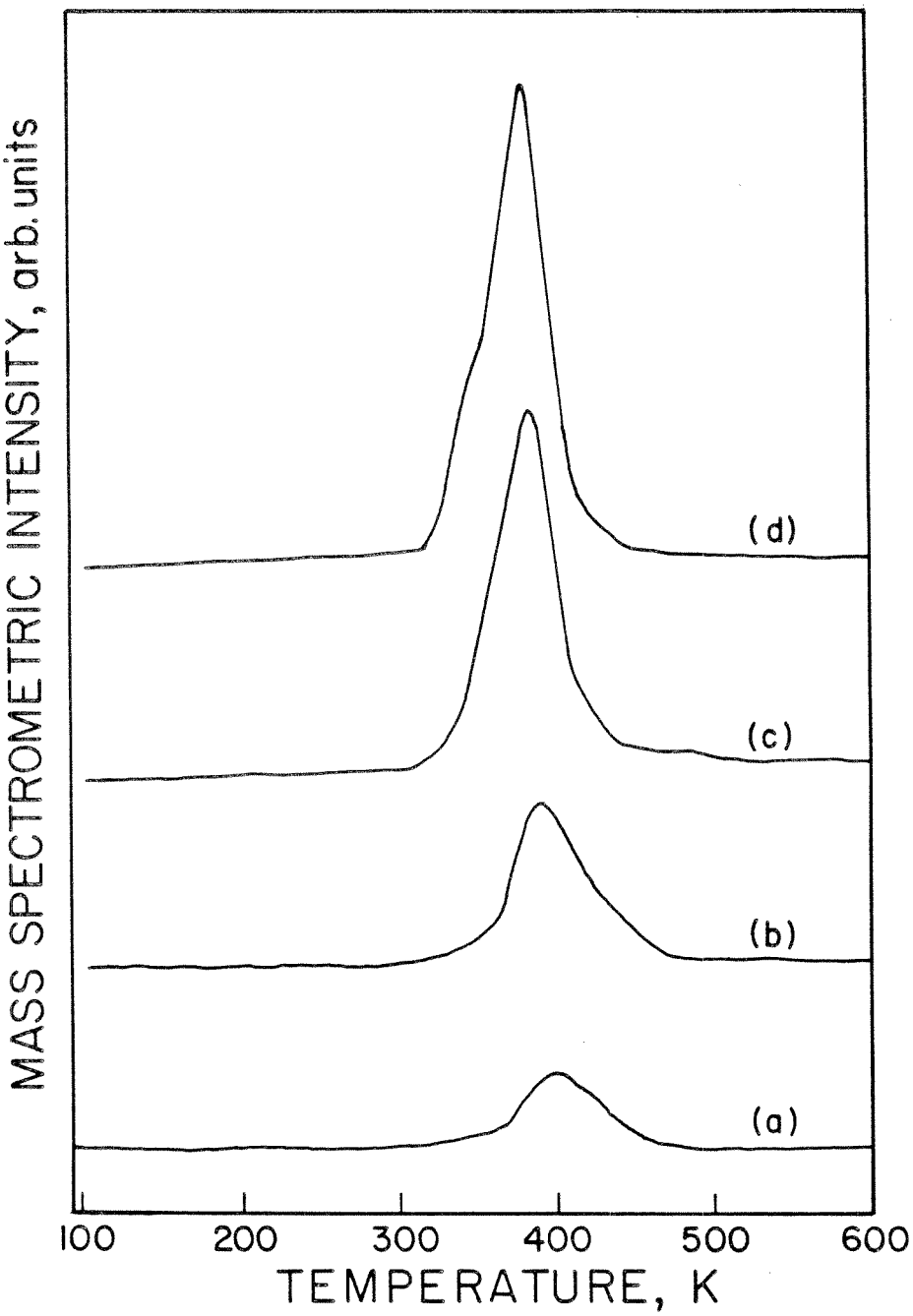
MASS SPECTROMETRIC INTENSITY, arb. units
(d)
(c)
(b)
(a)
100
200
300
400
500
600
TEMPERATURE, K

Figure 2

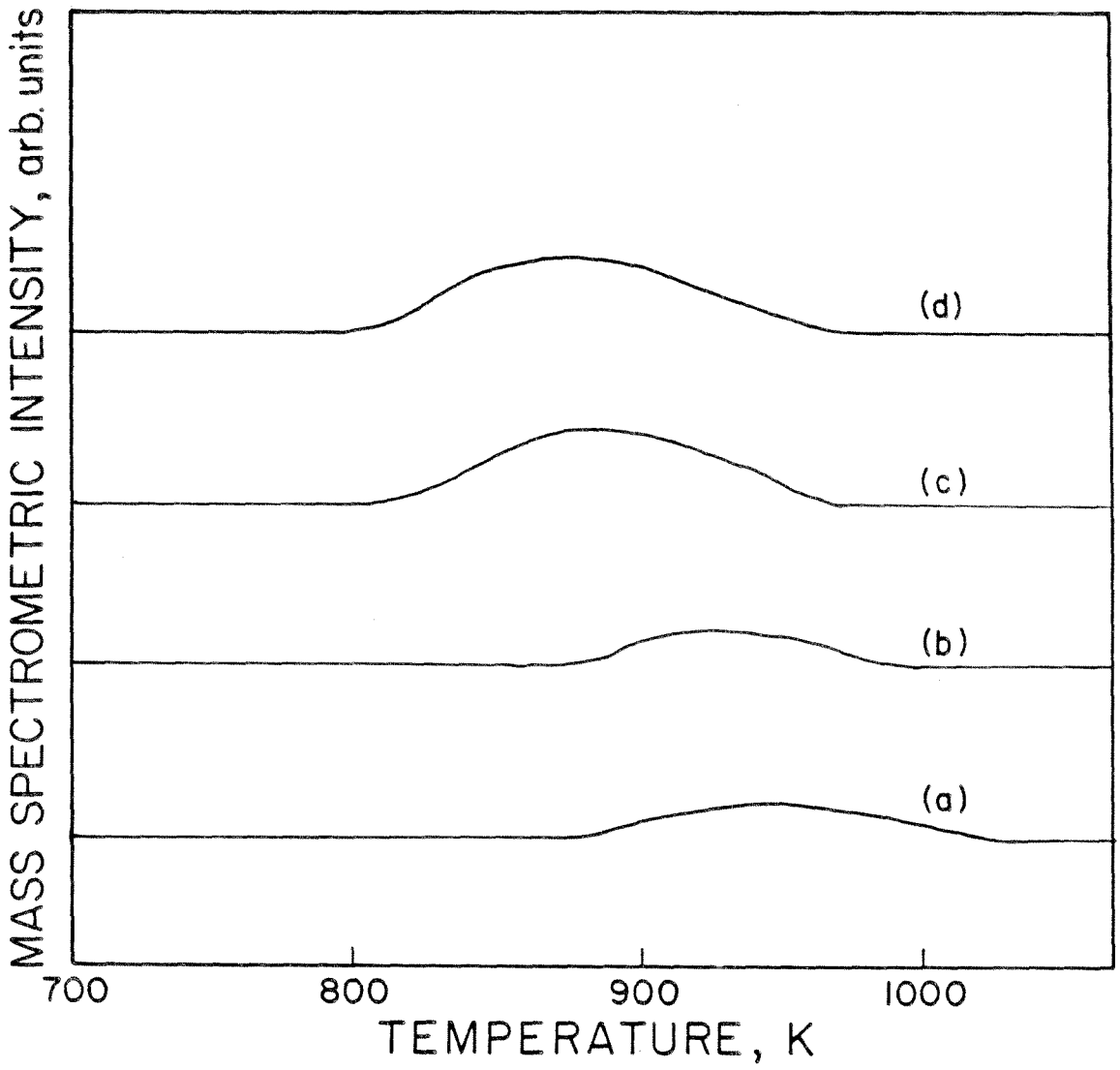
MASS SPECTROMETRIC INTENSITY, arb. units
(d)
(c)
(b)
(a)
700
800
900
1000
TEMPERATURE, K

Figure 3

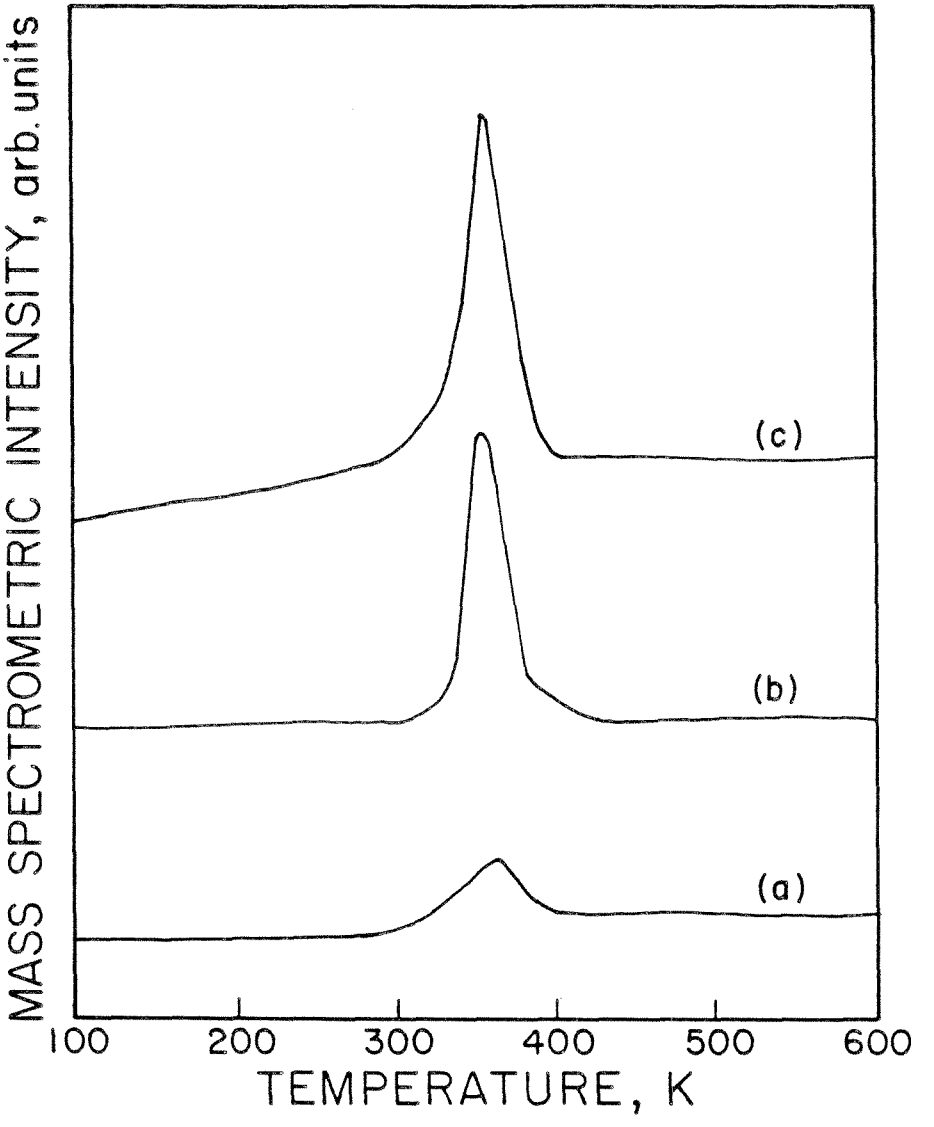
MASS SPECTROMETRIC INTENSITY, arb. units
(c)
(b)
(a)
100
200
300
400
500
600
TEMPERATURE, K

Figure 4

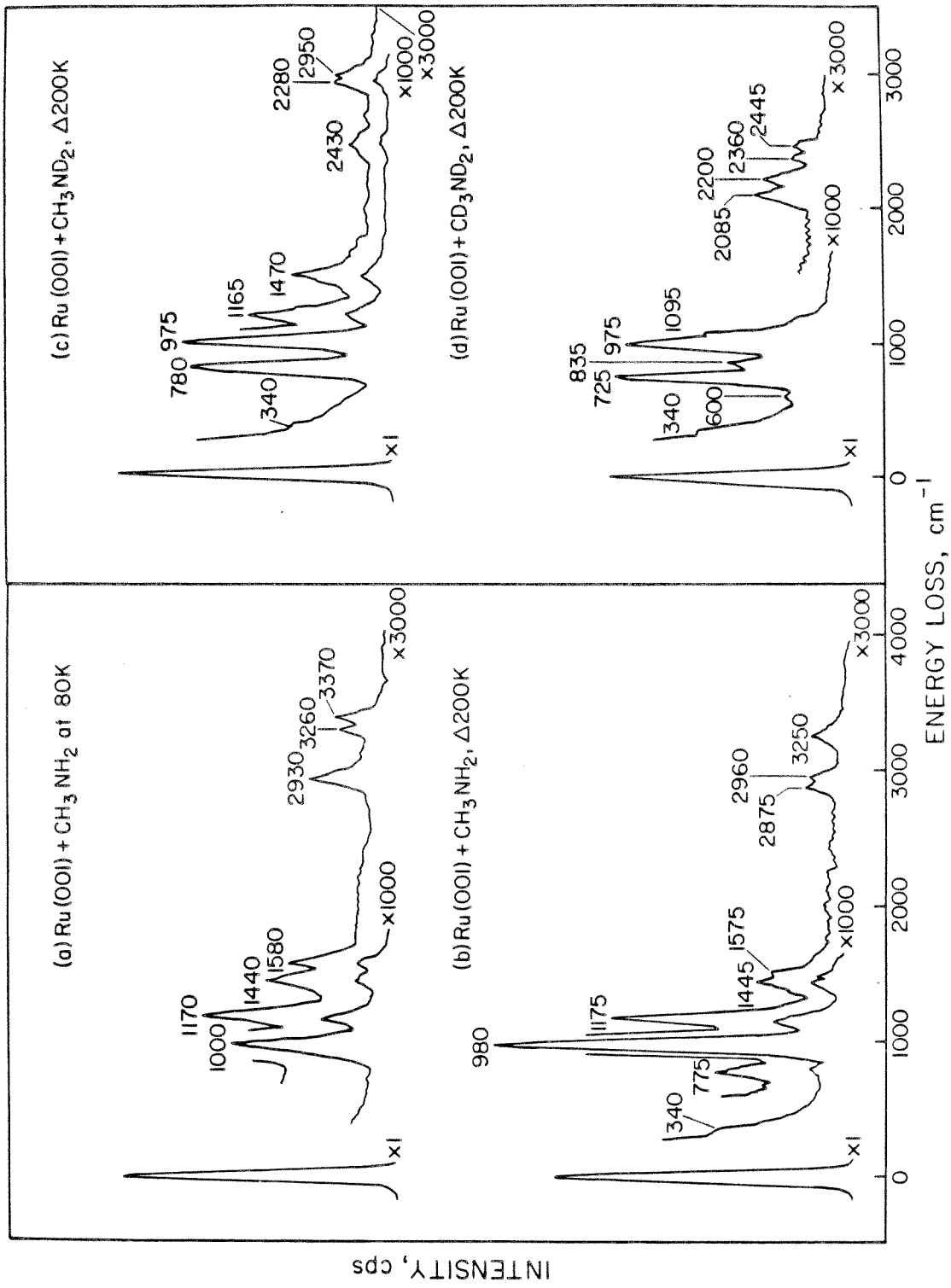
(a) Ru(001) + CH3NH2 at 80K
1170
1000
1440
1580
2930
3260
3370
×1000
×3000
×1
(b) Ru(001) + CH3NH2, Δ200K
980
1175
340
775
1445
1575
2875
2960
3250
×1000
×3000
×1
(c) Ru(001) + CH3ND2, Δ200K
780
975
340
1165
1470
2280
2950
2430
×1000
×3000
×1
(d) Ru(001) + CD3ND2, Δ200K
835
725
975
340
600
1095
2085
2200
2360
2445
×1000
×3000
×1
0
1000
2000
3000
4000
ENERGY LOSS, cm⁻¹
INTENSITY, cps

Figure 5

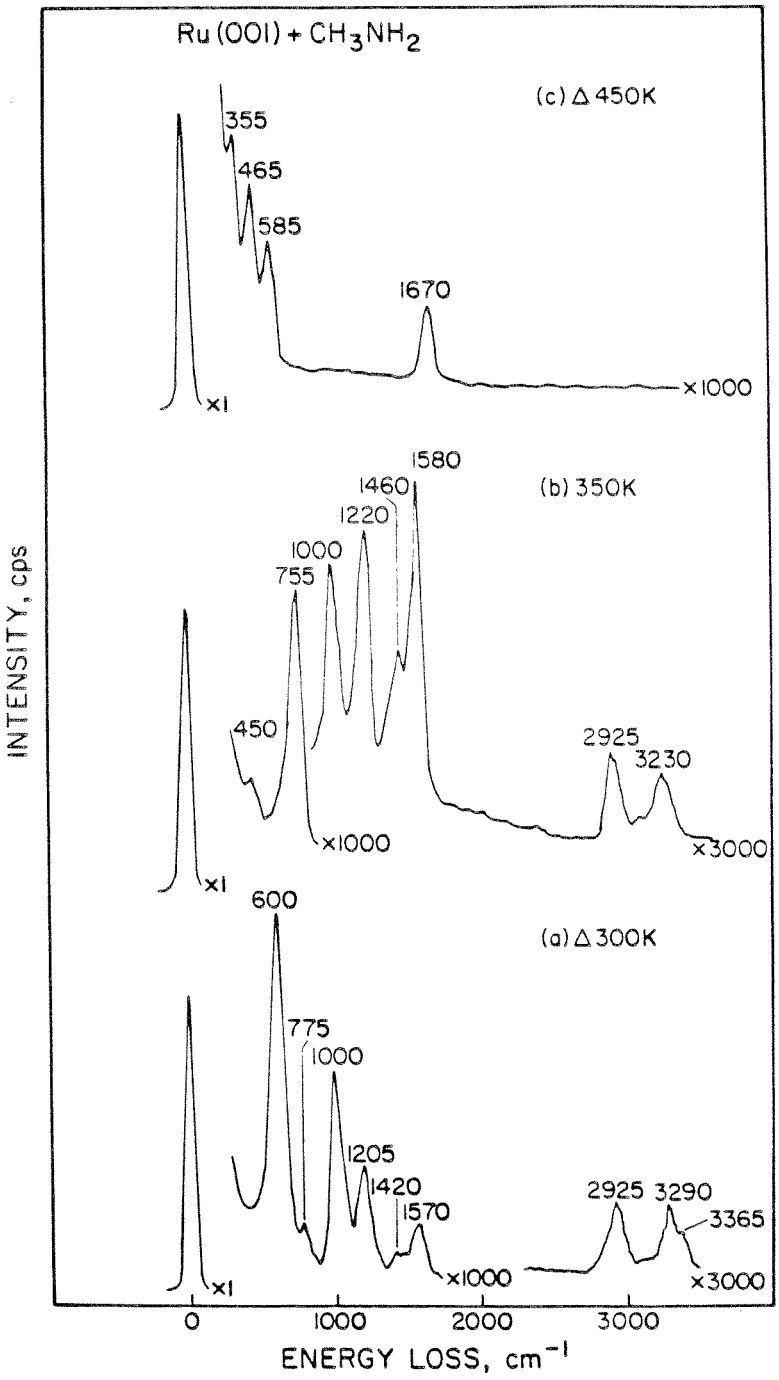
Ru(001) + CH3NH2
(c) Δ 450K
355
465
585
1670
×1
×1000
(b) 350K
1580
1460
1220
1000
755
450
2925
3230
×1000
×3000
×1
(a) Δ 300K
600
775
1000
1205
1420
1570
2925
3290
3365
×1000
×3000
×1
INTENSITY, cps
0
1000
2000
3000
ENERGY LOSS, cm⁻¹

Figure 6

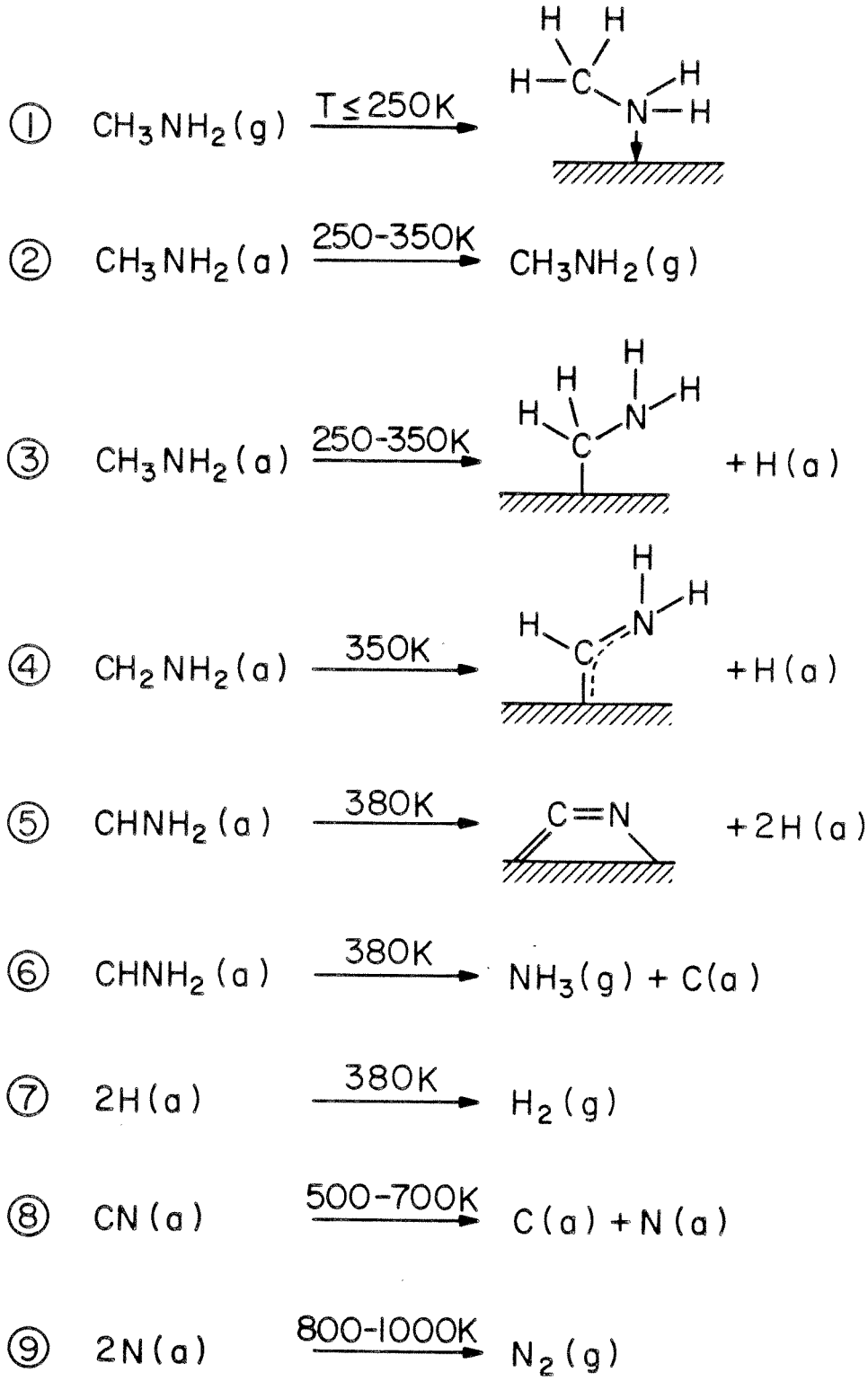
① $CH_3NH_2(g)$ $T \leq 250K$
② $CH_3NH_2(a)$ 250-350K $CH_3NH_2(g)$
③ $CH_3NH_2(a)$ 250-350K +H(a)
④ $CH_2NH_2(a)$ 350K +H(a)
⑤ $CHNH_2(a)$ 380K C=N +2H(a)
⑥ $CHNH_2(a)$ 380K $NH_3(g) + C(a)$
⑦ 2H(a) 380K $H_2(g)$
⑧ CN(a) 500-700K C(a) + N(a)
⑨ 2N(a) 800-1000K $N_2(g)$

Figure 7

# CHAPTER VII

## Conclusions

The combined results of Chapters II-V, Appendices 1 and 2, and a few additional electron energy loss spectroscopic experiments have led to the decomposition mechanisms for ethylene and acetylene adsorbed on Ru(001) and ethylene adsorbed on the Ru(001)-p(2x2)O surface that are depicted in Figs. 1(a) and (b), respectively. As shown in Fig. 1(a), the carbon atoms of both ethylene and acetylene rehybridize to nearly $sp^3$ following adsorption on Ru(001). These two molecularly chemisorbed species react between 150 and 280 K to form an $sp^3$ hybridized $HCCH_2$ species. The $HCCH_2$ is stable and observed via EELS following the coadsorption of hydrogen with acetylene at 150 K. Since ethylene, acetylene, and acetylene coadsorbed with hydrogen all generate the same decomposition products (acetylide and ethylidyne), the existence of the $HCCH_2$ intermediate may be inferred in the decomposition of ethylene and acetylene as well. In the absence of coadsorbed hydrogen, acetylene also forms some acetylide in addition to $HCCH_2$. The $HCCH_2$ dehydrogenates to a postulated, unstable, $sp^3$-hybridized $CCH_2$ species, which may either add a hydrogen atom to form ethylidyne or lose a hydrogen atom to form acetylide. The ethylidyne decomposes to elemental carbon with concurrent evolution of hydrogen between 330 and 350 K, while the acetylide undergoes carbon-carbon bond cleavage to carbon and methylidyne near 360 K. Finally, the methylidyne dehydrogenates above 500 K.

The postulation of the existence of an unstable $CCH_2$ intermediate in this decomposition reaction is based on coadsorption experiments of deuterium with $C_2H_2$, and, equivalently, hydrogen with $C_2D_2$. Electron energy loss (EEL) spectra of deuterium (hydrogen) and $C_2H_2$ ($C_2D_2$) coadsorbed at 80 K and annealed to 250 K show that the predominant isotope of ethylidyne formed is $CCD_2H$ ($CCH_2D$) with a symmetric methyl deformation mode near 1210 $cm^{-1}$ (1260 $cm^{-1}$). This indicates that during the hydrogenation reaction two deuterium atoms have bonded to a carbon atom of acetylene and the hydrogen-carbon bond of the second carbon atom has been broken. Note that ethylidyne does not undergo isotopic exchange with coadsorbed deuterium under these conditions. Thus, the reaction of acetylene must occur along the following pathway:

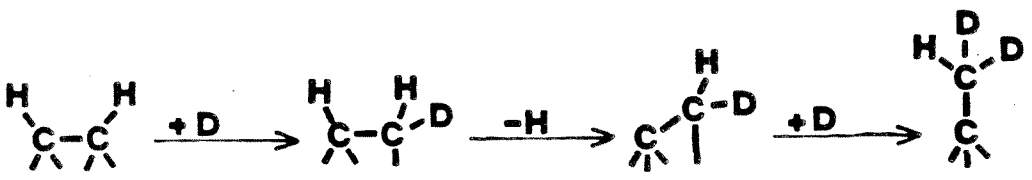

Intramolecular hydrogen transfer within acetylene or HCCHD may be ruled out on the basis of the above experiments because it would produce mainly $CCH_2D$.

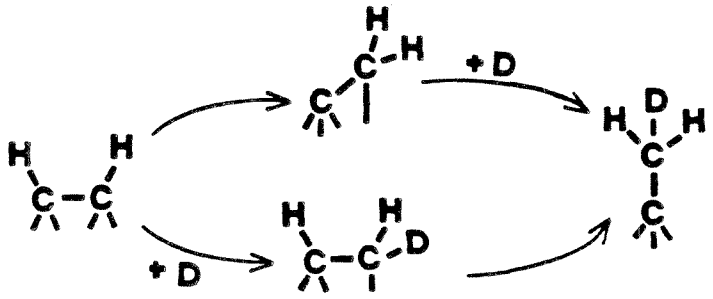

Moreover, the following mechanism:

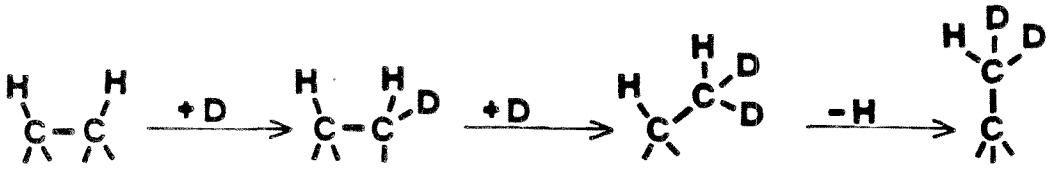

is eliminated for three reasons. First, considerable bond strain would be required in the $HCCHD_2$ intermediate to prevent the hydrogen and deuterium atoms on the $CHD_2$ group from nearing the surface and undergoing C-H or C-D bond cleavage with adsorption of the resulting free hydrogen or deuterium atom to the surface. Second, addition of deuterium to HCCHD would most likely form HDCCHD, not $HCCHD_2$, since $C_2H_2D_2$ is evolved following $C_2H_2$ and deuterium coadsorption, and is, in fact, the sole isotope of ethylene observed. Third, the existence of a $CCH_2$ decomposition intermediate is supported by the observed isotopic exchange of coadsorbed deuterium into acetylide. Thus, acetylene dehydrogenates via a $CCH_2$ intermediate, and it may be inferred that ethylene reacts through an identical $CCH_2$ species, as was the case for the $HCCH_2$ intermediate.

It has been shown that ethylene, acetylene and their decomposition products tend to be $sp^3$-hybridized on Ru(001) with $\eta^2$-bonding occurring. In contrast, on the Ru(001)-p(2x2)O surface, $sp^2$-hybridization and $\eta^1$-bonding are favored. This is shown in the decomposition mechanism depicted in Fig. 1(b). Ethylene is $\pi$-bonded to ruthenium in the presence of sufficient oxygen. Between 200 and

250 K, the ethylene dehydrogenates to ethylidyne, which decomposes at a higher temperature to vinylidene with concurrent hydrogen desorption. In the presence of hydrogen, this reaction is reversible, and ethylidyne may be reformed. This suggests that ethylene dehydrogenates to an unstable (in the presence of hydrogen) vinylidene species, which rehydrogenates rapidly to ethylidyne. Upon heating to desorb surface hydrogen, ethylidyne dehydrogenates back to vinylidene. The vinylidene is bridge-bonded and the carbon-carbon axis is tilted with respect to the surface normal such that $\pi$-electron density may be donated to the surface. Upon annealing to between 350 and 400 K, the vinylidene undergoes both carbon-carbon and carbon-hydrogen bond cleavage, forming methylidyne. This reaction may proceed via an acetylide intermediate because methylidyne is formed from acetylide on the clean surface, and this acetylide is unstable at these temperatures. Finally, the methylidyne dehydrogenates above 500 K.

In addition to the study of the reaction of unsaturated hydrocarbons on the Ru(001) and Ru(001)-p(2x2)O surface, coadsorption of ethylene and acetylene with hydrogen, deuterium and carbon monoxide have illuminated further the reaction mechanisms. For example, the coadsorption of CO with ethylene does not alter the bonding of molecularly chemisorbed ethylene or the identities of the reaction intermediates, but it does reduce the binding energy of hydrogen, causing it to desorb at a lower temperature. As described in Chapter III, the lower temperature hydrogen desorption confirmed the stoichiometry of the ethylene decomposition intermediates, $CCH_3$ and CCH. The coadsorption of hydrogen with ethylene indicated that ethane could be formed at surface temperatures as low as 200 K. Similarly, acetylene was hydrogenated to ethylene at 175 K. Coadsorption of deuterium and methylidyne followed by heating to 300 K showed that significant isotopic exchange occurred, presumably via an unstable methylene (CHD) intermediate. This suggests that methylidyne may be hydrogenated to methylene at higher hydrogen pressures. Methylidyne may therefore be an intermediate in Fischer-Tropsch synthesis in which carbon monoxide and hydrogen synthesize hydrocarbons. The extent of the inhibition of ethylene adsorption by preadsorbed hydrogen and carbon monoxide was also measured, and the inhibition appeared to result from a simple blocking of the ethylene adsorption sites. This situation contrasts with the electronic perturbation of the ruthenium surface by preadsorbed oxygen

adatoms, which both reduces the coverage of postadsorbed ethylene and alters the bonding of the chemisorbed ethylene, as discussed in Ch. V. Finally, it was shown that preadsorbed hydrogen increased the ratio of ethylidyne to acetylide formed, while preadsorbed CO reduced this ratio.

The interactions of ethylene and acetylene with ruthenium illustrate the similarity of the chemistry of unsaturated hydrocarbons on the Group VIII transition metals. In particular, the interactions are remarkably similar to those of ethylene and acetylene adsorbed on the hexagonal (111) faces of the fcc metals such as rhodium, palladium and platinum (**1-6**). Ethylene adsorbed on Ru(001), Rh(111) and Pt(111) at low temperatures is di-σ-bonded (**1,5**). The carbon atoms of acetylene are rehybridized to between $sp^2$ and $sp^3$ following adsorption on Ru(001), Pd(111) and Pt(111) (**3,4,6**). Ethylene adsorbed on all four surfaces forms ethylidyne upon heating to room temperature [and also acetylide on Ru(001)] (**1,2,5**). On Ru(001) and Pd(111) acetylene forms both ethylidyne and acetylide upon heating (**3,4**). Ethylidyne formation appears to be peculiar to the geometry of these hexagonal surfaces and must require a threefold site. The coadsorption of ethylene with oxygen on Ru(001) and Pt(111) are also remarkably similar. On both surfaces, ethylene is π-bonded and forms an $sp^2$-hybridized vinylidene species at higher temperatures (**5**). Indeed, the formation of π-bonded ethylene appears to be characteristic of all of the oxygen precovered Group VIII transition metal surfaces studied to date, such as Ru(001), Pd(100), Pt(111) and Fe(111) (**7,5,8**).

The different bonding configurations of ethylene on the clean and oxygen-precovered surface may be discussed in terms of the Dewar-Chatt-Duncanson model of the bonding of olefins to metal atoms (**9**). In this model, bonding occurs when ethylene donates electron density from the π-orbital to the metal, and electron density is donated from the d-orbital of the metal (or for a surface the d-band) into the previously unoccupied $\pi^*$-orbital. The extent of backdonation dictates the type of bonding; little or no backdonation leads to $sp^2$ hybridization and π-bonding, whereas significant backdonation of electron density, roughly equivalent to two electrons per ethylene, induces $sp^3$-hybridization and di-σ-bonding. An organometallic complex analogous to the first ethylene adsorbate is Zeise's salt ($K^+[Pt(C_2H_4)Cl_3]^-$) (**10**), in which an ethylene ligand is π-bonded to a platinum atom, and the electronegative chlorine ligands play the role of the oxygen atoms on the surface, which will be discussed later. The di-σ-

bonded ethylene is not so easily modeled, because bonding undoubtedly occurs to more than one metal atom (11). However, this $sp^3$-hybridized ethylene may be crudely thought of as a metallocyclopropane or metallocyclobutane (12). The extent of backdonation of electron density to the $\pi^*$-orbital is strongly affected by the presence of electronegative oxygen atoms. As discussed in Chapter V, the $\pi$su*-orbital of ethylene lies at an energy close to the Fermi level of the clean Ru(001) surface, permitting backdonation from the d-band to this orbital. Addition of oxygen to the surface lowers the Fermi level (with respect to the vacuum level), increasing the separation between the $\pi^*$-orbital and the Fermi level, inhibiting backdonation. Thus on the clean surface ethylene is di-$\sigma$-bonded, while on the oxygen precovered surface ethylene is $\pi$-bonded.

The addition of oxygen also reduces the binding energies of other coadsorbates, such as hydrogen and carbon, and this affects the decomposition mechanism of ethylene. For example, ethylidyne decomposes rapidly to elemental carbon with simultaneous evolution of hydrogen on the clean surface but dehydrogenates to vinylidene on the Ru(001)-p(2x2)O surface, possibly due to the effect of the reduced binding energy of hydrogen, which alters the energetics of this process. Thus, a poison may have a dramatic effect upon catalytic chemistry as demonstrated by the change in the decomposition mechanism of ethylene in the presence of oxygen.

The chemistry of ethylene adsorbed on the Ru(001)-p(2x2)O surface may also be compared to the reaction of ethylene with organometallic clusters in an effort to relate homogenous catalysis with heterogeneous catalysis by metallic surfaces. For example, ethylene reacts with $Os_3(CO)_{12}$ to form a vinyl complex $HOs_3(HC{=}CH_2)(CO)_{10}$, which forms a vinylidene complex $H_2Os_3(C{=}CH_2)(CO)_9$ upon heating (13). Infrared data of this vinylidene complex are very similar to EEL spectra of vinylidene on Ru(001)-p(2x2)O, and therefore the structure and bonding of these species must also be very similar. Thus, the structural data of the vinylidene ligand provide information on the bonding of the vinylidene adsorbate, indicating that this species is bridge-bonded to ruthenium with the carbon-carbon bond axis tilted with respect to the surface normal. Both the vinylidene ligand and adsorbate may be hydrogenated to ethylidyne, and the structure of the ethylidyne complex may also be used to model the ethylidyne observed on both the Ru(001)-p(2x2)O and Ru(001) surfaces. On this basis, the ethylidyne is adsorbed

in a threefold site with its carbon-carbon bond axis nearly perpendicular to the surface. The existence of the intermediate vinyl complex in the formation of vinylidene suggests that ethylene $\pi$-bonded on ruthenium in the presence of oxygen may dehydrogenate through a similar vinyl species that is unstable. The vinyl adsorbate dehydrogenates to vinylidene, which is rapidly hydrogenated to ethylidyne due to the presence of surface hydrogen. As discussed earlier, upon annealing, the hydrogen desorbs and the ethylidyne dehydrogenates back to vinylidene.

The above comparison also elucidates one of the differences between the bonding of hydrocarbons on metal clusters and surfaces. The Fermi level of a Group VIII transition metal surface lies approximately -5 to -6 eV below the vacuum level. As discussed above, the Fermi level of Ru(001) at -5.5 eV is sufficiently near the energy of the empty $\pi$-orbitals of ethylene and acetylene to permit back-donation from the metal d-band into this orbital and the formation of $sp^3$-hybridized adsorbates. The formation of $sp^2$-hybridized hydrocarbon species on Ru(001) requires the presence of an electronegative coadsorbate, such as oxygen, which lowers the Fermi level of the surface, inhibiting back-donation. Small metal clusters are much more electron-deficient than these metal surfaces. Clusters containing three or four metal atoms have ionization potentials that are much lower (at -7 to -9 eV) with respect to the vacuum than the analogous Fermi levels of the corresponding surfaces (**14**). These metal clusters lack the electron density to backdonate into the $\pi^*$-orbitals of hydrocarbon ligands, and so $sp^2$-hybridization and $\pi$-bonding of ligands are favored in these clusters. Thus, the different electronic properties of metal clusters and metal surfaces dictate the bonding of hydrocarbon ligands and adsorbates.

The chemisorption and reaction of methylamine on the Ru(001) surface have also been explored. Electron energy loss spectroscopic experiments have shown that the molecular methylamine is coordinated to the ruthenium via the lone pair of electrons on the nitrogen atom. Upon annealing to 300 K, the methylamine decomposes to $CH_2NH_2$, which is bonded to the ruthenium through the carbon atom. This species dehydrogenates to $CHNH_2$ after annealing to 350 K that is also coordinated to the surface via the carbon atom. The frequency of the carbon-nitrogen stretching mode of $CHNH_2$ occurs between those expected for unperturbed carbon-nitrogen single and double bonds. This probably results from the delocalization of the lone pair of electrons previously on the nitrogen over the nitrogen-carbon and

carbon-ruthenium bonds of the $CHNH_2$.

The $HCNH_2$ adspecies decomposes via two competing pathways upon annealing to 400 K. The minority pathway is the formation of carbon adatoms and ammonia, the latter of which desorbs immediately. The remaining $HCNH_2$ dehydrogenates completely to side-on bonded C=N, with simultaneous evolution of hydrogen. Annealing the CN adspecies to between 500 and 700 K induces carbon-nitrogen bond cleavage, leaving carbon and nitrogen adatoms on the surface. Thus, the presence of the lone pair of electrons on the nitrogen atom of methylamine affects both the coordination of molecularly chemisorbed methylamine and the nature of the decomposition intermediates on Ru(001). Molecularly chemisorbed methylamine is coordinated to the surface through the lone pair of electrons and decomposes to stable $CH_2NH_2$, $CHNH_2$ and C=N intermediates.

We have seen that EELS and thermal desorption experiments may delineate the decomposition mechanisms of fairly complex molecules. This information should prove useful for higher pressure studies of heterogeneous catalysis in which identification of reaction intermediates is not possible. It has also been shown that coadsorbates such as oxygen may radically alter the chemistry of these reactions via electronic perturbations of the surface. The chemistry of hydrocarbons adsorbed on the Ru(001) surface was shown to be similar to that of triatomic metal clusters. Finally, the existence of a lone pair of electrons on a molecule, such as methylamine, can have a profound effect upon the bonding of the molecularly chemisorbed species and the decomposition intermediates.

**References**


1. Dubois, L.H.; Castner, D.G.; Somorjai, G.A., *J. Chem. Phys.* **1980**, 72, 5234.

2. Gates, J.A.; Kesmodel, L.L., *Surface Sci.* **1983**,124, 68.

3. Gates, J.A.; Kesmodel, L.L., *J. Chem. Phys.* **1982**, 76 4281.

4. Kesmodel, L.L.; Waddill, G.D.; Gates, J.A., *Surface Sci.* **1984**, 138, 464.

5. Steininger, H.; Ibach, H.; Lehwald, S., *Surface Sci.* **1982**, 117, 685.

6. Ibach, H.; Lehwald, S., *J. Vacuum Sci. Technol.* **1978**, 15, 407.

7. Stuve, E.M.; Madix, R.J.; Brundle, C.R., *Surface Sci.* **1985**, 152/153, 532.

8. Seip. U.; Tsai, M.C.; Kuppers, J.; Ertl, G., *Surface Sci.* **1984**, 147 65.

9. Ittel, S.D.; Ibers, J.A., *Adv. Organomet. Chem.* **1976**, 14, 33.

10. Hiraishi, J., *Spectrochim. Acta Part A* **1969**, 25, 749.

11. Horsley, J.A.; Stohr, J.; Koestner, R.J., *J. Chem. Phys.* **1985**, 83, 3146.

12. Steigerwald, M.L.; Goddard, III, W.A., *J. Am. Chem. Soc.* **1985**, 107, 5027.

13. Andrews, J.R.; Kettle, S.F.A.; Powell, D.B.; Sheppard, N., *Inorg. Chem.* **1982**, 21, 2874.

14. Melius, C.F.; Upton, T.H.; Goddard, III, W.A., *Solid State Commun.* **1978**, 28, 501.

**Figure Captions**

Figure 1. The decomposition mechanisms of ethylene and acetylene on the Ru(001) surface.

Figure 2. The decomposition mechanism of ethylene on the Ru(001)-p(2x2)O surface.

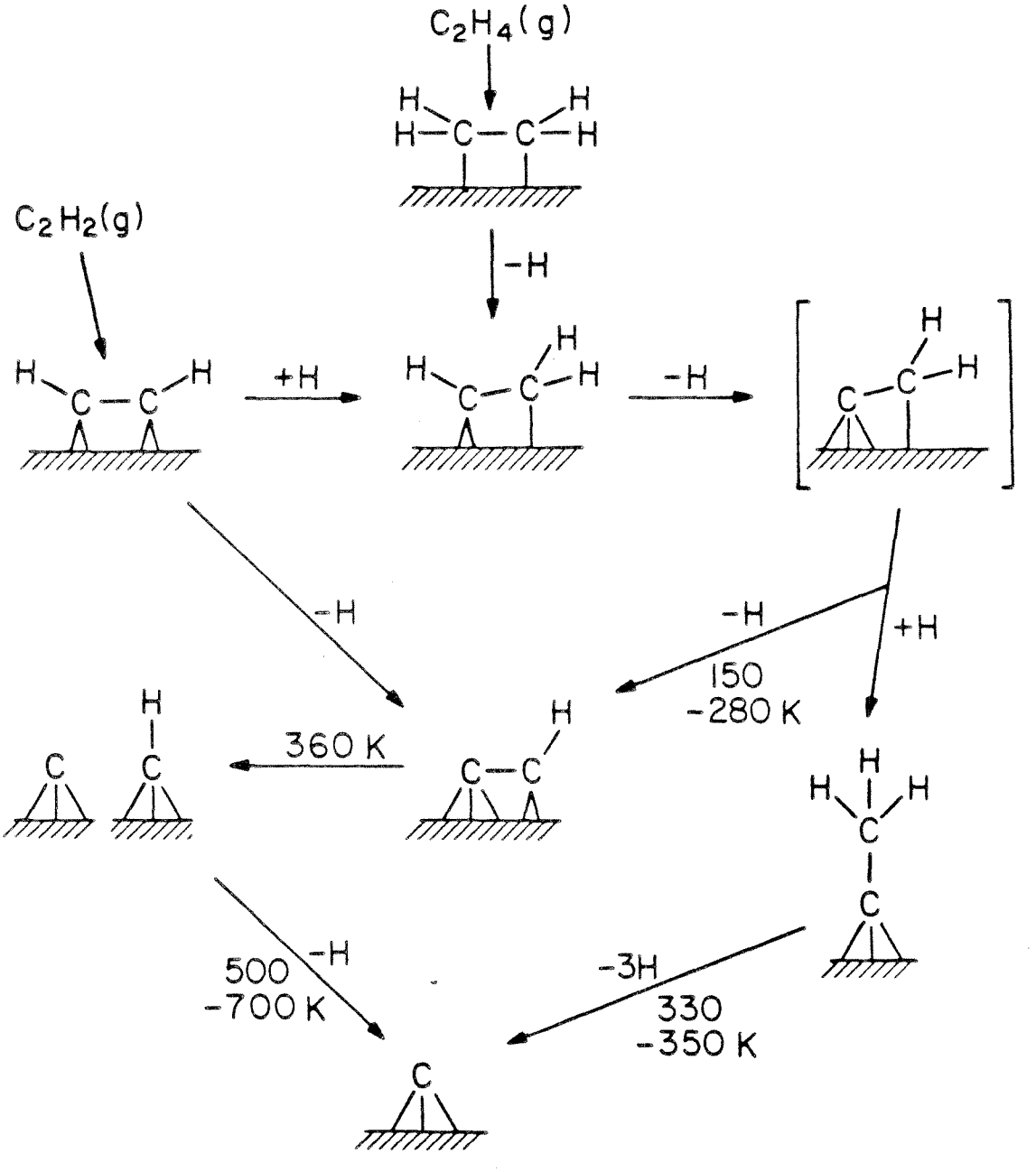


Figure 1

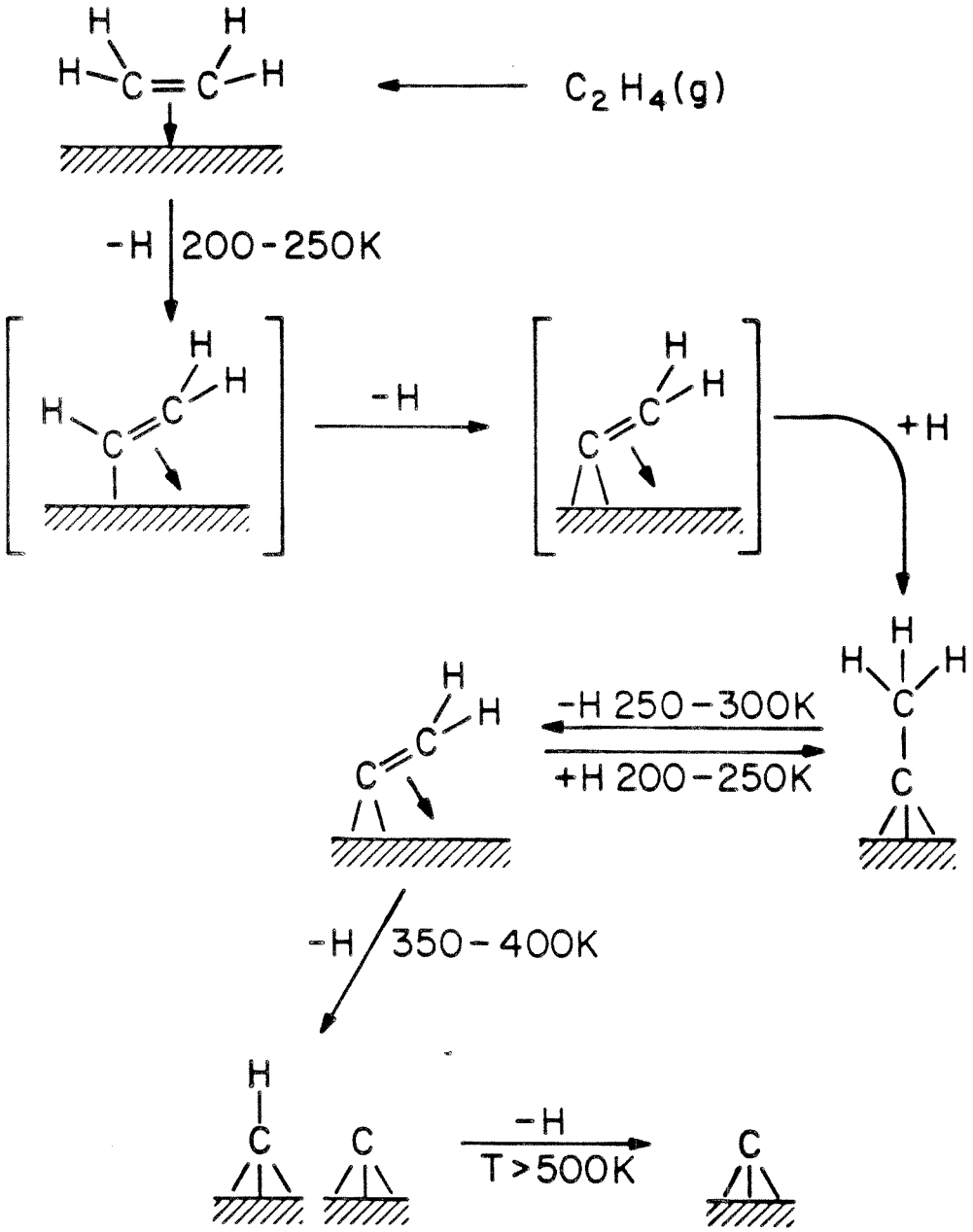


Figure 2

# CHAPTER VIII

## Appendices

1. The Interaction of Acetylene with the Ru(001) Surface.
2. The Coadsorption of Hydrogen and Acetylene on the Ru(001) Surface.
3. The Adsorption of Formic Acid and the Decomposition of the Formate Intermediate on the (001) Surface of Ruthenium.

# Appendix 1

## The Interaction of Acetylene with the Ru(001) Surface



[This chapter was published as a paper by J. E. Parmeter, M. M. Hills and W. H. Weinberg in *The Journal of the American Chemical Society* **108**, 3563 (1986).]

## Abstract

The adsorption and decomposition of acetylene on the hexagonally close-packed Ru(001) surface has been studied using high resolution electron energy loss spectroscopy and thermal desorption mass spectrometry. Below 230 K, acetylene is molecularly adsorbed on this surface with rehybridization of the acetylenic carbon atoms to nearly $sp^3$ occurring. Between 230 and 250 K, the acetylene undergoes both dehydrogenation and hydrogenation reactions, resulting in the formation of two stable surface intermediates, ethylidyne ($CCH_3$) and acetylide (CCH). Both the ethylidyne and the acetylide decompose near 350 K, accompanied by hydrogen desorption, leaving only methylidyne (CH) and carbon adatoms on the surface. The methylidyne decomposes with hydrogen evolution into the gas phase between approximately 480 and 700 K.

## I. Introduction

The interaction of unsaturated hydrocarbon molecules with a variety of low Miller index single crystalline transition metal surfaces has been the focus of much research in surface science recently (1). These studies are of obvious importance both in quantifying the relationships between the bonding of hydrocarbon ligands to multinuclear homogeneous complexes and their bonding to surfaces, and in view of the role that such hydrocarbons play in industrial, heterogeneous catalytic processes. The application of modern, sophisticated experimental techniques to the study of hydrocarbon adsorption and decomposition on metals has led to the identification of a number of surface species that may act as intermediates in these catalytic surface reactions and that have been observed in organometallic cluster compounds. Perhaps the most useful technique in understanding the structure and bonding of adsorbates on metal surfaces has been vibrationally inelastic electron scattering, which is usually termed high resolution electron energy loss spectroscopy (EELS), especially when employed in combination with thermal desorption mass spectrometry (TDMS). Recently, the results of two different EELS and TDMS studies of ethylene adsorption on the hexagonally close-packed Ru(001) surface have been reported (2,3). As a natural extension of this work, we report here a similar investigation of the adsorption and decomposition of acetylene on Ru(001).

Acetylene adsorption has been studied previously with EELS on a wide variety of metal surfaces, including Cu(111) (**4**), Cu(100) (**5**), Cu(110) (**5**), Ag(110) (**6**), Ni(111) (**7**), Ni(110) (**4**), Pd(111) (**8,9**), Pd(100) (**9,10**), Pd(110) (**4**), Pt(111) (**11**), Rh(111) (**12**), Fe(110) (**13**), Fe(111) (**14**), W(110) (**15**), W(111) (**16**) and W(100) (**17**). With the exception of the Ag(110) surface, on which the adsorption is weak and reversible below 160 K, acetylene is adsorbed molecularly, but with the molecule *strongly* distorted from its gas phase structure, in all the cases where adsorption below 200 K has been reported. Typically, the molecularly adsorbed acetylene is stable at temperatures below approximately 250-350 K. The single most important spectroscopic indication of the degree of rehybridization of molecular acetylene upon adsorption is the carbon-carbon stretching frequency, which is 1974 $cm^{-1}$ in gas phase acetylene (**18**). However, a large number of metal surfaces, including Cu(111), Cu(100), Cu(110), Pd(111), Pd(110), Ni(110) and Pt(111), on which acetylene is adsorbed molecularly, exhibit carbon-carbon

stretching frequencies in the 1300-1400 $cm^{-1}$ range, indicative of a rehybridization of the carbon atoms to between $sp^2$ and $sp^3$, and an approximate carbon-carbon bond order of 1.5. On other surfaces, even more extensive rehybridization of the acetylene molecule occurs, resulting in still lower carbon-carbon stretching frequencies. These surfaces include Fe(110) ($\nu_{CC}$ = 1240 $cm^{-1}$), Ni(111) ($\nu_{CC}$ = 1220 $cm^{-1}$), Pd(100) ($\nu_{CC}$ = 1210 $cm^{-1}$) and Fe(111) ($\nu_{CC}$ = 1145 $cm^{-1}$). Further insight into the degree of distortion which the molecule experiences upon adsorption is given by the reduction of the carbon-hydrogen stretching frequencies in going from the gas phase to the chemisorbed phase. Finally, the relative intensities of the carbon-hydrogen bending and carbon-carbon stretching modes may serve to delimit the geometry and the binding site of the adsorbed species (**4**). It is both to investigate these issues and to quantify the connection with ethylene adsorption that we have undertaken this study of acetylene adsorption on Ru(001).

The mechanism by which molecularly adsorbed acetylene decomposes on metal surfaces is also of great interest. The initial dissociation step may be either carbon-carbon bond cleavage to produce methylidyne (CH), or carbon-hydrogen bond cleavage and formation, which may result in a number of different adsorbed hydrocarbon intermediates. Initial cleavage of the carbon-carbon bond has been reported on Ni(111) at 400 K (**7**) and on Fe(110) at approximately 320 K (**13**), to form surface methylidyne. Initial cleavage of carbon-hydrogen bonds occurs on the Pt(111), Pd(100) and Pd(111) surfaces. On Pt(111), formation of a $CCH_2$ species via hydrogen transfer has been proposed as the initial step in acetylene decomposition (**11**). On Pd(100), a hydrogen atom is abstracted from the molecularly adsorbed species by the surface between 300 and 450 K, resulting in the formation of an acetylide (CCH) (**9**). The Pd(111) surface exhibits interesting and complex behavior, with the formation of both acetylide and ethylidyne ($CCH_3$) above 300 K (**9**). These species dehydrogenate thermally at higher temperatures, possibly via methylidyne intermediates. In view of the recent identification of both ethylidyne and methylidyne as decomposition products of ethylene on Ru(001) (**2,3**), a similar study of the decomposition of acetylene on this surface is of obvious importance.

In this paper, we first discuss thermal desorption measurements after acetylene adsorption on Ru(001), and then EEL spectra of both multilayer and chemisorbed molecular acetylene on this surface.

The EEL spectra provide evidence for a highly distorted, nearly $sp^3$ hybridized, molecularly adsorbed acetylene in the chemisorbed overlayer at temperatures below approximately 230 K. We then turn to a discussion of the thermal decomposition of acetylene, which leads to the formation of both acetylide and ethylidyne between approximately 230 and 350 K. These species decompose below 400 K, to yield methylidyne and surface carbon.

## II. Experimental Procedures

The EEL spectrometer used in these studies, as well as the ultrahigh vacuum (UHV) chamber in which it is contained, has been described in detail elsewhere (19). Briefly, the stainless steel UHV chamber is pumped by a 220 *l*/s Varian ion pump and a titanium sublimation pump, and base pressures below 5 x $10^{-11}$ Torr are obtained routinely. The home-built EEL spectrometer is of the Kuyatt-Simpson type, with 180° hemispherical deflectors serving as the energy dispersing elements in both the monochromator and the analyzer. The monochromator is spatially fixed, but the analyzer is rotatable to allow off-specular spectra to be measured. All spectra presented and referred to in this paper were collected in the specular direction unless otherwise noted. The impact energy of the incident electron beam was approximately 4 eV in all cases, and the beam was incident on the Ru(001) crystal at an angle of 60° with respect to the surface normal. The instrumental energy resolution in these studies, defined as the full-width at half-maximum of the elastically scattered beam, varied from 60 to 80 $cm^{-1}$, while count rates in the elastic peak varied from 1.5 x $10^5$ to 3 x $10^5$ counts per second.

The Ru(001) crystal was cooled using liquid nitrogen, and temperatures as low as 80 K were obtained routinely. Crystal cleaning was achieved using the well-established techniques of argon ion sputtering and heating the crystal in a background of oxygen (20). The cleanliness of the surface was verified with EELS. Some of the EEL spectra presented in Sect. III show a small amount of CO contamination (below 1-2% of a monolayer), due to adsorption from the background. Not surprisingly, it was found that these varying and low concentrations of coadsorbed CO did not affect the EEL spectra of acetylene and its decomposition products.

Thermal desorption mass spectrometry was performed in a separate UHV chamber also containing a Ru(001) crystal, and equipped with a quadrupole mass spectrometer (UTI 100C) with a skimmer to

discriminate between desorption from the crystal surface and desorption from the crystal edges and support leads, as well as an Auger electron spectrometer for verifying surface cleanliness. Heating rates between 5 and 20 K/s were used in the TDMS experiments. Crystal cooling and cleaning were accomplished as in the EELS chamber.

The $C_2H_2$ used in these studies was obtained from an industrial acetylene tank (95% purity) and was purified as it was introduced into a glass flask by passage through a dry ice/methanol slurry. The main purpose of this procedure was to remove acetone, which is always added to prevent explosions when acetylene is stored under high pressures. The $C_2D_2$ (99 atom % deuterated) was obtained from MSD Isotopes. The stainless steel leak lines through which the acetylene was introduced into the UHV chamber were flushed several times with $C_2H_2$ or $C_2D_2$, in order to passivate them towards acetylene decomposition, before any acetylene was introduced into the UHV chamber. Mass spectra of the $C_2D_2$ and $C_2H_2$ which were admitted into the UHV chamber showed no traces of any impurities. Multilayer EEL spectra also showed no detectable impurities.

## III. Results and Discussion

### A. Thermal Desorption Mass Spectrometry

Thermal desorption measurements after acetylene adsorption on Ru(001) at 80 K were performed for acetylene exposures in the range of 0.2 to 10 L (1 L ≡ 1 Langmuir = $10^{-6}$ Torr-s). The only desorption products detected in the temperature range between 80 and 800 K were molecular acetylene and hydrogen. Benzene, ethylene, ethane and methane were specifically looked for and were not detected under any circumstances.

Molecular acetylene desorbs only in a sharp peak at 95 K. Since this peak appears only for acetylene exposures greater than 5 L and does not saturate for increasing exposures above 5 L, it may be assigned unambiguously as the desorption of a multilayer state. *No* molecular acetylene desorbs from the chemisorbed monolayer state of acetylene on the Ru(001) surface.

The hydrogen thermal desorption spectra that result after 0.2, 0.8 and 10 L acetylene exposures on Ru(001) at 80 K are shown in Fig. 1. The 0.2 and 0.8 L exposures correspond, respectively, to

approximately 20 and 70% of saturation acetylene coverage, and the 10 L exposure, as the results discussed above suggest, is more than sufficient to saturate the monolayer. Indeed, hydrogen thermal desorption spectra are identical for all acetylene exposures greater than 5 L, confirming that a 5 L exposure corresponds to saturation coverage of chemisorbed acetylene on Ru(001), and that the hydrogen thermal desorption features shown in Fig. 1 correspond to the decomposition of these chemisorbed species. The spectra in Fig. 1 reveal two main desorption features, a low temperature ($\beta_1$) peak and a broad, high temperature ($\beta_2$) peak. The $\beta_1$ peak is centered at 425 K for a 0.2 L acetylene exposure and shifts downward to 380 K for saturation acetylene exposures. This behavior is characteristic of second-order desorption kinetics. The $\beta_2$ peak is quite broad, extending from about 480 to 580 K for 0.2 L acetylene exposures, and from 480 to 700 K for saturation exposures.

As will be shown from the EELS results, the only hydrocarbon species resulting from acetylene decomposition on Ru(001) above 400 K is methylidyne. Thus, the high temperature $\beta_2$ desorption peak of hydrogen results from methylidyne decomposition to yield carbon adatoms and $H_2(g)$. The $\beta_1$ desorption peak of hydrogen results from surface hydrogen that is formed from the dehydrogenation of ethylidyne (and to a lesser degree from acetylene decomposition to acetylide), as will be discussed later. For initial acetylene exposures of 0.4 L or more, the ratio of the $\beta_1$ to $\beta_2$ peak areas is 3:1 within experimental error, indicating that one-fourth of the hydrogen initially present in the chemisorbed acetylene is eventually present in methylidyne. For 0.2 L acetylene exposures, the ratio of the $\beta_1$ to $\beta_2$ peak areas is more difficult to determine due to peak overlap, but it is approximately 2:1, indicating that one-third of the hydrogen atoms initially present in the acetylene are eventually present in methylidyne. Thus, relatively more methylidyne is formed for low initial acetylene exposures.

Since neither monolayer acetylene nor other hydrocarbons desorb molecularly from Ru(001), all of the chemisorbed acetylene decomposes on the surface to yield eventually $H_2(g)$ and carbon adatoms. Thus, there is a one-to-one correspondence between the amount of acetylene adsorbed in the monolayer and the total amount of hydrogen desorbing in the $\beta_1$ and $\beta_2$ thermal desorption peaks.Consequently, the total amount of hydrogen desorbing following an acetylene exposure may be compared to the amount of hydrogen desorbing from the clean Ru(001) surface following a saturation exposure to $H_2$

(21), and this may be used to calculate the acetylene coverage. This yields a saturation fractional coverage of approximately 0.27 for acetylene adsorption on Ru(001).

## B. Electron Energy Loss Spectroscopy

### *1. The Multilayer State*

As indicated above, exposing the Ru(001) surface at 80 K to approximately 5 L or more of $C_2H_2$ or $C_2D_2$ results in the condensation of molecular multilayers of acetylene on the surface. The EEL spectra of $C_2H_2$ and $C_2D_2$ multilayers on the Ru(001) surface are shown in Fig. 2, and the observed vibrational frequencies are listed in Table 1, together with data for both gas phase and crystalline acetylene. These multilayer spectra are useful as a supplement to TDMS data, both in verifying the purity of the acetylene used in these experiments and in determining when saturation coverage of chemisorbed acetylene is obtained. For both $C_2H_2$ and $C_2D_2$, all fundamental modes are clearly resolved except $\nu_4$, the Raman active carbon-hydrogen symmetric bending mode, which is obscured by the intense, IR active asymmetric bending mode, $\nu_5$. As in the case of gas phase IR spectra of acetylene (18), the frequency of the $\nu_4$ mode may be estimated from the observed $\nu_5 + \nu_4$ combination band, which occurs at 1375 $cm^{-1}$ for $C_2H_2$ multilayers and 1110 $cm^{-1}$ for $C_2D_2$ multilayers. Not surprisingly, the IR active modes of the acetylene multilayers are close in frequency to both those of crystalline acetylene (22) and those of gas phase acetylene (18). The feature near 740 $cm^{-1}$ in Fig. 2(b) is probably due to a small amount of $C_2H_2$ in the deuterated acetylene. This impurity is on the order of 1% or less.

### *2. Molecularly Chemisorbed Acetylene*

Annealing the Ru(001) surface on which acetylene multilayers are present to above 95 K, or exposing the Ru(001) surface to less than 5 L of acetylene at 80 K, results in the formation of a surface species that is stable to approximately 230 K. This chemisorbed species is identified easily as molecularly adsorbed acetylene that has undergone extensive rehybridization upon adsorption. The observed vibrational modes for $C_2H_2$ and $C_2D_2$ are listed together with their assignments in Table 2, and the relevant EEL spectra are presented in Fig. 3. For comparison, the vibrational data for acetylene in two organometallic cobalt compounds are also listed in Table 2. These data will be discussed below in relation to possible bonding geometries for acetylene on Ru(001).

The mode assignments follow in a straightforward fashion from a comparison of the spectra of hydrogenated and deuterated acetylene. The loss feature at 2940 (2210) $cm^{-1}$ for $C_2H_2$ ($C_2D_2$) is clearly due to a carbon-hydrogen (carbon-deuterium) stretching vibration. In both cases, the symmetric and asymmetric stretching modes are not resolved. The intense mode at 765 $cm^{-1}$, which shifts down to 565 $cm^{-1}$ upon deuteration, is assigned to a carbon-hydrogen bending mode, as is the less intense mode, which shifts from 980 to 715 $cm^{-1}$ upon deuteration. The feature that appears at 1135 $cm^{-1}$ in the $C_2H_2$ spectrum and at 1085 $cm^{-1}$ in the $C_2D_2$ spectrum clearly does not shift sufficiently to be a hydrogenic mode and is thus assigned as the carbon-carbon stretching vibration. Modes at 520 and 375 $cm^{-1}$ in the $C_2H_2$ spectrum are assigned, respectively, to the asymmetric and symmetric metal-carbon stretching modes of adsorbed acetylene. The latter mode occurs at 350 $cm^{-1}$ for $C_2D_2$, while the asymmetric metal-carbon stretch in the deuterated species is obscured by the carbon-deuterium bending mode that is centered at 565 $cm^{-1}$. There is no other set of mode assignments that consistently accounts for the observed spectra.

Off-specular EEL spectra indicate that the carbon-carbon stretching vibration at 1135 $cm^{-1}$ in $C_2H_2$ and the carbon-hydrogen bending vibration at 765 $cm^{-1}$ are principally dipolar excited modes, while the carbon-hydrogen stretching vibration at 2940 $cm^{-1}$ and the carbon-hydrogen bend at 980 $cm^{-1}$ are excited primarily by nondipolar mechanisms (**23**). These data suggest that the carbon-hydrogen bend at 765 $cm^{-1}$ involves motion of the hydrogen atoms largely perpendicular to the surface, while the carbon-hydrogen bend at 980 $cm^{-1}$ involves motion of the hydrogen atoms largely parallel to the surface. However, without detailed knowledge of the surface binding site of chemisorbed acetylene, assignment of these bending modes as "in-plane" or "out-of-plane" is not possible. No additional vibrational modes are observed in off-specular spectra.

The observed carbon-carbon stretching frequency of 1135 $cm^{-1}$ for chemisorbed $C_2H_2$ corresponds to a carbon-carbon bond order nearly equal to one, with the carbon atoms being nearly $sp^3$ hybridized. This may be seen by comparison to the gas phase carbon-carbon stretching frequencies of ethane ($\nu_{CC}$ = 995 $cm^{-1}$) and ethylene ($\nu_{CC}$ = 1623 $cm^{-1}$) (**18**). Although this is the lowest carbon-carbon stretching frequency that has heretofore been observed for chemisorbed acetylene on any transi-

tion metal surface, it is quite close to the value of 1145 $cm^{-1}$, which has been observed for $C_2H_2$ on Fe(111) (14). The carbon-hydrogen stretching frequency of 2940 $cm^{-1}$ is also consistent with carbon atoms that are nearly $sp^3$ hybridized; typical values for $\nu_{CH}$ are 2800-3000 $cm^{-1}$ for $sp^3$ hybridized carbon atoms and 2950-3100 $cm^{-1}$ for $sp^2$ hybridized carbon atoms (18).

A comparison of the carbon-carbon stretching frequency of 1135 $cm^{-1}$ for acetylene chemisorbed on Ru(001) to the carbon-carbon stretching frequencies of the acetylene ligands in the cobalt compounds listed in Table 2 suggests that such a low value of $\nu_{CC}$ is not at all unreasonable for acetylene adsorbed on a metal surface. The decrease in frequency of 204 $cm^{-1}$, from $\nu_{CC}$ = 1403 to 1199 $cm^{-1}$, in going from a two-cobalt atom cluster to a four-cobalt atom cluster suggests that a further decrease in $\nu_{CC}$ might be expected as the metal "cluster" becomes infinitely large (i.e. a metal surface). This should be especially true of the surfaces of the relatively more reactive iron group metals, as opposed to surfaces of the nickel-palladium-platinum triad on which acetylene adsorption has been studied more extensively.

Based on the EELS data alone, any conclusions regarding the nature of the adsorption site for acetylene on Ru(001) must be somewhat speculative. It has been suggested (4) that adsorbed $C_2H_2$ species exhibiting strong carbon-hydrogen bending modes in the 670-770 $cm^{-1}$ region, together with relatively weak carbon-carbon stretching modes, are the result of a "di-$\sigma + \pi$" bonding structure in which the plane of a cis M-CH=CH-M complex is tilted significantly with respect to the surface normal through the interaction of the C=C bond with a third metal atom. Such a model accounts successfully for the dipolar enhancement of the intense carbon-hydrogen bending mode in these surface complexes, assigned as the $\gamma_{CH}$ out-of-plane bend. Such species occur when acetylene is adsorbed on Ni(110), Pd(111), Pd(110), Rh(111) and Pt(111). However, on all of these surfaces, the adsorbed acetylene is characterized by a carbon-carbon stretching frequency between 1300 and 1400 $cm^{-1}$. Consequently, it is not clear that the same structure should apply to $C_2H_2$ on Ru(001). Indeed, the low carbon-carbon stretching frequency of 1135 $cm^{-1}$ argues against any model that invokes $\pi$-bonding between the carbon-carbon bond and the surface. Possible alternative bonding geometries are suggested by the organometallic compounds listed in Table 2. In the compound $Co_2(CO)_6(C_2H_2)$ (24), the plane contain-

ing the $C_2H_2$ group bisects the cobalt-cobalt vector and is perpendicular to it. A similar bonding configuration could be obtained for acetylene on Ru(001) if the carbon atoms of acetylene occupy adjacent, inequivalent threefold hollow sites on the surface [Fig. 4(a)]. Since these adjacent adsites are separated by 1.56 Å on this surface (**25**), slightly farther apart than the length of a carbon-carbon single bond in a hydrocarbon molecule (1.54 Å), it is probable that the carbon atoms would not be centered directly above the threefold sites, if such a bonding geometry were to occur. In the compound $Co_4(CO)_{10}(C_2H_2)$ (**26**), the carbon-carbon bond of the acetylene ligand lies parallel to a cobalt-cobalt bond, with each carbon atom being σ-bonded to one of these two cobalt atoms and with a four-centered, μ-type bond between the carbon atoms and the remaining two cobalt atoms. An analogous bonding situation on Ru(001) would be achieved if the two carbon atoms of the acetylene are σ-bonded to nearest neighbor ruthenium atoms, and with a four-centered bond between the carbon atoms and the two ruthenium atoms on either side of this carbon-carbon bond [Fig. 4(b)]. It should be emphasized that the observation of a dipolar enhanced carbon-carbon stretching mode in specular EEL spectra does not rule out such bonding models in which the carbon-carbon bond lies very nearly parallel to the surface, since charge coupling between the adsorbed acetylene and the metal may result in a substantial dynamic dipole's being associated with the $\nu_{CC}$ vibration (**27**).

In summary, molecularly adsorbed acetylene on Ru(001) exhibits vibrational frequencies characteristic of essentially a carbon-carbon single bond and $sp^3$ hybridized carbon atoms. Although we have discussed two *possible* bonding configurations based on a comparison with organometallic cobalt complexes, we stress that this is speculative and feel that additional studies of the vibrational spectra of acetylene in cluster compounds and additional measurements with other surface sensitive techniques are necessary before firm conclusions may be drawn concerning the nature of the binding site on Ru(001).

*3. Thermal Decomposition of Chemisorbed Acetylene*

Upon heating the Ru(001) surface with molecularly chemisorbed acetylene to temperatures in the range of 250-350 K, marked changes occur in the EEL spectra. Figure 5(a) shows the EEL spectrum that results when the surface represented in Fig. 3(a) of adsorbed $C_2H_2$ is annealed to 300 K. The most obvious changes are the disappearance of the carbon-hydrogen bending mode of molecularly adsorbed

acetylene at 980 $cm^{-1}$ and the appearance of a new mode at 1360 $cm^{-1}$, which is comparable in intensity to the mode at 1140 $cm^{-1}$. In addition, the strong carbon-hydrogen bending mode, which occurs at 765 $cm^{-1}$ for molecularly adsorbed acetylene, shifts down slightly (~15 $cm^{-1}$) in frequency. Finally, the metal-carbon stretching modes of adsorbed acetylene at 375 and 520 $cm^{-1}$ are no longer present but are replaced by a new mode at 435 $cm^{-1}$.

Spectra of deuterated acetylene on Ru(001) that has been annealed to 300 K [Fig. 5(b)] show similar changes. The intense carbon-deuterium bend of molecularly adsorbed $C_2D_2$ shifts downward slightly from 565 to 550 $cm^{-1}$, the carbon-deuterium bend at 715 $cm^{-1}$ is greatly reduced in intensity or completely absent, and a new mode appears at 420 $cm^{-1}$. In addition, a relatively broad feature appears between 1080 and 1120 $cm^{-1}$, and a weaker feature appears at 1260 $cm^{-1}$.

These observed changes that occur in the EEL spectra when the surface is annealed to temperatures above 250 K might be accounted for in two different ways. One possibility is that acetylene remains molecularly chemisorbed on the surface under these conditions but has undergone a change in molecular orientation or adsorption site such that the observed spectral changes result. The second possibility is that a surface reaction has taken place, resulting in the formation of one or more new surface species. The first of these two possibilities is most unlikely in view of the previously discussed thermal desorption spectra. The fact that the low temperature tail of the $\beta_1$ hydrogen thermal desorption peak extends to below 250 K for saturation acetylene coverages indicates that some carbon-hydrogen bond cleavage has occurred by this temperature. Furthermore, attempting to rationalize the EEL spectra observed after heating to 300 K in terms of molecularly adsorbed acetylene would require assigning the 1360 $cm^{-1}$ peak in the $C_2H_2$ spectra to a carbon-hydrogen bending mode, which is inconsistent with all existing vibrational data for acetylene adsorbed on surfaces or inconsistent as a ligand in organometallic compounds (**28**). In addition, the bands at 1140 and 1360 $cm^{-1}$ in Fig. 5(a) disappear at a slightly lower temperature than the band at 750 $cm^{-1}$. Hence, these two modes cannot be assigned as belonging to the same surface species that gives rise to the 750 $cm^{-1}$ mode. *The possibility that the EEL spectra in Fig. 5 correspond to some altered form of molecularly chemisorbed acetylene may therefore be ruled out unambiguously.*

Consequently, it must be concluded that the EEL spectra shown in Fig. 5 are characteristic of at least two different reaction products that result from the thermally activated decomposition of acetylene on Ru(001). Indeed, the observed vibrational modes may be explained easily in terms of two species, namely, acetylide and ethylidyne. Mode assignments for both species are listed in Table 3. Ethylidyne has been isolated previously and identified as a product of ethylene decomposition on Ru(001) (2,3), and modes of approximately equal intensity at 1140 $cm^{-1}$ (carbon-carbon stretch) and 1360 $cm^{-1}$ [$\delta_s(CH_3)$] are characteristic of this species. To confirm further the identity of this species, off-specular EEL spectra were measured, which showed additional vibrational modes at 990 $cm^{-1}$ [$\rho(CH_3)$] and 1440 $cm^{-1}$ [$\delta_a(CH_3)$], as is the case for ethylidyne formed by ethylene decomposition. The remaining vibrational modes in Fig. 5 may be assigned to the acetylide species. The 750 $cm^{-1}$ mode is a carbon-hydrogen bend, and the 435 $cm^{-1}$ mode is a metal-carbon stretch. The latter is far too intense to be attributed solely to the metal-carbon stretch of coadsorbed CO, and since a mode of this intensity was not observed in the case of ethylidyne formed from ethylene on Ru(001), we attribute it mainly to the acetylide species. It is possible, however, that the symmetric metal-carbon stretch of ethylidyne, which occurs at 480 $cm^{-1}$ for ethylidyne formed from ethylene decomposition (3), also contributes to the intensity of this mode. As may be seen in Table 3, deuterated spectra are consistent with these assignments. The feature at 1085 $cm^{-1}$ in the $C_2D_2$ spectrum is due to the overlap of the carbon-carbon stretch and the $\delta_s(CD_3)$ mode of deuterated ethylidyne. In addition, the weak mode that appears at 1260 $cm^{-1}$ in the deuterated spectra may be assigned to the carbon-carbon stretch of the acetylide. This frequency is too high to be due to any sort of carbon-deuterium vibration, since no modes (except the carbon-hydrogen stretch) appear above 1360 $cm^{-1}$ in the specular spectra of acetylide and ethylidyne. The corresponding mode for acetylide is expected to be upshifted slightly (it appears at 1290 $cm^{-1}$ for acetylide formed from ethylene decomposition) and is thus obscurred by the $\delta_s(CH_3)$ mode of ethylidyne. Finally, it should be noted that the carbon-hydrogen (carbon-deuterium) stretching frequencies of the acetylide and the ethylidyne are not well resolved and therefore must be at approximately the same frequency.

Since ethylidyne has a larger hydrogen-to-carbon atom ratio than acetylene, it is obvious that not

all of the molecularly adsorbed acetylene on Ru(001) may be converted to ethylidyne when the surface is heated. This is consistent with the observation that ethylidyne is formed only when acetylide is formed simultaneously. Thus, the *overall* chemical conversion that results in ethylidyne formation may be written as the self-hydrogenation reaction

$$2C_2H_2(a) \rightarrow CCH(a) + CCH_3(a) .$$

This is not meant to imply, however, that acetylide and ethylidyne are formed in a ratio of 1:1, since it is obvious that acetylide formation may occur without ethylidyne formation. As written, this reaction says nothing concerning the mechanism of acetylide and ethylidyne formation from acetylene, an issue of obvious fundamental importance. We have not been able to isolate spectroscopically a $CCH_2$ species or any other intermediate in the formation of ethylidyne under these conditions. Coadsorption experiments with acetylene and hydrogen on Ru(001) are currently in progress, which may shed light on the mechanism of acetylide and ethylidyne formation (29).

The ethylidyne that is formed on Ru(001) has been discussed in detail in previous studies of ethylene adsorption (2,3) and, consequently, will not be considered further here. However, since we have not previously described the acetylide species in detail, a discussion of this species is in order. Very few acetylide species have been identified previously on metal surfaces. On Ag(110) with preadsorbed oxygen, an acetylide has been identified as the result of acetylene decomposition (6). However, since the carbon atoms in this species retain an sp hybridization, as evidenced by a carbon-hydrogen stretching frequency of 3250 $cm^{-1}$, this species is clearly not closely related to the acetylide that is formed on Ru(001). Acetylene decomposition on Pd(100) and Pd(111) (9), however, leads to the formation of an acetylide that is very similar to the one observed on Ru(001), the former being characterized by an intense carbon-hydrogen bend at 750 $cm^{-1}$, a weak carbon-carbon stretch at 1340 $cm^{-1}$, and a rather weak carbon-hydrogen stretch at 3000 $cm^{-1}$. From these data it was suggested that the acetylide on the palladium surfaces has both carbon atoms bonded to the surface, with the carbon-carbon bond axis either parallel or slightly skewed relative to the surface plane. This is consistent with a weak carbon-carbon stretching vibration and an intense carbon-hydrogen bending vibration, in accordance with the surface dipole selection rule for EELS (23). The same conclusions very likely apply to the

acetylide on Ru(001), and the somewhat lower carbon-carbon (1260 $cm^{-1}$ for CCD) and carbon-hydrogen (~2935 $cm^{-1}$) stretching frequencies on the ruthenium surface suggest a slightly lower carbon-carbon bond order than occurs in the acetylide on palladium, although in both cases the bond order is clearly between one and two. This slightly lower carbon-carbon bond order may be related to the lower decomposition temperature of acetylide on Ru(001). On this surface the acetylide has decomposed entirely by 400 K, while on Pd(100) at least some acetylide remains on the surface to 650 K. Finally, we note that it is quite reasonable that the carbon-carbon stretching frequency of adsorbed acetylide is somewhat higher than that of chemisorbed acetylene on Ru(001), since the former may have some double bond character due to the additional electron no longer involved in a carbon-hydrogen bond.

Annealing the Ru(001) surface to temperatures of 400 K or higher causes the decomposition of both the acetylide and the ethylidyne, and a new surface species appears which is characterized by vibrational modes at 440 (415), 800 (615) and 3010 (2255) $cm^{-1}$ in the case of $C_2H_2$ ($C_2D_2$). The vibrational spectra for the hydrogenated and deuterated forms of this species are shown in Fig. 6. Based on the previous studies of ethylene decomposition on Ru(001), and comparison to vibrational data for a number of previously identified surface species (**14,30-33**) and analogous organometallic compounds (**34,35**), the vibrational modes of this new species are identified easily, respectively, as the metal-carbon stretch, the carbon-hydrogen (carbon-deuterium) bend and the carbon-hydrogen (carbon-deuterium) stretch of a surface methylidyne. The carbon-hydrogen modes are listed in Table 4 and compared to those for other methylidyne species on surfaces and in the organometallic compounds $Ru_3(CO)_9H_3(\mu_3\text{-}CH)$ and $Co_3(\mu_3\text{–}CH)(CO)_9$. A significant feature of the methylidyne spectra is the complete lack of any vibrational features between 1000 and 2000 $cm^{-1}$ which might have been associated with a carbon-carbon stretching vibration. Note that the frequency of the carbon-hydrogen bend of methylidyne is approximately 50 $cm^{-1}$ higher than, and thus quite distinct from, the carbon-hydrogen bend of the acetylide which exists at lower temperatures, and that the carbon-hydrogen stretch is also upshifted by about 70 $cm^{-1}$. It should be pointed out that, in addition to methylidyne, there must be a rather large concentration (approximately 0.4 monolayer) of carbon adatoms on the Ru(001) surface at

400 K, since the thermal desorption spectra indicate a large fraction of the hydrogen initially present in the acetylene has desorbed from the surface by this temperature. Heating the surface to slightly over 700 K desorbs the remaining hydrogen, and EEL spectra measured at 800 K verify that all spectral features due to methylidyne have disappeared. All that remains is a weak loss feature near 600 $cm^{-1}$, which may be attributed to the presence of carbon adatoms.

Both chemical intuition and the structures of the organometallic complexes listed in Table 4 suggest that the most likely coordination site for methylidyne on Ru(001) is one in which the carbon atom occupies a threefold hollow site. Indeed, the observed carbon-hydrogen bending and stretching modes of methylidyne on Ru(001) resemble most closely those of methylidyne on the hexagonally close-packed Ni(111) surface, on which a structure has been proposed in which the carbon atom occupies a threefold hollow site, and the carbon-hydrogen bond axis is tilted slightly with respect to the surface normal. The latter allows the carbon-hydrogen bending mode to become dipolar active and could account for its relatively high intensity in the methylidyne spectra on Ru(001). Spectra taken 10° off-specular do indeed indicate a marked reduction in the intensity of the carbon-hydrogen bending mode on Ru(001), suggesting that this mode is dipolar enhanced in specular EEL spectra and that the carbon-hydrogen bond axis may be tilted slightly with respect to the surface normal. These conclusions are in agreement with those of Barteau et al. (2) for methylidyne formed from ethylene decomposition on Ru(001).

Two closely related issues remain to be addressed regarding acetylene decomposition on Ru(001). The first is the relative concentrations of acetylide and ethylidyne formed upon decomposition of molecularly chemisorbed acetylene between 230 and 250 K. Unfortunately, neither the EELS nor the TDMS results discussed here can provide an unambiguous answer to this question. Clearly, stoichiometry requires that unless some acetylene is dehydrogenated completely to $C_2$ dimers below 250 K, a possibility which seems unlikely and for which there is no spectroscopic evidence, no more than half of the chemisorbed acetylene may be converted to ethylidyne, while the rest decomposes to acetylide. Taking into account the saturation acetylene coverage of 0.27 monolayer, this places an upper limit of approximately 0.14 monolayer on the total concentration of ethylidyne produced. A suitable

lower limit is not so easily derived. Since the desorption of hydrogen begins slightly below 250 K for a saturation exposure of acetylene, it is obvious that not all of the hydrogen that results from acetylide formation contributes to ethylidyne formation. Rather, an overall reaction such as

$$C_2H_2(a) \rightarrow CCH(a) + \tfrac{1}{2} H_2(g)$$

also occurs to some extent. Consequently, the surface concentration of acetylide is greater than that of ethylidyne, although the exact ratio is not known.

The second remaining question involves the mechanism of methylidyne formation; i.e., is the methylidyne formed via carbon-carbon bond cleavage of acetylide, via decomposition of ethylidyne, or via a combination of both of these mechanisms? Since acetylide and ethylidyne decompose in very similar temperature ranges, the former between approximately 350 and 380 K and the latter between approximately 330 and 360 K [as judged both from this acetylene study and our previous ethylene study (3)], EEL spectra are of little use in answering this question. However, some information may be gleaned from the fact that the ratio of the areas of the $\beta_1$ to $\beta_2$ hydrogen thermal desorption peaks is less for low initial acetylene exposures compared to higher exposures. This implies that relatively more methylidyne is formed from acetylene decomposition at low initial coverages of the latter. In our study of ethylene decomposition on Ru(001) (3), it was found that the ratio of acetylide to ethylidyne formed upon ethylene decomposition was larger at lower initial ethylene coverages relative to higher initial coverages, and it would be expected that this is true in the case of acetylene as well. This is in accord with the fact that ethylidyne occupies only one site on the surface, while an acetylide and two hydrogen adatoms occupy at least three sites. Consequently, the former should be favored at higher initial coverages of acetylene. Therefore, a relatively greater amount of acetylide formation leads to a relatively greater amount of methylidyne formation, and it follows that acetylide must have a greater tendency to decompose to yield methylidyne than does ethylidyne. Thus, the dominant mechanism of acetylide decomposition appears to be carbon-carbon bond cleavage to give C(a) and CH(a), while the dominant mechanism of ethylidyne decomposition is to 2 C(a) and 3 H(a). This is in agreement with the more conclusive EELS results for ethylene decomposition on Ru(001) (3), which show more clearly the decomposition of ethylidyne prior to the decomposition of acetylide, and with little or no methylidyne

formation accompanying the ethylidyne decomposition.

Further evidence that methylidyne is formed largely from acetylide decomposition was provided by adsorbing acetylene at 350 K. A subsequent hydrogen thermal desorption spectrum showed that the area of the $\beta_2$ desorption peak (from methylidyne) is enhanced by approximately a factor of two compared with that observed after a saturation exposure of acetylene at 80 K. Since the desorption of surface hydrogen is rapid at 350 K, the probability of ethylidyne formation under these conditions is negligible. On the other hand, acetylide is stable at 350 K, and its surface concentration was found to be enhanced relative to adsorption at 80 K, followed by annealing. This enhancement in the surface concentration of acetylide correlated with the enhancement in the surface concentration of methylidyne that was observed, strongly implicating acetylide as the major source of methylidyne. However, the possibility that a small amount of ethylidyne decomposes to give methylidyne, or that a small amount of acetylide decomposes to 2C(a) + H(a) rather than to C(a) and methylidyne cannot be ruled out completely.

In summary, the overall mechanism of acetylene decomposition on Ru(001) may be written as

$$C_2H_2(g) \xrightarrow{<230K} C_2H_2(a)\ ,$$

$$C_2H_2(a) \xrightarrow{230\text{–}250K} CCH(a) + CCH_3(a)\ ,$$

$$CCH(a) \xrightarrow{350\text{–}380K} C(a) + CH(a)$$

$$CCH_3(a) \xrightarrow{330\text{–}360K} 2C(a) + 3H(a)$$

$$2H(a) \xrightarrow{\sim 380K} H_2(g)\ ,$$

and

$$CH(a) \xrightarrow{480\text{–}700K} C(a) + \frac{1}{2}\ H_2(g)\ .$$

## IV. Conclusions

The principal conclusions of this work may be summarized as follows:

1. Molecularly adsorbed acetylene on Ru(001) is stable below 230 K and is characterized by a carbon-carbon stretching frequency of 1135 $cm^{-1}$, corresponding to carbon atoms that are very nearly $sp^3$ hybridized. This is the lowest carbon-carbon stretching frequency yet observed for

molecularly adsorbed acetylene on a transition metal surface. The saturation coverage of molecularly adsorbed acetylene on Ru(001) is approximately 0.27 monolayer.

2. Molecularly adsorbed acetylene does not desorb intact from Ru(001), but rather is an intermediate to dehydrogenation and hydrogenation that occurs between 230 and 250 K, yielding acetylide and ethylidyne.

3. The acetylide and ethylidyne decompose near 350 K, leaving methylidyne as the only hydrocarbon species on the surface by 400 K, along with carbon adatoms. The decomposition of ethylidyne (and perhaps to some degree the decomposition of acetylide) produces surface hydrogen, which recombines and desorbs as $H_2(g)$. This desorption occurs at 425 K for very low initial coverages of acetylene and at 380 K for a saturation coverage of chemisorbed acetylene.

4. The methylidyne decomposes between 480 and 700 K, yielding $H_2(g)$ and leaving only carbon on the surface.

**Acknowledgments**

This work was supported by the National Science Foundation under Grant No. CHE-8516615. Acknowledgment is also made to the Donors of the Petroleum Research Fund, administered by the American Chemical Society, for the partial support of this research under Grant No. 15454-AC5.

**References**


1. For example, see Muetterties, E. L.; Rhodin, T. N.; Band, E.; Brucker, G. F.; Pretzer, W. R., *Chem. Rev.* **1979**, 79, 91.

2. Barteau, M. A.; Broughton, J. Q.; Menzel, D., *Appl. Surface Sci.* **1984**, 19, 92.

3. Hills, M. M.; Parmeter, J. E.; Mullins, C. B.; Weinberg, W. H., *J. Am. Chem. Soc.* **1986**, 108, 3554.

4. Bandy, B. J.; Chesters, M. A.; Pemble, M. E.; McDougall, G. S.; Sheppard, N., *Surface Sci.* **1984**, 139, 87.

5. Avery, N. R., to be published.

6. Stuve, E. M.; Madix, R. J.; Sexton, B. A., *Surface Sci.* **1982**, 123, 491.

7. (a) Lehwald, S.; Ibach, H., *Surface Sci.* **1979**, 89, 425. (b) Ibach, H.; Lehwald, S., *J. Vacuum Sci. Technol.* **1981**, 18, 625.

8. Gates, J. A.; Kesmodel, L. L., *J. Chem. Phys.* **1982**, 76, 4281.

9. Kesmodel, L. L.; Waddill, G. D.; Gates, J. A., *Surface Sci.* **1984**, 138, 464.

10. Kesmodel, L. L., *J. Chem. Phys.* **1983**, 79, 4646.

11. Ibach, H.; Lehwald, S., *J. Vacuum Sci. Technol.* **1978**, 15, 407.

12. Dubois, L. H.; Castner, D. J.; Somorjai, G. A., *J. Chem. Phys.* **1980**, 72, 5234.

13. Erley, W.; Baro, A. M.; Ibach, H., *Surface Sci.* **1982**, 120, 273.

14. Seip, U.; Tsai, M.-C.; Küppers, J.; Ertl, G., *Surface Sci.* **1984**, 147, 65.

15. Backx, C.; Willis, R. F.; Feuerbacher, B.; Fitton, B., *Surface Sci.* **1977**, 68, 516.

16. Backx, C.; Feuerbacher, B.; Fitton, B., Willis, R. F., *Surface Sci.* **1977**, 63, 193.

17. Hamilton, J. C.; Swanson, N.; Waclawski, B. J.; Celotta, R. J., *J. Chem. Phys.* **1981**, 74, 4156.

18. Herzberg, G., *Infrared and Raman Spectra of Polyatomic Molecules*, Van Nostrand, N.Y., **1945**.

19. Thomas, G. E.; Weinberg, W. H., *Rev. Sci. Instrum.* **1979**, 50, 497.

20. Thomas, G. E.; Weinberg, W. H., *J. Chem. Phys.* **1979**, 70, 954.

21. Shimizu, H.; Christmann, K.; Ertl, G., *J. Catal.* **1980**, 61, 412.

22. Glocker, G.; Morrell, C. E., *J. Chem. Phys.* **1936**, 4, 15.

23. For a discussion of EELS scattering mechanisms, see Ibach, H.; Mills, D. L., *Electron Energy Loss Spectroscopy and Surface Vibrations*, Academic Press, N.Y., **1982**.

24. Iwashita, Y.; Tamura, F.; Nakamura, A., *Inorg. Chem.* **1969**, 8, 1179.

25. This distance is calculated easily from the nearest neighbor separation of 2.71 angstrom in bulk ruthenium; see Kittel, C., *Introduction to Solid State Physics*, fifth edition, Wiley, N.Y., **1976**.

26. Gervasio, G.; Rossetti, R.; Stanghellini, P. L., *Organometallics* **1985**, 4, 1612.

27. Ref. 23, pp. 171-172.

28. To our knowledge, no CH bending mode above 1000 $cm^{-1}$ has been identified previously for acetylene in an organometallic complex. The only CH bending frequency identified previously for chemisorbed acetylene that lies above 1150 $cm^{-1}$ is one of 1415 $cm^{-1}$ on Fe(110), a surface species for which all four possible acetylene CH bending modes were observed in specular EEL spectra (**13**).

29. Parmeter, J. E.; Hills, M. M.; Weinberg, W. H., to be published.

30. Demuth, J. E.; Ibach, H., *Surface Sci.* **1978**, 78, L747.

31. Gates, J. A.; Kesmodel, L. L., *Surface Sci.* **1983**, 124, 68.

32. Ref. 23, Ch. 6.

33. Dubois, L. H.; Somorjai, G. A., in: *Am. Chem. Soc. Symp. Ser.*, Eds., A. T. Bell and M. L. Hair, Am. Chem. Soc., Washington, D.C., **1980**.

34. Howard, M. W.; Kettle, S. F.; Oxton, I. A.; Powell, D. B.; Sheppard, N.; Skinner, P., *J. Chem. Soc. Faraday Trans. II*, **1981**, 77, 397.

35. Eady, C. R.; Johnson, B. F. G.; Lewis, J., *J. C. S. Dalton*, **1977**, 477.

**Table 1.** Vibrational frequencies ($cm^{-1}$) for $C_2H_2$ and $C_2D_2$ in gas and crystalline phases, and for $C_2H_2$ and $C_2D_2$ multilayers on Ru(001) at 80 K.

$C_2H_2$

| Mode | Gas (18) | Crystalline IR (22)† | Multilayers on Ru(001) |
|---|---|---|---|
| CH s bend ($\nu_4$) | 612 | - | 605* |
| CH a bend ($\nu_5$) | 729 | 761,769 | 770 |
| CC stretch ($\nu_2$) | 1974 | - | 1970 |
| CH a stretch ($\nu_3$) | 3287 | 3226 | 3255 |
| CH s stretch ($\nu_1$) | 3374 | - | 3360 |

$C_2D_2$

| Mode | Gas (18) | Crystalline IR (22)† | Multilayers on Ru(001) |
|---|---|---|---|
| CD s bend ($\nu_4$) | 505 | - | 545* |
| CD a bend ($\nu_5$) | 539 | 562,568 | 565 |
| CC stretch ($\nu_2$) | 1762 | - | 1780 |
| CD a stretch ($\nu_3$) | 2439 | 2393 | 2440 |
| CD s stretch ($\nu_1$) | 2701 | - | 2705 |

*Estimated from frequency of $\nu_4 + \nu_5$ combination band.
†Crystalline IR data at 63 K.
s = symmetric, a = asymmetric.

**Table 2.** Vibrational modes of molecularly adsorbed acetylene on Ru(001) in the temperature range 80-230 K, with corresponding frequencies from the cobalt compounds $Co_2(CO)_6(C_2H_2)$ (**24**) and $Co_4(CO)_{10}(C_2H_2)$ (**26**) presented for comparison. All frequencies are reported in $cm^{-1}$.

| | Ru(001) | | | | |
|---|---|---|---|---|---|
| Mode | $C_2H_2$ | $C_2D_2$ | $\nu(C_2H_2)/\nu(C_2D_2)$ | $Co_2(CO)_6(C_2H_2)$ | $Co_4(CO)_{10}(C_2H_2)$ |
| CH a stretch | | | | 3116 | 3020 |
| | 2940 | 2210 | 1.33 | | |
| CH s stretch | | | | 3086 | 2993 |
| CC stretch | 1135 | 1085 | 1.05 | 1403 | 1199 |
| CH bend | 980 | 715 | 1.37 | 894 | 983,1120 |
| CH bend | 765 | 565 | 1.35 | 768 | 837,922 |
| MC a stretch | 520 | obscurred | - | 605 | 619 |
| MC s stretch | 375 | 350 | 1.07 | 551 | ? |

s = symmetric, a = asymmetric.

**Table 3.** Vibrational modes observed for ethylidyne and acetylide present on the Ru(001) surface in the temperature range 250-350 K due to acetylene decomposition. All frequencies are given in $cm^{-1}$.

| $CCH_3$ (ethylidyne) | | | |
|---|---|---|---|
| Mode | $C_2H_3$ | $C_2D_3$ | $\nu(C_2H_3)/\nu(C_2D_3)$ |
| CC stretch | 1140 | ~1150[†] | 0.98 |
| $\delta_s(CH_3)$ | 1360 | ~1030[†] | 1.30 |
| CH stretch[*] | ~2935 | ~2210 | 1.33 |
| $\delta_a(CH_3)$[**] | 1440 | - | - |
| $\rho(CH_3)$[**] | 990 | 800 | 1.24 |

| CCH (acetylide) | | | |
|---|---|---|---|
| Mode | $C_2H$ | $C_2D$ | $\nu(C_2H)/\nu(C_2D)$ |
| CH bend | 750 | 550 | 1.36 |
| CC stretch | obscurred | 1260 | - |
| CH stretch[*] | ~2935 | ~2210 | 1.33 |
| RuC stretch | 435 | 420 | 1.04 |

[†]These two modes overlap in the deuterated spectra, and the frequencies given are best estimates based on several different spectra.

[*]The CH and CD stretching modes of the acetylide and ethylidyne species are not well resolved.

[**]These modes are observed mainly in off-specular spectra; they are very weak or absent in specular EEL spectra.

**Table 4.** Vibrational frequencies ($cm^{-1}$) of the carbon-hydrogen bending and stretching modes of methylidyne in two organometallic compounds and on several metal surfaces.

| | $Co_3(\mu_3\text{–}CH)(CO)_9$ **(34)** | Fe(111) **(14)** | Ni(111) **(30)** | Pd(111) **(31)** | Pt(111) **(32)** | Rh(111) **(33)** | Ru(001) (this work) |
|---|---|---|---|---|---|---|---|
| CH bend | 850 | 795 | 790 | 762 | 850 | 770 | 800 |
| CH stretch | 3041 | 3015 | 2980 | 3002 | 3100 | 3025 | 3010 |

**Figure Captions**

Figure 1. The $H_2$ thermal desorption spectra resulting after the Ru(001) surface at 80 K is exposed to 0.2, 0.8 and 10 L of $C_2H_2$. The heating rate used in recording these spectra is approximately 20 $K\text{-}s^{-1}$.

Figure 2. The EEL spectra that result from 10 L exposures of (a) $C_2H_2$ and (b) $C_2D_2$ to the Ru(001) surface at 80 K. These spectra are characteristic of condensed acetylene multilayers.

Figure 3. The EEL spectra that result when the Ru(001) surface at 80 K is exposed to 5 L of (a) $C_2H_2$ and (b) $C_2D_2$ and heated to 150 K. The spectra were recorded at 80 K. These spectra are characteristic of chemisorbed acetylene.

Figure 4. (a) The metal-acetylene structure of the organometallic compound $Co_2(CO)_6(C_2H_2)$ (**24**), and an analogous bonding configuration for acetylene on the Ru(001) surface. (b) The metal-acetylene structure of the organometallic compound $Co_4(CO)_{10}(C_2H_2)$ (**26a**), and an analogous bonding configuration for acetylene on the Ru(001) surface.

Figure 5. The EEL spectra that result when the Ru(001) surface at 80 K is exposed to 5 L of (a) $C_2H_2$ and (b) $C_2D_2$ and heated to 300 K. These spectra were recorded at 80 K and show the characteristic features of acetylide and ethylidyne.

Figure 6. The EEL spectra that result after the Ru(001) surface at 80 K is exposed to 5 L of (a) $C_2H_2$ and (b) $C_2D_2$, annealed to 400 K, and recooled to 80 K. These spectra are characteristic of a methylidyne species.

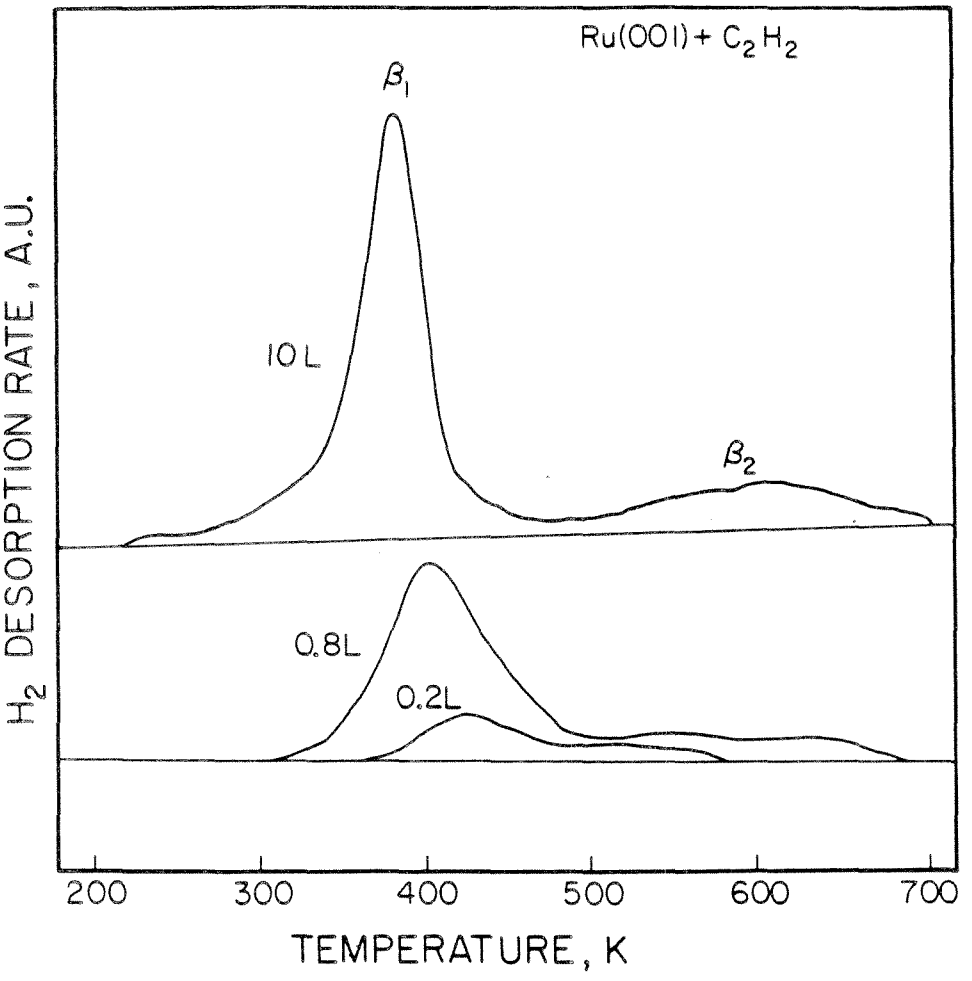
Ru(001) + $C_2H_2$
$\beta_1$
$\beta_2$
10 L
0.8L
0.2L
$H_2$ DESORPTION RATE, A.U.
200
300
400
500
600
700
TEMPERATURE, K

Figure 1

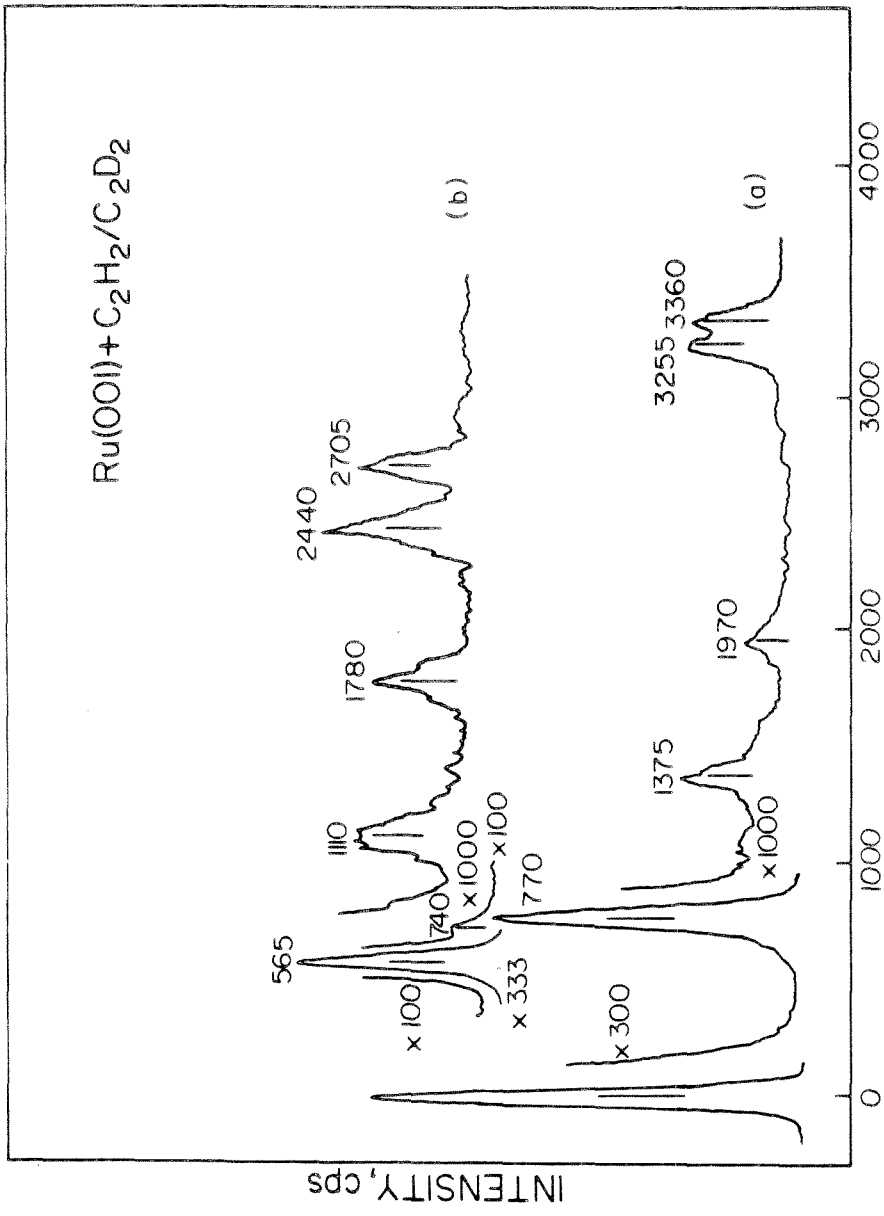
Ru(001)+C2H2/C2D2
INTENSITY, cps
ENERGY LOSS, cm-1
0
1000
2000
3000
4000
565
740
770
1110
1780
2440
2705
1375
1970
3255
3360
(a)
(b)
x100
x333
x300
x1000
x100
x1000

Figure 2

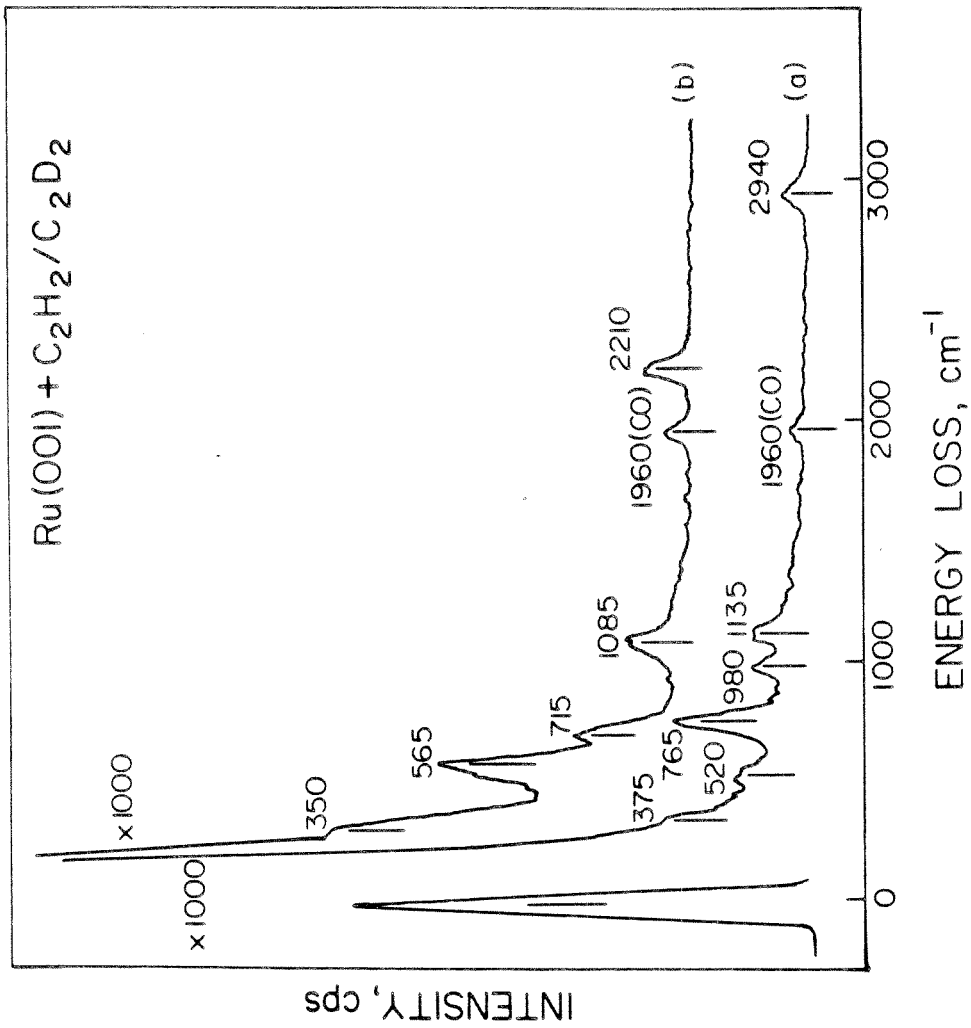
Ru(001) + C2H2/C2D2
INTENSITY, cps
ENERGY LOSS, cm-1
0
1000
2000
3000
x1000
x1000
350
565
715
1085
1960(CO)
2210
(b)
375
765
520
980
1135
1960(CO)
2940
(a)

Figure 3

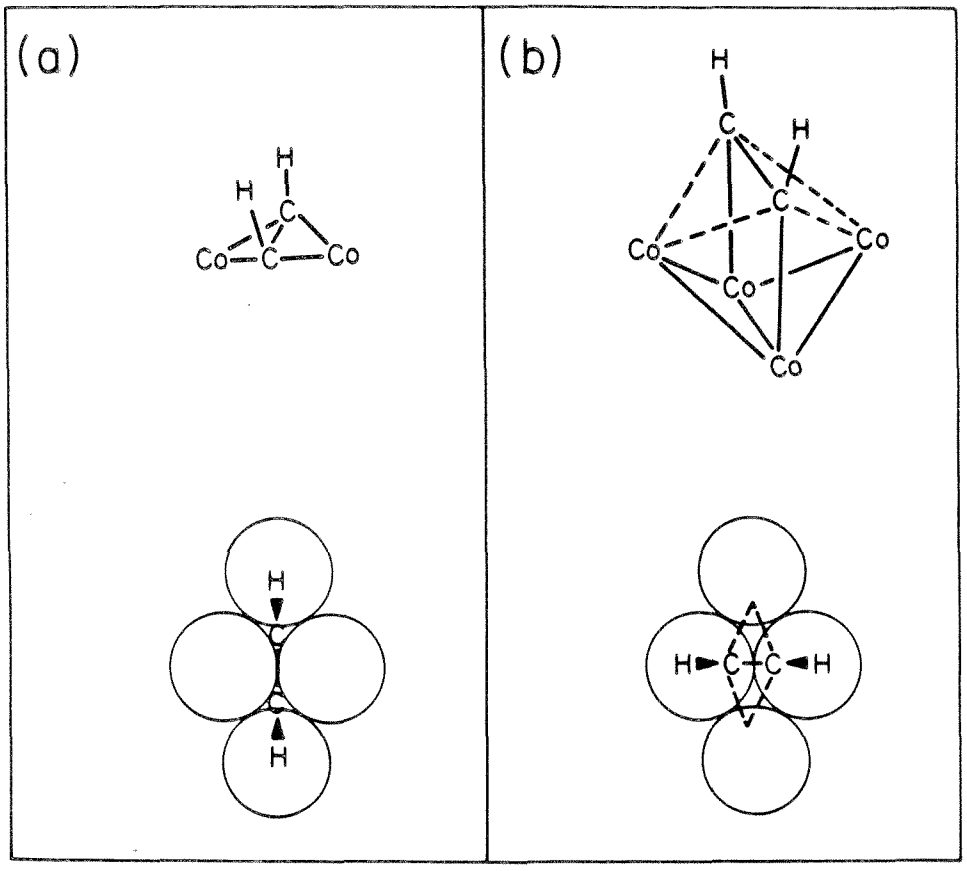


Figure 4

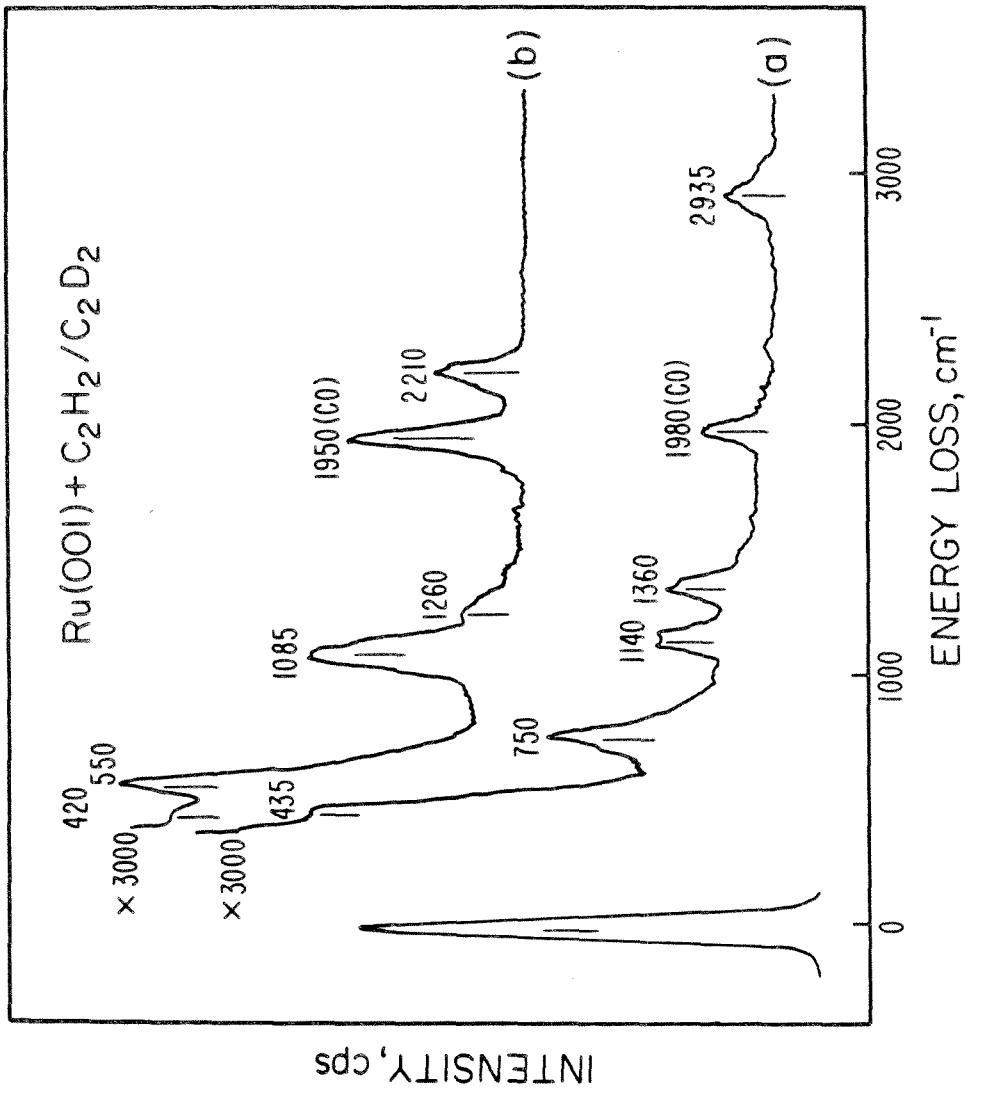
Ru(001) + C2H2 / C2D2
INTENSITY, cps
ENERGY LOSS, cm-1
0
1000
2000
3000
420
550
× 3000
× 3000
435
1085
750
1140
1360
1260
1950(CO)
2210
1980(CO)
2935
(b)
(a)

Figure 5

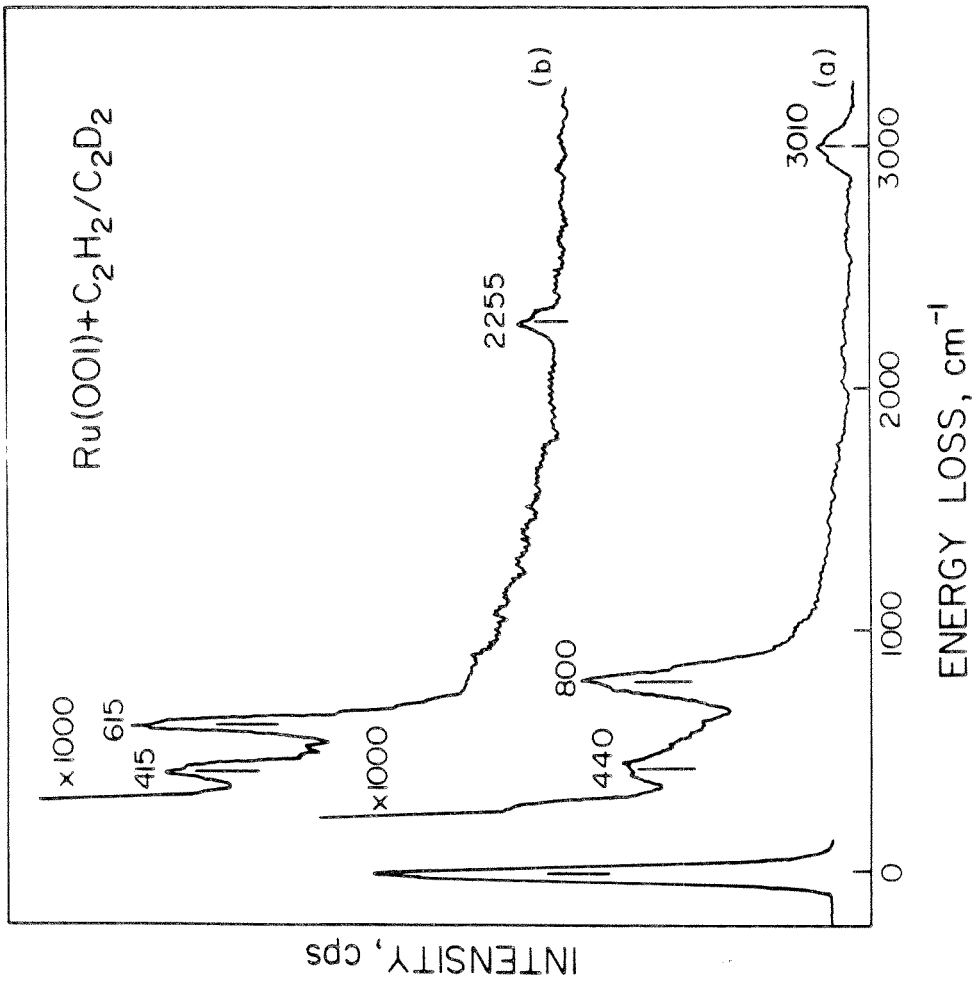
Ru(001)+C2H2/C2D2
INTENSITY, cps
ENERGY LOSS, cm-1
0
1000
2000
3000
3010
(a)
2255
(b)
800
440
615
415
×1000
×1000

Figure 6

## Appendix 2

## The Coadsorption of Hydrogen and Acetylene on the Ru(001) Surface



[This chapter has been accepted for publication as an article by J. E. Parmeter, M. M. Hills and W. H. Weinberg in *The Journal of the American Chemical Society*.]

**Abstract**

The adsorption of acetylene on Ru(001) surfaces with various coverages of preadsorbed hydrogen has been investigated using high resolution electron energy loss spectroscopy and thermal desorption mass spectrometry. The presence of a saturation coverage of dissociatively adsorbed hydrogen ($\theta_H \cong 0.85$) inhibits the subsequent adsorption of acetylene, reducing the fractional saturation coverage of chemisorbed acetylene at 80 K from approximately 0.25 to 0.11. Partial hydrogenation of the chemisorbed acetylene occurs as the surface is heated above 150 K, resulting in the formation of an $\eta^2$–$CHCH_2$ species. Further hydrogenation of $\eta^2$–$CHCH_2$ to ethylene occurs also, with 0.01 monolayer of ethylene desorbing at 175 K. The remainder of the chemisorbed acetylene is not hydrogenated to ethylene but undergoes carbon-hydrogen bond cleavage and formation to yield acetylide (CCH) and ethylidyne ($CCH_3$) above 230 K, as on clean Ru(001). The ratio of ethylidyne to acetylide is greater, however, on the hydrogen-presaturated surface.

## I. Introduction

The adsorption of acetylene has been studied on a number of single crystalline transition metal surfaces under ultrahigh vacuum (UHV) conditions (**1-15**), both to gain insight into the interaction of alkynes with such surfaces, and to isolate stable surface intermediates in order to make a connection with the bonding of similar ligands in organometallic complexes. In nearly all cases, acetylene adsorbs molecularly at low temperatures ($T \lesssim 250$ K), but with substantial rehybridization of the carbon-carbon triple bond occurring. We have recently reported the results of a study of acetylene adsorption and reaction on the hexagonally close-packed Ru(001) surface, using high resolution electron energy loss spectroscopy (EELS) and thermal desorption mass spectrometry (TDMS) (**16**). It was found that acetylene chemisorbs molecularly on this surface below 230 K with rehybridization of the carbon atoms to nearly $sp^3$, as judged by a carbon-carbon stretching frequency of 1135 $cm^{-1}$ (**17**). The chemisorbed acetylene undergoes both carbon-hydrogen bond cleavage and bond formation when the surface is heated above 230 K, yielding two stable intermediates on the surface, namely, acetylide (CCH) and ethylidyne ($CCH_3$). The acetylide and ethylidyne decompose below 400 K, leaving methylidyne (CH) and surface carbon, with desorption of $H_2$ centered at 375 K. The methylidyne decomposes below 800 K with further $H_2$ desorption between 480 and 800 K, leaving only carbon on the surface. The desorption of neither molecular acetylene nor any other hydrocarbons occurs.

An issue of fundamental importance in understanding alkyne hydrogenation reactions on transition metal surfaces is the interaction of chemisorbed acetylene with coadsorbed hydrogen. The reactions of coadsorbed hydrogen and acetylene have been studied previously on the hexagonally close-packed Pt(111) (**9**), Pd(111) (**6,7**), Rh(111) (**10**), and Ni(111) (**4**) surfaces and also on the stepped Ni[5(111)x($\bar{1}$10)] surface (**4**). Since the reactions of ethylene (**18,19**), hydrogen (**20-22**), and coadsorbed ethylene and hydrogen (**23**) on Ru(001) have all been studied previously with EELS and TDMS, this is an obviously desirable surface on which to conduct hydrogen and acetylene coadsorption experiments. We report here the results of such an investigation, also employing both EELS and TDMS, of acetylene coadsorption and reaction with preadsorbed hydrogen on Ru(001). These results provide unambiguous evidence for the hydrogenation of acetylene to ethylene under UHV conditions, and they

yield additional information that permits important comparisons to acetylene and ethylene decomposition on clean Ru(001).

## II. Experimental Procedures

The EEL spectrometer and the UHV chamber which houses it have been described in detail elsewhere (24). The resolution of the spectrometer varied between 60 and 80 $cm^{-1}$ (full-width at half-maximum), while maintaining a count rate of 2 x $10^5$ counts per second in the elastically scattered beam with an incident electron beam energy of approximately 4 eV. All EEL spectra presented and discussed here were measured in the specular direction, which was 60° from the surface normal. The angle of acceptance of the electron energy analyzer was approximately 2°.

Thermal desorption mass spectrometric measurements were performed both in the EELS chamber and in a separate UHV chamber that has been described elsewhere (25). This UHV chamber was equipped with a skimmer on the mass spectrometer in order to minimize the effects of desorption from the crystal edge (the area of which is approximately 8% of the oriented surface area) and the support leads. While most TDM spectra collected in the EEL chamber (including those in Figs. 1 and 3) employed a temperature base, the TDM spectra in this second chamber were time base spectra with a computer algorithm for baseline subtraction, and this provided more accurate coverage determinations. All coverages reported in this paper are based on this more accurate method. The desorption peak temperatures reported here are accurate to within approximately ±5 K, and the heating rate was approximately 8 $K\text{-}s^{-1}$ in all cases.

The Ru(001) crystals in both UHV chambers were cleaned using standard techniques of $Ar^+$ sputtering and annealing in oxygen (26). Surface cleanliness was monitored via EELS and TDMS in the EELS chamber, and via Auger electron spectroscopy and TDMS in the second UHV chamber.

The $H_2$ and $D_2$ used in this study were obtained from Matheson with reported purities of 99.9995 and 99.5%, respectively. These gases were used without further purification, and their mass spectra gave no indication of any impurities. Previous studies of $H_2$ adsorption on Ru(001) (20-22) have shown that the adsorption is dissociative at all temperatures examined ($T \gtrsim 75$ K), with the hydrogen adatoms

giving rise to very weak EELS loss features near 800 and 1150 $cm^{-1}$. In addition to the appearance of these loss features, hydrogen adsorption on clean Ru(001) resulted in an increase in the intensity of the elastically scattered peak (surface reflectivity) by about a factor of two, an effect that has been noted previously (27).

The $C_2D_2$ (99 atom % deuterated) was obtained from MSD Isotopes and used without further purification. The $C_2H_2$ was obtained from an industrial acetylene tank (95% purity) and was purified as described elsewhere (16). Both the $C_2H_2$ and $C_2D_2$ showed mass spectral cracking patterns that were virtually identical to those reported in the literature (28), and no impurities could be detected in either case. Thermal desorption measurements were performed with $C_2D_4$ in order to make a comparison with the observed desorption of ethylene following acetylene and hydrogen coadsorption on Ru(001). The $C_2D_4$ (99 atom % deuterated) was also obtained from MSD Isotopes, and its purity was verified via mass spectrometry.

Gas exposures were effected by backfilling the UHV chambers through leak valves. The stainless steel vacuum lines leading to the leak valves were flushed several times with the relevant gas prior to the introduction of the gas into the UHV chamber. All reported exposures were measured with a Bayard-Alpert ionization gauge, uncorrected for relative ionization probabilities. Exposures are reported in units of Langmuirs, where 1 Langmuir ≡ 1 L = $10^{-6}$ Torr-s.

## III. Results

### A. Thermal Desorption Mass Spectrometry

Thermal desorption mass spectra were measured for acetylene adsorbed at 80 K on the Ru(001) surface with varying coverages of preadsorbed hydrogen. Similar to acetylene adsorption on the clean Ru(001) surface (16), where hydrogen is the only thermal desorption product from chemisorbed acetylene, hydrogen is the principal thermal desorption product resulting from chemisorbed acetylene on the hydrogen precovered surface. There is no desorption, for example, of methane, ethane, benzene or acetylene (other than the desorption of condensed acetylene multilayers at 95 K). However, in contrast to acetylene adsorption on clean Ru(001), small amounts ($\lesssim$0.01 monolayer) of ethylene are observed to

desorb following acetylene adsorption on the Ru(001) surface with a sufficient concentration of preadsorbed hydrogen. This indicates clearly that chemisorbed acetylene and hydrogen adatoms can react on Ru(001) under these conditions.

*1. Hydrogen Thermal Desorption*

Figure 1 shows $H_2$ thermal desorption spectra for saturation exposures of both $H_2$(a) and $C_2H_2$(b) on Ru(001) and for a saturation exposure of $C_2H_2$ on a Ru(001) surface which had been presaturated with hydrogen (c). A saturation hydrogen exposure on Ru(001) gives rise to a broad thermal desorption peak centered at 325 K with a shoulder near 380 K, as shown in Fig. 1(a), and corresponds to a hydrogen adatom fractional surface coverage of 0.85 (**20**), i.e. 1.39 x $10^{15}$ atoms-cm$^{-2}$. The hydrogen adatoms occupy exclusively threefold hollow sites, and the peak splitting is due to adatom-adatom interactions (**22**). As may be seen in Fig. 1(b), a saturation exposure of acetylene on Ru(001) gives rise to a sharp hydrogen desorption peak centered near 375 K, with a less intense and very broad feature between approximately 480 and 800 K that displays three weak maxima. The saturation fractional coverage of acetylene adsorbed on clean Ru(001) is 0.25 ± 0.03, as judged by the $H_2$ thermal desorption spectra. (Recall that only $H_2$ is observed to desorb from the Ru(001) surface on which acetylene is adsorbed.)

Comparison of spectra (b) and (c) of Fig. 1 shows that the principal $H_2$ desorption peak is somewhat sharpened and downshifted by approximately 35 K, from 375 to 340 K, when the Ru(001) surface is presaturated with hydrogen. This peak corresponds to ethylidyne decomposition, which on the hydrogen precovered surface occurs at a slightly lower temperature than on the clean surface (see Sect. III.B). On the clean surface, the peak at 375 K also involves a small contribution from hydrogen adatoms that are formed when acetylene decomposes to acetylide, and that do not react further to form ethylidyne. On the hydrogen precovered surface, the peak at 340 K also involves substantial amounts of preadsorbed hydrogen adatoms. Clearly visible on both sides of the 340 K peak in Fig. 1(c) are shoulders that are characteristic of hydrogen desorption from the clean surface, and that result from the recombinative desorption of hydrogen adatoms that are not influenced significantly by the presence of coadsorbed hydrocarbon species. The leading edge of Fig. 1(c) is downshifted slightly relative to that of

Fig. 1(a) due to the increased hydrogen adatom *density* in the former case.

Between 480 and 800 K, the $H_2$ thermal desorption spectra for both acetylene and acetylene with preadsorbed hydrogen show very broad peaks of low intensity. Since the desorption of hydrogen from the clean Ru(001) surface is complete below 500 K, these features clearly result from reaction-limited hydrogen desorption due to the decomposition of a surface hydrocarbon species. Our previous EELS results for acetylene decomposition on Ru(001) have shown that methylidyne is the only hydrocarbon species present on the surface above 400 K (**16**). Consequently, hydrogen desorption above 480 K is necessarily due to methylidyne decomposition for acetylene adsorption on Ru(001). The fact that three desorption maxima are observed above 480 K for saturation acetylene coverages (only one maximum is observed for low coverages), and the broad temperature range for methylidyne decomposition results from variations in the local coverage of carbon and methylidyne. Similarly, EEL spectra for coadsorbed hydrogen and acetylene on Ru(001) demonstrate that methylidyne is the only hydrocarbon species on the surface above 400 K. Therefore, in this case also, hydrogen desorption above 480 K is due to methylidyne decomposition. The amounts of hydrogen that desorb between 480 and 800 K indicate that approximately 0.13 monolayer of methylidyne is formed for a saturation exposure of acetylene on clean Ru(001), while only about 0.04 monolayer of methylidyne is formed following a saturation exposure of acetylene on the hydrogen presaturated Ru(001) surface. The hydrogen thermal desorption peaks from the decomposition of methylidyne occur at somewhat lower temperatures for acetylene coadsorbed with hydrogen, similar to the case of lower acetylene coverages on the clean surface (**16**). The higher desorption temperatures on the initially clean surface are probably due to a stabilization of methylidyne by the higher concentration of coadsorbed carbon adatoms, which block surface sites that are necessary for carbon-hydrogen bond cleavage and also hinder hydrogen-hydrogen recombination. The lower concentration of carbon adatoms in the case of coadsorbed acetylene and hydrogen is a consequence of the fact that preadsorbed hydrogen partially inhibits the adsorption of acetylene on Ru(001).

By comparison to the amount of hydrogen that desorbs following a saturation exposure of $H_2$ on Ru(001), the amount of acetylene that adsorbs and decomposes to yield (eventually) $H_2(g)$ and surface

carbon on the hydrogen presaturated Ru(001) surface is estimated to be approximately 0.10 monolayer. To obtain this estimate, time-integrated TDM spectra corresponding to Fig. 1(a) are subtracted from similarly time-integrated TDM spectra corresponding to Fig. 1(c), with no peak deconvolution required. Since the only other desorption product resulting from acetylene adsorption on hydrogen presaturated Ru(001) is 0.01 monolayer of ethylene (see Sect. III.A.2), this indicates that approximately 0.11 monolayer of acetylene is chemisorbed on this surface. Thus, the presence of 0.85 monolayer of hydrogen adatoms on the Ru(001) surface inhibits acetylene chemisorption substantially, reducing the saturation acetylene coverage by approximately 60%.

Figure 2 shows $H_2$, HD and $D_2$ thermal desorption spectra from a Ru(001) surface, which has been exposed to 1 L of $H_2$ followed by a subsaturation exposure of 1 L of $C_2D_2$ at 80 K. A 1 L hydrogen exposure corresponds to 0.57 ± 0.05 monolayer of hydrogen adatoms, and the amount of $C_2D_2$ that adsorbs is approximately 0.11 monolayer. The equivalent coverages of the various hydrogen isotopes that desorb are approximately 0.22 monolayer of $H_2$, 0.12 monolayer of HD and 0.05 monolayer of $D_2$. Thus, the isotopic mixing of hydrogen and deuterium is not complete; a purely statistical distribution would be 0.21 monolayer of $H_2$, 0.16 monolayer of HD and 0.03 monolayer of $D_2$. Several aspects of these thermal desorption spectra are noteworthy. The first is that no $D_2$ and only a trivial amount of HD desorb below 230 K, the temperature at which acetylene decomposition begins on both the clean and the hydrogen precovered Ru(001) surfaces. This indicates that virtually no H/D exchange occurs between the coadsorbed hydrogen adatoms and chemisorbed acetylene. Thus, the reaction

$$DCCD(a) + H(a) \rightarrow HCCD(a) + D(a)$$

is not facile on this surface. Second, small amounts of both $H_2$ and HD are desorbed between 480 and 600 K, indicating the decomposition of a CH methylidyne species. Thus, a small amount (~0.01-0.02 monolayer) of the preadsorbed hydrogen adatoms have reacted with a hydrocarbon species below 480 K to become incorporated into the hydrocarbon adlayer and form eventually CH. It is also worth noting that methylidyne decomposition is complete below 700 K, consistent with the initial acetylene coverage of 0.11 monolayer.

2. *Ethylene Thermal Desorption*

Ethylene desorption following the coadsorption of hydrogen and acetylene on Ru(001) at 80 K was studied using four combinations of hydrogen and acetylene isotopes, namely, $H_2 + C_2H_2$, $H_2 + C_2D_2$, $D_2 + C_2H_2$, and $D_2 + C_2D_2$. Of these various combinations, $H_2 + C_2D_2$ and $D_2 + C_2H_2$ are the most useful since the presence of different hydrogen isotopes, in principle, allows different isotopes of ethylene to be desorbed. Consequently, the isotopes of ethylene that are observed to desorb provide mechanistic insight into the surface reaction (provided that desorption occurs at a temperature below which H/D exchange between adsorbed hydrogen and the adsorbed hydrocarbons is not important). The coadsorption of $H_2$ and $C_2H_2$ is the least useful for monitoring ethylene desorption, since any desorbed ethylene occurs at 28 amu ($C_2H_4$), and the presence of carbon monoxide (also at 28 amu) in the chamber background leads to a large, sloping background in the mass 28 thermal desorption spectra. This makes the detection of small amounts of $C_2H_4$ difficult.

Thermal desorption spectra of ethylene-$d_2$ ($C_2H_2D_2$) following the coadsorption of $H_2$ and $C_2D_2$ on Ru(001) at 80 K are shown in Fig. 3(a)-(e). The surface was exposed to various fluxes of hydrogen, as indicated, and then saturated with $C_2D_2$. The initial hydrogen coverages were calculated by comparing the amount of hydrogen desorbed following a given exposure on the clean Ru(001) surface to the amount desorbed following a saturation exposure on Ru(001). The $C_2D_4$ thermal desorption spectrum resulting from a saturation exposure of perdeuteroethylene on Ru(001) is shown in Fig. 3(f). Ethylene-$d_2$ is desorbed following $H_2$ and $C_2D_2$ coadsorption only for $\theta_H \geq 0.6$. The peak desorption temperature of 175 ± 5 K is in excellent agreement with thermal desorption data for ethylene adsorbed on Ru(001) [cf. Fig. 3(f) and Ref. 19], and the observations that the desorption peak temperature does not shift with increasing hydrogen adatom coverage and occurs at nearly the same temperature as ethylene desorption following ethylene adsorption on Ru(001) (**19**) suggest that this is a desorption-limited reaction with first-order desorption kinetics. Assuming a constant preexponential factor of the desorption rate coefficient of $10^{13}$ $s^{-1}$, an activation energy of desorption of approximately 10-11 kcal/mol is estimated (**29**).

Comparison to the thermal desorption spectrum for a saturation exposure of chemisorbed $C_2D_4$ on Ru(001), where approximately 0.06 monolayer of ethylene desorbs molecularly at 180 K, allows the

coverages of ethylene-$d_2$ that are desorbed to be estimated for various hydrogen precoverages (to within approximately a factor of two). For fractional hydrogen precoverages of 0.6, 0.75 and 0.85, approximately 0.002, 0.005 and 0.01 monolayer of $C_2H_2D_2$ are desorbed, respectively. Since approximately 0.10 monolayer of acetylene adsorbs and decomposes on Ru(001), which is presaturated with hydrogen, this indicates that approximately 9% of the chemisorbed acetylene is hydrogenated on this surface *and* desorbs as ethylene.

Ethylene-$d_2$ (at 30 amu) is the only isotope of ethylene that desorbs from Ru(001), following the coadsorption of $H_2$ and $C_2D_2$. No detectable desorption (i.e. <0.001 monolayer) is observed at 31 amu ($C_2HD_3$) or at 32 amu ($C_2D_4$), and only a very weak feature is observed at 29 amu, which is due to the $C_2HD_2$ cracking fragment of ethylene-$d_2$, rather than ethylene-$d_1$ ($C_2H_3D$). Thermal desorption spectra of coadsorbed $D_2$ and $C_2H_2$ on Ru(001) yield similar results: only ethylene-$d_2$ is observed as a desorption product. Thus, it is clear that the ethylene desorption at 175 K results from the reaction of chemisorbed molecular acetylene with two preadsorbed hydrogen adatoms, and that the sequential addition of the two hydrogen atoms is irreversible.

### B. Electron Energy Loss Spectroscopy

As noted in Sect. I, hydrogen adsorption on Ru(001) has been investigated previously with EELS (**21-22**). The observed loss features near 800 and 1150 $cm^{-1}$, due to the presence of hydrogen adatoms in threefold hollow sites, are extremely weak and are obscured by various hydrocarbon modes when either coadsorbed ethylene or acetylene is present (**16,19**). The molecular chemisorption of acetylene on clean Ru(001) below 230 K produces a very nearly $sp^3$ hybridized species, which is characterized by the following loss features in the case of $C_2H_2$ ($C_2D_2$): ruthenium-carbon stretching modes at 375 (350) and 520 $cm^{-1}$ (not resolved for $C_2D_2$); CH (CD) bending modes at 765 (565) and 980 (715) $cm^{-1}$; a carbon-carbon stretching mode at 1135 (1085) $cm^{-1}$; and a CH (CD) stretching mode at 2940 (2210) $cm^{-1}$ (**16**). The spectra in Fig. 4 also show loss features due to small amounts (<0.01 monolayer) of CO adsorbed from the chamber background. It has been found previously that these small and varying amounts of CO do not affect the EEL spectra of chemisorbed acetylene or its decomposition products (**16**). The EEL spectra for saturation exposures of $C_2H_2$ and $C_2D_2$ on Ru(001), corresponding to

approximately 0.25 monolayer of chemisorbed acetylene, are shown in Fig. 4(a) and (b).

Also shown in Fig. 4 are EEL spectra of $C_2H_2$ adsorbed on a hydrogen presaturated Ru(001) surface (c), and of $C_2D_2$ adsorbed on a deuterium presaturated Ru(001) surface (d). The major difference between these spectra and those of Fig. 4(a) and (b) is the appearance of a new vibrational mode, which occurs at 1440 $cm^{-1}$ for coadsorbed $H_2$ and $C_2H_2$ and at 1175 $cm^{-1}$ for coadsorbed $D_2$ and $C_2D_2$. The frequency of this mode is in the range characteristic of a $CH_2$ ($CD_2$) scissoring vibration, and the observed frequency shift upon deuterium substitution [$\delta(CH_2)/\delta(CD_2) = 1.23$] confirms this assignment. This indicates that a new surface species has been formed containing a $CH_2$ group, which is in agreement with our TDMS results, showing ethylene desorption at 175 K. However, the EEL spectra of Fig. 4(c) and (d) are not due to chemisorbed ethylene (or a combination of chemisorbed ethylene and acetylene), as judged by a comparison with previous studies of ethylene adsorption on Ru(001) (**18,19**). The $CH_2$ scissoring mode is thus assigned to an $\eta^2$–$CHCH_2$ species, the logical intermediate in the hydrogenation of acetylene to ethylene. (The $\eta^2$ designation indicates that both carbon atoms of the $CHCH_2$ species are bonded directly to the surface but does *not* imply nearly equal metal-carbon bond lengths or anything else regarding the structure of $CHCH_2$.) An $\nu^1$–$CHCH_2$ species containing a carbon-carbon double bond (vinyl) is ruled out due to the lack of a carbon-carbon stretching mode above 1500 $cm^{-1}$. Other $CH_2$-containing species such as $\eta^2$–$CCH_2$ or $CH_2$ (methylene), which require the breaking of carbon-hydrogen or carbon-carbon bonds of acetylene in order to be formed, are excluded in view of the observed lack of H/D exchange below 230 K, the fact that CH bonds of chemisorbed acetylene are not broken below 230 K on clean Ru(001), and the observed lack of carbon-carbon bond cleavage below 340 K.

Since the modes characteristic of chemisorbed acetylene are still present in Fig. 4(c) and (d), the surface contains a mixture of chemisorbed acetylene and $\eta^2$–$CHCH_2$ after annealing to 150 K. This observation is in agreement with previous results for hydrogen and acetylene coadsorption on the stepped Ni[5(111)x($\bar{1}$10)] surface, where the appearance of a $\delta(CH_2)$ mode at 150 K was taken as evidence for the formation of a mixed overlayer of $CHCH_2$ and chemisorbed acetylene (**4**). The $\eta^2$–$CHCH_2$ should also give rise to $CH_2$ wagging, twisting and rocking modes, which would be

expected, respectively, near 1150, 900 and 775 $cm^{-1}$, based on a comparison to chemisorbed ethylene on Ru(001) (**19**). These modes are not resolved due to overlap with various modes of chemisorbed acetylene (or, in some cases, perhaps because they are intrinsically weak). However, spectra (c) and (d) of Fig. 4 do exhibit slight changes in the frequencies and relative intensities of some modes compared to spectra (a) and (b), and these differences are no doubt due at least partially to the presence of additional modes of $\eta^2$–$CHCH_2$ that are not well resolved. This may also very well be the reason for the relatively poorer resolution in the 750-1150 $cm^{-1}$ region of spectrum (c), compared to spectrum (a).

Further hydrogention of $\eta^2$–$CHCH_2$ and desorption of ethylene occurs between 150 and 250 K, as indicated by the thermal desorption results of Fig. 3. EEL spectra show that a small amount of $\eta^2$–$CHCH_2$ is present on the surface at 200 K, but that it is completely gone by 250 K. Molecularly chemisorbed acetylene decomposes near 230 K, as on the clean surface, and the surface species present from 250 to 340 K are acetylide (which is stable to nearly 400 K) and ethylidyne, as in the case of acetylene adsorbed on clean Ru(001) (**16**). The acetylide is characterized primarily by a strong CH bending mode at 750 $cm^{-1}$, while ethylidyne is characterized by modes of nearly equal intensity at 1140 [$\nu$(CC)] and 1360 [$\delta_s(CH_3)$] $cm^{-1}$. The decomposition of acetylene on the hydrogen presaturated Ru(001) surface differs, however, from the decomposition of acetylene on clean Ru(001) in that the ratio of ethylidyne to acetylide is increased on the hydrogen presaturated surface. On the clean surface, there is slightly more acetylide than ethylidyne (as judged from both EELS and TDMS), while on the hydrogen precovered surface, the ratio of ethylidyne to acetylide is approximately 3:2, as estimated from EEL spectra, which are virtually identical to those resulting from ethylene decomposition for saturation ethylene coverages on clean Ru(001) (**19**). In addition, the ethylidyne decomposes at a slightly lower temperature on the hydrogen precovered surface, where EELS features due to this species have disappeared by 350 K. On the other hand, some ethylidyne is stable to at least 360 K when acetylene decomposes on the clean Ru(001) surface.

When $C_2H_2$ ($C_2D_2$) is adsorbed on Ru(001) and the surface is annealed between 400 and 700 K, a methylidyne species is formed that is characterized by the following vibrational modes: a ruthenium-carbon stretch at 440 (415) $cm^{-1}$, a CH (CD) bend at 800 (615) $cm^{-1}$, and a CH (CD) stretch at 3010

(2255) $cm^{-1}$. When $C_2H_2$ is adsorbed on a hydrogen presaturated Ru(001) surface and the surface is annealed to these same temperatures, the same CH species is formed in smaller concentrations, as discussed in Sect. III.A.1. The coadsorption of $H_2$ and $C_2D_2$ or $D_2$ and $C_2H_2$, followed by annealing to over 400 K, leads to the production of both hydrogenated (CH) and deuterated (CD) methylidyne on Ru(001), although CD predominates in the former case and CH in the latter. This mixing of hydrogen isotopes in the methylidyne is in agreement with our thermal desorption results, and provides unequivocal evidence for the incorporation of preadsorbed hydrogen into the hydrocarbon adlayer. The mechanisms of the incorporation of preadsorbed hydrogen into various hydrocarbon species will be discussed in a subsequent publication (30).

## IV. Discussion

All the TDMS and EELS results reported here are consistent with the partial hydrogenation of acetylene on a hydrogen presaturated Ru(001) surface to produce low concentrations of a $CHCH_2$ species and ethylene. The $CHCH_2$ is a stable intermediate in the synthesis of ethylene, and the ethylene formed desorbs near 175-180 K, as does ethylene that desorbs following ethylene adsorption. Furthermore, the data prove that the formation of both $CHCH_2$ and ethylene results from the reaction of preadsorbed hydrogen with chemisorbed acetylene, not from a disproportionation reaction involving hydrogen adatoms that originate from acetylene decomposition. (This is not surprising since neither $CHCH_2$ nor ethylene is observed via EELS or TDMS in the absence of preadsorbed hydrogen, and because chemisorbed acetylene is stable on the clean surface to 230 K.) Acetylene that is not hydrogenated to ethylene decomposes to acetylide and ethylidyne near 230 K as on the clean Ru(001) surface, although the ratio of ethylidyne to acetylide is increased. The data also indicate that H/D exchange does not occur to an appreciable extent between chemisorbed acetylene and preadsorbed hydrogen on this surface, but that such exchange does occur for at least one of the decomposition products of acetylene. The formation of detectable amounts of ethylene that desorb below 200 K after hydrogen and acetylene coadsorption on Ru(001) under UHV conditions is significant in view of the lack of precedent for this reaction on other metal surfaces.

Coadsorbed hydrogen and acetylene react near room temperature to form ethylidyne on the Pt(111) (**9**), Pd(111) (**6,7**) and Rh(111) (**10**) surfaces. Ethylidyne is also produced, along with acetylide, as a decomposition product of acetylene on both Pd(111) (**7**) and Ru(001) (**16**). The reactions of coadsorbed acetylene and hydrogen below 200-250 K, however, have received somewhat less attention. On Ni(111), coadsorbed hydrogen and acetylene do not react below 250 K (**4**). Experiments performed on Pt(111) are somewhat inconclusive. A recent TDMS study has reported ethylene desorption at 250 K following $H_2$ and $C_2H_2$ coadsorption on this surface (**31**), whereas a previous EELS study reported that coadsorbed hydrogen and acetylene do not react on Pt(111) below 280 K, at which temperature ethylidyne is formed (**9**).

Hydrogenation of acetylene to $CHCH_2$ has been observed with EELS, however, for coadsorbed hydrogen and acetylene at 150 K on the stepped Ni[5(111)x($\bar{1}$10)] surface (**4**). Adsorption of acetylene on this hydrogen presaturated surface produces a mixture of chemisorbed molecular acetylene and a $CHCH_2$ species similar to the case of Ru(001), as discussed in Sect. III.B. The ruthenium and nickel surfaces differ markedly, however, in the extent of H/D exchange observed between the adsorbed hydrocarbon species and the preadsorbed hydrogen at low surface temperatures. While little exchange occurs on Ru(001) below 230 K, exchange is facile on Ni[5(111)x($\bar{1}$10)] at 150 K. This difference may be correlated with the ability of the two surfaces to dehydrogenate acetylene. On the clean nickel surface, acetylene has been found to dehydrogenate partially even at 150 K (**4**), while chemisorbed acetylene is stable to 230 K on Ru(001). Unfortunately, no thermal desorption data are available for the nickel surface, so it is not known whether any ethylene is formed and desorbed from this surface. Given the dehydrogenation ability of this nickel surface, however, ethylene desorption would seem to be unlikely.

Although it is apparent that the ethylene formed from acetylene hydrogenation on Ru(001) is produced via a $CHCH_2$ intermediate, the bonding and hybridization of this intermediate are less obvious. Since only the $\delta(CH_2)$ mode of the $CHCH_2$ is distinguished clearly from the modes of coadsorbed molecular acetylene in the EEL spectra, conclusions concerning the hybridization of the carbon atoms in $CHCH_2$ are not easily drawn. The $CHCH_2$ species formed on Ni[5(111)x($\bar{1}$10)] was assigned, on the

basis of a $CH_2$ stretching mode at 3050 $cm^{-1}$, as being $sp^2$ hybridized, although no $\nu$(C=C) mode was identified (**4**). A $CHCH_2$ ligand has been identified in the organometallic complex $Os_3(CHCH_2)(H)(CO)_{10}$, which is $\sigma$-bonded to one osmium atom with a $\pi$-bond to a second osmium atom (**32**). The carbon atoms of the $CHCH_2$ ligand are intermediate between $sp^3$ and $sp^2$ hybridization with strongly coupled $\nu$(CC) and $\delta(CH_2)$ modes at 1310 and 1476 $cm^{-1}$. Although these precedents might suggest a $CHCH_2$ species with at least some double bond character, we believe that the $CHCH_2$ species formed on Ru(001) is more nearly $sp^3$ hybridized. The lack of any carbon-hydrogen stretching mode above 3000 $cm^{-1}$ or any carbon-carbon stretching mode above 1200 $cm^{-1}$ is suggestive of $sp^3$ hybridization, although this is not conclusive because these modes could be too weak to be detected. More significantly, both chemisorbed acetylene and ethylene on Ru(001) are essentially $sp^3$ hybridized, and since $CHCH_2$ is an intermediate in the conversion of acetylene to ethylene, it would be expected to have a similar structure. Such an $\eta^2$-$CHCH_2$ species would have both carbon atoms bonded directly to the surface, with the carbon-carbon bond either parallel or (more likely) slightly skewed with respect to the surface plane.

As stated previously, the decomposition products of chemisorbed acetylene are the same on the hydrogen presaturated Ru(001) surface as on the clean surface, namely, ethylidyne and acetylide. As would be expected, the presence of surface hydrogen shifts the ratio of these two decomposition products toward more ethylidyne, the product that contains more hydrogen atoms. This is evident both in EEL spectra measured after annealing to 250-300 K, and in the TDM spectra, which show a smaller amount of methylidyne [which forms primarily (or exclusively) from acetylide, rather than ethylidyne, decomposition (**16,19**)] decomposing on the hydrogen precovered surface. Another difference between the clean and hydrogen presaturated surfaces is the slightly higher decomposition temperature of ethylidyne on the clean surface, which is evident in both EEL and TDM spectra. This is due to the lower concentration of hydrocarbon species on the hydrogen presaturated surface.

## V. Conclusions

The adsorption of acetylene on Ru(001) with preadsorbed hydrogen has been studied using high resolution electron energy loss spectroscopy and thermal desorption mass spectrometry. The principal

conclusions of this work may be summarized as follows:

1. The dissociative adsorption of hydrogen on Ru(001) inhibits the subsequent adsorption of acetylene. The reduction in the saturation coverage of acetylene is approximately 60% if the surface is saturated with hydrogen (from 0.25 monolayer on the initially clean surface to 0.11 monolayer on the hydrogen presaturated surface with $\theta_H = 0.85$).

2. Hydrogen thermal desorption spectra following the adsorption of acetylene on the hydrogen presaturated Ru(001) surface show features that are characteristic of hydrogen and acetylene adsorbed separately, although the major $H_2$ desorption peak resulting from acetylene decomposition is downshifted by 35 K from 375 to 340 K. This is the result of a slightly lower decomposition temperature for ethylidyne (one of the two major decomposition products of acetylene) on the hydrogen presaturated surface.

3. Thermal desorption spectra of $H_2$, HD and $D_2$ from coadsorbed $H_2$ and $C_2D_2$ on Ru(001) indicate that some of the preadsorbed hydrogen is incorporated into surface hydrocarbon species, since both $H_2$ and HD are observed to desorb well above the temperature at which they desorb following adsorption on either the clean Ru(001) surface or the Ru(001) surface with various coverages of carbon adatoms. Electron energy loss spectra show that the stable hydrocarbon species leading to $H_2$ and HD desorption above 480 K is methylidyne. No $D_2$ and only a trivial amount of HD desorb from the surface below 230 K where acetylene decomposition begins, indicating that H/D exchange between chemisorbed acetylene and preadsorbed hydrogen is not facile. Thus, hydrogen is incorporated into surface hydrocarbon species by H/D exchange between preadsorbed hydrogen and one or more of the decomposition products of acetylene.

4. Following saturation acetylene exposures on hydrogen presaturated Ru(001), approximately 0.01 monolayer of ethylene desorbs from the surface at 175 K. Thus, ethylene desorption accounts for approximately 9% of the chemisorbed acetylene under these conditions. Furthermore, the coadsorption of $H_2$ and $C_2D_2$ shows that the desorbed ethylene consists entirely of mass 30, i.e. CHDCHD, implying that ethylene formation results from the reaction of two preadsorbed hydrogen adatoms with molecularly chemisorbed acetylene. Ethylene formation and desorption are

observed only if the initial surface coverage of hydrogen adatoms exceeds approximately 70% of saturation (about 0.6 monolayer). No other hydrocarbons desorb from Ru(001) following hydrogen and acetylene coadsorption at 80 K (except for condensed multilayers of acetylene).

5. Electron energy loss spectra show that at 150 K the hydrocarbon adphase is a mixture of molecularly chemisorbed acetylene and a $CH_2$-containing species that is inferred to be $CHCH_2$ (for $H_2$ and $C_2H_2$ coadsorption). In addition to the ethylene desorption at 175 K, annealing the surface to 230 K causes the decomposition of chemisorbed acetylene. The two decomposition products, ethylidyne and acetylide, are the same as in the case of acetylene decomposition on the initially clean surface, although the ratio of ethylidyne to acetylide is increased.

**Acknowledgment:** This research was supported by the National Science Foundation (Grant No. CHE-8516615).

**References**


1. Bandy, B. J.; Chesters, M. A.; Pemble, M. E.; McDougall, G. S.; Sheppard, N., *Surface Sci.* **1984**, 139, 87.

2. Avery, N. R., *J. Am. Chem. Soc.* **1985**, 107, 6711.

3. Stuve, E. M.; Madix, R. J.; Sexton, B. A., *Surface Sci.* **1982**, 123, 491.

4. Lehwald, S.; Ibach, H., *J. Surface Sci.* **1979**, 89, 425.

5. Ibach, H.; Lehwald, S., *J. Vacuum Sci. Technol.* **1981**, 18, 625.

6. Gates, J. A.; Kesmodel, L. L. *J. Chem. Phys.* **1982**, 76, 4281.

7. Kesmodel, L. L.; Waddill, G. D.; Gates, J. A., *Surface Sci.* **1984**, 138, 464.

8. Kesmodel, L. L., *J. Chem. Phys.* **1983**, 79, 4646.

9. Ibach, H.; Lehwald, S., *J. Vacuum Sci. Technol.* **1978**, 15, 407.

10. Dubois, L. H.; Castner, D. J.; Somorjai, G. A., *J. Chem. Phys.* **1980**, 72, 5234.

11. Erley, W.; Baro, A. M.; Ibach, H., *Surface Sci.* **1982**, 120, 273.

12. Seip, U.; Tsai, M.-C.; Küppers, J.; Ertl, G., *Surface Sci.* **1984**, 147, 65.

13. Backx, C.; Willis, R. F.; Feuerbacher, B.; Fitton, B., *Surface Sci.* **1977**, 68, 516.

14. Backx, C.; Feuerbacher, B.; Fitton, B., Willis, R. F., *Surface Sci.* **1977**, 63, 193.

15. Hamilton, J. C.; Swanson, N.; Waclawski, B. J.; Celotta, R. J., *J. Chem. Phys.* **1981**, 74, 4156.

16. Parmeter, J. E.; Hills, M. M.; Weinberg, W. H., *J. Am. Chem. Soc.* **1986**, 108, 3563.

17. For comparison, the carbon-carbon stretching frequencies of acetylene, ethylene and ethane in the gas phase are 1974, 1623 and 995 $cm^{-1}$, respectively. See, for example, Herzberg, G., *Infrared and Raman Spectra of Polyatomic Molecules*, Van Nostrand, N.Y., 1945.

18. Barteau, M. A.; Broughton, J. Q.; Menzel, D., *Appl. Surface Sci.* **1984**, 19, 92.

19. Hills, M. M.; Parmeter, J. E.; Mullins, C. B.; Weinberg, W. H., *J. Am. Chem. Soc.* **1986**, 108, 3554.

20. Shimizu, H.; Christmann, K.; Ertl, G., *J. Catal.* **1980**, 61, 412.

21. Barteau, M. A.; Broughton, J. Q.; Menzel, D., *Surface Sci.* **1983**, 88, 384.

22. Conrad, H.; Scala, R.; Stenzel, W.; Unwin, R., *J. Chem. Phys.* **1984**, 81, 6371.

23. Hills, M. M.; Parmeter, J. E.; Weinberg, W. H., *J. Am. Chem. Soc.* **1986**, 108, 7215.

24. Thomas, G. E.; Weinberg, W. H., *Rev. Sci. Instrum.* **1979**, 50, 497.

25. Williams, E. D.; Sobrero, A. C.; Weinberg, W. H., *J. Chem. Phys.* **1982**, 76, 1150.

26. Thomas, G. E.; Weinberg, W. H., *J. Chem. Phys.* **1979**, 70, 954.

27. Thiel, P. A.; W. H. Weinberg, *J. Chem. Phys.* **1980**, 73, 4081.

28. Cornu, A.; Massot, G., *Compilation of Mass Spectral Data*, Hayden and Son Ltd., London, 1975.

29. Redhead, P. A., *Vacuum* **1962**, 203.

30. Parmeter, J. E.; Hills, M. M.; Weinberg, W. H., in preparation.

31. Megiris, C. E.; Berlowitz, P.; Butt, J. B. Kung, H. H., *Surface Sci.* **1985**, 159, 184

32. Andrews, J. R.; Kettle, S. F. A.; Powell, D. B.; Sheppard, N., *Inorg. Chem.* **1982**, 21, 2874.

**Figure Captions**

Figure 1. The $H_2$ thermal desorption spectra resulting after the Ru(001) surface at 80 K is exposed to (a) 10 L $H_2$, (b) 5 L $C_2H_2$ and (c) 10 L $H_2$ followed by 5 L $C_2H_2$. Note that the baseline is not identical for the three cases, and that the abscissa are nonlinear. The abbreviation a.u. denotes arbitrary units.

Figure 2. Thermal desorption spectra resulting after the Ru(001) surface at 80 K are exposed to 1 L $H_2$, followed by 1 L $C_2D_2$: (a) $H_2$, (b) HD and (c) $D_2$. Dashed lines are approximate baselines for the three spectra.

Figure 3. Thermal desorption spectra of CHDCHD (m = 30 amu) recorded after the Ru(001) surface at 80 K is exposed to (a) 5 L $C_2H_2$, (b) 0.4 L $H_2$ followed by 5 L $C_2D_2$, (c) 1 L $H_2$ followed by 5 L $C_2D_2$, (d) 1.4 L $H_2$ followed by 5 L $C_2D_2$, and (e) 10 L $H_2$ followed by 5 L $C_2D_2$. In spectra (b)-(e) the initial absolute hydrogen adatom coverages are approximately 0.35, 0.6, 0.75 and 0.85, respectively. Spectrum (f) shows the $CD_2CD_2$ (m = 32 amu) desorption that results following a 5 L $C_2D_4$ exposure at 80 K. The apparent peak just above 100 K in spectra (a)-(e) is a spectrometer effect and should be ignored. Note that the abscissa are nonlinear.

Figure 4. The EEL spectra that result when the Ru(001) surface at 80 K is exposed to (a) 5 L $C_2H_2$, (b) 5 L $C_2D_2$, (c) 10 L $H_2$ followed by 5 L $C_2H_2$, and (d) 10 L $D_2$ followed by 5 L $C_2D_2$, and then annealed to 150 K and recooled to 50 K prior to spectral collection. Spectra (a) and (b) are characteristic of molecularly chemisorbed acetylene, while spectra (c) and (d) show features characteristic both of chemisorbed acetylene and $CHCH_2$ ($CDCD_2$). In spectra (c) and (d), the low frequency metal-carbon modes are not resolved due to the somewhat poorer cutoff of the elastic peak. The apparent shift of the high frequency metal-carbon mode in spectrum (c) compared to spectrum (a) is not very reproducible and may also be due to the poorer elastic peak cutoff.

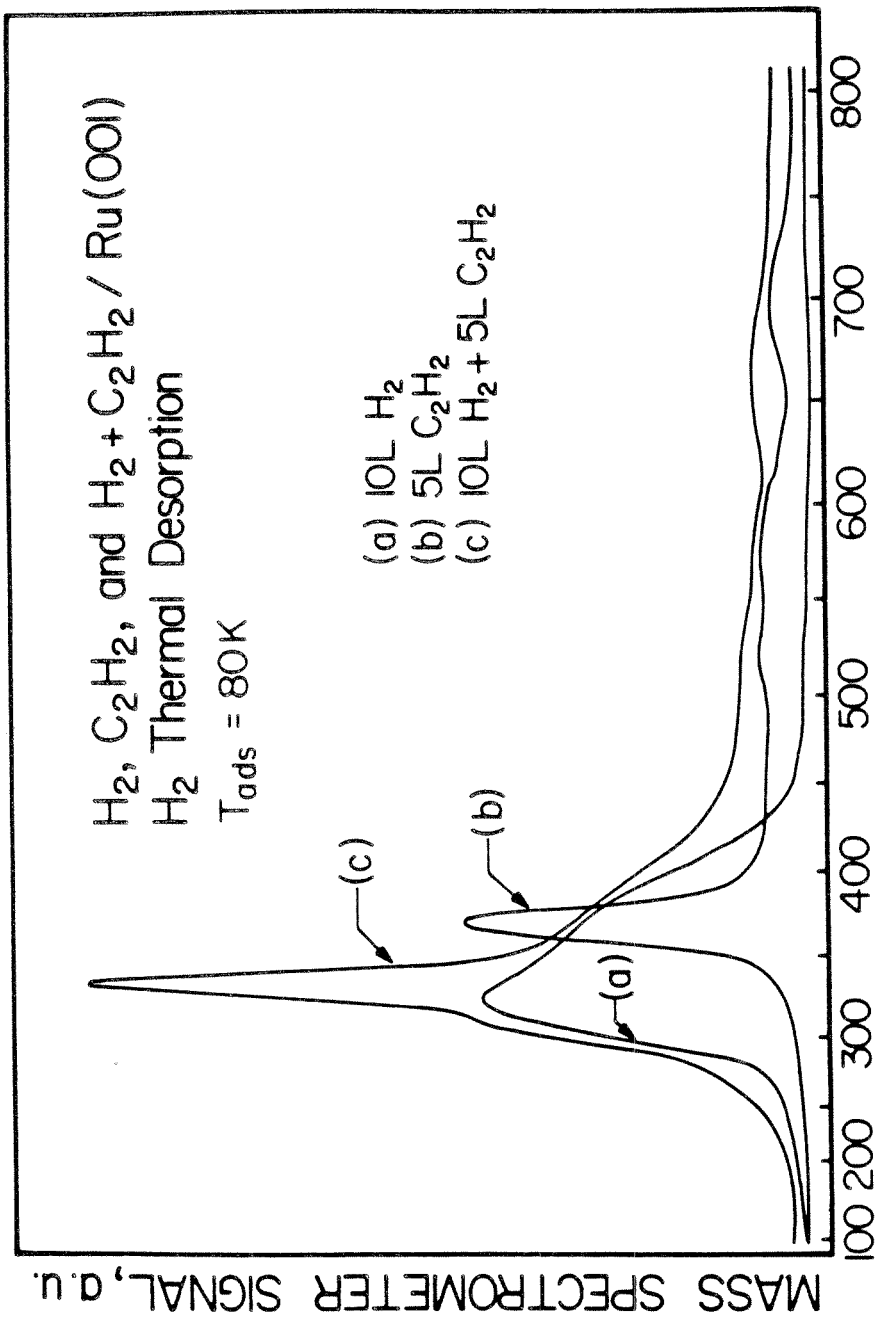
$H_2$, $C_2H_2$, and $H_2 + C_2H_2$ / Ru(001)
$H_2$ Thermal Desorption
$T_{ads}$ = 80K
(a) 10L $H_2$
(b) 5L $C_2H_2$
(c) 10L $H_2$ + 5L $C_2H_2$
(a)
(b)
(c)
MASS SPECTROMETER SIGNAL, a.u.
100 200 300 400 500 600 700 800
TEMPERATURE, K

Figure 1

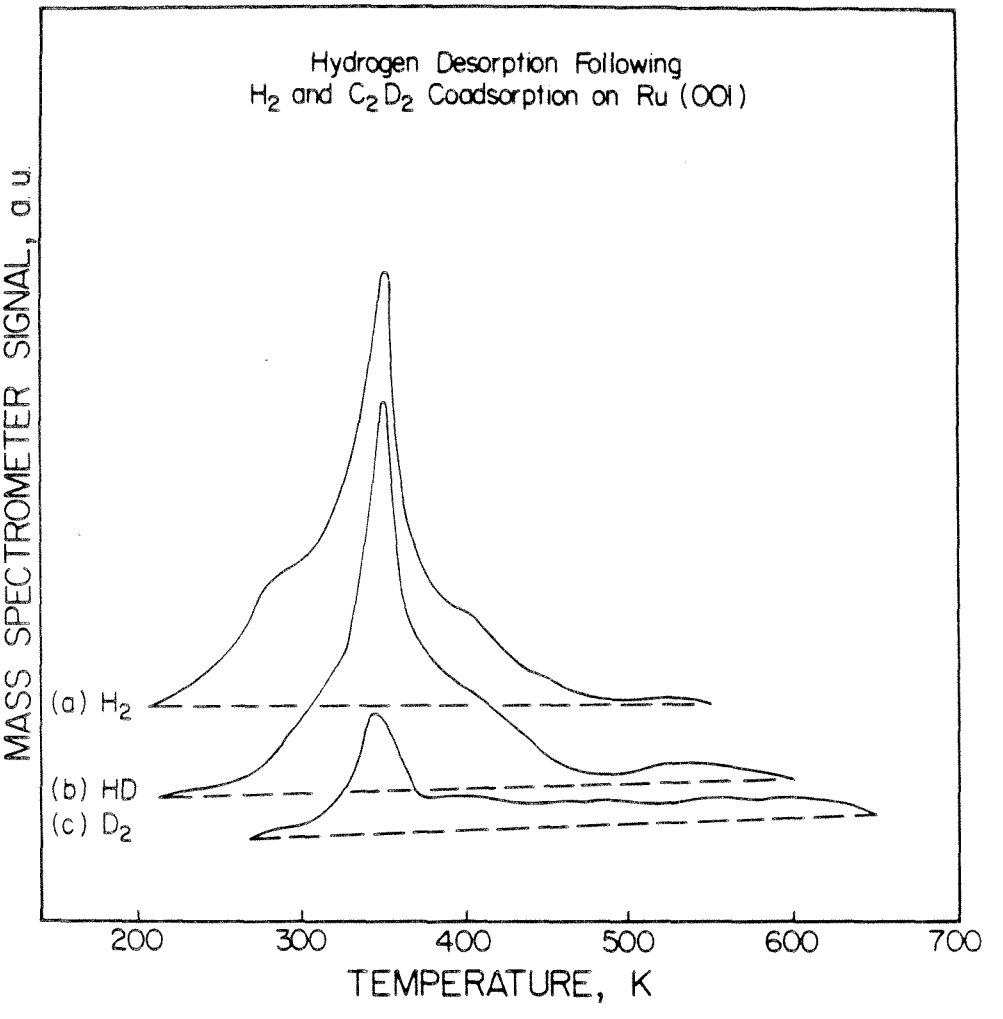
Hydrogen Desorption Following
$H_2$ and $C_2D_2$ Coadsorption on Ru (001)
MASS SPECTROMETER SIGNAL, a.u.
(a) $H_2$
(b) HD
(c) $D_2$
200
300
400
500
600
700
TEMPERATURE, K

Figure 2

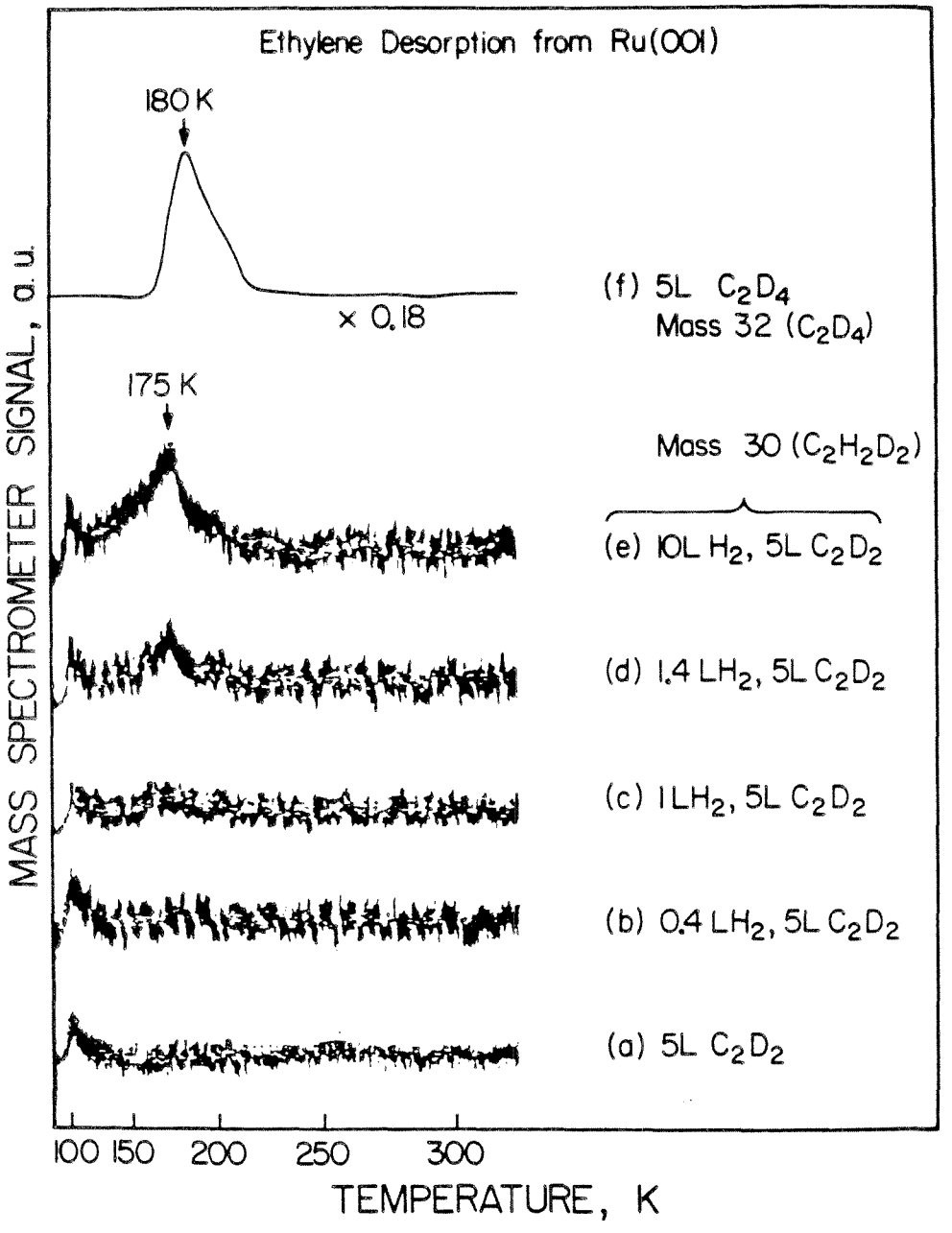
Ethylene Desorption from Ru(001)
180 K
× 0.18
175 K
(f) 5L $C_2D_4$
Mass 32 ($C_2D_4$)
Mass 30 ($C_2H_2D_2$)
(e) 10L $H_2$, 5L $C_2D_2$
(d) 1.4 L $H_2$, 5L $C_2D_2$
(c) 1 L $H_2$, 5L $C_2D_2$
(b) 0.4 L $H_2$, 5L $C_2D_2$
(a) 5L $C_2D_2$
MASS SPECTROMETER SIGNAL, a.u.
100 150 200 250 300
TEMPERATURE, K

Figure 3

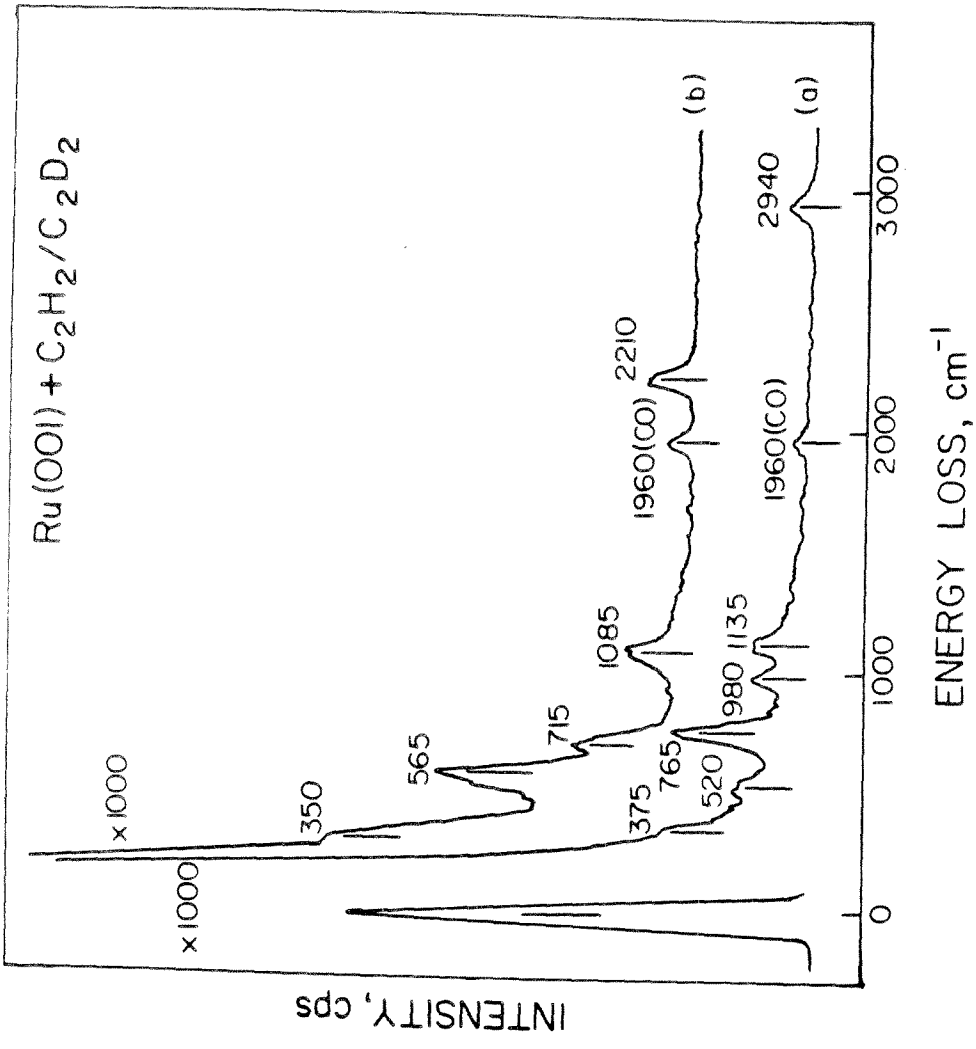
Ru(001) + C2H2/C2D2
INTENSITY, cps
ENERGY LOSS, cm-1
0
1000
2000
3000
×1000
×1000
350
565
715
1085
1960(CO)
2210
(b)
375
765
520
980
1135
1960(CO)
2940
(a)

Figure 4ab

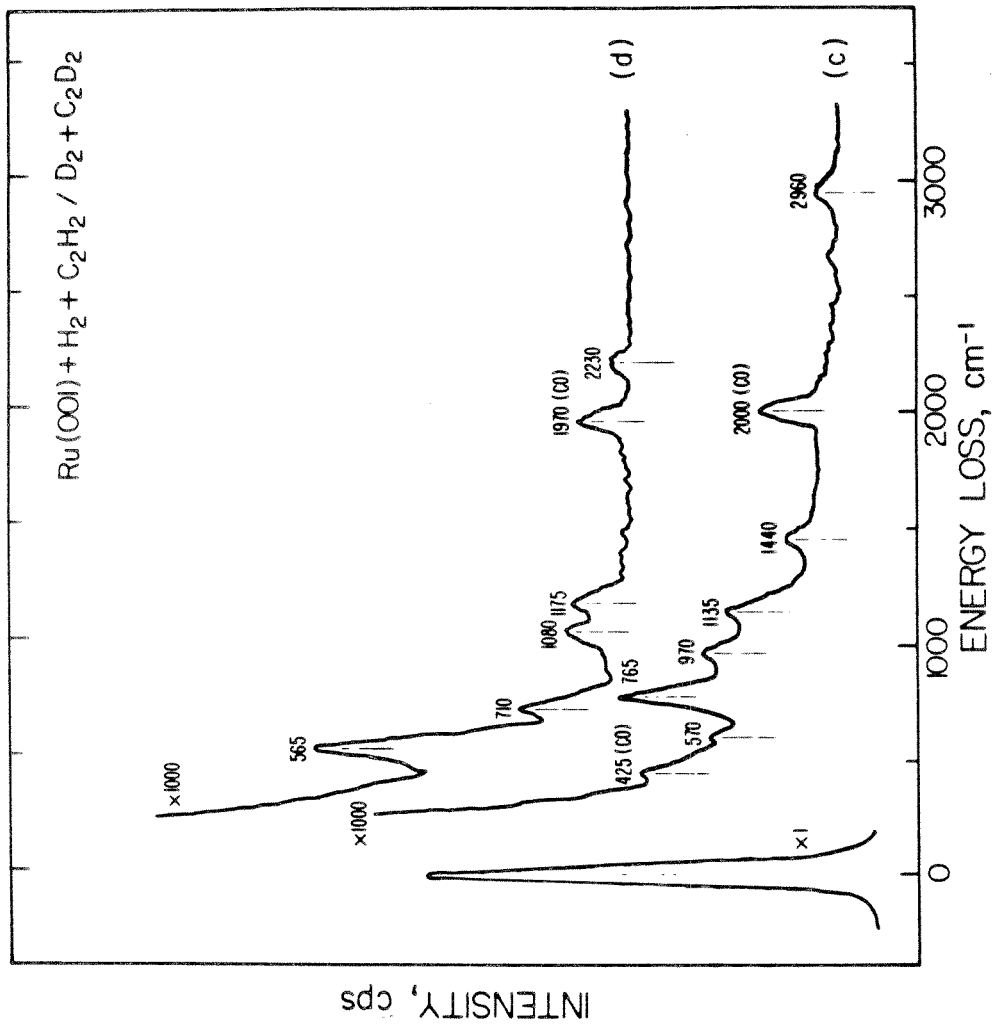
Ru(001) + H2 + C2H2 / D2 + C2D2
(d)
(c)
×1000
×1000
×1
565
710
425 (CO)
765
1080 1175
1970 (CO)
2230
570
970
1135
1440
2000 (CO)
2960
0
1000
2000
3000
ENERGY LOSS, cm-1
INTENSITY, cps

Figure 4 cd

# Appendix 3

## The Adsorption of Formic Acid and the Decomposition of the Formate Intermediate on the (001) Surface of Ruthenium

## Abstract

The adsorption of formic acid on the clean Ru(001) surface has been studied by electron energy loss vibrational spectroscopy and thermal desorption mass spectrometry. Large exposures of formic acid produce a molecular multilayer species with vibrational frequencies similar to those of crystalline formic acid. Two different formate species (a monodentate and a bidentate formate) and a surface hydroxyl have been identified as stable intermediates in the decomposition of formic acid on the Ru(001) surface. The monodentate formate species has a ν(C=O) mode at 1345 $cm^{-1}$ and a softened C-H stretching mode, characteristic of a surface-hydrogen interaction. The monodentate formate species is completely converted to the bidentate species by heating to 200 K. The bidentate formate species is believed to bridge two adjacent binding sites. The formic acid decomposition products are $CO_2$, CO, $H_2$, water and oxygen adatoms. The ratio of desorbed CO with respect to desorbed $CO_2$ increases both with slower heating rate and with lower formate coverages.

## 1. Introduction

Among the goals of surface science are the identification and characterization of adsorbed intermediates, which serve to delimit the number of possible reaction mechanisms in catalytic reactions. The study of adsorbate structure and bonding provides a basis for understanding the role of the catalytic surface in heterogeneous catalysis. Of particular interest are reactions of molecules containing carbon-oxygen bonds, since numerous catalytic reactions involve the formation or cleavage of C-O bonds or the activation of carbon centers bonded to oxygen atoms in elimination, addition or reduction reactions. For this reason, there has been considerable interest in the interactions of formic acid with metal and metal oxide surfaces as model systems for carboxylate catalysis (**1**). A goal of this work has been determining reaction mechanisms and the factors that influence catalytic specificity for different decomposition products.

Single crystalline surfaces offer the advantage of having well-defined geometrical structures to which a wide array of surface-sensitive spectroscopies may be applied. Using a number of these techniques, we have developed a large data base concerning the mechanism and the kinetics of the decomposition of formic acid. Most metal surfaces fall into two distinct classes with respect to the product selectivity of formic acid decomposition. On the majority of single crystalline surfaces that have been studied, including Fe(100) (**2**), Ni(111) (**3**), Ni(110) (**4**), Ni(100) (**5**) Ru(001) (**6**) and Ru(100) (**7**), the decomposition products are $CO_2$, CO, *water* and $H_2$. On Pt(111) (**8**), Cu(100) (**9**) and Cu(110) (**10**), however, the decomposition products are $CO_2$ and $H_2$. Coadsorbates have been found to affect both the reactivity and selectivity. For example, on the clean Ag(110) surface, formic acid adsorbs molecularly and desorbs reversibly, but on a surface with presaturated oxygen adatoms ($\theta \approx 0.33$), dissociative adsorption occurs with $CO_2$, *water* and $H_2$ desorption (**11**. The preadsorption of an ordered $(\sqrt{5} \times \sqrt{5})$O adatom on Mo(100) causes formic acid to decompose to $CO_2$, CO, *water*, $CH_4$ and $H_2$, as compared to the clean Mo(100) surface on which the decomposition products are CO, *water* and $H_2$ (**12**). The formation of CO on the Ni(110) surface can be completely inhibited by a ordered 4x5 carbide overlayer (**13**).

Vibrational spectroscopy of surfaces on which formic acid is adsorbed has been employed on the

Ag(110) (**11**), Al(110) (**14**), Au(110) (**15**), Au(111) (**15**), Cu(110) (**16**), Cu(100) (**9**), Mo(100) (**12**), Ni(110) (**13**), Pt(111) (**8**), Pt(110) (**17**) and Ru(001) (**16**) surfaces, using either electron energy loss spectroscopy (EELS) or infrared reflection-absorption spectroscopy (IRAS). Formate intermediates, usually symmetrically bound (i.e. bidentate with equivalent oxygen atoms), have been identified on all these surfaces. These symmetric formates are characterized by four strong vibrational modes, $\nu$(M-O), $\delta$(OCO), $\nu_s$(OCO) and $\nu$(CH). On the Cu(100) (**9**), Mo(100) (**12**), Pt(110) (**17**), Ru(001) (**6**), oxygen-saturated Ag(110) (**11**), and Ni(110)-(4x5)C (**13**) surfaces, the presence of additional dipolar enhanced vibrational modes, in particular the $\nu_a$(OCO) mode that is forbidden by the surface selection rule for a symmetric formate (**18**), indicates the presence of an asymmetrically bound formate, which may be either an asymmetric, bidentate formate or a monodentate formate. The $\nu$(C-O) and $\nu$(C=O) modes of monodentate formates are located at similar frequencies to the $\nu_s$(OCO) and $\nu_a$(OCO) modes of bidentate formates. These asymmetric formates are observed at low temperatures (usually below 200 K), and heating causes an irreversible change in orientation to a symmetric formate. Two exceptions to this pattern are Cu(100), where the intensity of the $\nu_a$(OCO) mode on the annealed surface increases if the surface is held at 100 K for 10 to 20 minutes, suggesting a reversible change in orientation (**9,19**), and Ni(110), where only the symmetric formate is observed on the clean surface and only the asymmetric formate is observed on the Ni(110)-(4x5)C surface (**13**). On Pt(110), the bonding configuration has been assigned as an asymmetric bidentate formate, where a vector through the oxygen atoms is at an angle of approximately 10° with respect to the plane of the surface (**17**). All of the other asymmetric formates appear to be monodentate (**8,12**)

Determinations of the bonding geometry of the symmetric formate intermediate on the Cu(110) (**20**) and Cu(100) (**21**) surfaces have been made using extended X-ray absorption fine structure (EXAFS) measurements. Different bonding geometries have been found for this formate on the two different surfaces. On Cu(100) each formate oxygen resides at a site between four copper surface atoms (**21**), while on Cu(110) each oxygen bonds in an "on-top" arrangement above adjacent Cu atoms, with the plane of the formate parallel to the [1$\bar{1}$0] lattice vector and perpendicular to the surface (**20**). *Ab initio* geometrical optimization calculations for a model of formate on a Ni(001) surface yield a similar

geometry to that determined by EXAFS for the Cu(100) surface (22). Vibrational spectroscopic comparisons of the two different geometrical bonding configurations on the Cu(100) and Cu(110) surfaces, as measured by EELS and IRAS, respectively, are limited by the restricted frequency bandwidth of the latter technique. Thus, only two modes may be contrasted. The $\nu_s$(OCO) mode at 1330 $cm^{-1}$ on Cu(100) is found at 1350-1360 $cm^{-1}$ on Cu(110) and the $\nu$(CH) modes at 2840 and 2910 $cm^{-1}$ on Cu(100) occur at 2900-2980 $cm^{-1}$ on Cu(110) (9,16).

In this extension of our previous studies of the adsorption of formic acid on the Ru(001) surface (6), we present EEL spectral assignments for condensed (molecular) formic acid, bidentate and monodentate formate species and the first direct spectroscopic evidence for a surface hydroxyl species on Ru(001). Thermal desorption mass spectrometry (TDMS) results demonstrate two decomposition pathways leading either to CO desorption or to $CO_2$ desorption. This study is part of our ongoing investigations into the interactions of organic carbonyl ligands with the Ru(001) surface. Other reactants that have been investigated include acetone (23) and formaldehyde (24).

## 2. Experimental Procedures

The ultrahigh vacuum system and the EEL spectrometer used for these studies have been described previously (25). EEL spectra were recorded with a beam energy of approximately 5 eV. Count rates were typically 1 to 3 $\times$ $10^5$ counts per second for the specularly scattered elastic beam, while maintaining a resolution equal to or better than 80 $cm^{-1}$ (full-width at half-maximum intensity of the elastically scattered beam). Changes in EEL spectra as a function of temperature were observed by heating the crystal to various temperatures, followed by immediate cooling before recording the spectrum. All EELS measurements were made with the surface at a temperature of approximately 80 K.

Thermal desorption spectra were recorded in a second ultrahigh vacuum system equipped with Varian low-energy electron diffraction (LEED) optics, a Varian single pass cylindrical mirror Auger electron spectrometer, and a UTI 100 C quadrupole mass spectrometer. A Digital Equipment Corp. LSI-11 computer was used to collect TDMS data, and the smoothing procedure of Savitzky and Golay was used to improve the signal-to-noise ratio (26). Since no ordered superstructures were observed, no LEED results are presented.

The Ru(001) surfaces were cleaned chemically by exposure to $O_2$ at pressure of $5 \times 10^{-8}$ torr, while cycling the surface temperature between 300 and 800 K, followed by annealing in vacuum at 1650 K to remove adsorbed oxygen, and with occasional $Ar^+$ sputtering cycles (27). Surface cleanliness was confirmed with Auger spectroscopy, EELS or by thermal desorption of $H_2$ and CO. Formic acid samples, HCOOH (MCB spectroscopic grade), DCOOD (Stohler spectroscopic grade, nominal 99% $D_2$), HCOOD and DCOOH (Merck spectroscopic grade, nominal 99 D), were given a minimum of three freeze-thaw-pump cycles for additional purification before use, and gas handling lines were exposed numerous times to the deuterated formic acid to reduce isotopic exchange. Despite these precautions there appeared to be significant isotopic exchange of the hydroxyl deuterium with hydrogen prior to the adsorption of formic acid on the surface.

The Ru(001) surfaces were exposed to formic acid by backfilling the bell jars. Exposures quoted are not corrected for ionization gauge sensitivities. The mass spectrometer sensitivity was calibrated by integrating TDMS from saturation coverages of CO and $H_2$. Mass spectrometer sensitivities for other species, relative to CO, were estimated using information provided by the manufacturer.

## 3. EELS Identification of Adsorbed Species

Formic acid adsorption on the Ru(001) surface gives rise to several adspecies, which can be identified by their characteristic EEL features. The species are described below, along with their spectral assignments.

### 3.1 Molecular Formic Acid

Molecular formic acid is observed by EELS on the Ru(001) surface following exposures greater than 6 L at 80 K. EELS spectra following greater exposures are similar, but spectra at exposures above 10 L are less well resolved. The HCOOH spectrum shown in Fig. 1(a) is characterized by intense bands at 720, 940, 1235, 1370 and 1690 $cm^{-1}$, which are assigned as the $\delta$(OCO), $\pi$(OH), $\nu$(C-O), $\delta$(CH), and $\nu$(C=O) modes, respectively, of condensed multilayer formic acid. Also present are weaker, broader bands at 2640 and 2960 $cm^{-1}$, which can be assigned as 0(OH) and 0(CH) modes, respectively. The significantly lowered frequency of the $\nu$(OH) mode compared to that in the HCOOH monomer,

3570 $cm^{-1}$, is a consequence of the extensive hydrogen bonding in crystalline formic acid (28). These assignments are confirmed by comparison to the DCOOD spectrum in Fig. 1b, where the bands observed at 970, 1260, and 1680 $cm^{-1}$ are assigned as the $\delta$(CD), $\nu$(C-O) and $\nu$(C=O) modes, respectively. The most intense band at 690 $cm^{-1}$ is the unresolved sum of the $\delta$(OCO) and $\pi$(OD) modes. The $\nu$(OD) and $\nu$(CD) modes shift to 2020 and 2260 $cm^{-1}$, respectively. The small band at 2960 $cm^{-1}$ is assigned as a $\nu$(CH) mode from an HCOOH or HCOOD impurity. Evidence is also seen for a broad $\nu$(OH) mode from a DCOOH or HCOOH impurity at approximately 2600 $cm^{-1}$. These energies agree well with those of crystalline formic acid and less well with those of liquid (dimerized) formic acid (cf. Table 1). The mode at 230 (220) $cm^{-1}$ in the HCOOH (DCOOD) spectrum is assigned as a frustrated translational mode of molecules within the condensed lattice. A band at similar frequencies is observed for crystalline formic acid (28), as well as for condensed formic acid on other metal surfaces (9,11.

### 3.2 Monodentate Formate

A monodentate formate species is observed on the Ru(001) surface following submonolayer exposures at 80 K as well as following the desorption of a formic acid multilayer at 170 K. Spectra of submonolayer exposures of HCOOH and DCOOD are shown in Fig. 2. The intense band at 1680 $cm^{-1}$ in Fig. 2(a) is assigned to the $\nu$(C=O) mode; this band cannot be the $\nu_a$(OCO) mode, which occurs at a similar frequency for symmetrical bidentate formates (8,9,11-17,29), since this mode would have a dipole parallel to the surface and thus is forbidden by the surface selection rule (18). The band observed at 2355 $cm^{-1}$ is the $\nu$(CH) mode. The downward shift of this mode by over 500 $cm^{-1}$ from its usual frequency implies that the hydrogen atom strongly interacts with the Ru(001) surface (18). The assignment of this mode is confirmed by the deutero-formate spectrum, where this mode shifts to approximately 1700 $cm^{-1}$ and is obscured by the 1650 $cm^{-1}$ $\nu$(C=O) mode. The observation of this "softened" CH mode has not been reported for any other monodentate surface formate species. These two modes allow the monodentate formate geometry to be assigned:

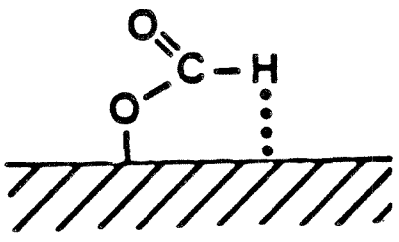

The EELS spectra exhibit bands at 370 (365), 775 (775), and 1345 (1315) $cm^{-1}$, which are assigned as the ν(Ru-O), dels(OCO) and nus(OCO) modes for the monodentate HCOO (DCOO) species, respectively. The 1160 $cm^{-1}$ band in the monodentate HCOO spectrum is assigned as a π(CH) mode. This mode is obscured in the DCOO spectrum by the dels(OCO) mode. The upward shift of this mode may be indicative of a hydrogen interaction with the surface. The 1015 $cm^{-1}$ band in the monodentate DCOO spectrum is assigned as a δ(CD) mode and is obscured in the HCOO spectrum by the $\nu_s$(OCO) mode.

The high frequency ν(CH) mode at 2935 $cm^{-1}$ is best explained by the presence of a bidentate formate, discussed further in Sect. 3.3. The assignment of the 610 $cm^{-1}$ peak observed in the monodentate DCOO spectrum will be discussed further in Sect. 3.4. Table 2 contains assignments for both Ru(001)-formate species, along with those for analogous metal-formate complexes and for formates adsorbed on other single crystalline metal surfaces.

### 3.3 Bidentate Formate

Annealing of the surface on the monodentate formate is present to temperatures above 200 K, leaving a formate species with only four bands at 380, 805, 1360 and 2915 $cm^{-1}$, which are assigned as the ν(Ru-O), dels(OCO), nus(OCO) and ν(CH) modes, respectively, of a symmetrically bonded bidentate formate species [cf. Figs. 3(a) and 4(a)]. As the surface is heated from 80 K to 200 K, the vibrational bands due to the monodentate formate disappear with little increase in the intensity of the CO vibrational modes and no $CO_2$ production. This indicates that most, if not all, of the monodentate formate converts to the bidentate formate, rather than decomposes directly.

Metal complexes of carboxylic acids, particularly acetate complexes, have been studied extensively (29). Two different bonding configurations of symmetrical bidentate formates are known: the bidentate bridging species, shown below as (a), and the bidentate chelating species, (b).

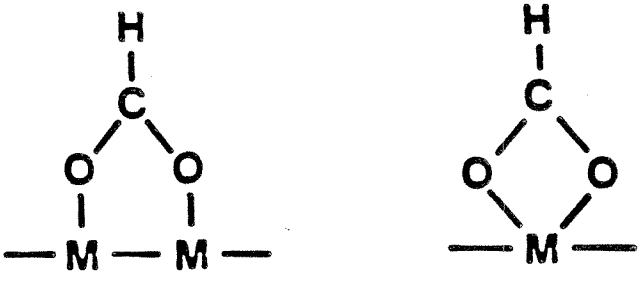


(a) (b)

While the difference in frequency between the $\nu_a$(OCO) and the $\nu_s$(OCO) modes provides the most conclusive diagnostic for discriminating between these two bonding geometries, the $\nu_a$(OCO) mode should not be observed in a symmetric bidentate formate because it does not have a dynamic dipole perpendicular to the surface. However, by comparison to the $\nu_s$(OCO) mode in transition metal formate and acetate species, the bonding geometry can be assigned as bridging bidentate. In group VIII transition metal acetate complexes, the $\nu_s$(OCO) mode has been reported in the range 1450-1465 $cm^{-1}$ for the chelating configurations contrasting the range of 1410-1440 $cm^{-1}$ for the bridging configurations (29). However, the $\nu_s$(OCO) mode of the the "free" (solvated) acetate ion at 1416 $cm^{-1}$ is very close to that of the bridging configuration acetate ligand. By analogy to the acetate results, the $\nu_s$(OCO) mode at 1360 $cm^{-1}$ in the bidentate surface formate closely correlates with the same mode in transition metal bridging formate complexes at approximately 1370 $cm^{-1}$ and in the "free" formate ion at 1351 $cm^{-1}$ (cf. Table 2).

### 3.4 Surface Hydroxyl

The weak band observed in the both the monodentate and the bidentate formate EEL spectra from DCOOD at 610 $cm^{-1}$ [cf. Figs. 2(b) and 4] cannot be assigned to either of these two species because no normal vibrational mode of either of these species corresponds to this frequency, and because its intensity correlates with neither species. It is observed in all DCOOD EELS spectra taken at temperatures up to 250 K, well above the conversion temperature for the monodentate formate, but it disappears by 300 K, while the bidentate formate modes remain strong. While water has been observed to desorb following formic acid exposures with a desorption maximum at 275 K (**6**), this mode cannot be due to adsorbed $D_2O$, which has been observed to have a frustrated rotational (librational) mode at 520 $cm^{-1}$ at low coverages, increasing to 620 $cm^{-1}$ at monolayer coverage, because submonolayer coverages of water desorb completely from the Ru(001) surface by 220 K (**30**). This mode at 610 $cm^{-1}$ is assigned as a $\delta$(Ru-OD) mode from a small concentration of surface-hydroxyl (OD) groups, which are produced along with CO by low temperature formate decomposition. The presence of this hydroxyl species has not been observed spectroscopically heretofore on the Ru(001) surface, but it has been reported on the Pd(100) (**31,32**), Ag(110) (**33** and Pt(111) (**34**) surfaces with $\delta$(M-OH) frequencies in the range between

670 and 1015 $cm^{-1}$ [490 and 750 $cm^{-1}$ for δ(M-OD)]. This assignment cannot be confirmed by comparison to HCOOH spectra, because the δ(Ru-OH) mode is obscured by the strong dels(OCO) mode at 775-805 $cm^{-1}$. The intensity of the ν(OH) mode for surface hydroxyl, which has been reported between 3200 and 3500 $cm^{-1}$ [ν(OD), between 2400 and 2600 $cm^{-1}$], is considerably less intense than the δ(M-OH) mode and would not be expected to be observed in these spectra, where the fractional coverage of surface OH is estimated to be on the order of 5%. The frustrated translational mode, ν(M-OH), which has been reported between 280 and 460 $cm^{-1}$, is obscured by the strong ν(Ru-O) formate mode at 380 $cm^{-1}$.

### 3.5 Formate Decomposition Products

As may have been seen in Figs. 2-4, there is spectroscopic conformation of two other adsorbed products of formate decomposition, CO and oxygen adatoms. Loss features from low concentrations of CO, ν(Ru-CO) at approximately 460 $cm^{-1}$ and ν(CO) at approximately 2000 $cm^{-1}$, appear in all spectra measured immediately following adsorption and increase in intensity as the surface is annealed. There is some formate decomposition below 200 K, as judged by the small increase in the intensity of the ν(CO) mode of CO, and the δ(Ru-OD) of surface-hydroxyl (OD), prompting speculation that the small amount of low temperature decomposition of formate to CO and OH takes place at defect sites. The weak Ru-O stretching mode at 540 $cm^{-1}$ from oxygen adatoms produced by formate decomposition is obscured by the ν(Ru-CO) mode of adsorbed CO, but it can be seen clearly at temperatures above those where CO desorbs [cf. Fig. 3(d)].

At temperatures above 300 K, formate continues to decompose, yielding CO, as evidenced by the increased intensity of the CO modes, yet no surface hydroxyl is observed by EELS above 300 K, nor is water observed as a decomposition product. Thus, at temperatures above 300 K, either the hydroxyl species quickly decomposes to O and H adatoms, or above 300 K another mechanism allows formate to decompose forming the CO, O and H adspecies directly, without the hydroxyl intermediate. These two mechanisms cannot be discerned on the basis of evidence presented in this study.

## 4. Thermal Desorption Mass Spectrometry Results

Six species, molecular formic acid, CO2, CO, water, $O_2$ and $H_2$, desorb from the Ru(001) surface following formic acid adsorption and heating of the surface. The thermal desorption spectra of molecular formic acid, CO2, CO, isotopes of hydrogen, and water are presented in Figs. 5, 6, 7, 9, and 10, respectively. Interpretations of these thermal desorption spectra are discussed in Sects. 4.1 through 4.5. The oxygen adatoms observed by EELS desorb as $O_2$ at approximately 1500 K. No attempt was made to record TDMS in this temperature range.

### 4.1 Formic Acid Desorption

Figure 5 exhibits desorption of molecular formic acid for several formic acid exposures. At an exposure of 5 L [cf. Fig. 5(c)], formic acid desorbs molecularly with a peak at approximately 200 K. With exposures in excess of 10 L, an additional lower temperature peak develops at 170 K, which does not saturate, due to multilayer (condensed) formic acid, as shown in Fig. 5(d). The 200 K feature is attributed to adsorption of a nondissociated layer of formic acid above the first layer of formate adsorbed on the Ru surface. This second layer comprised of molecular formic acid has a higher binding energy than condensed formic acid multilayers. The 200 K feature cannot be attributed to adsorbed formate recombining with surface hydrogen to yield formic acid. The peak does not shift with temperature as would accompany second-order desorption. There is no evidence for the recombination of surface formate with hydrogen adatoms; if a surface with adsorbed formate is heated to 200 K to desorb all molecular formic acid and then is cooled and exposed to $H_2$, no further molecular formic acid desorption is observed.

There is no molecular desorption of formic acid above 200 K. The tentative suggestion of formic acid desorption between 300 and 350 K (**6**) has been shown to be due to an overlap with significant desorption of $CO_2$ for the mass spectrometric resolution employed previously.

### 4.2 $CO_2$ Desorption

There is a negligible amount of $CO_2$ desorption following a formic acid exposure of 0.4 L, which corresponds to a formate coverage of 10% of the saturation formate coverage [cf. 6(a)], as estimated from the TDMS of CO and CO2. At higher formate coverages, a $CO_2$ desorption feature appears at

310 K, and the desorption peak shifts to higher temperatures with increasing coverage, reaching 365 K for a saturation formate coverage (cf. Fig. 6). This desorption of $CO_2$ is "reaction-limited" since it has been demonstrated that $CO_2$ does not adsorb on Ru(001) at temperatures above 77 K (35).

The presence of both CO and CO2 as decomposition products from surface formate demonstrates the existence of two decomposition pathways, since the probability of the reaction CO(a) + O(a) $\rightarrow$ $CO_2$ is less than $10^{-3}$ at temperatures below 400 K (35-37).

**4.3 CO Desorption**

The decomposition of the surface formate also yields adsorbed CO and hydroxyl fragments or hydrogen and oxygen adatoms, as discussed previously. While the onset of formate decomposition to CO is observed by EELS at temperatures below 200 K, all CO extrusion from the surface is "desorption-limited" (cf. Fig. 7) (38). Thus, no kinetic information concerning the decomposition of formate to CO may be derived from these thermal desorption spectra.

Integration of the thermal desorption peaks of CO and $CO_2$ establishes the saturation formate coverage to be 0.28 $\pm$ 0.04 monolayer (0.28 formate adspecies per surface Ru adatom). Two interesting effects are noted in the branching ratio, the relative amounts of desorbing CO and $CO_2$. Figure 8(a) shows the amounts of formate that decompose to yield CO and $CO_2$, relative to the saturation formate coverage, as well as the ratio of desorbed CO to $CO_2$. As noted previously, the onset of $CO_2$ desorption is at approximately 10% of saturation coverage. The CO desorption feature saturates well before the CO2 desorption feature saturates. In contrast, for formic acid decomposition on Ru(100), the branching ratio is independent of coverage (7). The branching ratio on Ru(001) is also influenced by the heating rate. Figure 8(b) shows the ratio of CO to $CO_2$ as a function of heating rate for a formate surface at approximately 40% of saturation coverage. The relative amount of $CO_2$ is minimized by reducing the heating rate. If the Ru surface is precovered with formate at 40% of the saturation coverage and is then annealed at 240 K for 5 minutes prior to the commencement of TDMS, the amount of $CO_2$ is decreased by a factor of five.

The change in branching ratio with coverage is explained by an increase in the activation barrier for the the CO decomposition reaction due to accumulation of product oxygen adatoms. Precoverage of

the surface with oxygen adatoms also lowers the ratio of CO to $CO_2$ (**39**). The change in branching ratio is consistent with the CO reaction having a lower preexponential factor than the CO2 decomposition reaction.

**4.4 Hydrogen Desorption**

Hydrogen adatoms may be produced from three different reactions:

$$HCOOH(a) \rightarrow HCOO(a) + H(a)\ , \qquad (A)$$

$$HCOO(a) \rightarrow CO(a) + H(a) + O(a)\ , \qquad (B)$$

and

$$HCOO(a) \rightarrow CO_2(g) + H(a)\ . \qquad (C)$$

Deuterium-labeled formic acid, DCOOH, was used in the thermal desorption measurements so that "hydrogen" from the dehydrogenation reaction (A) could be distinguished from that resulting from the formate decomposition reactions (B) and (C).

Thermal desorption spectra of $H_2$, HD and $D_2$ from DCOOH are shown in Figs. 9(A), 9(B) and 9(C), respectively. The poor signal-to-noise ratio seen for the D2 thermal desorption spectra compared to the $H_2$ and HD spectra results because the the mass spectrometer has a sensitivity of approximately 25% for $D_2$ with respect to $H_2$.

As demonstrated by the EELS results presented in Sect. 3.2, all adsorbed DCOOH decomposes below 200° K via reaction (A) to form adsorbed formate and H adatoms. These H adatoms combine to produce desorption-limited $H_2$ [cf. Fig 9(A)]. At formate coverages of approximately 10% of saturation, the peak for $H_2$ desorption is at 410 K, but shifts to lower temperature with increasing formate coverage. At saturation formate coverage, the desorption-limited peak shifts to 310 K and a second, reaction-limited peak is seen at 350 K, as the desorption-limited peak shifts to lower temperatures. The reaction-limited peak is 10 to 20 K below the $CO_2$ desorption peak temperature. The second peak correlates with the $CO_2$ desorption peak and is a result of a shift in the thermal desorption peak to lower temperatures due to the higher coverage of hydrogen adatoms.

Reaction (B), the decomposition of formate to produce CO, hydrogen, hydroxyl and O adspecies, is evidenced by the increased intensity of modes attributed to adsorbed CO in the EELS spectra, as dis-

cussed previously in Section 3.5. This reaction begins below the temperature for hydrogen desorption. The D adatoms from reaction (B) combine with the H adatoms from reaction (A), producing desorption-limited HD at the same temperatures as $H_2$ desorption [cf. Fig. 9(B)]. Reaction (C), the decomposition of formate to yield D adatoms and $CO_2$, has been discussed in Sect. 4.2. At low formate coverages, all decomposition occurs below the desorption temperature for hydrogen, and all evolution of HD from the surface is desorption-limited. At saturation formate coverage, there are two peaks, a desorption-limited peak at 310 K and a reaction-limited peak at 350 K, similar to $H_2$ TDMS.

Desorption of $D_2$ is qualitatively similar to HD desorption. At low formate coverages, all decomposition occurs below the hydrogen desorption temperature and all evolution of $D_2$ from the surface is desorption-limited [cf. Fig. 9(C)]. At higher formate coverages, desorption-limited hydrogen evolution shifts to lower temperatures. Consequently, the H adatom coverage is lower when reaction (C) is active, and this reaction produces increased amounts of $D_2$ with respect to HD. This is also reflected by a shift of the reaction-limited $D_2$ peak 10 to 20 K higher than the $H_2$ and HD peaks.

The peak temperatures for desorption-limited hydrogen evolution have shifted to lower temperatures with respect to $H_2$ on clean Ru(001), where hydrogen desorbs at 440 K at low coverage and 340 K at saturation coverage (**40**). Similar shifts have been seen for the coadsorption of CO and hydrogen (**41**).

### 4.5 Water Desorption

Water has been reported as a major decomposition product from formic acid on the (100) surface of Ru (**7**), but only very small amounts of water are a product on Ru(001), desorbing at 275 K [cf. Fig. 10]. The reaction of hydrogen and oxygen adatoms to give water does not occur on the Ru(001) surface at temperatures below that at which hydrogen adatoms recombine and desorb thermally as $H_2$ (**42**). Thus, this small amount of desorbed water must be produced by the recombination of hydroxyl fragments and surface hydrogen from formic acid dehydrogenation. Integration of CO, $CO_2$ and $H_2$ TDMS from HCOOH, with heating rates of approximately 15 K/s, yields an estimate for the total water production as $0.02 \pm 0.01$ molecule per surface Ru atom. Slow heating rates increase the amount of water, and the slow annealing cycles used for EELS measurements would be expected to increase the hydroxyl

coverage in those experiments.

## 5. Conclusions

This study has demonstrated the existence of two formate intermediates to formic acid decomposition on the Ru(001) surface, a monodentate formate and a bidentate formate. The bidentate formate bonds in a bridging configuration. The formate molecules decompose to produce CO, $CO_2$, water, O adatoms and hydrogen. Two forms of molecular formic acid are observed, a first-layer state that desorbs at 200 K and a multilayer state that desorbs at 170 K. Small exposures of formic acid dehydrogenate upon adsorption to produce a monodentate formate. The formate species do not recombine with H adatoms.

On the basis of EELS and TDMS results, the following reaction scheme can be constructed for formic acid decomposition of the Ru(001) surface.

$$\text{HCOOH(g)} \xrightarrow{<80\text{K}} \text{monodentate–HCOO(a)} + \text{H(a)}$$

$$\text{monodentate–HCOO(a)} \xrightarrow{80\text{–}200\text{K}} \text{bidentate–HCOO(a)}$$

$$\text{bidentate–HCOO(a)} \xrightarrow{<300\text{K}} \text{OH(a)} + \text{CO(a)}$$

$$\text{bidentate–HCOO(a)} \xrightarrow{200\text{–}350\text{K}} \text{O(a)} + \text{H(a)} + \text{CO(a)}$$

$$\text{bidentate–HCOO(a)} \xrightarrow{300\text{–}350\text{K}} \text{H(a)} + \text{CO}_2\text{(g)}$$

$$\text{OH(a)} + \text{H(a)} \xrightarrow{\sim 275\text{K}} \text{H}_2\text{O(g)}$$

$$2\text{H(a)} \xrightarrow{300\text{–}400\text{K}} \text{H}_2\text{(g)}$$

$$\text{CO(a)} \xrightarrow{450\text{–}500\text{K}} \text{CO(g)}$$

The ratio of products is influenced by two factors, the formate coverage and the heating rate. At a formate coverage of 10% of saturation, almost all decomposition yields CO. The amounts of both CO and $CO_2$ increase with formate coverage, but the CO decomposition channel saturates before the $CO_2$ channel. Slower heating rates are found to increase the relative amounts to water and CO. This is explained by deactivation of the surface by O adatoms and by a lower prefactor for HCOO decomposition to CO than to $CO_2$.

Two interesting features of this study are: the first spectroscopic evidence for a surface hydroxyl species on Ru(001) and the first reported observation of a softened ν(CH) mode for a surface formate species. While monodentate formate species have been proposed for other metal surfaces, this argument has been advanced solely on the assignment of a band at approximately 1660 $cm^{-1}$ as the ν(C=O) mode in a monodentate formate, rather than the $\nu_a$(OCO) mode of a bidentate formate, which would be dipolar allowed for an asymmetric bidentate bonding configuration. The observation of a softened ν(CH) mode provides additional evidence for the existence of a surface monodentate formate and indicates an interaction between the hydrogen atom and the surface, indicative of a short H-surface distance.

**Acknowledgments**

The authors wish to thank Dr. Theodore E. Madey, John Parmeter and Dr. Udo Schwalke for extremely useful discussions. This research was supported by the National Science Foundation under Grant No. CHE82-06487.

**References**


1. See for example, Madix, R.J., *Advan. Catal.* **1980**, 29, 1; Iglesia, E.; Boudart, M., *J. Catal.* 1983, 81, 224; Canning, N.D.S.; Madix, R.J., *J. Phys. Chem.* **1984**, 88, 2437.
2. Benziger, J.B.; Madix, R.J., *J. Catal.* **1980**, 65, 49.
3. Benziger, J.B.; Schoofs, G.R., *J. Phys. Chem.* **1984**, 88, 4439.
4. See Falconer, J.L.; Madix, R.J., *J. Catal.* **1978**, 31, 47, and references cited therein.
5. Benziger, J.B.; Madix, R.J., *Surface Sci.* **1979**, 79, 394.
6. Avery, N.R.; Toby, B.H.; Anton, A.B.; Weinberg, W.H., *Surface Sci.* **1982**, 122, L574; Toby, B.H.; Avery, N.R.; Anton, A.B.; Weinberg, W.H., *J. Electron Spect.***1983**, 29, 233.
7. Larson, L.A.; Dickinson, J.T., *Surface Sci.* **1979**, 84, 17.
8. Avery, N.R., *Appl. Surface Sci.* **1982**, 11/12, 774.
9. Sexton, B.A., *Surface Sci.* **1979**, 88, 319.
10. Ying, D.H.S.; Madix, R.J., *J. Catal.* **1980**, 61, 48.
11. Sexton, B.A.; Madix, R.J., *Surface Sci.* **1981**, 105, 177.
12. Miles, S.L.; Bernasek, S.L.; Gland, J.L., *Surface Sci.* **1983**, 127, 271.
13. Madix, R.J.; Gland, J.L.; Mitchell, G.E.; Sexton, B.A., *Surface Sci.* **1983**, 125, 481.
14. Liehr, M.; Thirty, P.A.; Pireaux, J.J.; Caudano, R., *Phys. Rev. B* **1985**, 31, 42.
15. Chtaib, M.; Thirty, P.A.; Delrue, J.P.; Pireaux, J.J.; Caudano, R., *J. Electron Spect.* **1983**, 29, 293.
16. Hayden, B.E.; Prince, K.; Woodruff, D.P.; Bradshaw, A.M., *Surface Sci.* **1983**, 133, 589.
17. Hofmann, P.; Bare, S.R.; Richardson, N.V.; King, D.A., *Surface Sci.* **1981**, 133, L459.
18. Ibach, H.; Mills, D.L., *Electron Energy Loss Spectroscopy and Surface Vibrations*, Academic Press, New York, 1982.
19. Other workers have suggested that the reappearance of the band assigned as the νA(OCO) mode is due to adsorption of molecular formic acid desorbing from other surfaces within the chamber **(14)**.

20. Puschmann, A.; Haase, J.; Crapper, M.D.; Riley, C.E.; Woodruff, D.P., *Phys. Rev. Letters* 1985, 54, 2250.

21. Stohr, J.; Outka, D.A.; Madix, R.J.; Dobler, U., *Phys. Rev. Letters* **1985**, 54, 1256.

22. Upton, T.H., *J. Chem. Phys.* **1985**, 83, 5084.

23. Avery, N.R.; Weinberg, W.H.; Anton, A.B.; Toby, B.H., *Phys. Rev. Letters* **1983**, 51, 682; Anton, A.B.; Avery, N.R.; Toby, B.H.; Weinberg, W.H., *J. Am. Chem. Soc.* **1986**, 108, 684.

24. Anton, A.B.; Parmeter, J.E.; Weinberg, W.H., *J. Am. Chem. Soc.*, in press.

25. Thomas, G.E.; Weinberg, W.H., *Rev. Sci. Instrum.* **1979**, 50, 497.

26. Savitzky, A.; Golay, M.J.E., *Anal. Chem.* **1964**, 36, 1627; Steinier, J.; Termonia, Y.; Deltour, J., *Anal. Chem* **1972**, 44, 1906.

27. Thomas, G.E.; Weinberg, W.H., *J. Chem. Phys.* **1979**, 70, 954.

28. Millikan, R.C.; Pitzer, K.S., *J. Am. Chem. Soc.* **1958**, 80, 3515.

29. K. Nakamoto, *Infrared and Raman Spectra of Inorganic and Coordination Compounds*, Wiley, New York, 1978.

30. Thiel, P.A.; Hoffmann, F.M.; Weinberg, W.H., *J. Chem. Phys.* **1981**, 75, 5556.

31. Stuve, E.M.; Jorgensen, S.W.; Madix, R.J., *Surface Sci.* **1984**, 146, 179.

32. Nyberg, C.; Tengsta l, C.G., *J. Chem. Phys.* **1984**, 80, 3463.

33. Stuve, E.M.; Madix, R.J.; Sexton, B.A., *Surface Sci.* **1981**, 111, 11.

34. Fisher, G.B.; Sexton, B.A., *Phys. Rev. Letters* **1980**, 44, 683.

35. Avery, N.R.; Anton, A.B., unpublished results.

36. Lee, H.I.; Praline, G.; White, J.M., *Surface Sci.* **1980**, 91, 581.

37. Madey, T.E.; Engelhardt, H.A.; Menzel, D., *Surface Sci.* **1975**, 48, 304.

38. Madey, T.E.; Menzel, D., *Japan. J. Appl. Phys.*, Suppl. 2, Pt. 2, **1974**, 229.

39. Toby, B.H.; Hills, M.M.; Weinberg, W.H., unpublished results.

40. Shimizu, H.; Christmann, K.; Ertl, G, *J. Catal.* **1980**, 61, 412.

41. Peebles, D.E., Schreifels, J.A.; White, J.M., *Surface Sci.* **1982**, 116, 117.

42. Shi, S.K.; Schreifels, J.A.; White, J.M., *Surface Sci.* **1981**, 105, 1.

43. Ito, K.; Bernstein, H.J., *Can. J. Chem.* **1956**, 634, 170.

44. Johnson, M.K.; Powell, D.B.; Cannon, R.D., *Spectrochim. Acta* **1981**, 37A, 995.

45. Darensbourg, D.J.; Fischer, M.B.; Schmidt, Jr., R.E. Baldwin, B.J., *J. Am. Chem. Soc.* **1981**, 103, 1297.

46. Immirzi, A.; Musco, A., *Inorg. Chim. Acta* **1977**, 22, L35.

Thomas, G.E.; Weinberg, W.H., *J. Chem. Phys.* **1979**, 70, 1437.

Johnson, S.W.; Madix, R.J., *Surface Sci.* **1977**, 66, 189.

Rahman, T.S.; Anton, A.B.; Avery, N.R.; Weinberg, W.H., *Phys. Rev. Letters* **1983**, 51, 1979.

Madey, T.E., Engelhardt, H.A.; Menzel, D., *Surface Sci.* **1975**,48, 304.

**Table 1.** Assignments of vibrational modes observed using EELS for molecular HCOOH and DCOOD on Ru(001) from this work. The fundamental mode assignments for formic acid monomers, dimers and crystalline formic acid are listed also (**28**). All frequencies are in $cm^{-1}$.

| Mode | HCOOH | | | DCOOD | | HCOOH | DCOOD |
|---|---|---|---|---|---|---|---|
| | Monomer | Dimer | Solid | Dimer | Solid | Ru(001) | |
| ν(OH) | 3570 | 3110 | 2532 | 2323 | 2041 | 2640 | 2020 |
| ν(CH) | 2943 | 2957 | 2958 | 2226 | 2272<br>2247 | 2960 | 2260 |
| ν(C=O) | 1770 | 1754 | 1703<br>1609 | 1720 | 1671<br>1590 | 1690 | 1680 |
| ν(C-O) | 1105 | 1218 | 1255<br>1224 | 1246 | 1270<br>1253 | 1235 | 1260 |
| δ(CH) | 1387 | 1365 | 1380(a) | 987<br>976 | 993 | 1370 | 970 |
| δ(OH) | 1229 | 1450 | 1560 | 1055 | 1090<br>1075 | | |
| π(CH) | 1033 | 1050 | 1083 | 890 | 899 | | |
| δ(OCO) | 636 | 397 | 720 | 642 | 662 | 720 | (b) |
| π(OH) | 636 | 917 | 974 | 678 | 708 | 940 | (b) |

(a) Composed of three bands at closely spaced frequencies.

(b) A band with intensity due to both these modes appears at 690 $cm^{-1}$. The exact positions of the two modes can not be determined.

**Table 2.** Assignments and frequencies (in $cm^{-1}$) of vibrational modes for various formate species. Numbers in parentheses are for the equivalent deuterated formate species.

| Mode | | | Inorganic Formate Complexes (IR) | | | | | Surface Formate Species (EELS) | | | | | |
|---|---|---|---|---|---|---|---|---|---|---|---|---|---|
| | | | Monodentate | | | Bidentate | | Monodentate | | | | Bidentate | |
| Bidentate | Monodentate | Solution | Cr | Fe | Pt | Cr | Fe | Ag(110)-O | Mo(110) | Ru(001) | Pt(110) | Ni(110) | Ru(001) |
| | | (Free) | | | | | | (tilted) | | this work | (tilted) | | this work |
| | | [29,43] | [44] | [45] | [46] | [44] | [44] | [11] | [12] | | [17] | [13] | |
| | ν(CH) | 2803 | | | | 2975 | 2975 | 2900 | 2910 | 2355 | 2950 | 2950 | 2915 |
| | | | | | | 2898 | 2953 | (2150) | | | (2185) | | (2200) |
| $\nu_s$(OCO) | ν(C-O) | 1351 | 1310 | 1293 | 1310 | 1374 | 1369 | 1340 | 1320 | 1345 | 1340 | 1370 | 1360 |
| | | | | | | | | (1310) | | (1315) | (1320) | | (1340) |
| | $\delta_s$(OCO) | 760 | 770(a) | | | | | 770 | 750 | 775 | 785 | 780 | 805 |
| | | | | | | 761 | | (770) | | (775) | (785) | | (800) |
| $\nu_a$(OCO) | ν(C=O) | 1585 | 1574 | 1620 | 1620 | 1644 | 1635 | 640 | 1650 | 1680 | 1560 | | |
| | | | | | | | 1625 | (1640) | | (1660) | (1560) | | |
| | $\delta_s$(CH) | 1385 | | | | 1391 | 1385 | (1010) | | (1015) | (1010) | | |
| | π(CH) | 1069 | 1050 | | | 1040 | 1052 | 1050 | | 1160 | 1050 | | |
| | ν(M-O) | | | | | | | 280 | 380 | 370 | 355 | 430 | 380 |
| | | | | | | | | (260) | | (365) | | | (410) |

(a) Raman frequency.

(b) Composed of three closely spaced bands.

**Figure Captions**

Figure 1: Electron energy loss spectra of molecular formic acid multilayers on Ru(001) at 80 K following exposures of 10 L of HCOOH, (a), and 10 L of DCOOD, (b).

Figure 2: Electron energy loss spectra of monodentate formate on Ru(001) at 80 K following exposures of 4 L of HCOOH, (a), and 2 L of DCOOD, (b).

Figure 3: Electron energy loss spectra showing bidentate formate decomposition on Ru(001) following a 10 L exposure of HCOOH at 80 K and annealing to the indicated temperatures.

Figure 4: Electron energy loss spectra showing bidentate formate on Ru(001) following a 4 L exposure of DCOOD at 80 K and annealing to the indicated temperatures. Note that the intensity of the 610 $cm^{-1}$ band due to a surface deuteroxyl does not correlate with the other spectral features.

Figure 5: Thermal desorption mass spectra of molecular formic acid desorption from Ru(001) following exposures of (a) 3 L, (b) 5 L, (c) 10 L and (d) 20 L of DCOOH.

Figure 6: Thermal desorption mass spectra of $CO_2$ desorption from Ru(001) following exposures of (a) 0.4 L, (b) 0.6 L, (c) 1 L, (d) 3 L, (e) 5 L and (f) 10 L of DCOOH.

Figure 7: Thermal desorption mass spectra of CO desorption from Ru(001) following exposures of (a) 0.4 L, (b) 0.6 L, (c) 1 L, (d) 3 L, (e) 5 L and (f) 10 L of DCOOH.

Figure 8: Formic acid decomposition products on Ru(001) as a function of reaction conditions: (A) the amounts of CO and $CO_2$ evolved relative to a saturation coverage of formate and the ratio of $CO_2$ to CO versus the formic acid exposure (in L) for a heating rate of approximately 15 K/s; (B) the ratio of $CO_2$ to CO versus the heating rate (in K/s) for a 1 L exposure (approximately 40% of saturation). The ratio of products from a surface annealed at 240 K for 300 s and then ramped at 13 K/s was used as the zero heating rate extrapolation.

Figure 9: Thermal desorption mass spectra of (A) $H_2$, (B) HD and (C) $D_2$ desorption from Ru(001) following exposures of (a) 0.4 L, (b) 0.6 L, (c) 1 L, (d) 3 L, (e) 5 L and (f) 10 L of DCOOH.

Figure 10: Thermal desorption mass spectra of *water* desorption from Ru(001) following an exposure of

5 L of DCOOH.

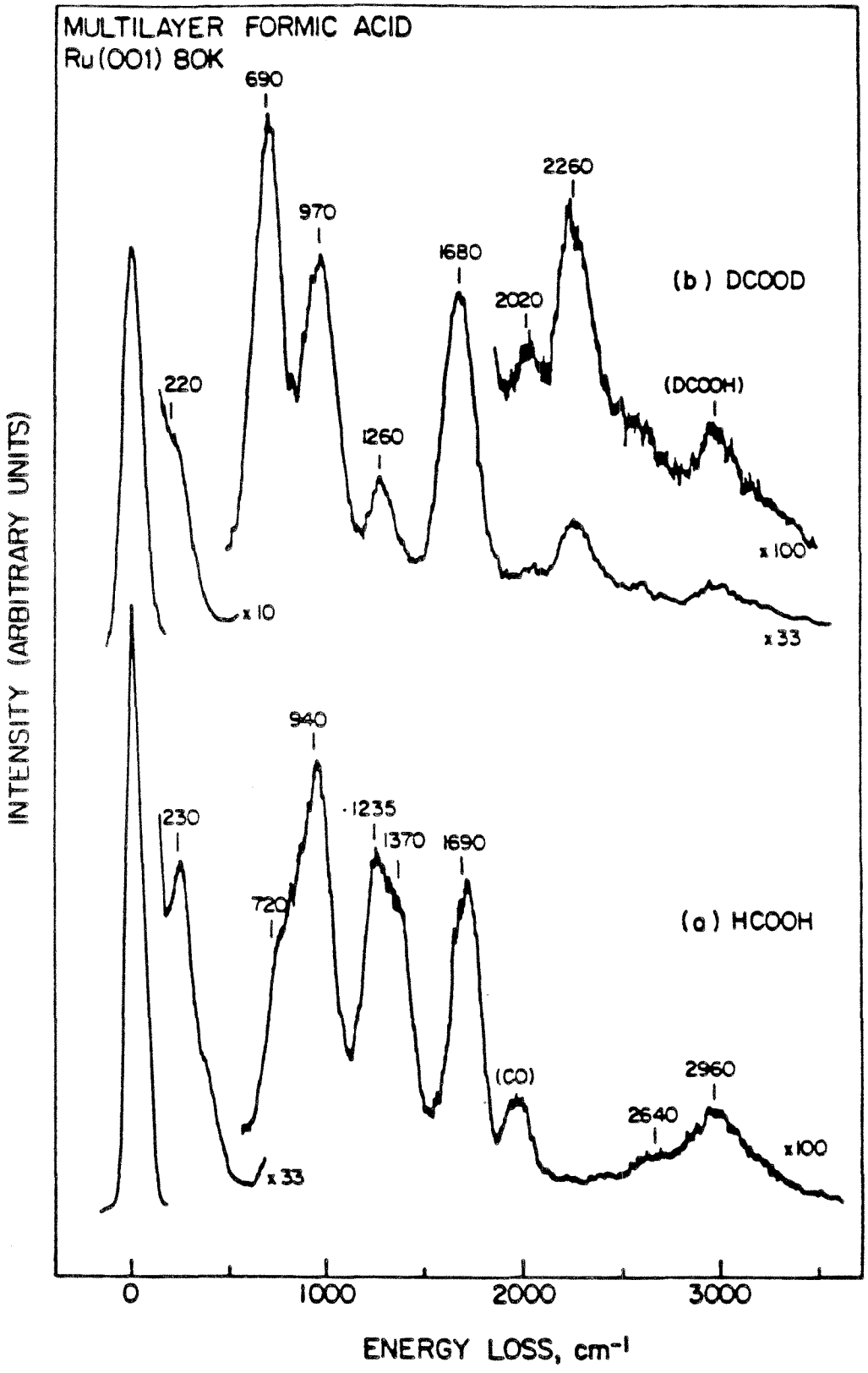
MULTILAYER FORMIC ACID
Ru(001) 80K
690
970
2260
1680
2020
(b) DCOOD
220
(DCOOH)
1260
x 100
x 10
x 33
940
230
1235
1370
1690
720
(a) HCOOH
(CO)
2960
2640
x 100
x 33
0
1000
2000
3000
ENERGY LOSS, cm-1
INTENSITY (ARBITRARY UNITS)

Figure 1

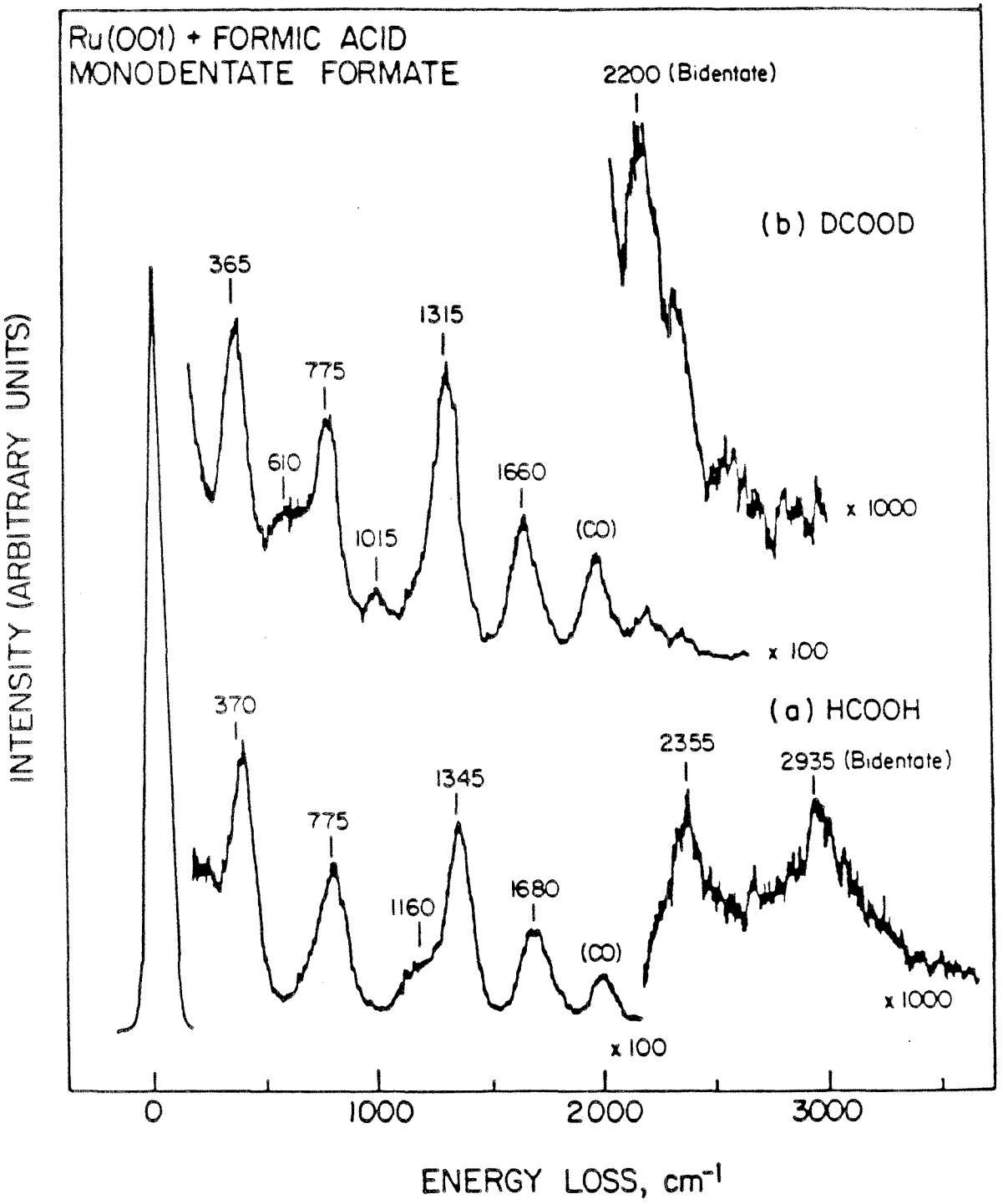
Ru(001) + FORMIC ACID
MONODENTATE FORMATE
2200 (Bidentate)
(b) DCOOD
365
1315
775
610
1660
1015
(CO)
x 1000
x 100
370
(a) HCOOH
2355
2935 (Bidentate)
1345
775
1160
1680
(CO)
x 1000
x 100
INTENSITY (ARBITRARY UNITS)
0
1000
2000
3000
ENERGY LOSS, cm⁻¹

Figure 2

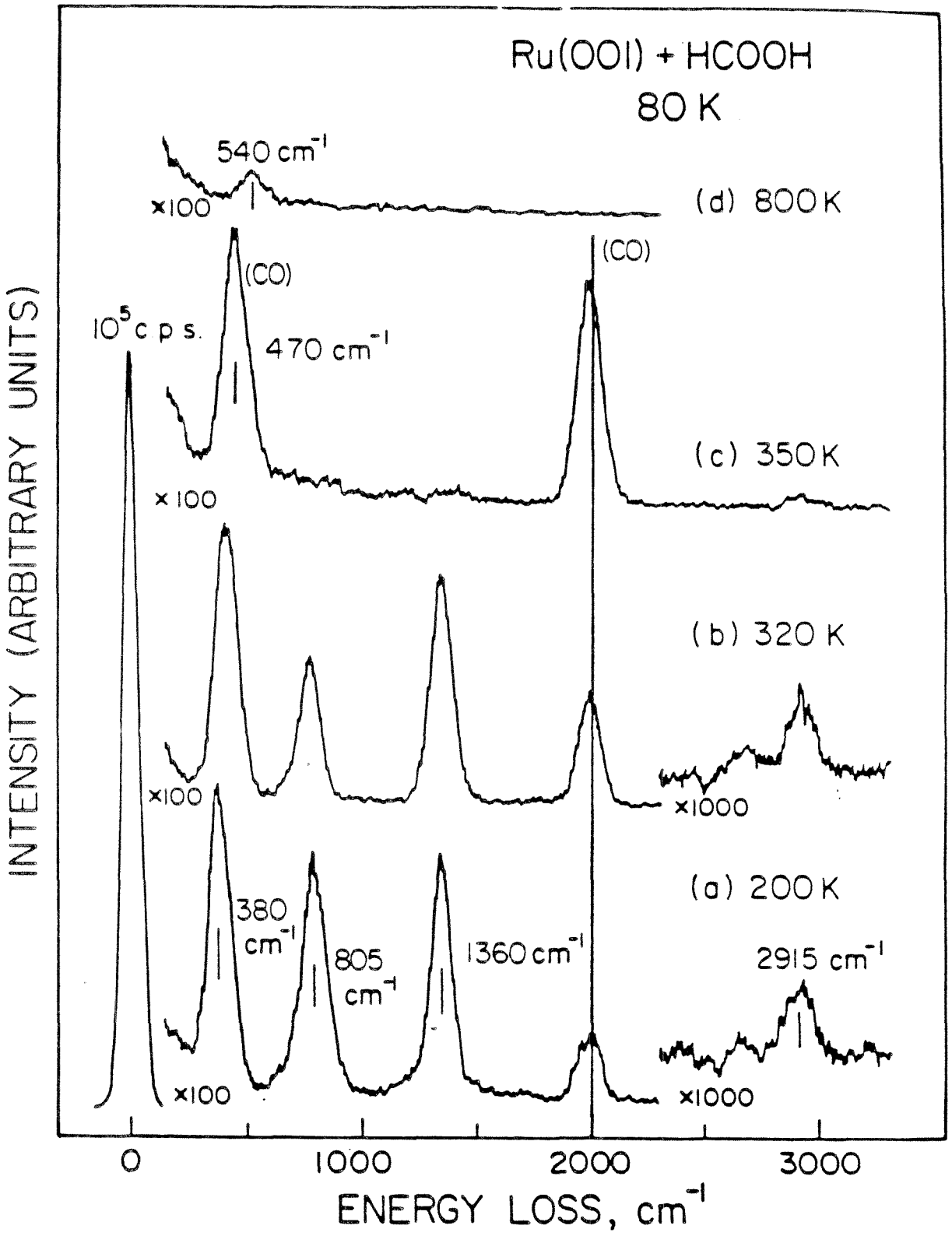
Ru(001) + HCOOH
80 K
540 cm⁻¹
×100
(d) 800 K
(CO)
(CO)
10⁵ c p s.
470 cm⁻¹
(c) 350 K
×100
(b) 320 K
×100
×1000
(a) 200 K
380 cm⁻¹
805 cm⁻¹
1360 cm⁻¹
2915 cm⁻¹
×100
×1000
INTENSITY (ARBITRARY UNITS)
0
1000
2000
3000
ENERGY LOSS, cm⁻¹

Figure 3

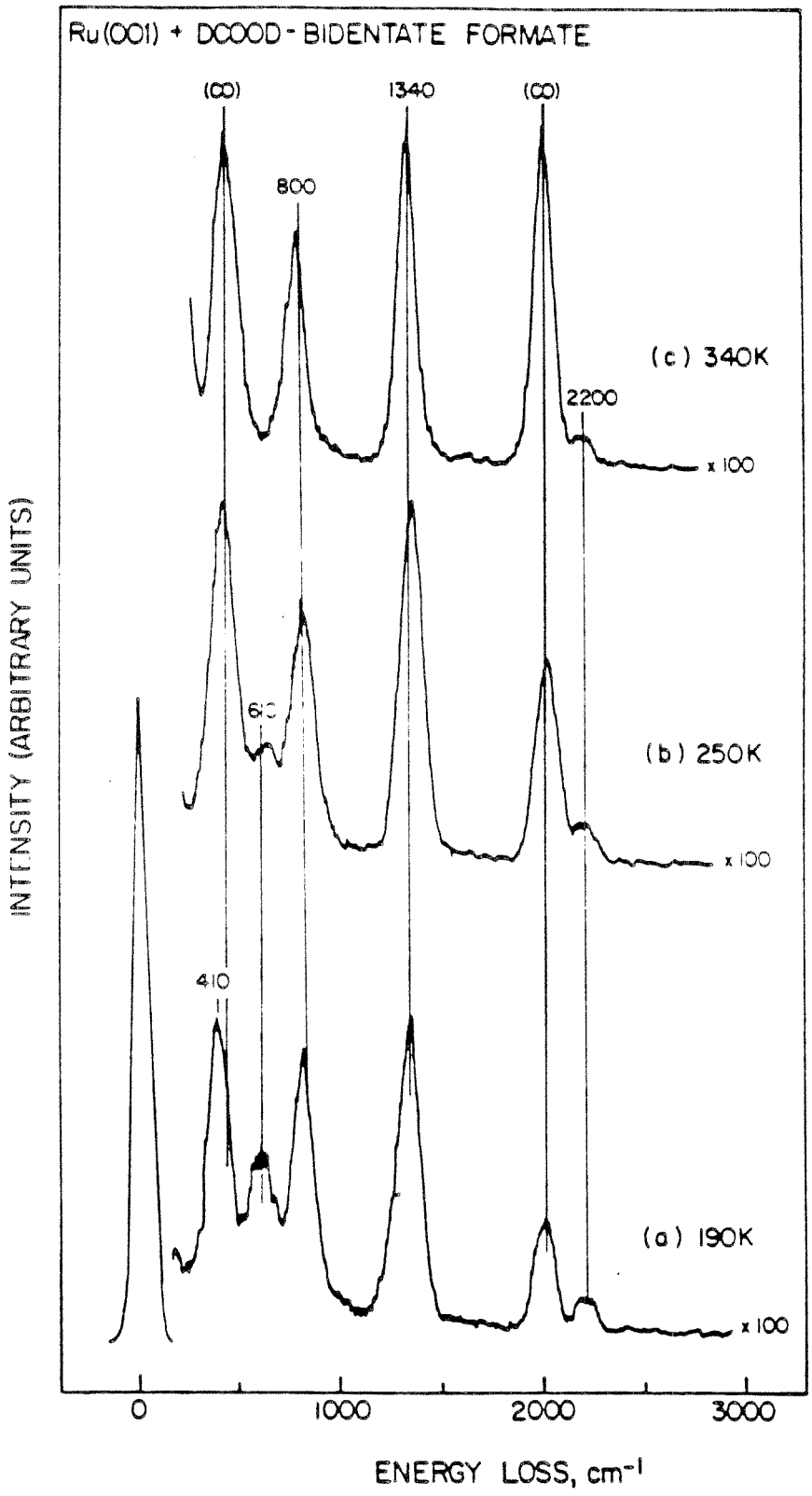
Ru(001) + DCOOD - BIDENTATE FORMATE
(CO)
1340
(CO)
800
(c) 340K
2200
x 100
(b) 250K
x 100
410
(a) 190K
x 100
INTENSITY (ARBITRARY UNITS)
0
1000
2000
3000
ENERGY LOSS, cm⁻¹

Figure 4

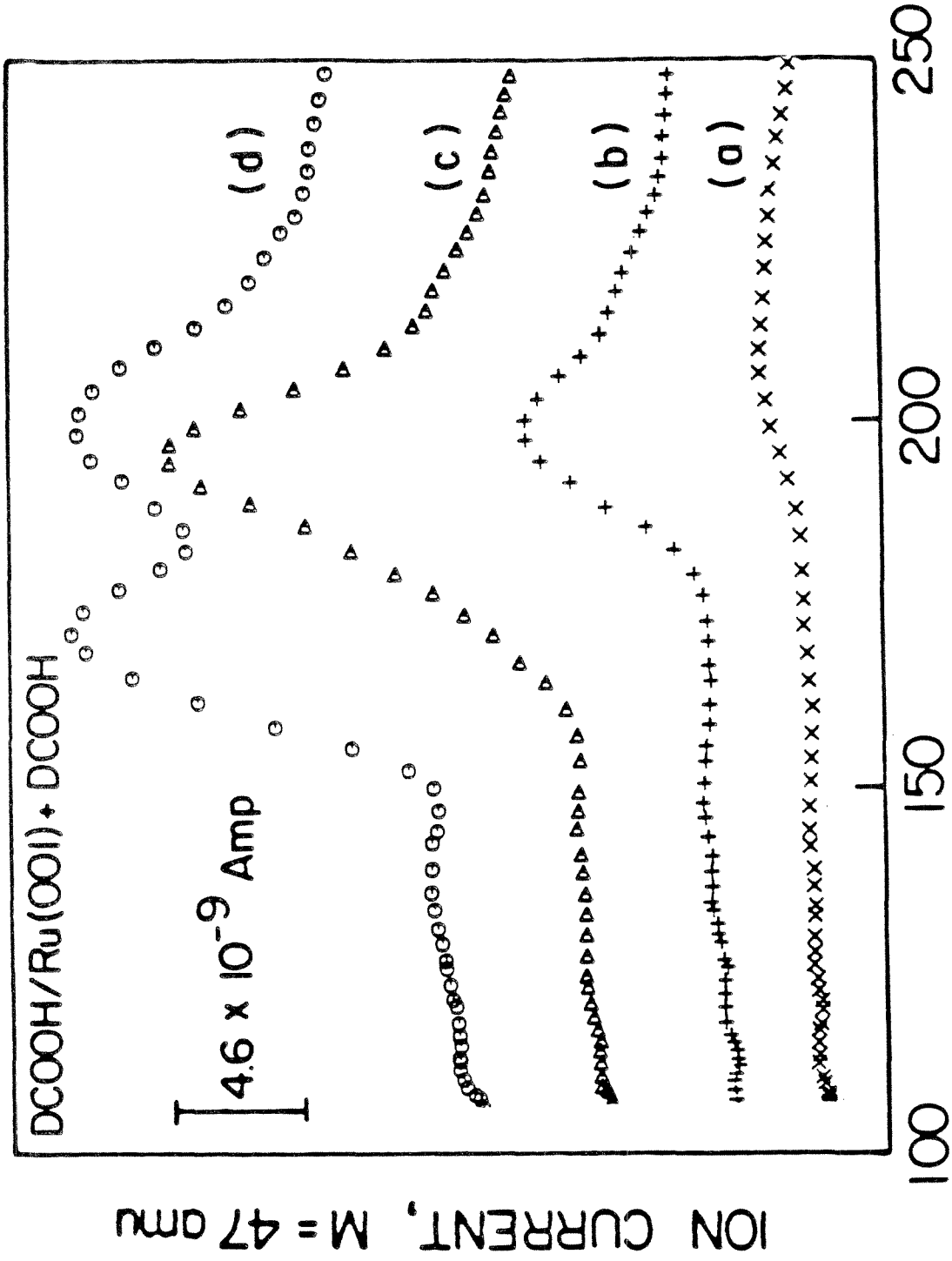
DCOOH/Ru(001) + DCOOH
4.6 x 10⁻⁹ Amp
(d)
(c)
(b)
(a)
100
150
200
250
TEMPERATURE
ION CURRENT, M = 47 amu

Figure 5

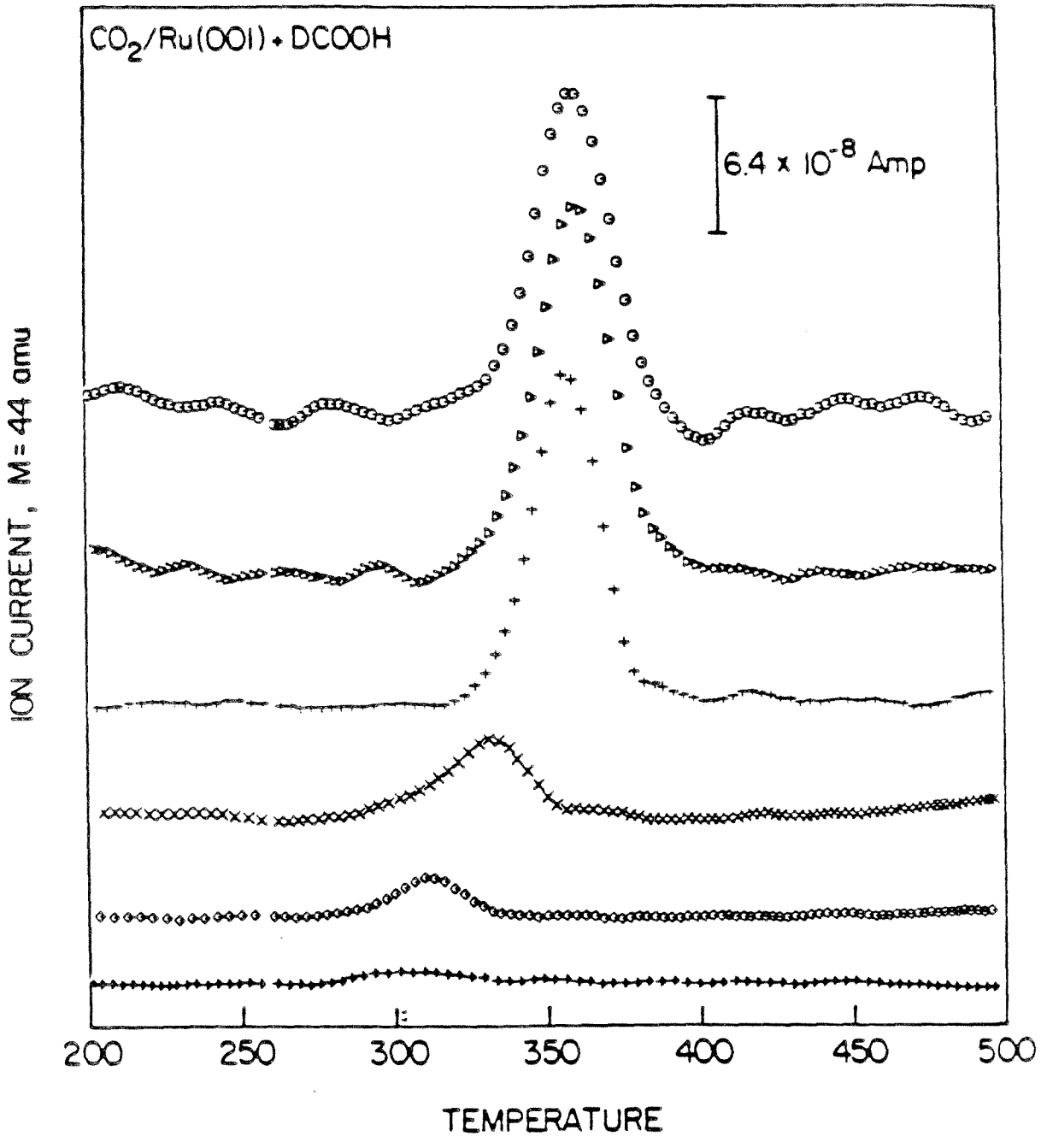
$CO_2$/Ru(001) + DCOOH
6.4 x $10^{-8}$ Amp
ION CURRENT, M = 44 amu
200
250
300
350
400
450
500
TEMPERATURE

Figure 6

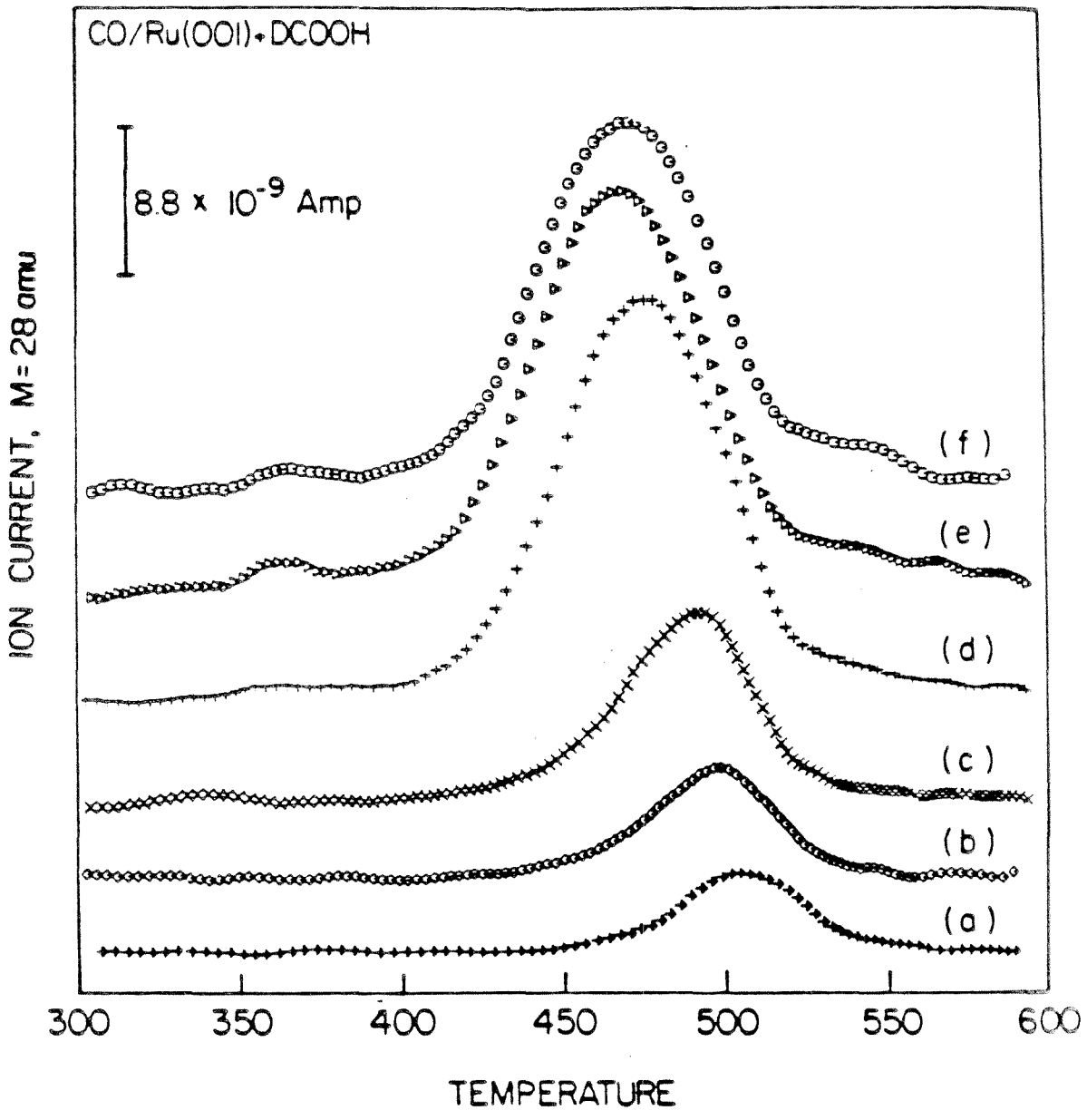
CO/Ru(001)+DCOOH
8.8 x 10⁻⁹ Amp
ION CURRENT, M=28 amu
(f)
(e)
(d)
(c)
(b)
(a)
300
350
400
450
500
550
600
TEMPERATURE

Figure 7

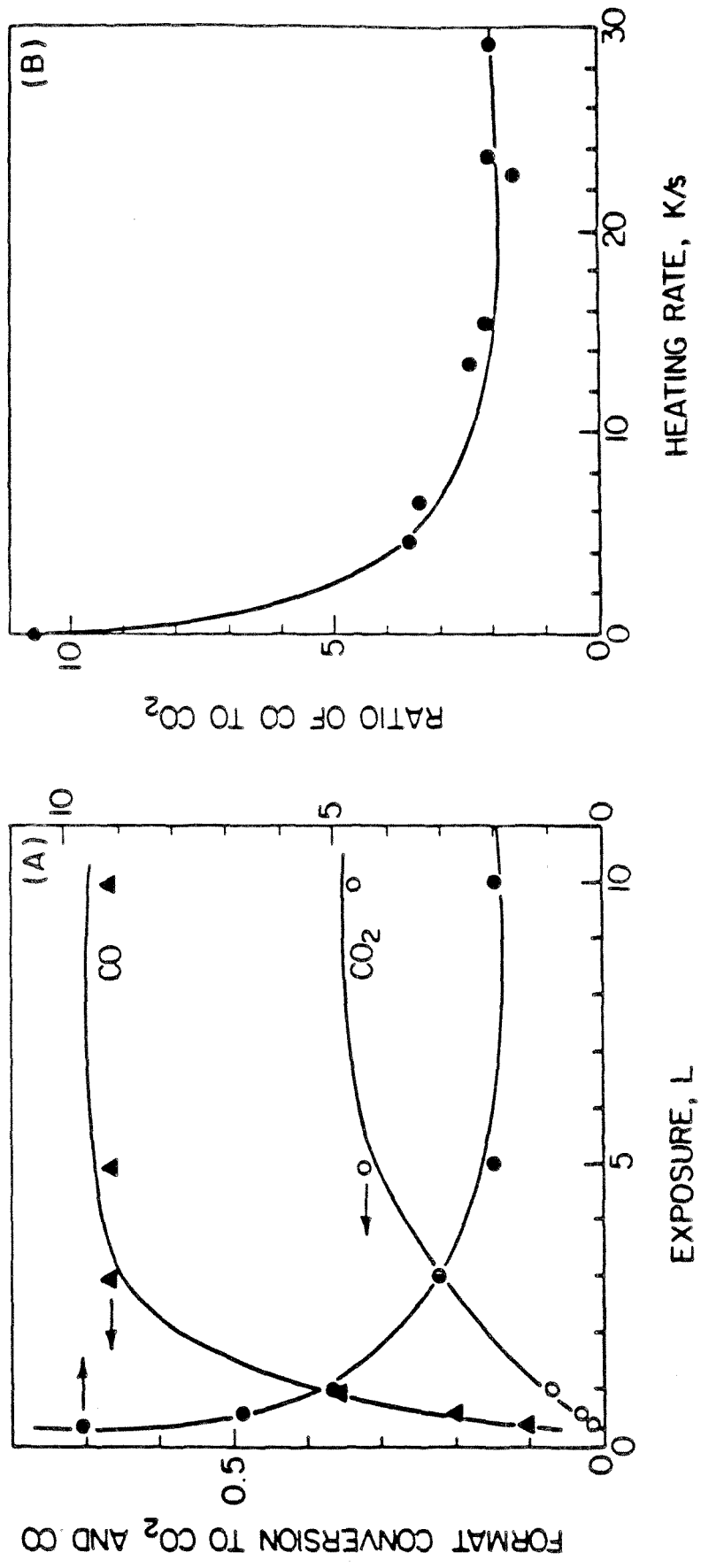
(A)
CO
$CO_2$
FORMAT CONVERSION TO $CO_2$ AND CO
EXPOSURE, L
(B)
RATIO OF CO TO $CO_2$
HEATING RATE, K/s

Figure 8

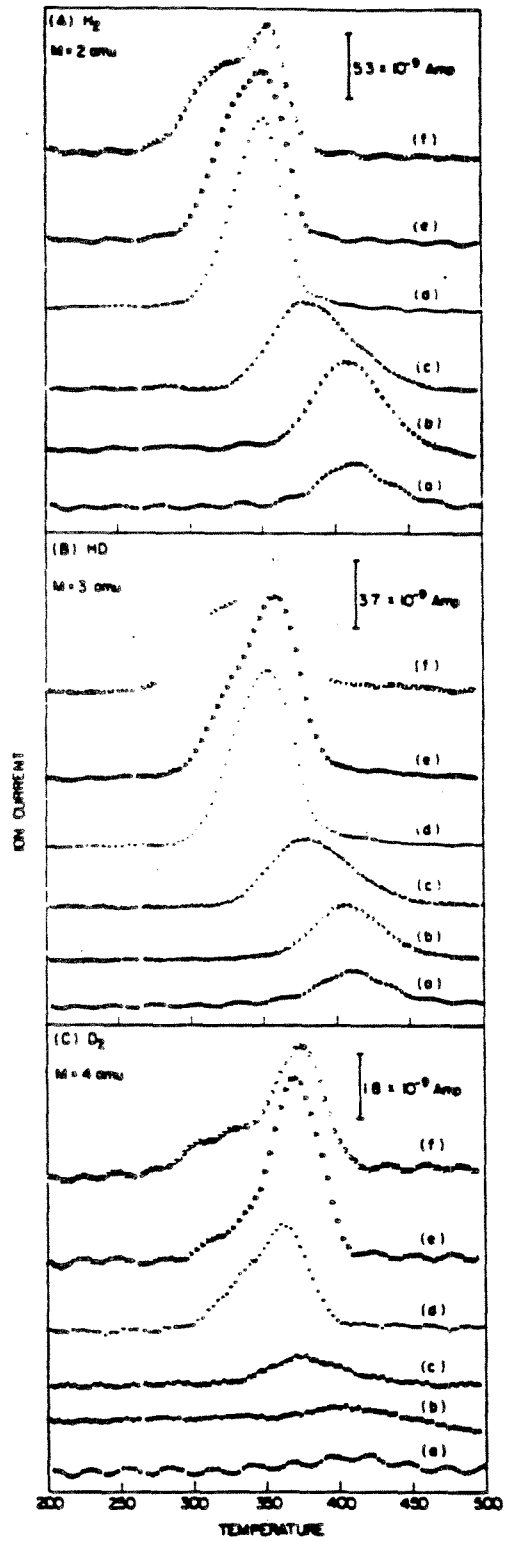
(A) $H_2$
M = 2 amu
5.3 × 10⁻⁹ Amp
(f)
(e)
(d)
(c)
(b)
(a)
(B) HD
M = 3 amu
3.7 × 10⁻⁹ Amp
(f)
(e)
(d)
(c)
(b)
(a)
(C) $D_2$
M = 4 amu
1.8 × 10⁻⁹ Amp
(f)
(e)
(d)
(c)
(b)
(a)
ION CURRENT
200
250
300
350
400
450
500
TEMPERATURE

Figure 9

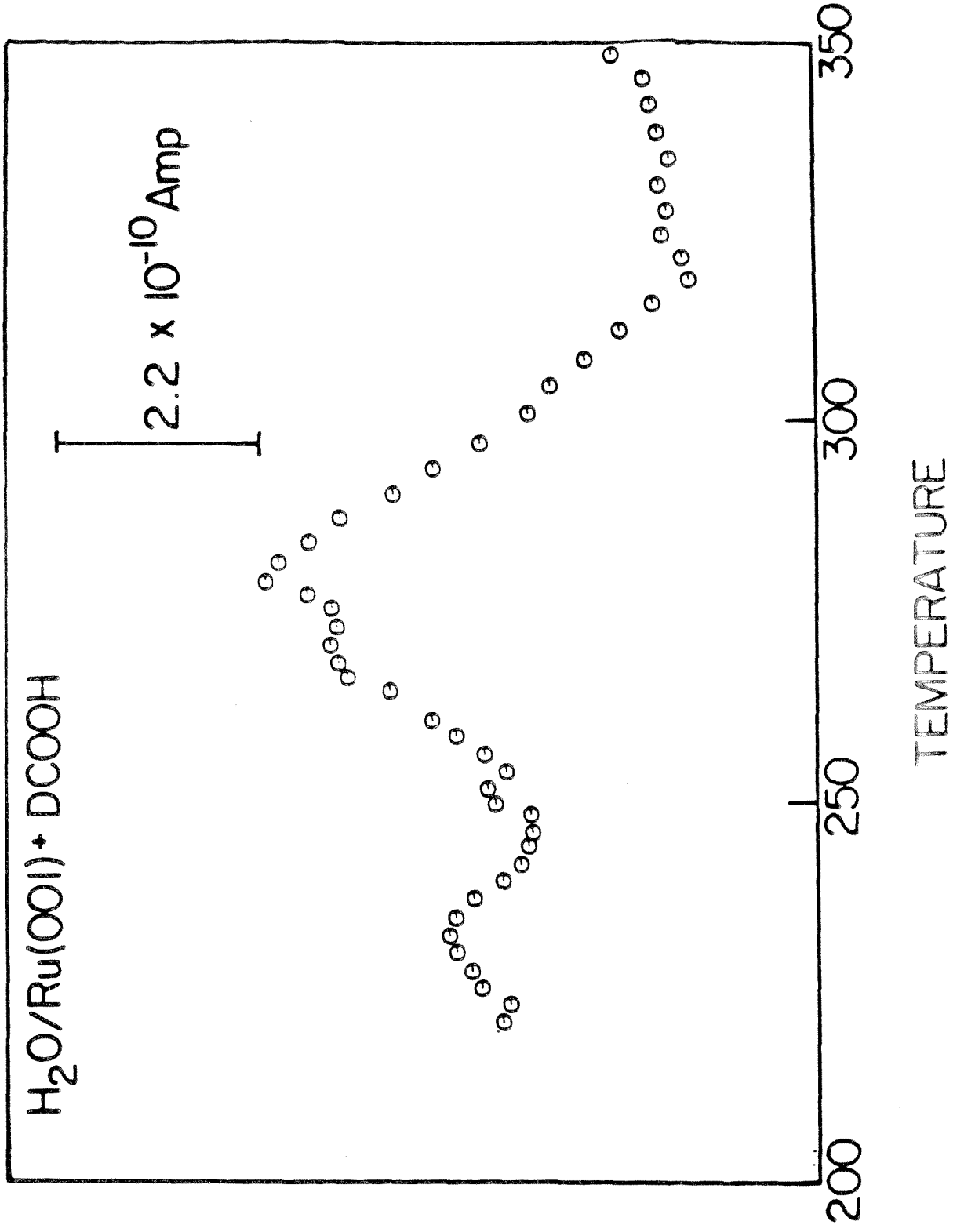


Figure 10